Curriculum Vitae
Da Shi

Education

INSTITUTION AND LOCATION	DEGREE *(if applicable)*	YEAR(s)	FIELD OF STUDY
University of Maryland, Baltimore County Baltimore, MD	B.S.	'03-'07	Biological Sciences
University of Maryland, Baltimore Baltimore, MD	Ph.D.	'11-'17	Biochemistry and Molecular Biology

Employment History

ACTIVITY/ OCCUPATION	BEGIN DATE (mm/yy)	END DATE (mm/yy)	FIELD	INSTITUTION/ COMPANY	SUPERVISOR/ EMPLOYER
Undergraduate Research Assistant	09/05	05/07	Behavioral Entomology	University of Maryland, Baltimore County, Dept. of Biological Sciences	Frank Hanson, PhD
Research Assistant	09/07	06/09	Pediatrics	University of Maryland, Baltimore, Dept. of Pediatrics	Mary C. McKenna, PhD
Research Assistant	06/09	08/11	Diagnostic Radiology	University of Maryland, Baltimore, Dept. of Diagnostic Radiology	Rao P. Gullapalli, PhD and Su Xu, PhD

Academic and Professional Honors

Invited speaker 43rd meeting of American Society for Neurochemistry Baltimore, MD. March 2012
Travel award for International Society for Neurochemistry Advanced School on New Approaches in Glial Cell Research in Barcelona, Spain. August 2012
Trainee (educational) stipend award from International Society of Magnetic Resonance in Medicine (ISMRM). May 2013 and May 2014
ISMRM Magna Cum Laude Merit Award. May 2013

Graduate Student Association Research Award. Spring 2014

Membership in Professional Societies

International Society of Magnetic Resonance in Medicine
American Society in Neurochemistry

Publications (in chronological order)

Peer-reviewed Publications

1. Scafidi S, Fiskum G, Lindauer SL, Bamford P, **Shi D**, Hopkins I, McKenna MC. Metabolism of acetyl-L-carnitine for energy and neurotransmitter synthesis in the immature rat brain. J Neurochem. 2010; 114(3):820-31.
2. Xu S, Zhuo J, Racz J, **Shi D**, Roys S, Fiskum G, Gullapalli R. Early microstructural and metabolic changes following controlled cortical impact injury in rat: magnetic resonance imaging and spectroscopy study. J Neurotrauma. 2011;(10):2091-102.
3. Raufman JP, Xu S, Cheng K, Khurana S, Johnson D, Shao C, Kane MA, **Shi D**, Gullapalli R, Polli J. In vivo magnetic resonance imaging to detect biliary excretion of 19F-labeled drug in mice. Drug Metab Dispos. 2011; 39(5):736-9.
4. McMillan AB, **Shi D**, Pratt SJ, Lovering RM. Diffusion tensor MRI to assess damage in healthy and dystrophic skeletal muscle after lengthening contractions. J Biomed Biotechnol. 2011;2011:970726.
5. **Shi D**, Xu S, Waddell J, Scafidi S, Roys S, Gullapalli R, McKenna MC. Longitudinal in vivo developmental changes of metabolites in the hippocampus of Fmr1 knockout mice. J Neurochem. 2012; 123(6):971-81.
6. Raufman JP, Xu S, Cheng K, Khurana S, Vivian D, **Shi D**, Gullapalli R, Polli J. Phrygian cap appearance of a mouse gallbladder on magnetic resonance imaging. J Vet Sci Med Diagn. 2013; 28;2(1).
7. Xu S, Waddell J, Zhu W, **Shi D**, Marshall AD, McKenna MC, Gullapalli RP. In vivo longitudinal proton magnetic resonance spectroscopy on neonatal hypoxic-ischemic rat brain injury: Neuroprotective effects of acetyl-L-carnitine. Magn Reson Med. 2015;74(6):1530-42.
8. Xu S, **Shi D**, Pratt SJ, Zhu W, Marshall A, Lovering RM. Abnormalities in brain structure and biochemistry associated with mdx mice measured by in vivo MRI and high resolution localized (1)H MRS. Neuromuscul Disord. 2015;25(10):764-72.

Published Abstracts

1. McKenna MC, Lindauer SL, Bamford P, **Shi D**, Hopkins IB, Zielke HR, Lindauer C. "MPEP attenuates altered glutamate metabolism in 18 day old Fragile X mouse brain." FRAXA Investigator's Meeting, Durham, NH. 2008.
2. Fiskum G, Mehrabian Z, Kristian T, Lindauer SL, **Shi D**, McKenna MC. NAD(H) depletion after neonatal cerebral hypoxia ischemia impairs brain mitochondrial bioenergetics. J Neurochem. 2009; Conference: 40th Annual Meeting of the American Society for Neurochemistry, Volume: 108.

3. Su X, Roys S, Racz J, **Shi D**, Zhou J, Gullapalli R, Fiskum G. "Early metabolic changes following focal traumatic brain injury in rats measured using 1H MRS." International Society of Magnetic Resonance Research, Stockholm, Sweden. 2010.
4. **Shi D,** Xu S, Roys S, Gullapalli R, McKenna MC. "Decrease of glutamate in the hippocampus of the fmr1 knockout mouse during myelingenesis detected by in vivo 1H MRS." International Society of Magnetic Resonance Research, Montréal, Québec, Canada. 2011.
5. **Shi D,** Xu S, Waddell J, Scafidi S, Roys S, Gullapalli R, McKenna MC. "Alteration of myelin components during critical development ages of *Fmr1* knockout mice." American Society for Neurochemistry, Baltimore, MD. 2012.
6. **Shi D,** Xu S, Waddell J, Scafidi S, Roys S, Gullapalli R, McKenna MC. "Alteration of myelin components during critical development ages of *Fmr1* knockout mice." Gordon Research Conference, Easton, MA. 2012.
7. **Shi D,** Xu S, Waddell J, Scafidi S, Roys S, Gullapalli R, McKenna MC. "Alteration of myelin components during critical development ages of *Fmr1* knockout mice." International Society for Neurochemistry Advanced School on New Approaches in Glial Cell Research, Barcelona, Spain. 2012.
8. **Shi D**, Zhou J, Xu S, Gullapalli RP. "Reduction of diffusion parameters in fixed brain sample of *Fmr1* KO compared to WT mice." International Society of Magnetic Resonance in Medicine, Salt Lake City, UT. 2013.
9. **Shi D,** Xu S, McKenna MC, Zhou J, Gullapalli R. "Different stages of white matter formation affected during peak myelination period in the developing *Fmr1* knockout mouse." American Society in Neurochemistry, Long Beach, CA. 2014.
10. **Shi D,** Xu S, McKenna MC, Zhou J, Gullapalli R. "Reduced magnetization transfer in gray and white matter in the developing *Fmr1* knockout mouse." International Society of Magnetic Resonance in Medicine, Milan, Italy. 2014.

Abstract

Title: Brain Development in the *Fmr1* KO Mouse Model of Fragile X Syndrome

Da Shi, Doctor of Philosophy, 2017

Dissertation Directed by: Rao P. Gullapalli, PhD. and Mary C. McKenna, PhD.

Fragile X syndrome (FXS) is the most commonly inherited form of intellectual disability resulting from silencing of *FMR1* gene and consequential absence of fragile X mental retardation protein. FXS is commonly studied in *Fmr1* KO mouse, which displays similar behavioral and neurological deficits as FXS patients. Many studies have investigated immature *Fmr1* KO brain, but little is known about alterations in brain maturation processes, including developmental changes in metabolites, white and gray matter morphology and brain network function. Alterations in metabolites from ^{1}H-magnetic resonance spectroscopy between *Fmr1* KO and WT mice revealed included *myo*-inositol at postnatal-day 30 (PND 30), and taurine at PND 18, 21, and 30. Next, developmental alterations in myelin and white matter were examined in fixed *Fmr1* KO mouse brains compared to WT at PND 18, 21, 30 and 60 with histological staining of myelin and MRI techniques to measure volume and magnetization transfer ratio, which is sensitive to myelin proteins and lipids. *Fmr1* KO mice revealed decreased myelin density and MTR at PND 18, increased at PND 30 and decreased at PND 60, suggesting altered pattern of myelin formation in *Fmr1* KO mouse. Diffusion tensor imaging was used to study microstructural properties of white matter to provide insight into myelin and axon properties in fixed *Fmr1* KO brains at PND 18, 21, 30 and 60. Decreased mean, axial and radial diffusivity was found at PND 21 and 30 in *Fmr1* KO brains, suggesting alterations in myelin compaction and axonal organization. Finally, alterations in functional

connectivity in *Fmr1* KO mouse were studied using resting-state functional-MRI. The longitudinal results showed decreased functional connectivity in the auditory and somatomotor networks in *Fmr1* KO brain compared to WT at PND 30 and not different by PND 60, suggesting a delay in development of the resting state networks in *Fmr1* KO mice. The work in this thesis characterized metabolic, structural, and functional alterations in developing *Fmr1* KO mouse brain.

Brain Development in the *Fmr1* KO Mouse Model of Fragile X Syndrome

by
Da Shi

Dissertation submitted to the Faculty of the Graduate School of the
University of Maryland, Baltimore in partial fulfillment
of the requirements for the degree of
Doctor of Philosophy
2017

Acknowledgements

I would like to thank my mentors Dr. Rao P. Gullapalli and Dr. Mary C. McKenna for first giving me the opportunity to join their respective labs as their technician and then allowing me to be their student. I would also like to thank my committee members Drs. Carolyn B. Smith, Kristen Varney, Alexandre Medina, and Celine Plachez for their insight and guidance, especially Dr. Smith for her time and effort in making me a better writer. I am grateful to Dr. Mike Tranfaglia who has taken an interest in my project and Dr. Becky Zorovic for allowing me to attend the FRAXA investigators meeting in 2008 where I first became interested in studying FXS. I would also like to thank members of the Gullapalli lab past and present, Dr. Su Xu for encouraging me to start the project that became Chapter 5, Dr. Jiachen Zhuo, Mr. Steven Roys, and Ms. Shiyu Tang for having the patience to answer my technical questions, and Drs. Chandler Sours and Jake Mullins for their friendship in the lab. In addition, I would like to thank members of Dr. McKenna's lab, past and present, including Ms. Penny Bamford, Ms. Irene Hopkins, Ms. Michele Diamond, and Ms. Danisha Gallop for their assistance with molecular techniques. I would like to especially thank Dr. Jaylyn Waddell for her friendship and her expertise. I also thank Dr. Gerald Wilson and Ms. Koula Cozmo from the Biochemistry department. Last but not least I would like to thank my loving and supportive family and friends, especially my parents who gave me endless encouragement, and the friends I have made at UMB, Dr. Cigdem Tosun, Dr. Jenny Browning, Ms. Shalon Edwards, Dr. Zephan Melville and Dr. Christina Young.

Table of Contents

Acknowledgements iii
Table of Contents iv
List of Tables x
List of Figures xi
List of Abbreviation xiii
CHAPTER 1: INTRODUCTION TO FXS 1
1.1. FRAGILE X SYNDROME 1
1.2. ANIMAL MODELS OF FXS 2
1.2.1. *Fmr1* KO mouse 2
1.2.2. *Drosophila* model of FXS 4
1.2.3. *Fmr1* KO rat model of FXS 5
1.3. NEURONAL PHENOTYPE IN THE *FMR1* KO MOUSE 6
1.3.1. Altered long-term depression in the *Fmr1* KO mouse 6
1.3.2. Downstream effects of mGluR5 dependent long-term depression in *Fmr1*KO mice 9
1.3.3. Altered long-term potentiation in the cortex of the *Fmr1* KO mouse 12
1.3.4. Excitatory and inhibitory signaling imbalance in the *Fmr1* KO mice 13
1.3.5. Morphological changes in FXS 14
1.3.5.1. Elevated levels of immature dendritic spines 14
1.3.5.2. Alterations in axon formation 18
1.4. ALTERATION OF GLIA IN THE *FMR1* KO BRAIN 19
1.4.1. Astrocytes 19
1.4.2. Oligodendrocytes 21
1.5. The importance of studying the developing *Fmr1* KO mouse brain 22
CHAPTER 2: IMAGING THE FXS BRAIN 24
2.1. INTRODUCTION TO BRAIN IMAGING STUDIES IN FXS AND THE *FMR1* KO MOUSE 24
2.1.1. Metabolic imaging in FXS AND THE *FMR1* KO MOUSE 24
2.1.1.1. Metabolism and tracer labeling using positron emission tomography 24
2.1.1.2. Brain metabolite levels from ^{1}H magnetic resonance spectroscopy 26
2.1.2. Changes in brain volume in children with FXS 27
2.1.3. Changes in brain volume in adolescents and adults with FXS 29
2.1.4. Volume changes in the *Fmr1* KO mouse brain 30

2.1.5. Altered white matter integrity in the FXS and *Fmr1* KO mouse brains 31
2.2. ALTERED BRAIN FUNCTION IN FXS 31
2.2.1. Resting state networks in the FXS brain 33
2.2.2. Resting state brain networks in rodents 36
2.3. SUMMARY 37
CHAPTER 3: PURPOSE AND SPECIFIC AIMS 39
3.1. RESEARCH QUESTIONS 39
3.2. PURPOSE 40
3.3. SPECIFIC AIMS 40
3.3.1. Determine longitudinal changes in hippocampal metabolites in developing *Fmr1* KO mouse brain compared to WT brain 41
3.3.2. Determine alterations in white matter of the developing *Fmr1* KO mice 41
3.3.3. Determine diffusion properties in the brain of developing *Fmr1* KO mice 42
3.3.4. Determine if there are alterations in resting state networks in the developing brain of *Fmr1* KO micecompared to WT mice 42
3.3.5. Pilot study of metformin on resting state networks in the developing brain of *Fmr1* KO mice 43
CHAPTER 4: ANIMALS AND GENOTYPING 45
4.1. ANIMALS 45
4.2. MICE BREEDING SCHEMES 45
4.3. GENOTYPING PROTOCOL 46
CHAPTER 5: LONGITUDINAL *IN VIVO* DEVELOPMENTAL CHANGES OF METABOLITES IN THE HIPPOCAMPUS OF *FMR1* KNOCKOUT MICE 48
5.1. INTRODUCTION 48
5.2. METHODS AND MATERIALS 50
5.2.1. Animal procedure 50
5.2.2. *In vivo* MRI/MRS 51
5.2.3. Statistical Analysis 53
5.3. RESULTS 55
5.3.1. Hippocampal volume 55
5.3.2. Neurochemical profile of *Fmr1* mice compared to wild type mice 56
5.3.3. Longitudinal changes in metabolites in the developing hippocampus 57

5.4. DISCUSSION 60
5.4.1. Change in *N*-acetylaspartate 64
5.4.2. Alterations in osmoregulatory molecules in the hippocampus of *Fmr1* KO mice 66
5.4.3. *Myo*-inostiol 67
5.4.4. Taurine 68
5.4.5. Neurotransmitters and related metabolites 69
5.4.6. Hippocampal volume differences 70
5.5. CONCLUSIONS 72
CHAPTER 6: WHITE MATTER ALTERATIONS IN *FMR1* KO MICE DURING EARLY POSTNATAL BRAIN DEVELOPMENT 73
6.1. INTRODUCTION 73
6.1.2. Detecting changes in myelin using MRI 75
6.2. METHODS AND MATERIALS 77
6.2.1. Animal procedure 77
6.2.2. Magnetic resonance imaging 78
6.2.3. Image Processing 79
6.2.4. Histology 80
6.2.5. Statistical Analysis 81
6.3. RESULTS 82
6.3.1. White matter volumes 82
6.3.2. T_2 relaxation time 86
6.3.3. Magnetization Transfer Ratio 88
6.3.4. Myelin staining 91
6.4. DISCUSSION 96
6.4.1. Myelination delay in white matter in the developing *Fmr1* KO mouse 97
6.4.2. Contribution of altered brain metabolites to myelination in the *Fmr1* KO mice 99
6.4.3. Implications for functional brain networks in the *Fmr1* KO mouse 101
6.4.4. White matter volume in the FXS brain 103
6.4.5. Imaging the fixed brain 103
6.5. CONCLUSIONS 104

CHAPTER 7: DIFFUSION PROPERTIES OF THE *FMR1* KO BRAIN AND REPRESENTATION OF AXON FIBER 106
7.1. INTRODUCTION 106
7.2. MATERIALS AND METHODS 110
7.2.1. Animal procedure 110
7.2.2. Magnetic resonance imaging 111
7.2.3. DKI reconstruction 112
7.2.4. Analysis of gray and white matter regions 114
7.2.5. White matter fiber tractography 114
7.2.6. Statistics 115
7.3. RESULTS 115
7.3.1. Diffusion tensor parameter changes in the *Fmr1* KO brain 117
7.3.1.1. Mean diffusivity 117
7.3.1.2. Axial diffusivity 120
7.3.1.3. Radial diffusivity 123
7.3.1.4. Fractional anisotropy 126
7.3.1.5. Fiber density 129
7.3.2. Kurtosis tensor parameter changes in the *Fmr1* KO brain 133
7.3.2.1. Mean Kurtosis 133
7.3.2.2. Axial Kurtosis 135
7.3.2.3. Radial Kurtosis 138
7.4. DISCUSSION 140
7.4.1. Insight regarding axonal fibers of the developing *Fmr1* KO mouse brain 140
7.4.2. Insight regarding myelination in the developing *Fmr1* KO mouse brain 142
7.4.3. Alterations in diffusivity in the brains of *Fmr1* KO mice and FXS patients 143
7.4.4. Diffusivity in normally developing rodents 144
7.5. CONCLUSIONS 146
CHAPTER 8: RESTING STATE NETWORKS IN THE DEVELOPING *FMR1* KO MOUSE BRAIN 147
8.1. INTRODUCTION 147
8.1.1. Functional connectivity and resting state networks in brain 147
8.1.2. Imbalance of neuronal signaling in the developing *Fmr1* KO mice 148

8.1.3. Altered functional connectivity in FXS and the *Fmr1* KO mice 148
8.1.4. Resting state networks in the rodent brain 150
8.1.5. The effect of anesthesia on resting state networks in the rodent brain.....152
8.1.6. Study aim.....153
8.2. MATERIALS AND METHODS 154
8.2.1. Animal procedure.....154
8.2.2. Magnetic resonance imaging 155
8.2.2.1. Anesthesia.....155
8.2.2.2. Image acquisition.....155
8.2.3. Data analysis.....156
8.2.3.1. Pre-processing procedures 156
8.2.3.2. Calculation of functional connectivity.....158
8.2.4. Statistical analysis 160
8.3. RESULTS 161
8.3.1. Developmental differences in the somatomotor network.....161
8.3.2. Developmental differences in the auditory and visual networks 165
8.3.3. Developmental differences in the default mode network.....168
8.4. DISCUSSION 173
8.4.1. Developmental changes in functional connectivity.....173
8.4.1.1. Somatomotor network.....175
8.4.1.2. Auditory network.....176
8.4.1.3. Visual network.....177
8.4.1.4. Default mode network.....178
8.4.2. Functional connectivity alterations in the autism spectrum disorder and relation to FXS 178
8.5. CONCLUSIONS.....180
CHAPTER 9: INTERVENTIONS FOR FRAGILE X SYNDROME AND PILOT STUDY WITH METFORMIN TREATMENT IN THE DEVELOPING *FMR1* KO MOUSE BRAIN.....181
9.1. TREATMENT OUTCOME MEASURES FOR FXS.....181
9.2. T REATMENTS FOR FXS 183
9.2. 1. Metabotropic glutamate receptor 5 antagonist 183

9.2.2. $GABA_B$ receptor agonist....185
9.2.3. Lithium....185
9.2.4. Minocycline....186
9.3. PILOT STUDY WITH METFORMIN....188
9.3.1. Current understanding of metformin in the *Fmr1* KO mouse and FXS patients....188
9.3.2. Materials and Methods....191
9.3.2.1. Animal procedure....191
9.3.2.2. Metformin treatment....192
9.3.2.3. Magnetic resonance imaging and data analysis....193
9.3.2.4. Statistical analysis....194
9.3.3. Results....194
9.3.3.1. Effect of Metformin on Functional Connectivity Networks....194
9.3.3.2. Changes in MTR following metformin treatment in the *Fmr1* KO mouse brain....200
9.3.4. Conclusions from the pilot study with metformin....203
CHAPTER 10: CONCLUSIONS AND FUTURE DIRECTIONS....205
10.1. DEVELOPMENTAL ALTERATIONS IN THE *FMR1* KO MOUSE BRAIN....205
10.2. FUTURE DIRECTIONS FOR STUDYING BRAIN DEVELOPMENT IN ANIMAL MODELS OF FXS....209
10.3. TREATMENT WITH METFORMIN....213
10.4. FUTURE DIRECTIONS FOR STUDYING METFORMIN TREATMENT IN FXS....213
References....215

List of Tables

Table 5-1: Comparison of the ratio of metabolites to total creatine (tCr) between *Fmr1* KO mice and WT mice at PND 18, 21, and 30.....57

Table 6-1: Whole brain volume (mm^3) of WT and *Fmr1* KO mice. 83

Table 6-2: Normalized white matter volume in *Fmr1* KO and WT mice.....84

Table 6-3: Summary of two-way ANOVA for the whole brain and regional white matter volumes.....85

Table 6-4: Summary of two-way ANOVA for normalized white matter volume.....86

Table 6-5: Summary of two-way ANOVA for T_2 relaxation 88

Table 6-6: Summary of two-way ANOVA for MTR 91

Table 6-7: Summary of two-way ANOVA for Black Gold II staining of myelin.....96

Table 7-1: Whole brain DTI and DKI parameters between WT and *Fmr1* KO mice at PND 18, 21, 30, and 60.....117

Table 7-2: Summary of two-way ANOVA for mean diffusivity.....120

Table 7-3: Summary of two-way ANOVA for axial diffusivity.....123

Table 7-4: Summary of two-way ANOVA for radial diffusivity 126

Table 7-5: Summary of two-way ANOVA for fractional anisotropy.....129

Table 7-6: Summary of two-way ANOVA for fiber density.....131

Table 7-7: Fiber density between WT and *Fmr1* KO mice at PND 18, 21, 30 and 60.....132

Table 7-8: Summary of two-way ANOVA for mean kurtosis.....135

Table 7-9: Summary of two-way ANOVA for axial kurtosis.....138

Table 7-10: Summary of two-way ANOVA for radial kurtosis 140

Table 9-1: Summary of two-way ANOVA for magnetization transfer ratio (MTR) of *Fmr1* KO and WT mice in metformin treated and vehicle groups.....203

List of Figures

Figure 1-1: The role of group 1 mGluR activation and FMRP in the WT and consequences from the lack of FMRP in the *Fmr1* KO mice 7

Figure 1-2: Downstream signaling of mGluR5 activation in the neurons of the hippocampus in WT mice and *Fmr1* KO mice 11

Figure 1-3: Representation of dendritic spine density in *Fmr1* KO and WT mice 16

Figure 5-1: Representative *in vivo* high resolution ^{1}H MR spectra in the hippocampus of *Fmr1* KO and WT mice 54

Figure 5-2: Hippocampal volume in the developing *Fmr1* KO and WT mouse brains 56

Figure 5-3: Mean ratio of each metabolite to total creatine in the hippocampus of *Fmr1* KO and WT mice studied longitudinally at PND 18, 21 and 30 60

Figure 6-1: White matter volume in the developing *Fmr1* KO and WT mouse brains 83

Figure 6-2: T_2 relaxation time in white matter regions of the developing *Fmr1* KO and WT mice 87

Figure 6-3: Magnetization transfer ratio (MTR) in white matter regions of the developing *Fmr1* KO and WT mice 90

Figure 6-4: Myelin density in white matter regions of the developing *Fmr1* KO and WT mice 94

Figure 7-1: Mean diffusivity in white and gray matter regions of *Fmr1* KO and WT mice . 119

Figure 7-2: Axial diffusivity in white and gray matter regions of *Fmr1* KO and WT mice . 122

Figure 7-3: Radial diffusivity in white and gray matter regions of *Fmr1* KO and WT mice 125

Figure 7-4: Fractional anisotropy in white and gray matter regions of *Fmr1* KO and WT mice 128

Figure 7-5: Mean kurtosis in white and gray matter regions of *Fmr1* KO and WT mice 134

Figure 7-6: Axial kurtosis in white and gray matter regions of *Fmr1* KO and WT mice 137

Figure 7-7: Radial kurtosis in white and gray matter regions of *Fmr1* KO and WT mice ... 139

Figure 8-1: Flowchart of pre-processing procedures with the rs-fMRI images 158

Figure 8-2: The mouse brain atlas 160

Figure 8-3: Difference in functional connectivity between PND 30 and PND 60 in the somatomotor network in *Fmr1* KO and WT mice.....163

Figure 8-4: Difference in functional connectivity between *Fmr1* KO and WT mice at PND 30 and PND 60 in the somatomotor network.....164

Figure 8-5: Difference in functional connectivity between PND 30 and PND 60 in the auditory and visual networks in *Fmr1* KO and WT mice.....167

Figure 8-6: Difference in functional connectivity between *Fmr1* KO and WT mice at PND 30 and PND 60 in the auditory and visual networks 168

Figure 8-7: Difference in functional connectivity between PND 30 and PND 60 in the default mode network in *Fmr1* KO and WT mice.....170

Figure 8-8: Difference in functional connectivity between *Fmr1* KO and WT mice at PND 30 and PND 60 in the default mode network.....172

Figure 9-1: Current pharmacological interventions for FXS and their intended targets 184

Figure 9-2: Possible metformin signaling pathways in FXS 190

Figure 9-3: The effect of metformin treatment on functional connectivity of the somatomotor network in the brains of *Fmr1* KO and WT mice.....196

Figure 9-4: The effect of metformin treatment on functional connectivity matrix of the auditory and visual networks in the brains of *Fmr1* KO and WT mice.....198

Figure 9-5: The effect of metformin treatment on functional connectivity matrix of the default mode network in the brains of *Fmr1* KO and WT mice.....200

Figure 9-6: The effect of short-term metformin treatment on MTR in white matter regions of *Fmr1* KO and WT mice.....202

Figure 10-1: Summary of findings in the developing *Fmr1* KO mouse brain compared to the WT mouse brain at PND 18, 21, 30 and 60 209

List of Abbreviations

^{1}H magnetic resonance spectroscopy (MRS)	Mammalian target of rapamycin (mTOR)
2',3'-Cyclic-nucleotide 3'-phosphodiesterase (CNP)	Motor cortex (M)
Aberrant Behavior Checklist-Community (ABC-C)	*Myo*-inositol (Ins)
α-amino-3-hydroxy-5-methyl-4-isoxazolepropionic acid (AMPA)	N-acetyl-aspartate (NAA)
Analysis of variance (ANOVA)	N-acetyl aspartyl glutamate (NAAG)
Auditory cortex (Aud)	N-methyl-D-aspartate (NMDA)
Autism syndrome disorders (ASD)	Parietal cortex (Par)
Blood oxygen level dependent (BOLD)	Phosphatidyl-inositol 3-kinase (PI3K)
Caudate putamen (CPu)	Phosphocholine (PCh)
Choline (Cho)	Phosphatidyl-inositol (PI)
Cingulate cortex (Cg)	Point-resolved spectroscopy (PRESS)
CRLB (Cramer-Rao lower bound)	Postnatal day (PND)
Diffusion kurtosis imaging (DKI)	Rapid acquisition with relaxation enhancement (RARE)
Diffusion tensor imaging (DTI)	Region of interest (ROI)
Fractional anisotropy (FA)	Repeated measures analysis of variance (RMANOVA)
Fragile X Mental Retardation protein (FMRP)	Resting state functional magnetic resonance imaging (rs-fMRI)
Fragile x syndrome (FXS)	Somatosensory cortex (S)
Frontal association cortex (Fra)	Thalamus (Thal)
Frontal orbital cortex (Orb)	Total creatine (tCr)
Functional MRI (fMRI)	Visual cortex (V)
γ-aminobutyric acid (GABA)	Wild-type (WT)
Glutamine (Gln)	
Glutamate (Glu)	
Glycerophosphocholine (GPC)	
Granular cortex (Gran)	
Insular cortex (Ins)	
Long term depression (LTD)	
Long term potentiation (LTP)	
Magnetic resonance imaging (MRI)	
Metabotropic glutamate receptor 5 (mGluR5)	

CHAPTER 1: INTRODUCTION TO FRAGILE X SYNDROME

1.1. FRAGILE X SYNDROME

Fragile X syndrome (FXS) occurs 1 in 5000 males and is the most common genetic cause of intellectual disability and single gene contributor to autistic spectrum disorder (Coffee et al., 2009; Kidd et al., 2014). FXS is caused the epigenetic methylation and consequent silencing of the *FMR1* gene (Verkerk et al., 1991; Wang et al., 2012) following the mutational insertion of more than 200 CGG repeats in the untranslated promoter region of the gene. In the unaffected population, the *FMR1* gene has up to 40 CGG repeats in the untranslated promoter region. Carriers of FXS have between 50 and 200 CGG repeats on the *FMR1* gene and can pass the *FMR1* gene with expanded CGG repeats to the offspring, which puts the offspring at high risk for FXS (Xu et al., 2012; Yrigollen et al., 2014). The silencing of the *FMR1* gene can be partial or complete, leading to mild to severe behavioral and cognitive outcomes, respectively (Bailey et al. 2009; Garber et al. 2008; Kidd et al., 2014). Male FXS patients have an average IQ of 40 and are likely to have severe cognitive and behavioral deficits (Bailey et al., 2009; Garber et al., 2008; Kidd et al., 2014). Female FXS patients can range from having nearly normal to severe deficits in behavior and cognition (Bailey et al., 2009; Freund et al., 1993; Garber et al., 2008). Children with FXS are usually diagnosed between 3 to 4 years old (Bailey et al., 2009). Behavioral issues in FXS include hyperactivity, hypersensitivity to tactile and auditory stimuli, impulsivity, social and attention problems, anxiety, and autistic-like behavior (Bailey et al., 2009; Garber et al., 2008; Hall et al., 2009; Rotschafer & Razak, 2013). The FXS population also has higher incidences of seizures

and sleep problems compared to the normal population (Kidd et al., 2014). The cognitive and behavioral problems in FXS are often severe enough that FXS patients may not be able to perform basic tasks and require full-time care (Vekeman et al., 2015). Caretakers are often family members, many of whom have reported changes in lifestyle and increasing financial hardships when caring for FXS patients (Vekeman et al., 2015).

The *FMR1* gene on the X chromosome codes for the fragile X mental retardation protein (FMRP) (Verheij et al., 1993; Verkerk et al., 1991). FMRP is a RNA binding protein that binds to 4% of total brain mRNA (Ashley et al., 1993), including mRNAs of over one hundred pre- and post-synaptic proteins as well as myelin proteins (Darnell et al., 2011). FMRP is thought to have two key roles in the brain, repressing mRNA translation and the transport of mRNA to dendritic spines (Darnell et al., 2009; Darnell et al., 2011; Dictenberg et al., 2008; Kao et al., 2010). FMRP binds to mRNA directly or to the ribosome at the elongation step of translation (Darnell et al., 2009; Darnell et al., 2011). FMRP may also be involved in the transport of mRNAs to the dendritic spines by binding with kinesin light chains (Dictenberg et al., 2008; Kao et al., 2010). Therefore, FMRP plays important regulatory roles in the brain, and the lack of FMRP leads to intellectual disability and abnormal behavior. The molecular changes resulting from the lack of FMRP are often studied using animal models.

1.2. Animal models of FXS

1.2.1. *Fmr1* KO mouse model of FXS

The *Fmr1* knockout (KO) mouse is the most commonly used model to study the consequences of *Fmr1* gene silencing (Bakker et al., 1994) and current understanding of

the molecular changes associated with *FMR1* gene silencing and identification of potential therapeutic interventions have come from studying the *Fmr1* KO mouse (Hagerman et al., 2012; Kazdoba et al., 2014; T. Wang et al., 2012). The mouse model of FXS recapitulates many of the cognitive and behavioral features of FXS (Kazdoba et al., 2014). The *Fmr1* KO mice compared to the wild-type (WT) mice show hyperactive behavior with increasing total distance moved in open field maze (Dansie et al., 2013; Qin et al., 2015; Yan et al., 2005), stereotypy and repetitive behavior from increase in marble burying behavior (Dansie et al., 2013), reduced sociability by spending less time investigating a novel stranger mouse (Gantois et al., 2017; Qin et al., 2015), and reduced capability during reversal learning in Morris water maze (Baker et al., 2010; Bakker et al., 1994). The two background strains of *Fmr1* KO mice, FVB and C57Bl6J mice, share common phenotypic traits including increased density of immature dendritic spines (Grossman, et al., 2006; Nimchinsky et al., 2001) and increased rates of protein synthesis (Qin et al., 2005; Qin et al., 2015). Animal models of FXS have also revealed major disruptions in brain function including increased metabotropic glutamate receptor 5 (mGluR5)-dependentlong-term depression (LTD) and an imbalance of excitatory to inhibitory neuronal signaling (Huber et al., 2002; Gibson et al., 2008). Morphological alterations in the *Fmr1* KO mouse include increased numbers of immature dendritic spines in the cortex, hippocampus and amygdala (Bilousova et al., 2009; Grossman et al., 2006; Grossman et al., 2010; Nimchinsky et al., 2001; Pan et al., 2010; Qin et al., 2011), and abnormal axon arborization in the somatosensory cortex (Bureau et al., 2008). Several studies have also shown that astrocytes from the *Fmr1* KO mouse brain contribute considerably to neuronal dysfunction (Cheng et al., 2012; Jacobs & Doering,

2010; Jacobs et al., 2012). Astrocytes from *Fmr1* KO mouse brain are co-cultured with neurons from WT mouse brain, the morphology of the WT neuron show increased axonal branching and immature dendritic spine density (Cheng et al., 2012; Jacobs & Doering, 2010; Jacobs et al., 2012). In addition, reduced myelin thickness and decreased concentration of myelin proteins are reported in the developing *Fmr1* KO mouse brain (Pacey et al., 2013). These studies have shown that the *Fmr1* KO mouse model has contributed considerably to the understanding of the neurological and molecular changes in FXS.

1.2.2. *Drosophila* model of FXS

The *dfmr1* gene in *Drosophila* is a homolog of the mammalian *FMR1* gene and its gene product shows similar sequence homology to FMRP (Wan et al., 2000). The *Drosophila dfmr1* gene product also binds to mRNA and the *dfmr1* protein is most abundant during embryonic development (Wan et al., 2000). The *Drosophila* model of FXS (*dfmr1* null) displays morphological alterations in the brain including larger synaptic boutons with an elevated number of vesicles that suggest altered synaptic function and synaptogenesis (Pan et al., 2004). Increased axonal branching and longer axon length are found in the *dfmr1* null fly compared to the WT fly (Pan et al., 2004; Pan et al., 2008). *Dfmr1* null flies show altered circadian rhythm (McBride et al., 2012; Monyak et al., 2016) perhaps providing some insight into sleep troubles experienced by FXS patients (Kronk et al., 2009; Kronk et al., 2010). Similar to the human condition, social interaction and memory deficits are observed in the male *dfmr1* null fly (Monyak et al., 2016; Tessier & Broadie, 2012). The *Drosophila* model of FXS has contributed novel insights

into the morphological and behavioral changes as well as possible treatment options for FXS, including lithium and metformin (Choi et al., 2010; McBride et al., 2005; McBride et al., 2012; Monyak et al., 2016).

1.2.3. *Fmr1* KO rat model of FXS

Recently the *Fmr1* KO rat model of FXS has been developed to provide additional insights into cognitive processes, social behaviors, and to query developmental process through *in vivo* imaging (Hamilton et al., 2014; Kenkel et al., 2016; Till et al., 2015). The juvenile *Fmr1* KO rats at postnatal day 25-45 (PND 25-40) show reduced play behavior and increased repetitive behavior compared to WT rat (Hamilton et al., 2014). However, the absence of FMRP in *Fmr1* KO rats can result in behavioral differences compared to the *Fmr1* KO mice. In juvenile *Fmr1* KO rats, tests of anxiety showed no differences compared to WT rats (Hamilton et al., 2014). In contrast, anxiety levels in developing FVB *Fmr1* KO mice has increased (3 weeks old) (Bilousova et al., 2009) and anxiety has decreased in the adult FVB *Fmr1* KO mice (PND 95-97) (Qin et al., 2011). In addition, spatial learning and reversal learning in Morris water maze in adult *Fmr1* KO rat are not different compared to WT rat (3-6 months old) (Till et al., 2015). However, adult *Fmr1* KO mice have shown deficits with reversal learning in Morris water maze (10-13 weeks old) (Bakker et al., 1994). Hippocampal deficits have been demonstrated in adult *Fmr1* KO rat, including increased mGluR5-dependent LTD, protein synthesis and immature dendritic spine density (Till et al., 2015), similar to findings in the *Fmr1* KO mice (Bilousova et al., 2009; Huber et al., 2002; Qin et al., 2005).

The *Fmr1* KO rat has been used to study brain function by training rats to remain still during functional magnetic resonance imaging without the use of anesthesia (Kenkel et al., 2016). In response to a trained reward odor, WT rats have shown increased brain activity in brain regions associated with reward, whereas *Fmr1* KO rats did not show this increase (Kenkel et al., 2016). Also, *Fmr1* KO rats show no preference in odor discriminating task for the trained reward odor, suggesting an alteration in the learned reward pathway (Kenkel et al., 2016). *Fmr1* KO rats are recently introduced, and this model has already shown novel uses in the study of social behavior and *in vivo* imaging (Hamilton et al., 2014; Kenkel et al., 2016; Till et al., 2015).

1.3. NEURONAL PHENOTYPE IN THE *FMR1* KO MOUSE

1.3.1. Altered long-term depression in the *Fmr1* KO mouse

Synaptic plasticity in the brain is dependent on long-term depression (LTD) which can lead to weakening and elimination of synapses and long-term potentiation (LTP) which can lead to strengthening of synapses (Bear, 1998). LTD and LTP are the electrophysiological basis of learning and memory (Bear, 1998). LTP and LTD depend on depolarization from ionotropic and metabotropic receptors at the synapse, and FMRP modulates group 1 metabotropic glutamate receptor 5 (mGluR5)-dependent LTD specifically (Bassell & Warren, 2008; Bear et al., 2004; Weiler et al., 1997; Weiler & Greenough, 1999). To better understand the role of FMRP at the synapse and how the absence of FMRP contributes to FXS, the mGluR theory of FXS has been proposed based on the following findings (Figure 1-1, adapted from Dolen and Bear 2008 (Dolen & Bear, 2008)) (M. F. Bear et al., 2004):

1) Group 1 mGluR activation leads to the synthesis of FMRP normally (Weiler et al., 1997).

2) Normal mGluR dependent LTD is proteins synthesis dependent (Oliet et al., 1997; Weiler & Greenough, 1993).

3) FMRP may act to repress mRNA translation at the synapse (Bassell & Warren, 2008; Weiler et al., 1997; Weiler & Greenough, 1999).

4) mGluR-dependent LTD is exaggerated in the absence of FMRP (Huber et al., 2002).

5) In the absence of FMRP, mGluR-dependent LTD is no longer protein synthesis dependent (Nosyreva & Huber, 2006).

Activation of group 1 mGluR normally leads to protein synthesis and FMRP can regulate protein synthesis during translation (Figure 1-1a). However, in the *Fmr1* KO mouse, mGluR activation can lead to elevated protein synthesis due to the lack of FMRP regulation on translation of mRNAs (Figure 1-1b). It has been suggested that the exaggerated mGluR-dependent LTD can lead to neurological and behavioral issues in FXS (Bear et al., 2004).

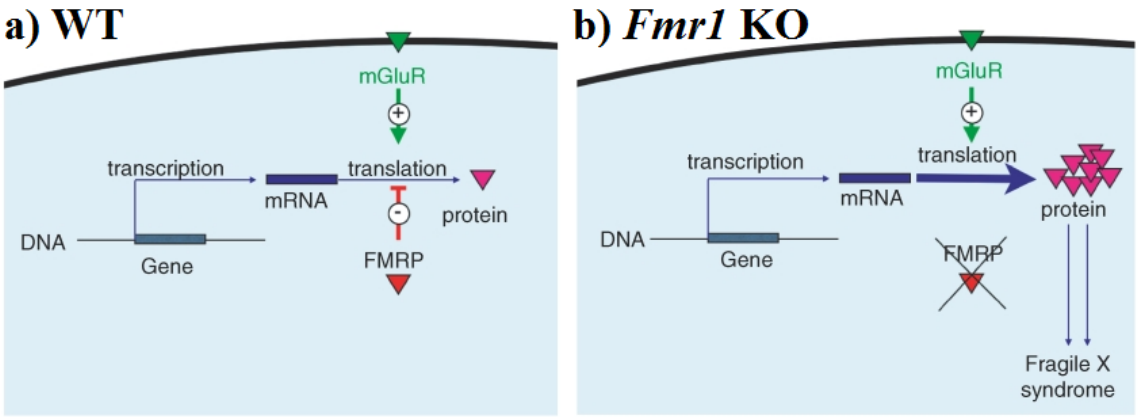

Figure 1-1: The role of group 1 mGluR activation and FMRP in the a) WT and b) consequences from the lack of FMRP in *Fmr1* KO mice. The figure was adapted from Dolen and Bear 2008 (Dolen & Bear, 2008).

The juvenile *Fmr1* KO mouse brain show increased mGluR5-dependent LTD in the hippocampus (PND 25-30) and cerebellum (PND 21-49) (Huber et al., 2002; Koekkoek et al., 2005). However, the ionotropic glutamate receptor N-methyl-D-aspartate (NMDA) receptor-dependent LTD is normal in hippocampus of juvenile *Fmr1* KO mice (PND 25-30) and does not contribute to the exaggerated LTD (Huber et al., 2002). These studies show specifically that mGluR5-dependent LTD is dysregulated in the absence of FMRP and may contribute to neuronal dysfunction in *Fmr1* KO mouse (Huber et al., 2002; Koekkoek et al., 2005). Furthermore, LTP is normal in hippocampus of adult *Fmr1* KO mice compared to WT (Godfraind et al., 1996; Li et al., 2002; Paradee et al., 1999). It should be noted that the mGluR5 mRNA levels are not different between *Fmr1* KO and WT mice, although reduction of mGluR5 protein has been reported in the synaptic membrane extracted from the whole brain of *Fmr1* KO mice at PND 21 (Giuffrida et al., 2005). In the post-mortem human FXS brain, increased mGluR5 proteins are found in prefrontal cortex and show increased mGluR5 receptor binding in a competitive binding assay using a selective mGluR5 antagonist, [^{3}H]-labeled 3-methoxy-5-pyridin-2-ylethynylpyridine (Lohith et al., 2013). Therefore, the alteration of synaptic plasticity in the *Fmr1* KO mice can be attributed to the increase of mGluR5-dependent LTD and lead to elevated downstream activity following mGluR5 activation (Giuffrida et al., 2005; Pfeiffer & Huber, 2009).

Genetic reduction of mGluR5, from mating mGluR5 knockdown mice to *Fmr1* KO mice, reduces mGluR5-dependent LTD, normalizes the immature dendritic spine density and protein synthesis in hippocampus of *Fmr1* KO mice compared to WT (Dolen et al., 2007). The finding of increased mGluR5-dependent LTD has led to the proposal

that mGluR5 antagonists may be used therapeutically to treat FXS (Bear et al., 2004; Dolen & Bear, 2009). Many types of mGluR5 antagonists have been tested in adult *Fmr1* KO mouse model and resulted in the normalization of behavior and immature dendritic spine levels (Levenga et al., 2011; Thomas et al., 2012; Yan et al., 2005).

1.3.2. Downstream effects of mGluR5-dependent long-term depression in *Fmr1* KO mice

In the normal post-synaptic terminal, mGluR5 activation leads to the dissociation with the scaffolding protein Homer (Ronesi & Huber, 2008). Homer then binds to the phosphatidylinositol 3-kinase (PI3K)-enhancer protein (PIKE) leading to the downstream activation of protein kinase B (AKT) and the PI3K-mammalian target of rapamycin (mTOR) complex (Hou & Klann, 2004; Ronesi & Huber, 2008) (Figure 1-2a, modified from (Huber et al., 2015)). The activation of the mTOR complex leads to phosphorylation of the 4E-binding protein and dissociation with the eukaryotic initiation factor 4E (eIF4E). The eIF4E binds to eIF4G and eIF4A to form the eukaryotic initiation factor 4 complex (eIF4F), leading to cap-dependent translation initiation of mRNA (Figure 1-2a) (Hou & Klann, 2004; Ronesi & Huber, 2008; Sharma et al., 2010). One of the proteins synthesized is FMRP (Weiler et al., 1997), which can act to repress translation by binding to the mRNA or the ribosome (Darnell et al., 2011). In addition to promoting translation, the activation of the mTOR pathway can result in cellular growth and proliferation in the brain (Huber et al., 2015).

In the hippocampus of developing *Fmr1* KO mouse (PND 19-55), mGluR5 association with the long isoform of Homer protein is decreased and association to the

short isoform of Homer (H1a) is increased (Ronesi et al., 2012). Genetic deletion of the short isoform in *Fmr1* and *H1a* double KO mice is able to rescue mGluR association with the long isoform of Homer and normalize the elevated PI3K and mTOR signaling, but not the exaggerated mGluR-dependent LTD (Ronesi et al., 2012). The hippocampus of juvenile and adult *Fmr1* KO mice show elevated activity with PIKE, AKT, mTOR, and eIF4F leading to increased translation of mRNA (Figure 1-2b, modified from (Huber et al., 2015)) (Liu et al., 2012; Ronesi et al., 2012; Sharma et al., 2010). The mitogen-activated protein kinase kinase (MEK) and extracellular signal-regulated kinase (ERK) activities are normal in hippocampus of developing (PND 19-55) and adult (12 weeks old) *Fmr1* KO mice (Figure 1-2b) (Liu et al., 2012; Ronesi et al., 2012). However, one recent study has shown increased MEK/ERK activity in hippocampus of *Fmr1* KO mouse (8-12 weeks old) (Gantois et al., 2017), suggesting that alterations in MEK/ERK signaling may be age dependent. At least one study demonstrated that rapamycin, a mTOR inhibitor, was ineffective at normalizing elevated mGluR5-dependent LTD in hippocampus of *Fmr1* KO mouse (Sharma et al., 2010). The inability of the mTOR inhibitor to normalize LTD may be due to the presence of accumulated proteins required for mGluR5 dependent LTD in hippocampus of *Fmr1* KO mice (Huber et al., 2015).

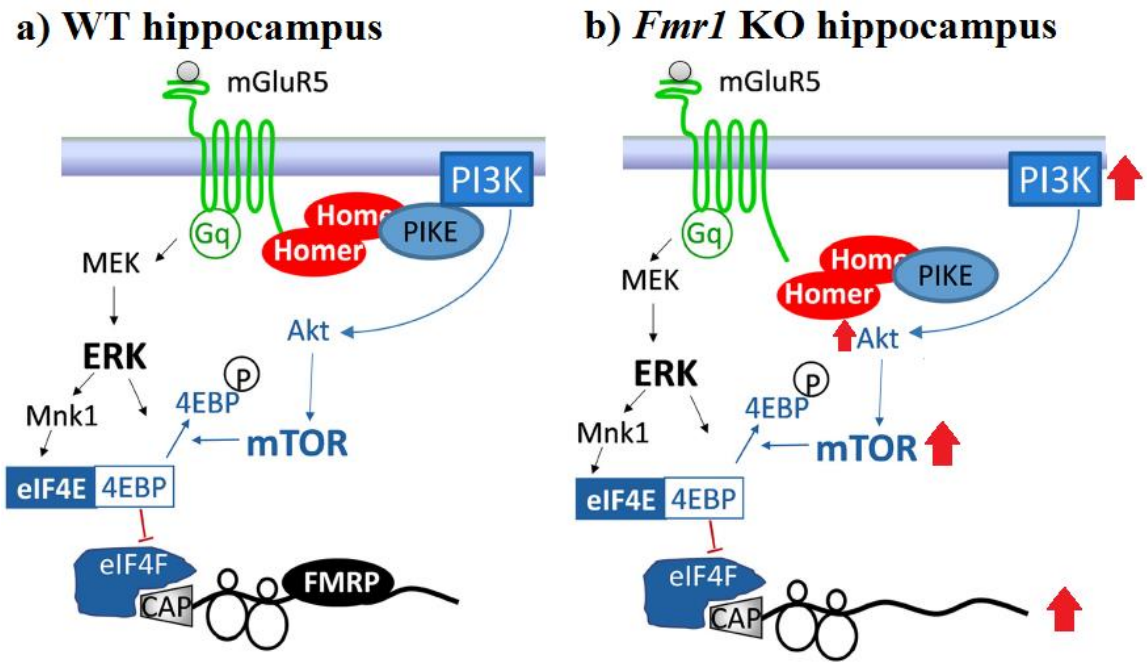

Figure 1-2: Downstream signaling of mGluR5 activation in the neurons of the hippocampus in a) WT mice and b) *Fmr1* KO mice. a) In the hippocampus of the WT mice, mGluR5 activation causes dissociation with Homer, and binding of Homer to PIKE. PIKE activates PI3K and leads to downstream activation of AKT and mTOR. mTOR phosphorylates 4EBP, allowing the formation of eIF4F and initiation of cap-dependent translation. However, FMRP can stall translation by binding to the mRNA. b) In the hippocampus of the *Fmr1* KO mice, the binding of mGluR5 to Homer is reduced, which can lead to increased activity of PI3K, AKT, and mTOR. Elevated mTOR activity leads to increased formation of the eIF4F and increases in translation in *Fmr1* KO mice. The absence of FMRP further increases translation in the synapse of *Fmr1* KO mice. No differences in the activation of the MEK/ERK pathway have been reported in the hippocampus of the developing *Fmr1* KO mice. This figure was modified from Huber et al. (Huber et al., 2015).

Activation of mGluR5 in neocortex of the WT mice results in downstream activation of MEK, ERK, and MAPK-interacting kinase 1 (Mnk1) pathway, leading to phosphorylation of 4EBP and increase in eIF4F cap-dependent translation initiation of mRNA (Sawicka et al., 2016). In contrast to the signaling deficiencies in the developing hippocampus, increases of MEK, ERK, Mnk1, and eIF4F activity have been reported in the neocortex of immature *Fmr1* KO mouse brain (PND 28-32) (Sawicka et al., 2016). In addition, mTOR levels in the neocortex of immature *Fmr1* KO mice are not altered

compared to the WT (Sawicka et al., 2016). Increased MEK and ERK activity are reported in prefrontal cortex and hippocampus of the adolescent/adult *Fmr1* KO mice (8-12 weeks old) (Gantois et al., 2017). The increase in the activity of MEK/ERK pathway may be due to the decrease of LTP reported in the cortex of the *Fmr1* KO mice (Harlow et al., 2010; Li et al., 2002; Sidorov et al., 2013; Wilson & Cox, 2007). Thus, the alterations in signal transduction in the neocortex of developing *Fmr1* KO mouse may be different compared to findings in the hippocampus.

1.3.3. Altered long-term potentiation in the cortex of the *Fmr1* KO mouse

In *Fmr1* KO mice, abnormal LTP is reported in the cortex (Harlow et al., 2010; Li et al., 2002; Sidorov et al., 2013; Wilson & Cox, 2007), whereas no difference in LTP is reported in the hippocampus of *Fmr1* KO mice (Huber et al., 2002). In visual cortex of developing *Fmr1* KO mice compared to WT (PND 13-25), mGluR5-dependent LTP is reduced, and treatment with the mGluR5 antagonist, 2-methyl-6-(phenylethynyl)pyridine, did not reverse this effect (Wilson & Cox, 2007). Altered LTP is also reported in somatosensory cortex of developing *Fmr1* KO mice compared to WT (PND 3-10) (Harlow et al., 2010). LTP potentiation in WT mice shows that the window of synaptic plasticity in somatosensory cortex is between PND 3 to 7 (similar to a preterm to term infant (Semple et al., 2013)), with the peak LTP potentiation observed at PND 3 and steadily reduced until PND 10 (Harlow et al., 2010). Whereas, the window for *Fmr1* KO mice is between PND 4 to 10, with LTP potentiation low at PND 4 and reaches peak potentiation between PND 6-7 followed by steady decline (Harlow et al., 2010). Time course studies over the course of cortical development indicate a developmental delay in

the window of synaptic plasticity in somatosensory cortex of *Fmr1* KO mouse brain (Harlow et al., 2010).

1.3.4. Excitatory and inhibitory signaling imbalance in the *Fmr1* KO mice

In addition to decreased LTP at synapses in somatosensory cortex (Harlow et al., 2010), an excitatory/inhibitory imbalance is observed in the developing somatosensory cortex of the *Fmr1* KO mice compared to WT (PND 14 and PND 28) (Gibson et al., 2008). A decreased connection frequency between excitatory and inhibitory neurons indicates that inhibitory neurons are less likely to be excited which may result in reduced inhibitory signaling in somatosensory cortex of *Fmr1* KO mice than WT (Gibson et al., 2008). Excitatory neurons show increased membrane excitability and can fire significantly greater numbers of action potentials in the *Fmr1* KO mouse brain (Gibson et al., 2008). Moreover, neural network excitability, measured in the form of synchronous depolarization in a network of neighboring neurons, is increased in developing *Fmr1* KO mice compared to WT (PND 14 and PND 28) (Gibson et al., 2008). These results provide evidence of altered excitability between excitatory and fast-spiking inhibitory neurons on a cellular and network level (Gibson et al., 2008). The hyperexcitability of excitatory neurons in somatosensory cortex may be associated with hypersensitivity to tactile stimuli in *Fmr1* KO mice and FXS patients (Castren et al., 2003; Gibson et al., 2008; Miller et al., 1999; Zhang et al., 2014).

Inhibitory neurotransmission is mediated by γ-aminobutyric acid (GABA) resulting in hyperpolarization of the postsynaptic membrane in adult rodents (Paluszkiewicz et al., 2011). mRNAs of select $GABA_A$ and $GABA_B$ subunits are targets

of FMRP (Darnell et al., 2011). Activation of the metabotropic G-protein coupled $GABA_B$ receptors promotes FMRP expression in neurons from WT mice *in-vitro* (W. Zhang et al., 2015). In adult *Fmr1* KO mouse brain (8-12 weeks old), there are reduced levels of $GABA_A$ receptor subunit mRNAs and proteins in the cortex and hippocampus compared to the WT (D'Hulst et al., 2006; El Idrissi et al., 2005). Treatment with $GABA_A$ agonists, diazepam, and ganaxolone, reduced audiogenic seizures in adult *Fmr1* KO mice (10 weeks) (Heulens et al., 2012). In the cortex and midbrain, the R1a subunit of the $GABA_B$ receptor is decreased in developing *Fmr1* KO mice (5 weeks old), but the mRNA level is unaffected (Kang et al., 2017). In hippocampal slices, inhibitory signaling from $GABA_B$ receptor activation by R-baclofen is normal in *Fmr1* KO mice (Kang et al., 2017). Furthermore, an elevated ratio of excitatory/inhibitory postsynaptic frequency in hippocampal slices in *Fmr1* KO mice is reduced by R-baclofen treatment (Kang et al., 2017), indicating that R-baclofen can normalize the excitatory/inhibitory imbalance in *Fmr1* KO mouse brain (Kang et al., 2017). In addition, acute R-baclofen treatment has led to normalization of social behavior, motor activity, motor learning, protein synthesis, and immature dendritic spine density in *Fmr1* KO mice (Henderson et al., 2012; Kang et al., 2017; Qin et al., 2015). Thus, the imbalance of excitatory/inhibitory signaling and reduced GABA receptor activity may contribute to neuronal dysfunction in *Fmr1* KO mice.

1.3.5. Morphological changes in FXS

1.3.5.1. Elevated levels of immature dendritic spines

One of the hallmark morphological features of FXS pathology in humans is the

increase in the number of thin and flagella-like immature dendritic spines (Figure 1-3a, adapted from Grossman et al. (Grossman et al., 2006)) (Hintonet al., 1991; Rudelli et al., 1985) and the decrease of mature, mushroom-shaped dendritic spines in the cortex of FXS patients (Figure 1-3a) (Irwin et al., 2001). An increase of immature dendritic spines is reported in somatosensory and visual cortices, hippocampus and amygdala of *Fmr1* KO mice (Figure 1-3, from Dolen et al. (Dolen et al., 2007)) (Bilousova et al., 2009; Dolen et al., 2007; Grossman et al., 2006; Grossman et al., 2010; Pan et al., 2010). Dendritic spine elimination and formation are also reported to occur at higher rates in somatosensory cortex in both developing (1 month old) and adult *Fmr1* KO mice (4 months old) compared to the WT mice (Pan et al., 2010). In addition, newly formed spines in developing *Fmr1* KO mouse brain have smaller head diameter compared to new spines in the WT at PND 30 (Pan et al., 2010). Experiments to determine if tactile hypersensitivity is associated with higher rates of dendritic spine elimination and formation in somatosensory cortex indicated no difference between *Fmr1* KO mice that had undergone whisker trimming sensory deprivation for 2 weeks compared to *Fmr1* KO mice without sensory deprivation (Pan et al., 2010). Therefore, the high turnover rate of dendritic spines does not appear to be the result of tactile hypersensitivity in *Fmr1* KO mouse brain and suggests a possible role of FMRP regulation of elimination and formation of dendritic spines (Pan et al., 2010).

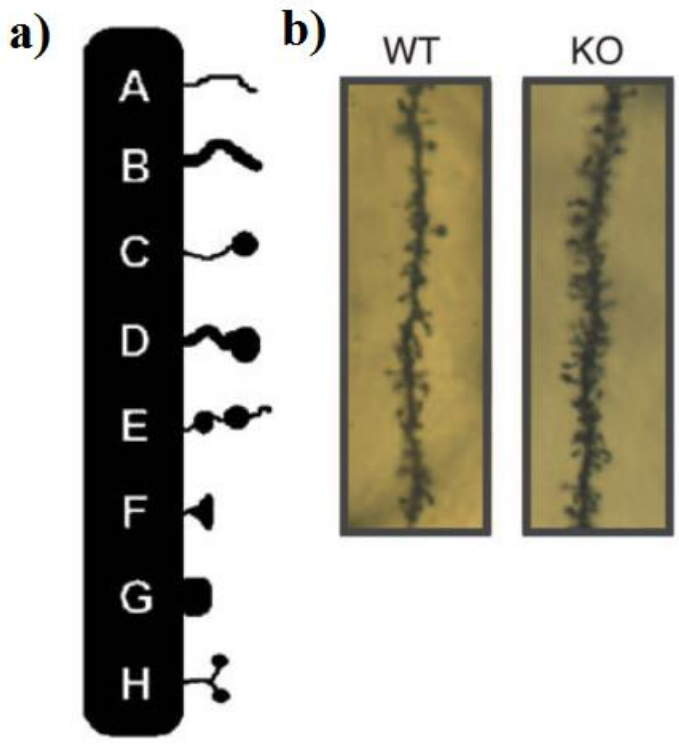

Figure 1-3: Representation of dendritic spine density in *Fmr1* KO and WT mice. a) A cartoon representation of the immature (A, B, C, D, and E) and mature (F, G, and H) dendritic spine morphology in the mouse brain. Figure 1-3a was adapted from Grossman et al. (Grossman et al., 2006). b) Representative images of dendritic spines from WT and *Fmr1* KO mice in the visual cortex with Golgi-Cox staining technique. Figure 1-3b was adapted from Dolen et al. (Dolen et al., 2007).

The molecular changes in *Fmr1* KO mouse brain that are responsible for the increase in immature dendritic spines remain unknown (Bilousova et al., 2009; Grossman et al., 2006). However, it has been suggested that the abnormal dendritic spine morphology in *Fmr1* KO mice may be from altered protein-protein interactions and the dysregulation of local protein synthesis at the dendritic spine resulting from the exaggerated mGluR5-dependent LTD (Grossman et al., 2006). Activation of mGluR5 with the group 1 mGluR agonist (S)-3,5-dihydroxyphenylglycine shows an increase of elongated dendritic spines *in vitro* in WT neurons (Vanderklish & Edelman, 2002). In addition, reducing mGluR5 by genetic reduction or with mGluR5 antagonists results in

reduced levels of immature dendritic spines in the hippocampus of adult *Fmr1* KO mice (Dolen et al., 2007; Levenga et al., 2011; Pop et al., 2014). Treatment with R-baclofen also normalized immature dendritic spine density presumably by normalizing the excitatory/inhibitory imbalance in *Fmr1* KO mouse brain (Henderson et al., 2012).

Increased immature dendritic spine density and decreased mature dendritic spine density are also found in the CA1 region of hippocampus in *Fmr1* KO mice at PND 7, 8, 21 and 60 compared to WT (Bilousova et al., 2009; Sidhu et al., 2014). The developing hippocampus show elevated matrix metalloproteinase 9 (MMP-9) activity and reducing MMP-9 activity with the broad spectrum antibiotic minocycline, normalized the number of immature dendritic spines in *Fmr1* KO mice at PND 7 (Bilousova et al., 2009). Early minocycline treatment also normalized the elevated anxiety levels in *Fmr1* KO mice at PND 21 (Bilousova et al., 2009). Continuous minocycline treatment is administered through the drinking water and is passed from the mother mouse to the pups through the milk (Bilousova et al., 2009). Genetic reduction of the elevated MMP-9 activity has normalized the densities of mature and immature dendritic spines in the hippocampus of the double *Fmr1* and MMP-9 KO mice compared to the WT (PND 8, 14, 21 and 60) (Sidhu et al., 2014). In the hippocampus of double KO *Fmr1* and MMP-9 mice, mGluR5-dependent LTD as well as AKT, mTOR, and eIF4F activities are normalized compared to the WT (Sidhu et al., 2014). It is thought that the elevated MMP-9 activity may contribute to the immature dendritic spine morphology by excessive cleavage of the extracellular matrix proteins in the hippocampus of *Fmr1* KO mice (Bilousova et al., 2009; Sidhu et al., 2014). Thus, the correction of altered molecular changes in the *Fmr1* KO mouse brain, including mGluR5 dependent LTD, imbalance of excitatory and

inhibitory signaling, or from excessive cleavage of the extracellular matrix by MMP-9, can normalize immature dendritic spine density (Bilousova et al., 2009; Grossman et al., 2006; Henderson et al., 2012; Sidhu et al., 2014).

1.3.5.2. Alterations in axon formation

In cultured WT neurons, FMRP is observed in axonal growth cones and throughout the axon shaft (Antar et al., 2006). In cultured *Fmr1* KO neurons, axon growth cones display excess filopodia and reduced axon motility, which may reduce the number of connections to dendritic spines and contribute to increased immature dendritic spines (Antar et al., 2006). Axonal architecture is also compromised in the brain of *Drosophila* model of FXS, with increased axonal branching and longer axonal branches that can protrude into other brain regions compared to the control flies (Pan et al., 2004). Overexpression of the *Drosophila fmr1* gene reduces axonal branching and outgrowth, suggesting a role for FMRP in the regulation of axon formation (Pan et al., 2004).

Diffuse axon arbors, displaying shorter and more disperse axons, have been demonstrated in neurons connecting layer 4 to layer 2/3 in somatosensory cortex of developing *Fmr1* KO mice compared to WT (PND 13-15) (Bureau et al., 2008), suggesting that FMRP may be involved in axon guidance and/or pruning (Bureau et al., 2008). However, the amplitude of the action potentials along diffuse axons in *Fmr1* KO mice are not significantly different from the axons in WT brain, indicating excitatory signaling from layer 4 to layer 3 of somatosensory cortex is not affected (Bureau et al., 2008). No differences in axon distribution or altered signaling have been observed from layer 5 to layer 3 of the somatosensory cortex in developing *Fmr1* KO and WT mice,

demonstrating the abnormal axon morphology may not necessarily affect all axons in *Fmr1* KO mouse brain (Bureau et al., 2008). The diffuse axon morphology in somatosensory cortex of *Fmr1* KO mice (PND 13-15) is no long different at an older age (PND 20-22) compared to WT mice (Bureau et al., 2008) suggesting a developmental delay in axon growth. There are also non-neuronal influences contributing to axon morphology, including the influence of *Fmr1* KO astrocytes in causing increased axonal branching and reductions in mature dendritic spines in WT neurons (Jacobs & Doering, 2010).

1.4. Alteration of glia in the *Fmr1* KO brain

1.4.1. Astrocytes

Astrocytes outnumber neurons 3 to 1 in the rodent brain and 1.4 to 1 in the human brain and astrocytes are critical to the health and function of the brain (Nedergaard, Ransom, & Goldman, 2003). Astrocytes control the pH and ion concentrations of the extracellular milieu, take up the neurotransmitter glutamate released into the synaptic cleft to maintain lower resting concentration of glutamate needed for neurotransmission, and convert glutamate into glutamine to avoid excitotoxicity (M. C. McKenna, 2007). FMRP is present in astrocytes in both the developing and mature mouse brain (Gholizadeh et al., 2015). Normally astrocytic FMRP regulates the level of the glutamate transporter GLT1 which is critical in maintaining glutamate homeostasis (Higashimori et al., 2013).

Recent studies in the *Fmr1* KO mouse have revealed glial dysfunction as a contributing factor to pathological features of FXS (Higashimori et al., 2013; Jacobs &

Doering, 2010; Jacobs et al., 2012). In the *Fmr1* KO mouse, the glutamate transporter GLT1 mRNA and protein levels, along with glutamate uptake are reduced at PND 4 and PND 40 compared to WT (Higashimori et al., 2013). Thus, reduced uptake of glutamate by astrocytes may contribute to the enhanced neuronal excitability observed in *Fmr1* KO mouse brain (Higashimori et al., 2013).

In a co-culture experiment, astrocytes from *Fmr1* KO mouse brain influenced neurons from WT brain to display characteristics of *Fmr1* KO neurons, including increased axonal branching and reduction of mature dendritic spine density (Jacobs & Doering, 2010). The study by Jacobs et al. (Jacobs & Doering, 2010) suggests that astrocytes from *Fmr1* KO brain can have a considerable influence on the morphology of neurons (Jacobs & Doering, 2010). Another study has shown elevated levels of neurotrophin-3 in the growth media of *Fmr1* KO astrocytes and WT neurons that are cultured with conditioned medium also displayed increased immature dendritic spines density (Yang et al., 2012). However, injection of *Fmr1* KO astrocytes transfected with neurotropin-3 short hairpin RNA to reduce neurotrophin-3 levels into the prefrontal cortex of the adult *Fmr1* KO mice did not normalize fear conditioning, whereas injection of WT astrocytes normalized fear conditioning (Yang et al., 2012). The study by Yang et al. (Yang et al., 2012) suggests that astrocytes can have considerable influence on neurological deficits in *Fmr1* KO mouse brain and that a limited rescue of FMRP from WT neurons can normalize behavior in *Fmr1* KO mice (Yang et al., 2012). Given the close anatomical proximity and the dynamic metabolic relationship between neurons and astrocytes in the brain, it is not surprising that astrocytes in *Fmr1* KO mouse brain can

contribute to the neuronal phenotype of FXS (Jacobs & Doering, 2010; Yang et al., 2012).

1.4.2. Oligodendrocytes

Mature oligodendrocytes are essential in forming myelin sheaths that insulate and protect axons. Myelination in the rodent brain is a postnatal event; peaking between PND 20-21, and continuing into adulthood (Andersen, 2003; Semple et al., 2013) and declining around 18 months (Xie et al., 2013). FMRP concentration is high in normal oligodendrocyte precursor cells in corpus callosum and FMRP levels in oligodendrocyte precursor cells decrease following maturation into oligodendrocytes (Gholizadeh et al., 2015; Wang et al., 2004). A low level of FMRP in oligodendrocytes does not eliminate its importance in FXS but rather indicates that the decrease in FMRP from birth to adulthood may be intricately tied to the normal developmental process (Gholizadeh et al., 2015).

The exact role of FMRP in oligodendrocytes remains unknown, but FMRP binds to the mRNA and may repress translation of myelin proteins (Darnell et al. 2011). The FMRP polyribosomal complex binds to the mRNA of many essential myelin proteins including myelin basic protein, 2',3'-Cyclic-nucleotide 3'-phosphodiesterase (CNP), myelin-associated glycoprotein, and proteolipid protein (Darnell et al., 2011; Wang et al., 2004). Myelin basic protein is a key and abundant myelin protein necessary for compacting myelin sheaths (Harauz et al., 2009). CNP binds to and organizes microtubules and may contribute to the structural integrity of myelin (Bifulco, Laezza, Stingo, & Wolff, 2002). Normally, both myelin basic protein and CNP protein levels are

found only in maturing oligodendrocytes and are commonly used as indicators for mature oligodendrocytes (Harauz et al., 2009; Hinman et al., 2008). In the cerebellar white matter of developing *Fmr1* KO mice, reduced myelin thickness at PND 7 and concentrations of myelin basic protein and CNP are found at PND 7 and PND 15 compared to WT mice (Pacey et al., 2013). The reduction in myelin thickness and myelin protein levels are similar at PND 30 between *Fmr1* KO and WT mice (Pacey et al., 2013), and myelin basic protein levels are elevated in cerebellar white matter of adult *Fmr1* KO mice (2-4 months) (Pacey et al., 2013). The authors suggest that their results demonstrate delayed myelination during early postnatal brain development in the cerebellum of *Fmr1* KO mice (Pacey et al., 2013).

1.5. THE IMPORTANCE OF STUDYING THE DEVELOPING *FMR1* KO MOUSE BRAIN

As previously mentioned, the developing *Fmr1* KO mouse show alteration in synaptic plasticity, dendritic spine morphology, axon growth and myelination that may have detrimental effects on brain maturation (Bilousova et al., 2009; Gibson et al., 2008; Huber et al., 2002; Pacey et al., 2013; Shi et al., 2012; Wilson & Cox, 2007). In addition, FMRP has been shown to influence cortical migration patterns in normally developing mouse embryo by affecting multipolar to bipolar transition in neurons (La Fata et al., 2014). Whereas, change in migration patterns in embryonic *Fmr1* KO mouse brain can result in abnormal development of the functional network and alter excitatory and inhibitory networks in cortex (La Fata et al., 2014). Reintroduction of FMRP to *Fmr1* KO mouse embryos rescued neuronal migration patterns, demonstrating the critical role of FMRP in normal brain development (La Fata et al., 2014).

Recently, increasing number of studies has incorporated translational imaging techniques to study FXS patients and rodent models of FXS (D'Hulst et al., 2015; Gothelf et al., 2008; Haas et al., 2009; Haberl et al., 2015; Hall et al., 2013; Hall et al., 2016; Hazlett et al., 2012; Hoeft et al., 2010; Lai et al., 2016; Qin et al., 2013). These imaging methods can offer additional insight to developmental changes in the brains of FXS patients and *Fmr1* KO mice on metabolism, morphology, and function. However, further studies in the developing brain at different time points are needed to determine developmental alterations between *Fmr1* KO and WT mice.

CHAPTER 2: IMAGING THE FXS BRAIN

2.1. INTRODUCTION TO BRAIN IMAGING STUDIES IN FXS AND THE *FMR1* KO MOUSE

In vivo brain imaging methods have recently been used to study alterations in metabolism, morphology, and function in FXS patients. The benefit of the imaging methods lies in their ability to non-invasively image human brains *in vivo* and determine differences between FXS patients and both age-matched and IQ-matched controls. In addition, brain imaging studies have also been performed in *Fmr1* KO mouse to determine whether the animal model show similarities to the alterations in brain metabolism, morphology, and function found in FXS patients (Ellegood et al., 2010; Haberl et al., 2015; Shi et al., 2012).

2.1.1. Metabolic imaging in FXS AND THE *FMR1* KO MOUSE

2.1.1.1. Metabolism and tracer labeling using positron emission tomography

Metabolic imaging studies in the mouse using autoradiography showed the cerebral metabolism rate of glucose and the rate of protein synthesis were increased in the brains of *in vivo Fmr1* KO mice compared to WT (Qin et al., 2002; Qin et al., 2005). Glucose metabolism was studied by infusion of [^{14}C]deoxyglucose into awake and behaving *Fmr1* KO and WT mice for 45 minutes and then sacrificed to measure the cerebral metabolism rate of glucose in the autoradiogram (Qin et al., 2002). Increased rates of glucose metabolism were reported in the hippocampus, prefrontal, auditory, motor, and visual cortices, and the thalamus of adult *Fmr1* KO mice compared to WT (4-5 months old) (Qin et al., 2002). Similarly, the rate of cerebral protein synthesis was

measured using autoradiography after the incorporation of the radiolabeled tracer L-[1-^{14}C]leucine for 60 minutes in the awake and behaving adult *Fmr1* KO and WT mice (4 and 6 months old) (Qin et al., 2005). A regional selective increase of protein synthesis was observed in the hippocampus, frontal association and posterior parietal cortices and the thalamus of the adult *Fmr1* KO mice at both ages (Qin et al., 2005). Thus, the studies by Qin et al. (Qin et al., 2002; Qin et al., 2005) demonstrate increased metabolism of glucose and protein synthesis in the *Fmr1* KO mouse brain and have led to recent studies of protein synthesis and ligand binding in human patients with FXS (D'Hulst et al., 2015; Qin et al., 2013).

Human studies in young adults with FXS used a PET-based method for measuring rates of cerebral protein synthesis with radiolabeled tracer L-[1-^{14}C]leucine, indicated that rates were *decreased* rather than increased (Qin et al., 2013). It was not clear whether the opposite finding in patients was due to the use of propofol anesthesia, which would greatly suppress overall brain metabolism, or there was a difference between the disease in humans and the mouse model. Further studies in mice revealed that propofol reduced brain protein synthesis in *Fmr1* KO mice but not in the WT mice, indicating that the sedating agent can have selective effects on brain protein synthesis in the absence of FMRP (Qin et al., 2013). A reduction in $GABA_A$ receptor binding to [^{11}C] flumazenil, a high-affinity ligand for $GABA_A$ receptor, was found in parietal and cingulate cortices as well as in the thalamus of adult FXS patients compared to normal controls (D'Hulst et al., 2015). The reduction in $GABA_A$ receptors in FXS patients was supported by previous findings of reduced $GABA_A$ receptor subunit mRNAs and proteins in the cortex of adult *Fmr1* KO mice (D'Hulst et al., 2006; El Idrissi et al., 2005). Metabolic imaging in the

Fmr1 KO mice has revealed widespread alterations in glucose metabolism and protein synthesis in the brain (Qin et al., 2002; Qin et al., 2005) and similar approaches have been performed in FXS patients (Qin et al., 2013).

2.1.1.2. Brain metabolite levels from ^{1}H magnetic resonance spectroscopy

^{1}H magnetic resonance spectroscopy (MRS) can determine the concentration of unbound metabolites in specific regions of the brain *in vivo* and can indicate differences in neurotransmitter levels as well as molecules associated with signal transduction (Fan, 1996). Reduced choline levels, which can include phosphocholine, glycerophosphocholine, and phospholipids, was reported in dorsolateral prefrontal cortex of male FXS patients (18 ± 4 years old) compared to normal controls (Kesler et al., 2009), and in the caudate nucleus of young adults with FXS (21 ± 3 years old) compared to IQ-matched controls (Bruno et al., 2013). The findings suggest that reduced choline levels may be specific to FXS and can reflect altered availability of choline for synthesis of acetylcholine and/or choline containing phospholipids which are incorporated into membranes (Bruno et al., 2013; Kesler et al., 2009). A recent finding showed reduced muscarinic acetylcholine receptor expression and reduced acetylcholine levels in the striatum of adult *Fmr1* KO mice, as well as increased acetylcholinesterase, an enzyme that breaks down acetylcholine (Qiu et al., 2016). Thus, specific molecular changes to the muscarinic acetylcholine signaling in *Fmr1* KO mice could also reflect reduced cholinergic signaling, as was suggested in FXS patients (Bruno et al., 2013; Kesler et al., 2009; Qiu et al., 2016). In addition, the glutamate plus glutamine pool was decreased in the caudate nucleus in adolescents and young adults with FXS compared to IQ-matched

controls and could indicate altered metabolism in the glutamate-glutamine cycle and abnormal glutamatergic neurotransmission (Bruno et al., 2013; McKenna et al., 2011). No differences were reported in metabolite levels between the male and female FXS patients (Bruno et al., 2013). Our studies using developing *Fmr1* KO mice compared to WT showed elevated levels of taurine, and reduced *myo*-inositol levels in the hippocampus (Shi et al., 2012). The implications of these findings to the *Fmr1* KO mouse brain are discussed in Chapter 5 (Shi et al., 2012). Taken together these studies show evidence of metabolite alterations that may contribute to the molecular changes in the FXS brain.

2.1.2. Changes in brain volume in children with FXS

It is well documented in both young and adult FXS populations that overall and regional brain volumes differ from those of normal, idiopathic autism (without FXS diagnosis), and developmentally delayed populations (Gothelf et al., 2008; Hazlett et al., 2012; Hoeft et al., 2011). One developmental study of boys (3 years old), reported a general finding that idiopathic autistic boys had increased whole brain volumes compared to normally developing boys; in contrast, decreased whole brain volume were found in boys with FXS compared to the normally developing boys (Hoeft et al., 2011). The results by Hoeft et al. (Hoeft et al., 2011) were also confirmed in another study of FXS, idiopathic autistic and typically developing boys from 2-5 years old (Hazlett et al., 2012).

Regional brain volume in the human FXS brain showed increased and decreased volumes depending on the region and age (Bray et al., 2011; Gothelf et al., 2008; Hazlett et al., 2012; Hoeft et al., 2011; Qin et al., 2013). A study of boys with FXS (2.5 ± 0.6 y)

compared to age-matched normal controls reported increased gray matter volumes in cingulate cortex and caudate nucleus and decreased volumes in the insula, frontal, parietal, and temporal lobes (Hoeft et al., 2011). These boys with FXS also showed increased white matter volume in the medial frontal gyrus, temporal gyrus, and insular cortex, as well as decreased white matter volume in the inferior and superior frontal gyrus, and precentral and postcentral gyrus (Hoeft et al., 2011). In a separate study of boys with FXS between 2-5 years old, Hazlett et al. (Hazlett et al., 2012) reported increased volume of the caudate nucleus and white matter volume in the temporal lobe compared to age-matched normal controls. The boys with FXS also showed a decrease in gray matter volume in frontal, temporal, parietal-occipital lobes, amygdala and hippocampus compared to age-matched normal controls (Hazlett et al., 2012). These two studies show similarities in regional brain volume change in boys with FXS (Hazlett et al., 2012; Hoeft et al., 2011).

The cause of whole brain and regional volume changes in the FXS brain is still unknown, but the correlation of volume change to behavior scores may link volume change to behavioral issues in FXS patients. The increase of the caudate nucleus volume in boys with FXS correlates with poor performance scores in motor functions and repetitive behavior (Hazlett et al., 2012). Reduced amygdala volume in boys with FXS correlated with lower IQ scores and with poor sociability (Hazlett et al., 2012). The volume change in the insular, frontal and orbitofrontal regions suggest altered prefrontal cortex development that may be related to increased anxiety and eye-gaze aversion in boys with FXS (Hoeft et al., 2011). Thus, the changes in brain volume could play a role in altered behavioral and cognitive function in FXS patients (Hazlett et al., 2012; Hoeft et

al., 2011).

2.1.3. Changes in brain volume in adolescents and adults with FXS

In a relatively large study by Gothelf et al. (Gothelf et al., 2008) which included male and female FXS patients that ranged in age from 1-22 years old (mean age of 12 ± 6 years), brain volumes were compared between the FXS patients and age-matched normal controls. Increased volumes in gray matter include the occipital and parietal lobes, dorsal and middle superior cortices, and the caudate nucleus in FXS patients (Gothelf et al., 2008). Increased white matter volume in FXS patients was found in the inferior frontal region of the brain and decreased white matter volume in the superior temporal region (Gothelf et al., 2008). Bray et al. reported (Bray et al., 2011) increased volume of the caudate nucleus and whole brain white matter, normalized to whole brain volume, in both male and female FXS patients (9-22 years old, mean age 16 ± 3) compared to age-matched normal controls. (Gothelf et al., 2008). The caudate nucleus in male FXS patients was larger than that of the female FXS patients (Bray et al., 2011; Gothelf et al., 2008). The male and female FXS patients that showed greater caudate nucleus volume also displayed repetitive behaviors, lower IQ and greater *FMR1* gene silencing (Bray et al., 2011; Gothelf et al., 2008).

Decreased volumes in the amygdala, temporal lobe, and cerebral vermis were found in FXS patients (12 ± 6 years old) compared to normal controls, and lower cerebral vermis volume was found in FXS patients that displayed stereotyping behavior (Gothelf et al., 2008). Similar regional volume alterations were found in boys with FXS suggest that the alterations in cortical and caudate nucleus volumes may be consistent throughout

brain development in FXS (Gothelf et al., 2008; Hazlett et al., 2012; Hoeft et al., 2010). The prefrontal cortex in male, but not female, FXS patients (9-22 years old) showed increased volume and these patients also performed poorly in cognitive, spatial and verbal tasks compared to normal controls (Bray et al., 2011).

In young adult males with FXS (18-24 years old), reduced volume in the hippocampus, thalamus, and putamen compared to normal controls, and no differences were found in the caudate nucleus, frontal and parietal cortices, and white matter region of the corona radiate (Qin et al., 2013). Interestingly, no change in the caudate nucleus volume was reported by Qin et al. (Qin et al., 2013) in a young adult FXS population, suggesting the increased caudate nucleus volume reported in younger FXS patients may have normalized with age (Bray et al., 2011; Gothelf et al., 2008; Hazlett et al., 2012; Hoeft et al., 2010). The findings in brain volume between children and adolescents to adults with FXS showed dynamic morphological changes occur in the FXS brain during development and suggest that the trajectory of volume change in FXS brain is different from normal controls (Bray et al., 2011; Gothelf et al., 2008; Hazlett et al., 2012; Hoeft et al., 2010; Qin et al., 2013).

2.1.4. Volume changes in the *Fmr1* KO mouse brain

In mouse models of FXS, changes in brain volume may depend on the strain of the mouse (Lai et al., 2016). Fewer volume differences were found at PND 60 in the C57Bl6J *Fmr1* KO mice compared to WT, including decreased striatal volume and increased parietal-temporal lobe volume (Lai et al., 2016). The FVB strain of *Fmr1* KO mice reported increased basal forebrain and parietal-temporal lobe volumes in gray

matter, as well as decreased cerebral peduncle volume and increased corpus callosum, internal capsule, and fimbria volumes in white matter, compared to WT mice (Lai et al., 2016). This suggest that at least the volumes in the adult male C57Bl6J *Fmr1* KO mice may not recapitulate volume changes observed in FXS patients. However, findings of altered behavior, impaired learning, altered synaptic plasticity, increasing immature dendritic spine levels, delayed myelin, and elevated rates of protein synthesis have been reported in C57Bl6J *Fmr1* KO mouse strain (Bilousova et al., 2009; Huber et al., 2002; Pacey et al., 2013; Qin et al., 2015). Other studies using the developing male C57Bl6J *Fmr1* KO mice have revealed increasing hippocampal volume and decreasing cerebellar vermis volume at PND 30 compared to WT mice (Ellegood et al., 2010; Shi et al., 2012). Similarly, children (7 ± 5 years old) and adolescents (13 ± 6 years old) with FXS also showed increased hippocampal volume (Kates et al., 1997; Reiss, et al., 1994) and decreased cerebellar vermis volume in toddlers with FXS (2-5 years old) (Hoeft et al., 2010). Thus, the FVB *Fmr1* KO mouse may show greater number of changes in regional brain volume compared to the WT, but the C57Bl6 *Fmr1* KO mouse can still be used to measure brain volume especially during development.

2.1.5. Altered white matter integrity in the FXS and *Fmr1* KO mouse brains

White matter integrity is commonly studied using diffusion tensor imaging (DTI) by measuring water diffusion within the biological tissue in multiple directions from which the microstructural environment of the tissue can be inferred in human and rodent brains (Bockhorst et al., 2008; Mori & Zhang, 2006). The model of diffusivity in the brain assumes that water diffusion is isotropic, being able to diffuse in any direction if

unhindered in an uniform sample (Mori & Zhang, 2006). However, diffusion is hindered in both gray and white matter due to morphological structures, with white matter exhibiting more anisotropic diffusion because of restriction in water diffusion across the axon and myelin membranes, and the gray matter exhibiting more isotropic diffusion behavior (Mori & Zhang, 2006). Mean diffusivity (MD), a measure of the average distance water molecules diffuse after a period of time, decreases as the brain develops due to more restriction in water diffusion (Lebel et al., 2012; Qiu et al., 2008) and increases in MD have been demonstrated in edema, axonal and myelin injuries (Lee et al., 2014). Fractional anisotropy (FA), a measure of the preferential direction of diffusion (Mori & Zhang, 2006), increases in white matter during development as the water molecule is freely able to diffuse along the axon due to relatively less restricted diffusion while it is more restricted across the axon. FA is used as a measure of white matter integrity (Lee et al., 2014; Mori & Zhang, 2006).

In FXS patients (10-23 years old), MD in the inferior longitudinal fasciculus, the white matter tract connecting the temporal and occipital lobes, decreased compared to IQ-matched control, suggesting the presence of increased axon fibers in the FXS brain (Hall et al., 2016). In the same study, elevated FA was reported in the inferior longitudinal fasciculus, the uncinated fasciculus (white matter tract connecting the limbic system), and white matter in the cingulate gyrus in children and young adults FXS compared to IQ-matched controls (Hall et al., 2016). This study suggested that white matter integrity was greater in FXS patients compared to IQ-matched controls but no comparisons to normal controls were made (Hall et al., 2016). Increased fiber density was observed in the left ventral frontostriatal pathway of male toddlers with FXS (1-4 years

old) compared to normally developing controls (Haas et al., 2009). In a study of girls with FXS (7-14 years) compared to normal age-matched controls, decreased FA and increased MD were reported in the fronto-striatal pathway and white matter in parietal, motor, and somatosensory cortices (Barnea-Goraly et al. 2003). Decreased FA and increased MD were also reported in a separate study of adolescent girls and women with FXS (13-23 years) in the internal capsule, as well as white matter in the thalamus and precentral gyrus (Villalon-Reina et al., 2013). In the adult male *Fmr1* KO mouse brain (9-12 weeks old), reduced FA was reported in the anterior and posterior regions of the corpus callosum (Haberl et al., 2015). Thus, current studies suggest there is impaired white matter integrity in FXS patients and *Fmr1* KO mice compared to normally developing and WT controls (Barnea-Goraly et al., 2003; Haberl et al., 2015; Villalon-Reina et al., 2013).

2.2. ALTERED BRAIN FUNCTION IN FXS

2.2.1. Resting state functional networks in the FXS brain

Resting state functional MRI (fMRI) detects spontaneous, synchronous oscillations of blood oxygen level dependent (BOLD) signal that can provide insight into the intrinsic functional organization of the brain (Ogawa et al., 1990). The concept of functional connectivity comes from the discovery of spontaneous fluctuation of BOLD signals that are temporally correlated among disparate regions of the brain while the brain is at rest, which is thought to facilitate coordination between multiple networks resulting in efficient communication (Biswal et al., 1997; Liska et al., 2015; Sours et al., 2015; Stafford et al., 2014). The resting state networks were determined by spontaneous

fluctuations in BOLD signal that showed a high degree of functional connectivity between brain regions (Mantini et al., 2007). Adult resting state networks include the default mode, attention, visual, auditory, somatomotor and salience networks (Mantini et al., 2007; Peters et al., 2016). The default mode, visual, auditory, somatomotor networks have been reported in children (Fair et al., 2008; Hoff et al., 2013). The visual, auditory, and somatomotor networks are associated with the brain activity involved in the processing of visual, auditory, tactile and motor information that corresponds to increased BOLD activity in visual, auditory, somatosensory and motor cortices, respectively (Mantini et al., 2007). The default mode network, which involves functional connectivity between the medial prefrontal cortex, posterior cingulate cortex, and the medial and lateral parietal cortex, is active (meaning there is a temporal correlation between these regions) when an individual is awake and alert but in a situation that does not demand attention or goal-oriented activity (Li et al., 2014; Raichle et al., 2001). The default mode network is attenuated upon initiation of a task-based activity that requires attention, whereby functional connectivity increases and results in increased correlation within the attention network between the dorsolateral prefrontal cortex, posterior cingulate cortex, inferior parietal cortex and the supplementary motor area (Li et al., 2014; Mantini et al., 2007).

Reduced functional connectivity has been determined in male and female FXS patients (10-23 years old) and compared to IQ-matched controls, although normal controls were not included in the study, in brain regions associated with known adult resting state networks (Hall et al., 2013). Specifically, reductions of functional connectivity were found in the insular cortex, as well as frontal, temporal, parietal, and

occipital lobes in the brain of FXS patients (Hall et al., 2013), and these regions have been associated with the default mode, attention, auditory, visual and somatomotor networks (Mantini et al., 2007).

An important region affected in FXS was the insular cortex, a region that facilitates switching between the default mode and the attention network (Sridharan et al., 2008). The anterior insular cortex is also part of the salience network in the human brain, including the dorsal anterior cingulate cortex, dorsal striatum, and thalamus (Peters et al., 2016; Seeley et al., 2007). The salience network is involved in cognition, motivation, attention and motor control in normal humans (Peters et al., 2016). Alterations of functional connectivity in the salience network can contribute to impaired regulation of cognition, emotion, and behavior (Peters et al., 2016); decreased functional connectivity in the salience network was found in schizophrenic patients (Wang et al., 2016) and in patients with obsessive-compulsive disorder (Anticevic et al., 2014). A decrease in the functional connectivity of the insular cortex to other regions associated with the salience and the attention networks was observed in FXS patients compared to IQ-matched controls; this decrease may reflect attention problems associated with FXS (Hall et al., 2013). Functional connectivity in the insular cortex of the female FXS patients was higher than the male, but still reduced compared to IQ-matched controls (Hall et al., 2013). This difference may be due to IQ, as a positive correlation of IQ to BOLD signal in the insular cortex of FXS patients was reported, and the average IQ in female FXS patients in the study was 80 compared to an average IQ of 60 in male FXS patients (Hall et al., 2013). Therefore, the reduction of functional connectivity of the insular cortex within the salience network may reflect impaired cognition and emotion regulation in

FXS patients (Hall et al., 2013).

To test for differences in brain activity associated with gaze aversion and sociability in FXS, experimenters using a task-based functional MRI (fMRI) test, instructed adolescent male FXS patients (15.5 ± 2.4 years old) to focus on pictures of strangers making direct eye contact to the camera (Watson et al., 2008). The results of the eye contact study show increased BOLD signal in the insular cortex and decreased BOLD signal in the prefrontal cortex of male FXS patients compared to normal controls (Watson et al., 2008). The altered activity in the insular cortex from both resting state and task-based fMRI in FXS patients indicates that the insular cortex may play a role in the attention problems and social aversion in FXS (Hall et al., 2013; Watson et al., 2008). The use of resting state fMRI (rs-fMRI) to study FXS is relatively recent but the findings have revealed important insights into brain function and functional brain network of FXS patients, and suggest that the differences observed compared to normal and IQ-match populations may be associated with behavioral problems in FXS.

2.2.2. Resting state brain networks in rodents

In normal rats, functional and structural connections between the prefrontal and somatosensory cortices, as well as connection to the caudate putamen and thalamic nuclei are similar to those present in humans (D'Souza et al., 2014). The default mode, attention, auditory, visual and somatomotor resting state networks have been observed in WT adult rodents (Jonckers et al., 2014; Liska et al., 2015; Ma et al., 2016; Stafford et al., 2014; Zerbi et al., 2015). In addition, rs-fMRI show similar spatial activation patterns as fluorodeoxyglucose PET signals that measure glucose metabolism and synaptic activity

in normal adult rodent brain (Attwell & Laughlin, 2001; Shah et al., 2016). Findings in adult rodent functional connectivity studies show the cingulate cortex may serve as a functional hub for the default mode network, similar to the cingulate cortex in the adult human brain (Liska et al., 2015; Ma et al., 2016). In addition, the functional connectivity in the default mode network in the adult mouse is largely conserved with respect to adult primates and humans (Stafford et al., 2014).

Reduced functional connectivity between the visual cortex and the somatosensory, auditory and motor cortices, hippocampus, and caudate putamen has been reported in the brain of adult *Fmr1* KO mice (9-12 weeks old) compared to WT (Haberl et al., 2015). In agreement with findings in FXS patients, reduced functional connectivity was observed in the visual, auditory and somatomotor networks (Hall et al., 2013). Therefore, functional connectivity in *Fmr1* KO mouse brain showed a similar decrease to that of FXS patients. However, more studies are needed to determine changes in the default mode network and to study functional connectivity in developing *Fmr1* KO mouse brain.

2.3. SUMMARY

With the exception of volumetric studies, *in vivo* imaging modalities were not commonly used to study FXS patients or *Fmr1* KO mice. Only recently studies in FXS patients and *Fmr1* KO mice have incorporated different imaging modalities to reveal alterations in brain metabolism, morphology and function. Regional brain volume alterations in the FXS patient population were reported in children, adolescents, and adults when compared to age-matched normal controls. Recent studies also demonstrated

alterations in the FXS brain using metabolic imaging to show differences in metabolite concentrations and ligand binding, reduced white matter integrity using DTI, and functional imaging studies demonstrated altered in brain activity and reduced connectivity in the functional brain network in FXS patients. In addition, these techniques have also been used sparingly in the past to study the *Fmr1* KO mouse brain. These methods can be used in future studies to improve our understanding of brain development in *Fmr1* KO mice.

CHAPTER 3: PURPOSE AND SPECIFIC AIMS

3.1. RESEARCH QUESTIONS

The research in this thesis studied brain development in *Fmr1* KO mouse and determined whether imaging methods could identify differences during brain development between *Fmr1* KO and WT mice. Specifically, the following questions regarding brain maturation differences between *Fmr1* KO and WT mice were probed in this thesis:

- Are brain metabolites altered in the developing *Fmr1* KO mouse brain and can these alterations indicate neuronal and signal transduction deficits?
- Can developmental differences in gray and white matter structure be measured in the *Fmr1* KO mouse brain using magnetic resonance imaging?
- Is the functional brain network altered in the developing *Fmr1* KO mouse?
- Can the imaging and spectroscopy studies in the *Fmr1* KO mouse brain reveal altered patterns of brain development compared to the WT?
- Can the observed developmental differences between *Fmr1* KO and WT mice be used to guide treatment plans during brain development?

This research project was designed to find answers to the above questions in the *Fmr1* KO mouse model. While there remains much more that can be learned regarding the developmental aspects of FXS, the studies in this thesis have contributed new findings on the metabolic, anatomical and functional differences in the brain of *Fmr1* KO mouse compared to the WT during the key developmental stages.

3.2. PURPOSE

The purpose of this thesis was to study brain metabolism, morphology, and functional connectivity at specific stages of brain development in the *Fmr1* KO mouse brain compared to the WT. Differences in the brain were studied at critical stages of development that include before and during the peak of myelination and synaptogenesis at postnatal day 18 (PND 18) and 21, respectively, neural network specialization at PND 30, and maturation of the neural network at PND 60 (Semple et al., 2013). Studying the brain over many time points provided a better understanding of alterations in white and gray matter regions during the critical periods of brain development in the *Fmr1* KO mouse and may reveal altered patterns of brain development compared to the WT. The morphological and functional differences between *Fmr1* KO and WT mice could potentially be used to help plan intervention studies during critical developmental periods that show deficits in the *Fmr1* KO mouse brain. Taken together, the work in this thesis contributed to the understanding of overall brain development in the *Fmr1* KO mouse.

3.3. SPECIFIC AIMS

3.3.1. Determine longitudinal differences in hippocampal metabolites in developing *Fmr1* KO mouse brain compared to WT brain

The first aim was to characterize developmental changes in hippocampal metabolite levels in the *Fmr1* KO mouse brain. The objective of this study was to conduct a longitudinal assessment of the hippocampus in *Fmr1* KO mice to determine if metabolic alterations might contribute to the abnormal development of the hippocampus compared to WT mice. The metabolite levels were measured using ^{1}H magnetic

resonance spectroscopy in *Fmr1* KO and WT mice at PND 18, 21 and 30, during a period of myelination and neural network development. The hippocampus is well studied in the *Fmr1* KO mouse, and studies in the literature reported exaggerated mGluR5-dependent LTD (Huber et al., 2002), increased PI3K-mTOR signaling (Sharma et al., 2010), and increased immature dendritic spine density (Bilousova et al., 2009). Determining metabolite levels would reveal potential alterations in neurotransmitters, signaling molecules, and cellular structural components in the hippocampus of *Fmr1* KO mouse brain.

3.3.2. Determine alterations in white matter of the developing *Fmr1* KO mice

The objective of this study was to determine whether myelination in white matter regions during postnatal development is different in *Fmr1* KO mouse brain compared to the WT. A previous study demonstrated delayed myelination in cerebellar white matter of *Fmr1* KO mice (Pacey et al., 2013). Since myelin is the major component in white matter, we hypothesized that reduced myelin is found in white matter regions during brain development in *Fmr1* KO mouse. The volume of white matter regions, T_2 relaxation time, and magnetization transfer ratio were measured in fixed *Fmr1* KO and WT mouse brains at PND 18, 21, 30 and 60. These parameters are commonly used to study white matter using magnetic resonance imaging (MRI) (Bonnier et al., 2014; Ou et al., 2009; Schmierer et al., 2004; Thiessen et al., 2013; Wozniak & Lim, 2006). Histological staining of myelin with Black Gold II was used to quantify myelin density and determine how well myelin staining corresponded to the data obtained using MRI. Any observed deficits in myelin would potentially help to explain differences in the

development of white matter tracts in *Fmr1* KO mice compared to WT mice.

3.3.3. Determine diffusion properties in the brain of developing *Fmr1* KO mice

This aim investigated the microstructure differences in white and gray matter regions of the *Fmr1* KO mouse brain compared to WT using diffusion tensor imaging (DTI). DTI, which measures the diffusion distance of water with respect to time, was used to provide insights into axon and myelin morphology in developing *Fmr1* KO mouse brain. Previous reports of altered axon morphology suggest there are differences in the organization of axons in models of FXS, including increased axonal branching (Pan et al., 2004) and diffuse axonal arborization (Bureau et al., 2008). The objective of this study was to determine whether differences in the organization and density of axon fibers were present in the *Fmr1* KO mouse brain compared to WT. The fixed brains of *Fmr1* KO and WT mice were studied using DTI at PND 18, 21, 30 and 60. Insights into axon morphology and density would contribute to the understanding of morphological deficits in the developing *Fmr1* KO mouse brain.

3.3.4. Determine if there are alterations in resting state networks in the developing brain of *Fmr1* KO mice compared to WT mice

This aim determined functional connectivity in the brains of developing *Fmr1* KO mice compared to WT at an earlier age during brain development (PND 30) and when the brain is more mature (PND 60). The objective of this study was to study potential differences in the functional organization of developing *Fmr1* KO mouse brain using resting state network analysis. A previous study demonstrated increased local neuronal

network excitability in somatosensory cortex in developing *Fmr1* KO mouse (Gibson et al., 2008). The altered neural network excitability led to our hypothesis that functional connectivity is decreased in developing brain of *Fmr1* KO mice compared to the WT. Functional connectivity between brain regions was selected based on known resting state networks related to sensory functions (somatomotor, auditory, and visual), as well as the default mode network (Jonckers et al., 2014; Liska et al., 2015; Ma et al., 2016; Stafford et al., 2014; Zerbi et al., 2015). Currently little is known about functional connectivity changes during postnatal brain development in rodents and this project would contribute to the understanding of functional organization in the developing *Fmr1* KO and WT mouse brains.

3.3.5. Pilot study of metformin on resting state networks in the developing brain of *Fmr1* KO mice

A pilot study investigated the changes in functional connectivity and MTR following treatment with metformin during brain development in *Fmr1* KO mice compared to WT. Metformin is commonly used to treat type 2 diabetes (Hatoum & McGowan, 2015) and a recent study demonstrated the efficacy of metformin as a potential therapeutic agent in adult *Fmr1* KO mice (Gantois et al., 2017). We predicted that treating the developing brain from PND 21 to PND 60 in the *Fmr1* KO mouse brain would normalize differences in functional connectivity and MTR in *Fmr1* KO brain compared to WT. Functional connectivity was studied at PND 30 and PND 60 to reflect short and long-term metformin treatment, respectively. This preliminary study determined whether change in functional connectivity can be used to measure the

efficacy of metformin treatment in *Fmr1* KO mice. This study would be the first to evaluate treatment efficacy using MRI in *Fmr1* KO mouse brain.

Many studies have demonstrated neuronal alterations during development, but changes in white matter morphology and brain network dysfunction are only beginning to be studied in *Fmr1* KO mouse (Haberl et al., 2015; Pacey et al., 2013). The goal of this thesis was to improve our understanding of the metabolic, structural, and functional alterations in the developing *Fmr1* KO mouse brain.

CHAPTER 4: ANIMALS AND GENOTYPING

4.1. ANIMALS

Fmr1 KO mice (JAX B6.129P2-fmr1^{tmICgr} mice; Jackson Laboratory, Bar Harbor, ME, USA) on a C57Bl6J background and wild-type (WT) mice (JAX C57Bl6J; Jackson Laboratory, Bar Harbor, ME, USA) were bred at the University of Maryland, Baltimore. Animal use and breeding were approved by the Institutional Animal Care and Use Committee at the University of Maryland, Baltimore. Mice were housed at the University of Maryland, Baltimore with 12 hours of light and 12 hours of darkness. Food and water were provided *ad libitum*. All mice were weaned at PND 21. Weaned male mice were placed in cages with 2-5 littermates. Only male mice were used for this study because males are more affected by FXS than females in the human population due to the *FMR1* gene being on the X chromosome (Bailey et al., 2009; Garber et al., 2008; Kidd et al., 2014).

4.2. MOUSE BREEDING SCHEMES

In Chapters 5, 6 and 7, the *Fmr1* KO mice were generated by mating *Fmr1* KO female ($Fmr1^{-/-}$) to *Fmr1* KO males ($Fmr1^{-/y}$). The WT mice were generated by mating the WT female ($Fmr1^{+/+}$) to the WT male ($Fmr1^{+/y}$). The *Fmr1* KO mice were backcrossed for more than 10 generations.

In Chapters 8 and 9, *Fmr1* KO and WT mice were generated by mating a heterozygous ($Fmr1^{+/-}$) female mouse to a male WT mouse ($Fmr1^{+/y}$). The male offspring from this mating pair would be *Fmr1* KO ($Fmr1^{-/y}$) or WT ($Fmr1^{+/y}$). The WT mice

served as within litter controls to the *Fmr1* KO mice.

4.3. GENOTYPING PROTOCOL

A small section of the tail was taken for genotype determination at the time of sacrifice using methods previously described in Bakker et al.(Bakker et al., 1994). Female mice for breeding were also genotyped. The tools used and tail clippings were washed in 70% ethanol. The tail clipping was frozen at -20°C until polymerase chain reaction (PCR). Mouse DNA was extracted using the DirectAmp Tissue Genomic DNA Amplification kit (Denville Scientific Inc., Holliston, MA). Each tail clipping was incubated in 25 µl extraction solution and 6 µl of preparation solution from the DNA amplification kit in room temperature for 10 minutes, then incubated for 3 minutes at 95°C. Next, 30 µl of neutralization solution from the kit was added and the sample vortexed. The extracted DNA sample was used for PCR.

The thermocycler used was an Applied Biosystems 2720 Thermal Cycler (Thermo Fisher Scientific Inc., Waltham, MA). PCR was performed using HotStarTaq Polymerase from Qiagen (Qiagen Sciences, Germantown, MD): 10 µl PCR buffer, 5 µl manganese chloride, 2 µl deoxynucleotide mix, 0.5 µl DNA polymerase. In addition, 4 µl of DNA were added to the PCR solution, along with 1 µl of the WT, mutant, and common primers (Sigma-Aldrich Corp., The Woodlands, TX), and 3 µl of Milli-Q filtered water. Primers (from 5' to 3') (Bakker et al., 1994):

Mutant forward: CAC GAG ACT AGT GAG ACG TG

Wildtype forward: TGT GAT AGA ATA TGC AGC ATG TGA

Common: CTT CTG GCA CCT CCA GCT T

The PCR cycling conditions were as follows: 15 minutes at 95 °C to activate the DNA polymerase followed by 30 cycles of denaturation at 94 °C for 1.5 minutes each, annealing at 63°C for 1.5 minutes, and extension at 72 °C for 2.5 minutes. A final extension step was performed at 72 °C for 10 minutes. The bands were separated by gel electrophoresis on a 1.5% agarose gel at 110 volts for 1 hour. The *Fmr1* KO band was at 400 basepairs (bp), and the WT band was at 131 bp. The heterozygote bands were at 400 bp and 131 bp, and were only found in breeding females.

CHAPTER 5: LONGITUDINAL *IN VIVO* DEVELOPMENTAL CHANGES OF METABOLITES IN THE HIPPOCAMPUS OF *FMR1* KNOCKOUT MICE[1]

5.1. INTRODUCTION

Fragile X syndrome (FXS) is the most commonly inherited form of X-linked mental retardation (Garber et al., 2008), and is caused by mutational insertion of CGG tri-nucleotide repeats that leads to hypermethylation and silencing of the *FMR1* gene (Garber et al., 2008; Oostra et al., 1993). The rodent *Fmr1* gene and the human *FMR1* gene code for the fragile X mental retardation protein (FMRP), which acts as a translational repressor and binds specific mRNAs (Brown et al., 2001), including group 1 metabotropic glutamate receptor (mGluR) mRNA (Darnell et al., 2011). Silencing of the *Fmr1* gene can result in structural, biochemical and physiological changes in brain that impact development, and contribute to the pathology exhibited in the *Fmr1* KO mouse (Bassell & Warren, 2008; Dolen & Bear, 2008; Greenough et al., 2001). The mGluR5-dependent increase in long-term depression (LTD) involves dynamic translation and degradation of FMRP, which is thought to serve as a regulatory system controlling synaptic plasticity (Hou et al., 2006). The increased protein synthesis that occurs in the absence of FMRP accompanies enhanced LTD (Huber et al., 2002; Qin et al., 2005).

---

1. Shi D, Xu S, Waddell J, Scafidi S, Roys S, Gullapalli R, McKenna MC. Longitudinal *in vivo* developmental changes of metabolites in the hippocampus of *Fmr1* knockout mice. *J Neurochem*. 2012; 123(6):971-81.

The *Fmr1* KO mice exhibit behavioral and cognitive alterations similar to patients with FXS such as hyperactivity, anxiety, and deficits in learning and memory (Bakker et al., 1994; Brennan et al., 2006; Paradee et al., 1999; Smith et al., 2012; Spencer et al., 2005). The hippocampus has a crucial role in learning and memory formation (Eichenbaum, 1996; Scoville & Milner, 2000), and this region shows increased volume in young FXS patients (7 ± 5 years old) (Reiss et al., 1994). An increased density of morphologically immature dendrites has been observed in the dentate gyrus (Grossman et al., 2010), and the CA1 region of the hippocampus (Levenga et al., 2011) of *Fmr1* KO mice compared to controls.

Most studies in *Fmr1* KO mouse have focused on alterations in dendritic spines, electrophysiological properties, signaling and RNA processing pathways and behavior (Bardoni et al., 2006; Bassell & Warren, 2008; Dolen & Bear, 2008; Garber et al., 2008; Liu-Yesucevitz et al., 2011; Narayanan et al., 2008). Little emphasis has been placed on metabolic and biochemical changes. Metabolites offer a glimpse into functional processes under FMRP regulation (beyond the well studied protein and mRNA interactions) which can offer additional insight into regulatory pathways of the brain (Davidovic et al., 2011). Many alterations in metabolism can contribute to impaired brain development and dysfunction (Moffett et al., 2007; Yudkoff, 1999); however, few groups have studied metabolic or biochemical alterations in *Fmr1* KO mouse brain (Davidovic et al., 2011; Gruss & Braun, 2001; Qin et al., 2002). Evidence of alterations in cholinergic pathways has been reported in patients with FXS (Kesler et al., 2009). Both structural and biochemical alterations have been reported in brain regions of children with autism spectrum disorders (ASD) (Chugani, 2012), which share many features with FXS (Garber

et al., 2008).

Alterations in metabolites in the hippocampus of the FVB strain of juvenile *Fmr1* KO mice have been reported at postnatal day 12 (PND 12) using nuclear magnetic resonance spectroscopy (Davidovic et al., 2011) and at PND 28-32 using high performance liquid chromatography (HPLC) (Gruss & Braun, 2001) with *ex vivo* brain tissue. However, no studies have determined *in vivo* longitudinal changes in the hippocampus of developing *Fmr1* KO mice. Non-invasive methods such as *in vivo* magnetic resonance imaging (MRI) and ^{1}H magnetic resonance spectroscopy (MRS) allow monitoring of brain structure and metabolic integrity longitudinally during brain development and provide information on changes in neurotransmitters such as glutamate, taurine, and GABA, as well as metabolites including *N*-acetylaspartate, *myo*-inositol, and choline containing compounds.

The present study was performed during the critical period of myelination and synaptogenesis, at PND 18, 21 and 30, in the hippocampus where developmental alterations in metabolites could be affected by a lack of FMRP. We measured volumetric and metabolic changes over time in the hippocampus of *Fmr1* KO mice compared to wild-type C57Bl6J (WT) mice using *in vivo* MRI and ^{1}H-MRS, respectively. To our knowledge, the present study is the first report on *in vivo* ^{1}H-MRS assessment of longitudinal metabolic changes in the developing *Fmr1* KO mouse brain.

5.2. METHODS AND MATERIALS

5.2.1. Animal procedure

Male *Fmr1* KO mice (JAX B6.129P2-fmr^{1tmICgr} mice, Jackson Laboratory, Bar

Harbor, Maine) from a C57Bl/6J background were obtained from a breeding colony at the University of Maryland, Baltimore. All protocols were approved by the Institutional Animal Care and Use Committee at University of Maryland, Baltimore. Ten *Fmr1* KO mice and thirteen WT (JAX C57Bl6J) mice were used for each group; the mice used in this study came from 3 different litters, respectively. Food and water were given ad libitum. All mice were weaned at PND 21. Serial MRI and ^{1}H-MRS data sets were acquired at PND 18, 21 and 30 for each mouse. Breeding and genotyping protocols were listed in Chapter 4.

5.2.2. *In vivo* MRI/MRS:

All experiments were performed on a Bruker Biospec 7.0 Tesla 30 cm horizontal bore scanner using Paravision 5.1 software (Bruker Biospin MRI, Ettlingen, Germany). A four channel Bruker ^{1}H surface array coil was used as the receiver and a Bruker 72 mm linear-volume coil as the transmitter. Mice were anesthetized using 2% isofluorane during the set up and maintained between 1-1.5% isoflurane at 1 L/min oxygen administration via a nose-cone for the rest of the experiment. *Fmr1* KO and WT mice were carefully exposed to the same duration and level of isoflurane at each age to control for the potential effect of isoflurane exposure on developing brain metabolism (Kulak et al., 2010). The anesthetized mice were placed prone on a specialized holder with warm circulating water flowing through a pad that was placed over the body. Pain and discomfort were minimized by limiting scanning time to less than two hours, maintaining body temperature at 36-37°C, and respiration was monitored throughout the experiment (SA Instruments, Stony Brook, NY, USA).

Proton density-weighted MR images covering the entire brain were obtained using a 2D rapid acquisition with relaxation enhancement (RARE) sequence (TR/TE=5500/9.5 ms; slice thickness 0.5 mm; 16 slices) that served as anatomic reference at for ^{1}H MRS (10 minutes). Shimming over the hippocampus, on average yielded a water line of 11± 2 Hz in both the WT and *Fmr1* KO mice. A point-resolved spectroscopy (PRESS) pulse sequence (TR/TE=2500/20 ms) with water suppression was used for data acquisition from a 2 x 4 x 2 mm^3 voxel that covered the hippocampus area (Figure 5-1). The ^{1}H MRS voxel used was larger than the actual mouse hippocampus and included part of the cortex and the corpus callosum, but the majority of the scanned volume was over the hippocampus. A larger voxel was used to improve the signal to noise ratio and to minimize MRS scanning time. For each spectrum, 300 acquisitions were averaged for a total of 13 minutes. Shimming was performed using the Fastmap technique (Gruetter, 1993a) over the voxel of interest. ^{1}H MRS data were fitted using the LCModel software package (Provencher, 2001). Only those metabolite ratios relative to total creatine (tCr) that passed the Cramer-Rao lower bound (CRLB) of 25% were used for further analysis. The CRLB values for tCr were all less than 10 percent.

Hippocampal volume was measured with Medical Image Processing, Analysis and Visualization tool (MIPAV v5.3.1, CIT, NIH, Bethesda, MD) from the proton density-weighted images. The region of interest (ROI) was manually outlined in the proton density-weighted images for each image from around interaural 2.74 mm to interaural 0.28mm [regions referenced from Franklin and Paxinos (Franklin & Paxinos, 2007)], then these ROIs were grouped and volumes were calculated.

5.2.3. Statistical Analysis

A repeated measures analysis of variance (RMANOVA; SPSS) was used to determine differences between *Fmr1* KO and WT mice across the 3 ages for the hippocampal volume and each metabolite ratio separately, with genotype being the between subject factor and age being the within subject factor. In the cases in which the (age X genotype) interaction was statistically significant we probed further for the specific differences by means of independent Student's T-tests. To control for multiple pairwise comparisons, a false discovery rate with threshold of alpha = 0.05 was performed on the p-values. The threshold assumes 5% of significant p-values may be false positives, and if a significant p-value does not pass false discovery rate then that p-value may be a false positive. Metabolites that had a CRLB value higher than 25% were excluded from analysis. The decreased sample numbers for creatine and phosphocreatine are due to incomplete peak separation in some samples.

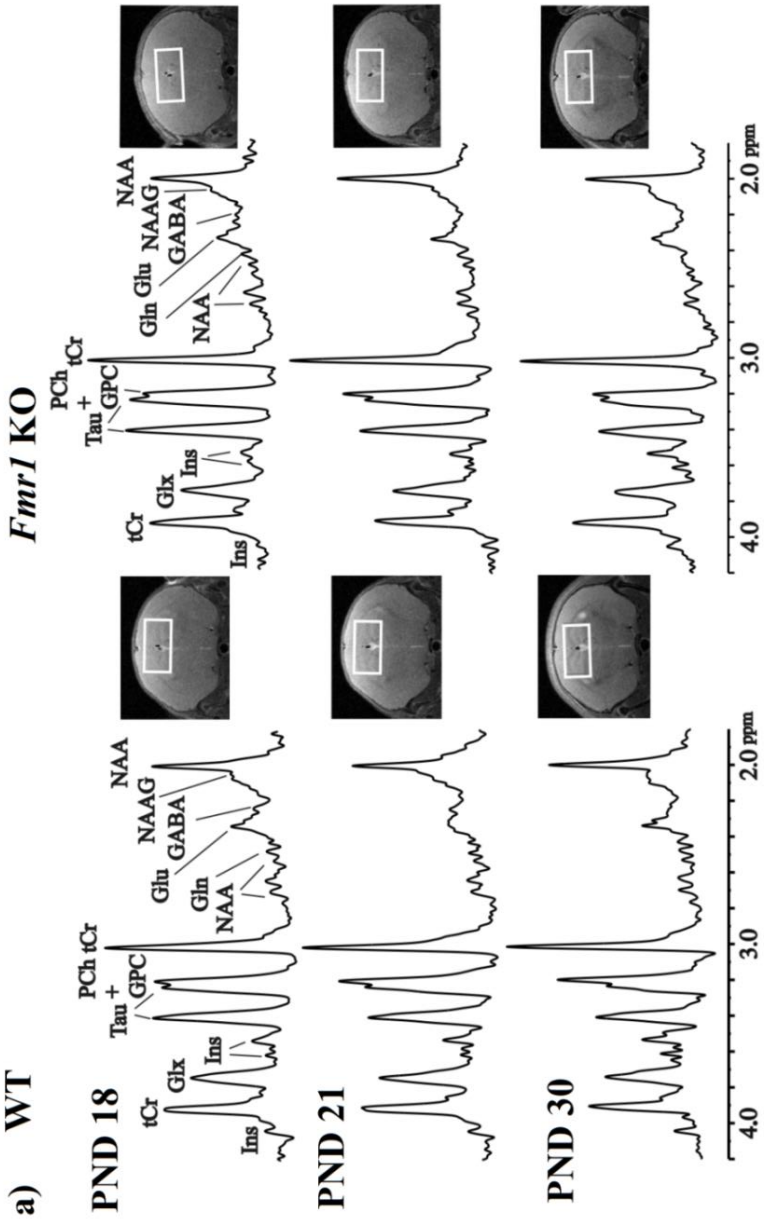

Figure 5-1: Representative *in vivo* high resolution ^{1}H MR spectra in the mouse hippocampus (16 µl) from wild type (left column) and *Fmr1* knockout (right column) during development. The spectra location is indicated in the respective MR images. Spectra were acquired using PRESS with TR = 2500 ms, TE= 20 ms, and total acquisition time is 13 minutes. Free induction decays were enhanced using Lorentzian-Gaussian transformation scheme (gb = 0.07, lb = - 4) before Fourier transformation. The spectra were phased using zero-order phase only without any baseline correction. GABA = γ-aminobutyric acid, Gln = glutamine, Glu = glutamate, Glx = glutamine + glutamate, GPC = glycerophosphocholine, Ins = *myo*-Inositol, NAA = *N*-acetylaspartate, NAAG = *N*-acetylaspartylglutamate, PCh = phosphocholine, tCr = creatine + phosphocreatine, Tau = taurine.

5.3. RESULTS

Fmr1 KO and WT control mice were studied at postnatal days (PND) 18, 21, and 30, as this time frame encompasses the critical period of synaptogenesis and rapid myelination in mice (Gruss & Braun, 2001; Massa et al., 2004; McKenna et al., 1994). At these ages, FMRP is expressed above adult levels in the brains of WT mice (Davidovic et al., 2011; Lu et al., 2004).

5.3.1. Hippocampal volume

The hippocampi were manually outlined in the proton density-weighted images for each mouse at each age and the volumes were calculated. Analysis of hippocampal volume revealed a significant effect of age, $F(2,36)= 8.28$, $p < 0.005$ and of genotype $F(1,18)= 24.35$, $p < 0.001$ (Figure 5-1); however, no significant (age X genotype) interaction was observed. The hippocampal volume in *Fmr1* KO mice was larger than WT control mice at all ages: 16.6% average increase at PND 18, 19.3% average increase at PND 21 and 11.0% average increase at PND 30 (Figure 5-2). In both genotypes, hippocampal volume was greatest at PND 21 and decreased by PND 30. Movement artifacts prevented analysis of three images from PND 21 and one from PND 30. The results agree with clinical reports of increased hippocampal volume in children with FXS (Kates et al., 1997; Reiss et al., 1994).

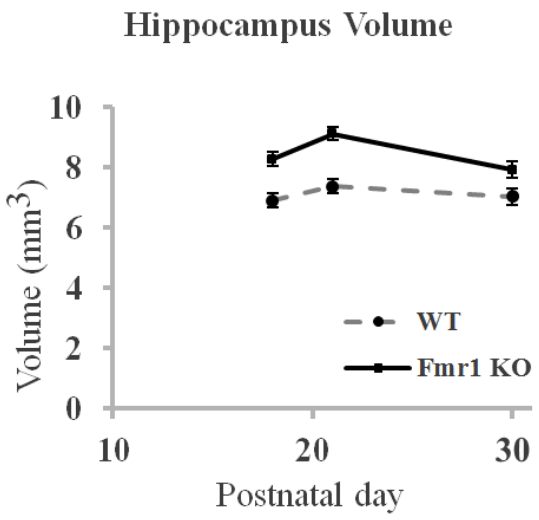

Figure 5-2: Mean volume of the hippocampus in *Fmr1* KO (black line) and WT control mice (gray dotted line) studied at PND 18, 21 and 30. Values are means ± standard error for mm^3 hippocampal volume from 10 *Fmr1* KO and 13 WT control mice studied longitudinally at PND 18, 21 and 30. However, only 9 *Fmr1* KO and 10 WT mice were included for analysis due to motion artifacts that prevented volume measurement in 4 mice. Repeated measures ANOVA revealed a significant effect of age $F(2,36)= 8.28$, $p < 0.005$, and a significant effect of genotype $F(1,17)= 24.35$, $p < 0.001$.

5.3.2. Neurochemical profile of *Fmr1* KO mice compared to wild type mice

High quality ^{1}H spectra of the hippocampal region were obtained at PND 18, 21 and 30 from both WT control and *Fmr1* KO mice. Typical *in vivo* ^{1}H MR spectra from the hippocampus at each age are shown in Figure 5-1. Data from 12 metabolites were compared between the hippocampus of WT and *Fmr1* KO mice. The peak from *N*-acetylaspartate (NAA) methyl singlet at 2.01 ppm was assigned as the reference from which the rest of the metabolites were identified. The ratio of metabolites to total creatine (tCr; creatine plus phosphocreatine) in the hippocampus was determined longitudinally in the WT and *Fmr1* KO mice at each age (Table 5-1 and Figure 5-3). There was no difference in total creatine content between WT and *Fmr1* KO mice at any of the ages studied (Table 5-1). Metabolite data from many *in vivo* studies of human and rodent brain

are reported relative to the value for tCr (Mukonoweshuro et al.,, 2001; Xu et al., 2011).

Metabolite/tCr	WT n	*Fmr1* KO n	**PND 18** WT Mean ± SE	**PND 18** *Fmr1* KO Mean ± SE	**PND 21** WT Mean ± SE	**PND 21** *Fmr1* KO Mean ± SE	**PND 30** WT Mean ± SE	**PND 30** *Fmr1* KO Mean ± SE
N-acetylaspartate †‡	13	9	**0.46 ± 0.02**	**0.38 ± 0.03**	0.49 ± 0.02	0.47 ± 0.02	0.55 ± 0.02	0.51 ± 0.01
Taurine†‡§	13	8	**1.80 ± 0.05**	**2.03** ** ± 0.06**	**1.54 ± 0.02**	**1.75*** ± 0.03**	**1.34 ± 0.02**	**1.39* ± 0.02**
Choline†	12	8	0.14 ± 0.01	0.15 ± 0.01	0.15 ± 0.01	0.15 ± 0.01	0.18 ± 0.01	0.17 ± 0.01
myo-Inositol †§	13	8	0.42 ± 0.03	0.53 ± 0.12	0.48 ± 0.02	0.38# ± 0.04	**0.74 ± 0.02**	**0.65* ± 0.02**
Glutamate†	13	8	0.88 ± 0.05	0.83 ± 0.06	0.82 ± 0.04	0.93 ± 0.03	0.99 ± 0.02	0.96 ± 0.03
Glutamine	13	7	0.55 ± 0.03	0.56 ± 0.03	0.50 ± 0.04	0.59 ± 0.03	0.55 ± 0.07	0.53 ± 0.02
GABA	11	6	0.33 ± 0.02	0.33 ± 0.04	0.35 ± 0.03	0.36 ± 0.02	0.33 ± 0.02	0.37 ± 0.02
Creatine†	7	5	0.23 ± 0.02	0.23 ± 0.01	0.27 ± 0.01	0.25 ± 0.03	0.32 ± 0.02	0.31 ± 0.02
Phosphocreatine†	8	6	0.78 ± 0.02	0.79 ± 0.03	0.75 ± 0.02	0.76 ± 0.03	0.68 ± 0.02	0.69 ± 0.02

Table 5-1: Comparison of the ratio of metabolites to total creatine (tCr) between *Fmr1* KO mice and WT mice at PND 18, 21, and 30. Values are the means ± SE of the relative concentration of each metabolite with respect to tCr obtained at each age as described in the methods. A total of 13 WT mice and 10 *Fmr1* KO mice were scanned longitudinally. The n's reflect the number of mice that passed the CRLB of 25% that were included for analysis. † indicates significant effect of age, ‡ indicates significant effect of genotype, and § indicates significant (age X genotype) interaction. The level of significance is indicated by asterisks *p < 0.05, **p < 0.005, *** p <0.0001; # p < 0.07 indicates a trend.

5.3.3. Longitudinal changes in metabolites in the developing hippocampus

N-acetylaspartate is a well accepted marker of neuronal health (Moffett et al., 2007). Analysis of *N*-acetylaspartate /tCr revealed a significant effect of age, $F(2,42)=19.643$, $p<0.001$ as well as a significant effect of genotype, $F(1,21)= 4.777$, $p < 0.05$ (Figure 5-3a). The interaction of (age X genotype) was not significant. However, the

results suggest that *N*-acetylaspartate/tCr in the hippocampus of the *Fmr1* KO mouse may be lower than the WT mouse at PND 18 (Figure 5-3a).

Analysis of taurine/tCr confirmed a significant effect of age, $F(2,40)=140.4$, $p < 0.001$, genotype, $F(1,20)=43.5$, $p < 0.001$, as well as a significant (age X genotype) interaction, $F(2,40)= 4.83$, $p < 0.05$ (Figure 5-3b). The ratio of taurine/tCr was significantly increased in the hippocampus of *Fmr1* KO mice compared to the WT controls (Figure 5-3b) at PND 18 $t(19)=3.60$, $p < 0.005$; PND 21 $t(21)=6.22$, $p < 0.005$ and PND 30 $t(21)=2.16$, $p < 0.05$. The significant p-values from multiple pairwise comparisons passed false discovery rate, with the threshold of alpha = 0.05.

Analysis of *myo*-inositol/tCr confirmed a significant effect of age, $F(2,40)= 13.87$, $p < 0.001$ and a significant (age X genotype) interaction, $F(2,40)= 7.06$, $p < 0.004$ (Figure 5-3c). The effect of genotype was not significant. A significant decrease was detected in the ratio *myo*-inositol/tCr in *Fmr1* KO mice compared to the WT controls (Figure 5-3c) at PND 30 $t(21)= 3.06$, ($p < 0.01$) and trend towards decrease was observed at PND 21 $t(20)= 1.95$, ($p < 0.07$). The significant p-value passed false discovery rate (alpha = 0.05).

Analysis of total choline/tCr showed a significant effect of age, $F(2,38)=15.53$, $p < 0.0001$ (Figure 5-3d). There was no significant (age X genotype) interaction between WT and *Fmr1* KO mice, and the main effect of genotype was not significant. Analysis of glutamate/tCr showed a significant effect of age, $F(2,38)=5.28$, $p < 0.01$. There were no significant effects of genotype or (age X genotype) interaction (Figure 5-3e) in *Fmr1* KO mice compared to WT controls. Analysis of glutamine/tCr (Figure 5-3f) and γ-aminobutyric acid (GABA)/tCr (Figure 5-3g) did not show any significant within or between group effects.

Analysis of creatine/tCr and phosphocreatine/tCr, the sum of which equals tCr, confirmed no significant interaction of (age X genotype) and no significant difference in genotype (Table 5-1). A significant effect of age was observed in both creatine, $F(2,22)=5.29$, $p < 0.05$ and phosphocreatine, $F(2,26)=8.51$, $p < 0.01$ in both *Fmr1* KO mice and WT controls.

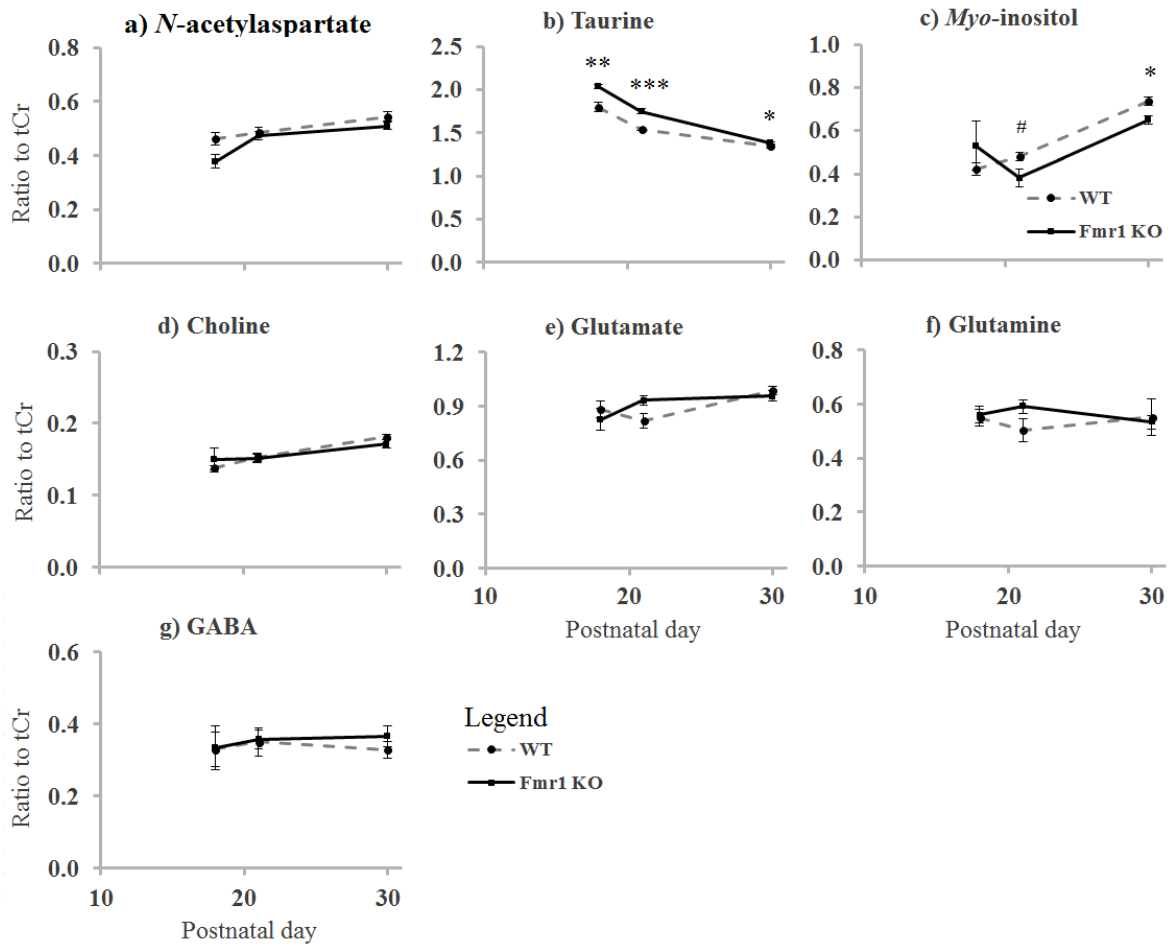

Figure 5-3: Mean ratio of each metabolite to total creatine (tCr) in the hippocampus of *Fmr1* KO (solid black line) and WT mice (gray dotted line) studied longitudinally at PND 18, 21 and 30. (a) *N*-acetylaspartate, (b) taurine, (c) *myo*-inositol, (d) Choline, (e) Glutamate, (f) Glutamine, (g) GABA. Data were collected longitudinally by *in vivo* ^{1}H MRS and fitted using the LCModel package (Provencher, 2001). Relative concentration is normalized to tCr as described in the Methods. Values are means ± standard error for each ratio from *Fmr1* KO and WT mice. The number of animals measured for each metabolite is listed in Table 5-1. Effect of age, genotype, and interaction of (age X genotype) were determined by RMANOVA. Asterisks indicate significant difference between *Fmr1* KO mice and age-matched WT mice; *$p < 0.05$, **$p < 0.005$, and ***$p < 0.0001$ as determined by independent Student t-test. $^{\#}p < 0.07$ indicates a trend determined by Student's t-test.

5.4. DISCUSSION

To our knowledge, this study is the first to characterize the longitudinal changes of metabolites *in vivo* in the developing hippocampus of the *Fmr1* KO mouse compared

to WT controls. We determined the metabolites on PND 18, 21 and 30, during the critical developmental period of synaptogenesis and myelination. Our study found increased hippocampal volume as well as alterations in *N*-acetylaspartate, taurine, and *myo*-inositol in the hippocampus of *Fmr1* KO mice. An imbalance of these metabolites that are involved in osmoregulation, signal transduction, and neuromodulation during this important period of synaptogenesis and early myelination could have long lasting effects that profoundly alter brain development.

A recent study by Kulak et al. (Kulak et al., 2010) used high field *in vivo* ^{1}H MRS to determine longitudinal changes in the neurochemical profiles of developing anterior and posterior cortex in C57Bl6J WT mice from PND 10-60 providing useful reference data for the WT controls in this present study. These authors (Kulak et al., 2010) reported significant changes over time in the concentration of many of the metabolites studied. In the present study, values are reported relative to total creatine as is frequently done in ^{1}H-MRS studies (Kumar et al., 2003; Mukonoweshuro et al., 2001; Xu et al., 2011). The developmental profile of the data for our WT mice can be compared to the data from Kulak et al. (Kulak et al., 2010) (their data are also expressed as metabolite/tCr). Kulak et al. (Kulak et al., 2010) reported a gradual increase in *N*-acetylaspartate and more striking increases in *myo*-inositol and choline in the anterior and posterior cortex from PND 20 to 30 in C57Bl6J WT mice. The developmental patterns between PND 18 and 30 for metabolites in the hippocampus in the C57Bl6J WT mice in the present study parallel the developmental patterns in cortex found by Kulak et al. (Kulak et al., 2010) in that we observed a relatively small increase in *N*-acetylaspartate and choline and a much larger increases in *myo*-inositol with age. The increase in choline in the WT mice reported by

Kulak et al. (Kulak et al., 2010) between PND 20 and 30 was much greater in the lipid rich cortex (~100%) than we observed in the hippocampal region (~28%) of the WT mice in the present study. However, it should be noted that an *ex vivo* study by Yao et al. (Yao, Caserta, & Wyrwicz, 1999) reported a decrease in phosphatidyl choline and total choline from PND 21 to adult in the whole brain of C57Bl6J WT mice. In addition, Tkac et al. (Tkac et al., 2003) reported a small decrease in choline in the hippocampus from PND 21 to 28 in Sprague Dawley rat brain.

Kulak et al. (Kulak et al., 2010) observed a striking decrease in taurine concentration in the cortex from PND 20 to 30, and in our study we found a 26% decrease in taurine in the hippocampus of WT mice from PND 18 to 30. The same group also found a small increase in glutamate and region specific changes in GABA and glutamine between PND 20 and 30 (Kulak et al., 2010). They found no change in GABA in anterior cortex and a slight decrease in posterior cortex, as well as an increase in glutamine in anterior cortex, but no change in the posterior cortex (Kulak et al., 2010). In the present study, we found a small age related increase in glutamate (~13%) in the hippocampus in WT mice from PND 18 to 30 and no change in either GABA or glutamine. Overall, the longitudinal developmental changes in metabolites in the hippocampus of WT mice in the present study are remarkably similar to the longitudinal changes from day 20-30 reported by Kulak et al. (Kulak et al., 2010) for cortex of C57Bl6J WT mice.

There is relatively little information about the metabolite changes in the hippocampus of *Fmr1* KO mice, and the two studies in the literature report *ex vivo* values for hippocampal metabolites in male FVB strain of *Fmr1* KO mice. An HPLC study by

Gruss and Braun (Gruss & Braun, 2001) reported values for hippocampal metabolites in PND 28-32 and adult brain, and an *ex vivo* study by Davidovic et al. (Davidovic et al., 2011) that reported metabolite values from PND 12 mouse brain. The recent study by Davidovic et al. (Davidovic et al., 2011) using ^{1}H high-resolution magic angle spinning nuclear magnetic resonance spectroscopy reported alterations in metabolites in the cortex, striatum, hippocampus and cerebellum in the FVB *Fmr1* KO mice at PND 12, an age at which FMRP concentration is high in the brains of WT mice (Davidovic et al., 2011). Metabolite values showed regional variation in the WT mouse brain, reflecting maturational differences of region-specific function at this early developmental time point (Davidovic et al., 2011). The FVB *Fmr1* KO mice, however, displayed a poorly differentiated, more homogenous metabolic state across the same regions (Davidovic et al., 2011). The authors suggested that this less diverse metabolic profile in the brain regions studied in FVB *Fmr1* KO mice was due to delayed brain maturation and delayed functional anatomical differentiation (Davidovic et al., 2011).

In the present study, *in vivo* longitudinal developmental pattern of several important metabolites including the neurotransmitters glutamate and GABA, and also glutamine and choline were not different in the hippocampus of *Fmr1* KO mice compared to WT. In contrast, several key metabolites had different developmental profiles in *Fmr1* KO mice compared to controls. *Myo*-inositol/tCr was not different on PND 18 but was significantly decreased in *Fmr1* KO mice at PND 30 compared to controls. Taurine/tCr was significantly higher in the hippocampus of *Fmr1* KO mice than controls at all ages studied, and decreased 32% from PND 18 to 30 in *Fmr1* KO mice, compared to a 25% decrease in WT mice. The longitudinal data in the present study are

consistent with the findings of an HPLC study of brain amino acids (Gruss & Braun, 2001) that found increased taurine in the hippocampus of juvenile FVB *Fmr1* KO mice (PND 28-32), and no differences in glutamate, glutamine, and GABA between *Fmr1* KO and WT mice. Interestingly, the same study (Gruss & Braun, 2001) did not find any differences in the metabolite levels in the hippocampus or in the other brain regions studied between the adult FVB *Fmr1* KO mice and the adult WT mice (Gruss & Braun, 2001). The differences observed in metabolite levels *in vivo* in the present study, as well as data from the HPLC study of Gruss and Braun (Gruss & Braun, 2001) suggest that some of the alterations in hippocampal metabolites that occur in the young *Fmr1* KO mice from PND 18 to 30 can be transient. Indeed, the genotype difference in *N*-acetylaspartate /tCr was most apparent at PND 18 as the ratios were similar to controls at the older ages. The increased ratio of taurine/tCr at PND 18 and 21 in *Fmr1* KO mice were closer to, but still significantly higher than the values for WT mice at PND 30. However, this was not the case for all metabolites as the decrease of *myo*-Inositol/tCr ratio in *Fmr1* KO mice was more pronounced at 30 days compared to the WT, than at PND 21 where it only approached significance.

5.4.1. Change in *N*-acetylaspartate

N-acetylaspartate increases significantly in the brain from birth to adulthood (Birken & Oldendorf, 1989), and is a widely used clinical marker for neuronal health and/or neuronal mitochondrial integrity (Moffett et al., 2007). *N*-acetylaspartate is synthesized in neurons, released and taken up by oligodendrocytes where it is cleaved by the glial enzyme aspartoacylase to aspartate and acetyl CoA, which serves as an

important precursor for the synthesis of myelin lipids in the developing brain (Burri et al., 1991; Moffett et al., 2007; Urenjak et al., 1992). Decreased formation of *N*-acetylaspartate in neurons has been shown to impair myelination in developing brain (Degaonkar et al., 2002). Decreased *N*-acetylaspartate/tCr has been observed in the hippocampus of children with ASD (Chugani, 2012; Gabis et al., 2008; Kleinhans et al., 2007) and in other related disorders characterized by psychomotor delay (Chugani, 2012; Gabis et al., 2008). Such observations are particularly important since Kleinhans et al. (Kleinhans et al., 2007) demonstrated that the decrease of *N*-acetylaspartate concentration was correlated with decreased brain activation in the prefrontal cortex determined by functional MRI. The effect of genotype on *N*-acetylaspartate/tCr in *Fmr1* KO mice compared to WT suggests impairment in neuronal development, and/or in neuronal mitochondrial function in the hippocampus in this model of FXS.

N-acetylaspartate acts as an agonist to N-methyl-D-aspartic acid (NMDA) receptors in neurons (Rubin et al., 1995); suggesting the lower *N*-acetylaspartate at PND 18 in the *Fmr1* KO mice may be related to decreased activation of NMDA receptors in the hippocampus. However, the NMDA receptor-dependent LTD in the hippocampus of the developing *Fmr1* KO mice (PND 21-30) was not impaired (Huber et al., 2002) and previous findings show decreased long-term potentiation and decreased amplitude of excitatory postsynaptic current upon activation of NMDA receptors in the dentate gyrus of the young adult *Fmr1* KO mouse (2-4 months) (Bostrom et al., 2015; Yun and Trommer, 2011). Therefore, the lower *N*-acetylaspartate at PND 18 may not affect with reports of lower NMDA receptor activity in the adult *Fmr1* KO mouse (Bostrom et al., 2015; Yun and Trommer, 2011).

5.4.2. Alterations in osmoregulatory molecules in the hippocampus of *Fmr1* KO mice

N-acetylaspartate, taurine, and *myo*-inositol can all function as osmolytes in brain cells (Baslow, 2010; Estevez et al., 1999; Heilig et al., 1989). Baslow (Baslow, 2010) has proposed that release of *N*-acetylaspartate and *N*-acetylaspartylglutamate from neurons has a key role in regulating neuronal water and in overall brain function. Extracellular taurine has been shown to increase in response to hypoosmotic swelling (Davies, Gotoh, Richards, & Obrenovitch, 1998). Decreased *myo*-inositol/tCr has been reported in the hippocampus of ASD patients (Gabis et al., 2008), and in the temporoparietal junction in high functioning ASD patients (Bernardi et al., 2011) compared to age matched controls.

The significant effect of age in the present study shows that taurine/tCr and *myo*-inositol/tCr are also changing during development in both WT control and *Fmr1* KO mice. However, the increase of taurine and decrease of *myo*-inositol could cause alterations in brain osmoregulation. An increase in both taurine and *myo*-inositol was found in the hippocampus of the FVB *Fmr1* KO mice at PND 12 and such an increase could affect osmoregulation and phosphatidyl-inositol (PI) metabolism (Davidovic et al., 2011). The increase of *myo*-inositol at PND 12 in the hippocampus reported by Davidovic et al. (Davidovic et al., 2011) could be an age specific change or may reflect differences between the FVB model and the C57Bl6 strain of *Fmr1* KO mice. However, as noted below, alterations of *N*-acetylaspartate, taurine, and *myo*-inositol can have other effects beyond osmoregulation.

5.4.3. *Myo*-inositol

The enzyme phosphoinositide 3-kinase (PI3K) phosphorylates PI, and PI3K signaling plays an important role in differentiation and cell growth (Peltier et al., 2007; Sanchez et al., 2004). PI signaling involves continuous breakdown to *myo*-inositol by phosphatases and lipid resynthesis of PI from *myo*-inositol (Shears, 1989). The decreased *myo*-inositol/tCr in the hippocampus of *Fmr1* KO mice at PND 30 could contribute to alterations in PI3K signaling pathways during brain development. Increased PI3K activity in the hippocampus of *Fmr1* KO mice was shown in two different studies (Gross et al., 2010; Sharma et al., 2010) and a PI3K antagonist was able to rescue neurons from the *Fmr1* KO phenotype *in vitro* (Gross et al., 2010). PI increases steadily from gestational day 15 to PND 21 in WT mice (Yao et al., 1999). In the present study, we found *myo*-inositol/tCr increased from PND 21 to 30, consistent with the developmental profile reported by Kulak et al. (Kulak et al., 2010) for C57Bl6J WT mice. However, at PND 30 values for *myo*-inositol/tCr in the hippocampus of *Fmr1* KO mice in the present study were only 65% of the WT mice. Phosphatidylinositol 4,5-bisphosphate has a crucial role in the attachment of myelin basic protein to oligodendrocyte membranes (Nawaz et al., 2009). Reducing phosphatidylinositol 4,5-bisphosphate led to detachment of myelin basic proteins from oligodendrocyte membrane and loss of myelin compaction in the corpus callosum (Nawaz et al., 2009). Thus, the decrease of *myo*-inositol/tCr at PND 30 in *Fmr1* KO mice compared to WT mice could potentially contribute to alterations in both myelination and signal transduction in the hippocampus. The importance of *myo*-inositol in the brain is underscored by the report that the *myo*-inositol/tCr level was directly associated with performance IQ scores in ASD patients

(Gabis et al., 2008).

5.4.4. Taurine

The non-protein inhibitory amino acid taurine is present in high concentration in immature brain and decreases with age (Kulak et al., 2010; Lima et al., 2004). Taurine is a key osmolyte and also protects against the effects of glutamate excitotoxicity *in vitro* by stabilizing calcium concentration in the cytoplasm to basal levels (El Idrissi & Trenkner, 1999). Thus, an increased level of taurine could potentially protect mitochondria from the potentially harmful increase in intracellular calcium (Nicholls, 2009) resulting from NMDA receptor and/or mGluR5 activation. In the present study, the increased taurine/tCr in *Fmr1* KO mice at all ages may reflect delayed or altered maturation of the hippocampus compared to WT mice.

El Idrissi et al. (El Idrissi et al., 2010) showed that the taurine dependent decrease in paired-pulse inhibition observed in hippocampal slices from WT mice was not seen in hippocampal slices from adult *Fmr1* KO mice (2 months old). The same group showed that supplementation with taurine improved performance in inhibitory avoidance task in *Fmr1* KO mice (2 months old) compared to the non-treated group (El Idrissi et al., 2009). During the developmental window in the present study, taurine can have an inhibitory function in the brain (Curtis & Watkins, 1960) as the high concentration of taurine, found in the developing brain, can activate glycine and $GABA_A$ receptors of pyramidal cells in the immature rat hippocampus (Wu & Xu, 2003). The increased levels of taurine at PND 18, 21 and 30 in *Fmr1* KO compared to WT mice could contribute to neuroprotection by modulating the intracellular calcium levels, and by contributing to the inhibitory activity

in hippocampal neurons.

5.4.5. Neurotransmitters and related metabolites

Choline and choline containing lipids are important constituents of plasma membranes which are increased with cell density, thus the total choline peak is used as a marker of proliferation (Usenius et al., 1994; Warren et al., 2000). The total choline peak at 3.21 ppm contains both the excitatory neurotransmitter acetylcholine (Fan, 1996), which is involved in learning and plasticity (Broide & Leslie, 1999; Hasselmo, 2006; Shinoe et al., 2005), and phosphatidyl-choline which is a necessary component of myelin, which increases during brain development (Diamond, 1971; Loffelholz, 1998; Martinez & Mougan, 1998). *In vivo* MRS in FXS patients showed a decrease in relative choline concentration in the dorsolateral prefrontal cortex relative to control subjects (Kesler et al., 2009). Altered activity of muscarinic acetylcholine receptors in the *Fmr1* KO mice suggested a decrease in the cholinergic driven plasticity in the subiculum (D'Antuonoet al., 2003) and in the CA1 region of the hippocampus (Volk et al., 2007). These previous studies demonstrated deficits in the subregions of the hippocampus that may contribute to altered choline concentration, whereas our study found no differences in the developmental profile of Cho/tCr in the whole hippocampus in *Fmr1* KO mice compared to WT. However, acetylcholine released by cholinergic terminals innervating the hippocampus is likely to be synthesized within the lateral septum of the brain where these projections originate (McKinney et al., 1983; Parent & Baxter, 2004).

Glutamate is the major excitatory neurotransmitter in the brain, synthesized from α-ketoglutarate that is derived from glucose metabolism via the TCA cycle, or by

deamination of the metabolite glutamine which is synthesized in astrocytes (Danbolt, 2001; McKenna, 2007; Schousboe et al., 1997; Sonnewald & Kondziella, 2003). Consistent with the findings of Gruss and Braun (Gruss & Braun, 2001), we did not find any alteration in the ratios of glutamate, glutamine or GABA to tCr levels in the hippocampus between *Fmr1* KO and WT mice during the critical development period of myelination and synaptogenesis. It is important to note that glutamate and GABA are both highly compartmentalized in brain (Waagepetersen et al., 2003), thus the overall ratio in the hippocampus may mask alterations in specific hippocampal regions or changes in the distribution of these neurotransmitters. Indeed, reports from other groups demonstrate that the GABAergic system is affected by the absence of FMRP in *Fmr1* KO mice without an overall alteration of the GABA neurotransmitter concentration (El Idrissi et al., 2005; Gibson et al., 2008). There is clear evidence of an imbalance in excitatory versus inhibitory neurotransmission in *Fmr1* KO brain (Gibson et al., 2008). Decreased excitation of inhibitory neurons in the somatosensory cortex of FVB *Fmr1* KO mice at PND 14 and PND 28 has been reported (Gibson et al., 2008), as well as alterations in $GABA_A$ receptor activation (El Idrissi et al., 2005), receptor subunit expression in the cortex (D'Hulst et al., 2006) and decreased expression of glutamate decarboxylase (D'Hulst et al., 2009). These studies in GABAergic system of *Fmr1* KO mouse suggest that the reduction of inhibitory signaling may be due to altered GABA receptors rather than GABA neurotransmitter.

5.4.6. Hippocampal volume differences

The most striking difference observed was the increased hippocampal volume in

the brains of the *Fmr1* KO mice at all ages compared to WT mice. However, hippocampus volume have been shown to vary with age in FXS patients, decreased hippocampal volume was reported in boys with FXS (2-5 years old) (Hazlett et al., 2012), increased hippocampal volume has been reported in children with FXS (7 ± 5 years old) (Reiss et al., 1994), and decreased hippocampal volume was reported in young adults with FXS (18-24 years old) (Qin et al., 2013). The hippocampus is rich in FMRP in normal brain and it has been suggested that the altered growth of the hippocampus may be related to the absence of this protein in FXS (Bray et al., 2011). Increased density of dendritic spines and delayed morphological development of spines were found in the dentate gyrus (PND 15, 21, 30 and 60) (Grossman et al., 2010) and the CA1 region of the hippocampus (PND 8, 14, 21 and 60) (Sidhu et al., 2014) of developing *Fmr1* KO mice compared to the WT. Although differences in FMRP have not been reported for hippocampal subregions, the increased mGluR5-dependent LTD is thought to contribute to the alterations in dendritic spines in the hippocampus of *Fmr1* KO mice (Grossman et al., 2010; Sidhu et al., 2014). Reports that mGluR5 dependent LTD is altered in the CA1 region of the hippocampus in *Fmr1* KO mouse (PND 21-30) (Huber et al., 2002) suggests that alterations in the mGluR5 signaling pathway may be restricted to the CA1 region and may contribute to the regional differences in altered spine phenotype in the hippocampus of *Fmr1* KO mice (Grossman et al., 2010; Levenga et al., 2011). The increase of hippocampus volume we observed *in vivo* at PND 18, 21 and 30 in *Fmr1* KO mice (Figure 5-1) may reflect a developmental delay in the hippocampus as well as increased dendritic branching and branch densities, or may be related to alterations in the osmolyte profile, or altered synaptic plasticity in this region.

5.5. CONCLUSIONS

During the critical developmental period of synaptogenesis and early myelination included in this study, a number of alterations were observed, particularly in metabolites involved in osmoregulation, signal transduction, and neuromodulation in the hippocampus of *Fmr1* KO mice when compared to age matched controls. Although some alterations may be normalized in adulthood (Gruss & Braun, 2001), such profound metabolic perturbations during synaptogenesis and modulation of enduring neuronal connections could result in lifelong alterations in the hippocampus and can affect both neuronal and astrocytic functions. The alterations observed in these metabolites may contribute to the FXS phenotype observed in the *Fmr1* KO mouse.

Acknowledgements:

This study was supported by the Core for Translational Imaging at Maryland (C-TRIM), the FRAXA Research Foundation, and NIH P01 grant HD016596.

The authors do not have any conflicts of interests.

CHAPTER 6: WHITE MATTER ALTERATIONS IN *FMR1* KO MICE DURING EARLY POSTNATAL BRAIN DEVELOPMENT[1]

6.1. INTRODUCTION

Fragile X syndrome (FXS) is the most commonly inherited form of sex-linked intellectual disability affecting 1 in 5000 males (Coffee et al., 2009). FXS causes intellectual disability and behaviors commonly seen in the autism spectrum disorder, including hyperactivity, social anxiety, and attentional problems (Coffee et al., 2009; Garber et al., 2008). FXS is caused by the mutational insertion of CGG trinucleotide repeats which leads to the epigenetic silencing of the *FMR1* gene (Verkerk et al., 1991). The silencing results in the loss of the mRNA binding protein (Ashley et al., 1993), the fragile X mental retardation protein (FMRP) (Devys et al., 1993). FMRP regulates the translation of hundreds of neuronal mRNAs, including many proteins necessary for synaptic integrity and function (Darnell et al., 2011). The loss of FMRP leads to elevated levels of protein synthesis in the brain (Qin et al., 2005), impaired regulation of neuronal signaling and synaptic plasticity (Bailey et al., 2012; Berry-Kravis et al., 2012; Cea-Del Rio & Huntsman, 2014; Gross et al., 2012; Hagerman et al., 2012; Martin & Huntsman, 2012; Paluszkiewicz et al., 2011), and elevated levels of immature dendritic spines in the cortex and hippocampus (Bilousova et al., 2009; Grossman et al., 2010; Irwin et al., 2001; Pan et al., 2010). These morphological alterations may contribute to symptoms associated with FXS (Garber et al., 2008; Kidd et al., 2014). A preclinical model of FXS,

[1] Da Shi, Su Xu, Jiachen Zhuo, Mary C. McKenna, and Rao P. Gullapalli. In preparation for submission.

the *Fmr1* knockout (KO) mouse (Bakker et al., 1994), is commonly used to study FXS and models many of the clinical manifestations of FXS.

6.1.1. Alteration of myelin in fragile X syndrome

While much of the research in FXS focuses on elucidating the biological changes associated with neurodevelopmental symptoms (Bailey et al., 2012; Berry-Kravis et al., 2012;), recent findings have shown alterations of astrocytes and oligodendrocyte function in the *Fmr1* KO mouse brain (Jacobs & Doering, 2010; Pacey et al., 2013; Wang et al., 2004). Astrocytes from *Fmr1* KO mouse brain can influence co-cultured neurons from the WT mouse brain to express increased axonal branching and immature dendritic spine density (Cheng et al., 2012; Jacobs & Doering, 2010; Jacobs et al., 2012). Previous studies have demonstrated that FMRP binds to many of the mRNAs of myelin proteins (Darnell et al., 2011), including myelin basic protein (Darnell et al., 2011; Wang et al., 2004), an abundant and key protein that ensures the stability of myelin sheaths (Harauz et al., 2009). FMRP also binds to other essential proteins found in mature oligodendrocytes including 2' 3'-cyclic-nucleotide 3'-phosphodiesterase (CNP), proteolipid protein, and myelin-associated glycoprotein (Darnell et al., 2011). Although the role of FMRP in oligodendrocyte maturation is still unknown, pre- and immature oligodendrocytes contain FMRP, while FMRP levels are greatly reduced in mature oligodendrocytes (Gholizadeh et al., 2015; Wang et al., 2004).

A recent study has provided evidence of delayed myelination in the cerebellar white matter of *Fmr1* KO mice during early postnatal development (Pacey et al., 2013). The study by Pacey et al. (Pacey et al., 2013) show reduced myelin thickness and reduced

concentrations of myelin basic protein and CNP at PND 7, followed by a normalization of cerebellar myelin thickness and protein levels at PND 30 (Pacey et al., 2013). Myelin basic protein levels then become elevated in cerebellar white matter of adult *Fmr1* KO mice (2-4 months old) (Pacey et al., 2013). Thus, the loss of FMRP regulation has a developmental influence on myelination and may cause a delay in myelination in the *Fmr1* KO mouse brain (Pacey et al., 2013).

Imaging studies of the *Fmr1* KO mouse brain have also revealed differences in regional brain volume, including an increase in hippocampal and a decrease in cerebellar volumes, as well as changes in brain metabolite concentrations that may influence myelination (Ellegood et al., 2010; Pacey et al., 2013; Shi et al., 2012). In children with FXS, increased overall white matter volume and changes in regional white matter volume during brain development have been reported (Hazlett et al., 2012; Hoeft et al., 2010). However, very little has been done to further characterize the underlying alterations associated with changes in brain volume using advanced imaging techniques in FXS patients and *Fmr1* KO mouse brains. Taken together, these studies provide evidence that alterations in white matter development may contribute to the neurodevelopment of FXS pathology.

6.1.2. Detecting changes in myelin using MRI

Changes in the relative levels of macromolecules can be detected using magnetization transfer (MT), a technique that exploits the exchange between the bound protons in the macromolecules and the protons in free water, providing a contrast that is reflective of the concentration of macromolecules present in tissue (Finelli et al., 1996;

Finelli et al., 1998; Henkelman et al., 2001; Wolff & Balaban, 1989). In white matter, such a contrast would be reflective of myelin water content since myelin macromolecules serve as the major pool of bound protons and it has been demonstrated that cholesterol and myelin lipids contribute significantly to the MT effect (Koenig et al., 1990; Stanisz et al., 1999). Normal myelin is composed of 70-85% lipids and 15-30% proteins (Quarles et al., 2012). Thereby, MT would provide an index of relative molecular content of white matter (Wozniak & Lim, 2006). As myelin macromolecule levels decrease, the MT is also expected to decrease between the free proton pool and the bound pool, indicating a decrease in myelin proteins and lipids. The decrease of MT would be expected in the white matter of *Fmr1* KO mice since reduced myelin proteins have been found in developing cerebellar white matter (Pacey et al., 2013) and reduced cholesterol and low density lipoproteins in FXS patients (Berry-Kravis et al., 2015). Transverse relaxation time T_2 provides information on the white matter environment with T_2-values decreasing with the extent of myelination within white matter (Paus et al., 2001). Together, these MRI techniques are sensitive to the chemical and physical environments of water protons and are commonly used to characterize developmental and pathological changes in white matter (Bonnier et al., 2014; Ou et al., 2009; Schmierer et al., 2004; Thiessen et al., 2013; Wozniak & Lim, 2006).

Given the strong evidence for the involvement of white matter and the myelin changes associated with FXS, including altered white matter volumes, reduced myelin thickness and alteration of myelin protein concentration (Hazlett et al., 2012; Hoeft et al., 2010; Pacey et al., 2013), we hypothesized decreased myelin is found in white matter during brain development in *Fmr1* KO mouse. Using MT and T_2 imaging, we assessed

white matter development in the corpus callosum, external capsule, internal capsule, cerebral peduncle and hippocampal fimbria in *ex vivo* preparations of *Fmr1* KO and WT mouse brains. We made measurements at critical time points in the course of myelination and neural network development, with PND 18 being before, and PND 21 during the peak of myelination and synaptogenesis in rodents (Semple et al., 2013). Additionally, neural network development has been shown to occur between PND 25-35 and is essentially mature by PND 60 (Semple et al., 2013). Myelination is ongoing throughout the ages studied and only declines in late adulthood, around 18 months, in rodents (Andersen, 2003; Xie et al., 2013). Histological myelin staining was used to verify results from T_2 relaxation time and MT imaging.

6.2. METHODS AND MATERIALS

6.2.1. Animal procedure

Fmr1 KO mice (JAX B6.129P2-fmr1^{tmICgr} mice; Jackson Laboratory, Bar Harbor, ME, USA) from a C57Bl6J background were bred at the University of Maryland, Baltimore. The Institutional Animal Care and Use Committee at the University of Maryland, Baltimore approved the protocol used in this study. All mice were weaned at PND 21. Food and water were given ad libitum. Breeding and genotyping protocols were listed in Chapter 4.

We studied mice at PND 18 (9 *Fmr1* KO, 9 WT), PND 21 (12 *Fmr1* KO, 14 WT), PND 30 (13 *Fmr1* KO, 12 WT, and PND 60 (6 *Fmr1* KO, 6 WT). Once animals reached the appropriate age, the male *Fmr1* KO and WT mice were anesthetized with 4% isoflurane and perfused through the left ventricle with 1X phosphate buffered saline

(PBS), followed by 4% paraformaldehyde fixative. The whole brain was removed from the skull and immersed in fixative for 48 hours. The fixed brain was then immersed in PBS for 1 week to decrease the effect of the fixative on T_2 relaxation time and MTR (Schmierer et al., 2008; Shepherd et al., 2009). These steps were tightly controlled in order to minimize any variations associated with tissue processing. The fixed brains were placed in a customized conical tube filled with a proton-free susceptibility-matching fluid Fluorinert (3M, St. Paul, MN) prior to MR imaging. Fluorinert does not degrade the sample because it is biologically inert (Flaim, 1994) and has been safely used for *in vivo* molecular imaging (Giraudeau et al., 2013; Kaneda, et al., 2009; Liao et al., 2013).

6.2.2. Magnetic resonance imaging

All experiments were performed on a Bruker Biospec 7.0 Tesla 30 cm horizontal bore scanner (Bruker Biospin MRI, Ettlingen, Germany) using Paravision 5.1 software. A Bruker 72-mm linear-volume coil as the transmitter and a four-channel Bruker ^{1}H surface array coil as the receiver were used for imaging. Prior to imaging, magnetic field inhomogeneity was adjusted using the FASTMAP technique (Gruetter, 1993b). Anatomical images were obtained using a 3D TurboRARE sequence covering a slab of 15 mm in thickness to obtain T_2-weighted images at a spatial resolution of 113 μm X 150 μm X 170 μm, using an echo time (TE) and repeat time (TR) of 11 ms and 2500 ms, respectively, with two averages. Quantitative information on T_2-relaxation time was obtained using an eight echo multi-echo spin echo sequence with three continuous slices centered on the hippocampus at Bregma -1.82, without any gap. The spatial resolution was 200 μm X 200 μm, acquired with 1 mm slice thickness, TEs of 9.3, 27.9, 46.5, 65.1,

83.7, 102.3, 120.9, and 139.5 ms at a TR of 10000 ms, and 2 averages.

MT imaging provides contrast based on the chemical exchange between free protons in water and bound protons in macromolecules such as proteins and lipids (Finelli et al., 1996; Finelli et al., 1998; Henkelman et al., 2001; Wolff & Balaban, 1989). The signal differences in MT images with and without the off-resonance saturation pulse to saturate the protons in the macromolecules reveals relative macromolecule abundance, and is measured as magnetization transfer ratio (MTR) (Henkelman et al., 2001; Wolff & Balaban, 1989).The MT images were obtained using a fast low shot (FLASH) T_1 technique. Acquisition parameters were slice thickness 0.5 mm, 0.5 mm gap, 16 slices that covered the cerebral cortex and the cerebellum, spatial resolution of 200 μm X 200 μm over a field of view of 1.5 cm X 1.5 cm, TE/TR = 3.6/280 ms, and 32 averages. For the MT images (M_s), a Gaussian off-resonance saturation pulse was used with duration of 12.6 ms and flip angle of 180 degrees at an off-resonance frequency of 5000Hz from the center frequency of water protons. The reference MT image (M_o) was scanned using the same parameters except without the off-resonance pulse.

6.2.3. Image Processing

Images were transferred offline to an independent database for further processing. Medical Image Processing, Analysis and Visualization tool (MIPAV v5.3.1, CIT; NIH, Bethesda, MD, USA) was used to obtain volumes of different regions and to extract information for computing MTR. MTR was calculated as $[(M_0-M_s) / M_0] \times 100$, where M_0 is the signal intensity from images obtained without the off-resonance pulse and M_s is the signal intensity from images where the saturation pulse was applied (Henkelman et

al., 2001). Normalized white matter volume was obtained by dividing each regional white matter volume by whole brain volume. Regions of interest (ROIs) were drawn manually on both the 3D T_2 anatomical and MT images by comparison with an anatomical reference (Franklin & Paxinos, 2007). ROIs included the whole brain, corpus callosum, external capsule, internal capsule, cerebral peduncle, fimbria, and cerebellar white matter. T_2 relaxation time was measured using an in-house Matlab program (Mullins et al., 2013). The data from all echo times for each ROI were fitted to a mono-exponential decay curve. The first echo at 9.3 ms was ignored to minimize potential contamination from the stimulated echo. The volumes, the T_2 relaxation time, and the MTR values from each ROI were obtained and analyzed for statistically significant differences. The cerebellar white matter T_2 was not available since the coverage for the multi-echo T_2 acquisition did not extend into the cerebellum and only MTR data was available for the cerebellar white matter.

6.2.4. Histology

Following MRI, six of the perfused brains from each genotype and age were placed in 30% sucrose solution for cryoprotection. Brains were then frozen and coronal sections 40 μm in thickness were prepared with a cryostat at -20ºC . One section was collected for every 12 sections, approximately 0.50 mm apart. Sections were stained for myelin with Black Gold II (EMD Millipore, Billerica, MA) by the following procedure described by Schmued et al. (Schmued et al., 2008). Mounted slides were rehydrated with two washes of de-ionized water, followed by staining in 0.3% Black Gold II and saline solution at 60ºC. After staining was complete, the slides were washed in 1%

sodium thiosulfate solution at 60ºC followed by three washes in water at room temperature (Schmued et al., 2008). Images were taken on a brightfield Olympus BX53 Research Microscope at 10X magnification and analyzed using Bioquant Life Sciences 2013 v13.5.6 software (Bioquant Image Analysis Inc. Nashville, TN). A white field correction was applied to all images prior to obtaining integrated optical density. The red channel was used to determine density because Black Gold II stains myelinated fibers red-brown. Optical densities were measured between Bregma 0.50 mm to -2.46 mm which included 5-6 sections of the corpus callosum and external capsule, 1-2 sections with the internal capsule, 2-3 sections for cerebral peduncle, and 3-4 sections for the fimbria. The intensity of myelin staining in white matter regions was measured as optical density. The optical density was calculated as the log of the intensity of the ROI divided by the intensity of the background (Kayser et al., 1994). The optical density value was normalized to the area (in μm^2) of the ROI.

6.2.5. Statistical Analysis

All statistical analyses were performed in SPSS (IBM Corp. 2013. IBM SPSS Statistics for Windows, Version 22.0. Armonk, NY). A separate two-way analysis of variance (ANOVA) was performed for each region in each parameter, including volume, normalized volume, MTR, T_2 relaxation, and myelin density. Each two-way ANOVA compared the effect of genotype, age, as well as the interaction of (genotype X age). Genotype and age effects were analyzed by Student's t-tests if the interaction between factors was statistically significant ($p < 0.05$). To control for multiple pairwise comparisons, a false discovery rate with threshold of alpha = 0.05 was performed on the

p-values. The threshold assumes 5% of significant p-values may be false positives, and if a significant p-value does not pass false discovery rate then that p-value may be a false positive.

6.3. RESULTS

6.3.1. White matter volumes

Previous studies showed regional brain volumes in both FXS patients and *Fmr1* KO mice were different compared to controls (Ellegood et al., 2010; Hazlett et al., 2012; Hoeft et al., 2010; Pacey et al., 2013; Shi et al., 2012). However, no differences in whole brain or white matter volumes were found between *Fmr1* KO and WT mice (Table 6-1 and Figure 6-1, respectively). The white matter volume normalized to whole brain volume was also not significantly different between *Fmr1* KO and WT mice (Table 6-2). The (genotype X age) interaction was not statistically significant in the whole brain volume, regional white matter volumes (Table 6-3), as well as normalized regional white matter volumes (Table 6-4), indicating that the developmental courses of change in white matter volumes were similar between the two genotypes. The normalized white matter volume from this study was similar to a recent study which reported no differences in whole brain volumes and regional white matter normalized to whole brain volume at PND 60 between *Fmr1* KO and WT C57Bl6J mouse brains (Lai et al., 2016).

Whole brain volume (mm^3)				
Age	WT	SE	*Fmr1* KO	SE
PND 18	352.09	22.64	341.82	5.94
PND 21	342.47	9.58	376.16	14.71
PND 30	360.60	5.13	302.66	37.65
PND 60	387.02	4.72	412.60	15.97

Table 6-1: Whole brain volume (mm^3) of WT and *Fmr1* KO mice. The mean and standard error (SE) for the whole brain volume are shown at PND 18, 21, 30 and 60. No significant interaction of (genotype X age) was found with whole brain volume.

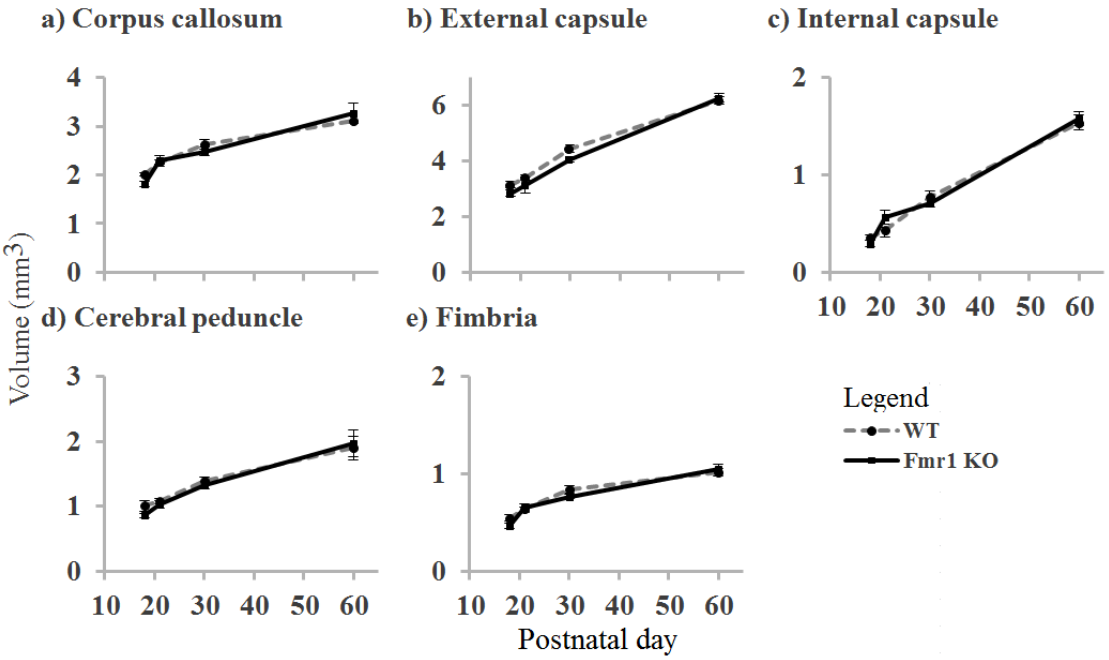

Figure 6-1: Regional white matter volume (mm^3; mean ± standard error) in the developing WT (gray dashed line) and *Fmr1* KO (black solid line) brains; a) the corpus callosum, b) external and c) internal capsule, d) cerebral peduncle, and e) fimbria. The ages studied were PND 18, 21, 30, and 60. Interaction of (genotype X age) was not significant in white matter regions.

Mean Normalized Volume				
Corpus callosum	WT	SE	*Fmr1* KO	SE
PND 18	0.0061	0.0004	0.0055	0.0002
PND 21	0.0067	0.0002	0.0061	0.0002
PND 30	0.0072	0.0002	0.0069	0.0002
PND 60	0.0080	0.0002	0.0079	0.0003
External capsule	WT	SE	*Fmr1* KO	SE
PND 18	0.0096	0.0009	0.0086	0.0005
PND 21	0.0100	0.0004	0.0091	0.0004
PND 30	0.0123	0.0004	0.0113	0.0002
PND 60	0.0160	0.0003	0.0152	0.0004
Internal capsule	WT	SE	*Fmr1* KO	SE
PND 18	0.0011	0.0001	0.0009	0.0001
PND 21	0.0013	0.0001	0.0014	0.0001
PND 30	0.0021	0.0002	0.0020	0.0001
PND 60	0.0040	0.0002	0.0038	0.0001
Cerebral peduncle	WT	SE	*Fmr1* KO	SE
PND 18	0.0031	0.0004	0.0026	0.0000
PND 21	0.0032	0.0001	0.0028	0.0001
PND 30	0.0038	0.0001	0.0037	0.0001
PND 60	0.0049	0.0005	0.0048	0.0006
Fimbria	WT	SE	*Fmr1* KO	SE
PND 18	0.0017	0.0002	0.0014	0.0001
PND 21	0.0019	0.0001	0.0017	0.0001
PND 30	0.0023	0.0001	0.0021	0.0001
PND 60	0.0026	0.0001	0.0026	0.0001

Table 6-2: Normalized white matter volumes in *Fmr1* KO and WT mice. Normalized volume was calculated by dividing regional white matter volume (mm^3) by its respective whole brain volume (mm^3). The mean normalized volume and SE for each white matter region in the *Fmr1* KO and WT mouse brain are presented at PND 18, 21, 30 and 60.

Volume	Region	df	F-value	p-value
Genotype	Whole brain	1	0.701	0.405
	Corpus callosum	1	0.315	0.577
	External capsule	1	1.535	0.220
	Internal capsule	1	0.048	0.827
	Cerebral peduncle	1	0.038	0.846
	Fimbria	1	0.266	0.608
Age	Whole brain	3	238.515	< **0.001**
	Corpus callosum	3	46.699	< **0.001**
	External capsule	3	189.351	< **0.001**
	Internal capsule	3	203.613	< **0.001**
	Cerebral peduncle	3	50.557	< **0.001**
	Fimbria	3	77.064	< **0.001**
Genotype X age	Whole brain	3	1.861	0.144
	Corpus callosum	3	1.095	0.357
	External capsule	3	1.394	0.252
	Internal capsule	3	1.369	0.260
	Cerebral peduncle	3	0.273	0.845
	Fimbria	3	0.884	0.453
Error	Whole brain	73		
	Corpus callosum	73		
	External capsule	73		
	Internal capsule	73		
	Cerebral peduncle	73		
	Fimbria	73		

n	WT	*Fmr1* KO
PND 18	9	9
PND 21	14	12
PND 30	12	13
PND 60	6	6

Table 6-3: Summary of two-way ANOVA for the whole brain and regional white matter volumes. The F-value and p-value for genotype, age, and interaction of (genotype X age) are presented. An interaction with p-value of 0.05 or less was considered significant (in bold). An independent Student's T-test was performed if there was a significant interaction with (genotype X age).

Normalized white matter volume Two way ANOVA Normalized volume	Region	df	F-value	p-value
Genotype	Corpus callosum	1	0.001	0.978
	External capsule	1	0.080	0.779
	Internal capsule	1	0.176	0.676
	Cerebral peduncle	1	0.061	0.806
	Fimbria	1	0.018	0.893
Age	Corpus callosum	3	23.729	< **0.001**
	External capsule	3	0.912	0.440
	Internal capsule	3	49.319	< **0.001**
	Cerebral peduncle	3	0.146	0.932
	Fimbria	3	3.313	0.025
Genotype X age	Corpus callosum	3	0.029	0.993
	External capsule	3	0.185	0.906
	Internal capsule	3	1.405	0.249
	Cerebral peduncle	3	0.293	0.831
	Fimbria	3	0.134	0.940
Error	Corpus callosum	73		
	External capsule	73		
	Internal capsule	73		
	Cerebral peduncle	73		
	Fimbria	73		

n	WT	*Fmr1* KO
PND 18	9	9
PND 21	14	12
PND 30	12	13
PND 60	6	6

Table 6-4: Summary of two-way ANOVA for normalized white matter volume. The normalized volume was calculated by dividing the regional white matter volume by the whole brain volume for each mouse. The F-value and p-value for genotype, age, and interaction of (genotype X age) are presented.

6.3.2. T_2 relaxation time

T_2 relaxation time can provide insights into white matter environment; generally T_2 relaxation time decreases following development of white matter (Paus et al., 2001). T_2 relaxation time was measured in the corpus callosum, external capsule, internal capsule, cerebral peduncle, and fimbria (Figure 6-2a-e, respectively). Poor signal to noise prevented analysis of one *Fmr1* KO mouse brain at PND 30. The (genotype X age) interaction was not statistically significant in the white matter regions studied (Table 6-5) indicating that changes in T_2 relaxation time over the course of development were not different between the two genotypes. In all five white matter regions T_2 relaxation times

decreased between PND 18 and PND 30 in WT mice as expected over the course of myelination. In *Fmr1* KO mice, however, decreases were seen between PND 21 and PND 30, suggesting that myelination was delayed.

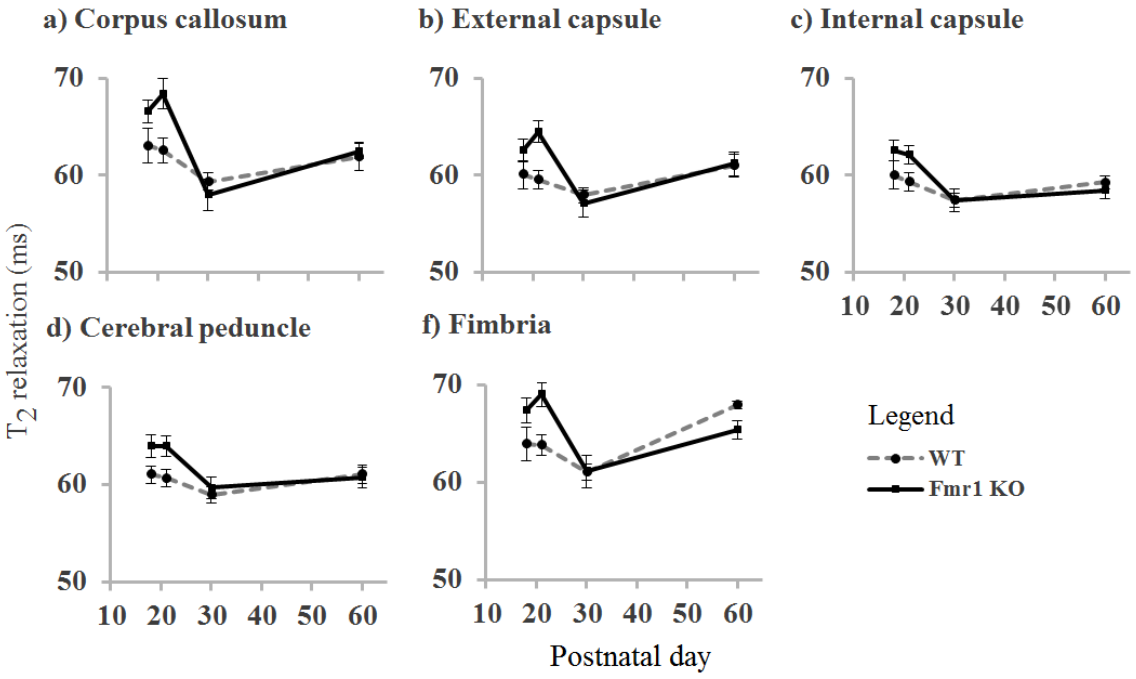

Figure 6-2: T_2 relaxation times (ms ± standard error) between WT (gray dashed line) and *Fmr1* KO (black solid line) mice at PND 18, 21, 30 and 60. Relaxation times were measured in white matter regions of the a) corpus callosum, b) external and c) internal capsule, d) cerebral peduncle, and e) fimbria. No significant (genotype X age) interaction was found in T_2 relaxation.

T_2 relaxation	Region	df	F-value	p-value
Genotype	Corpus callosum	1	2.091	0.153
	External capsule	1	3.050	0.085
	Internal capsule	1	0.594	0.443
	Cerebral peduncle	1	0.927	0.339
	Fimbria	1	1.393	0.242
Age	Corpus callosum	3	8.662	< **0.001**
	External capsule	3	6.186	< **0.001**
	Internal capsule	3	2.573	0.061
	Cerebral peduncle	3	2.084	0.110
	Fimbria	3	6.036	< **0.001**
Genotype X age	Corpus callosum	3	1.337	0.269
	External capsule	3	1.504	0.221
	Internal capsule	3	0.685	0.564
	Cerebral peduncle	3	1.659	0.184
	Fimbria	3	1.854	0.145
Error	Corpus callosum	72		
	External capsule	72		
	Internal capsule	72		
	Cerebral peduncle	72		
	Fimbria	72		

n	WT	*Fmr1* KO
PND 18	9	9
PND 21	14	12
PND 30	12	12
PND 60	6	6

Table 6-5: Summary of two-way ANOVA for T_2 relaxation. The F-value and p-values for genotype, age, and (genotype X age) interaction are presented. Statistically significant effects (p-value of 0.05 or less) are indicated in bold. The genotype X age interactions were not statistically significant in any of the white matter regions.

6.3.3. Magnetization Transfer Ratio

Magnetization transfer ratios are an index of macromolecular content in white matter, including myelin proteins and lipids that contribute to the structural integrity of white matter (Wozniak & Lim, 2006). The alterations in white matter maturation as indicated by MTR differed between the genotypes (Figure 6-3). Significant (genotype X age) interaction was found in all white matter regions studied (Table 6-6). Before the peak of myelination at PND 18, MTR in the white matter regions of *Fmr1* KO mice was decreased in the internal capsule ($t(2.56)$ $p<0.05$), cerebral peduncle ($t(2.41)$ $p<0.05$), and

fimbria ($t(2.42)$ $p<0.05$) (Figure 6-3) compared to WT mice. MTR in the *Fmr1* KO mouse brain showed a steep increase between PND 18 and PND 30 followed by a decrease or leveling off between PND 30 and PND 60 (Figure 6-3). In WT mice, MTR tended to be fairly level between PND 18 and PND 30 and increased thereafter (Figure 6-3). At PND 60 when the brain networks are more mature (Semple et al., 2013), MTR in all regions examined was higher in WT mice compared with *Fmr1* KO mice (Figure 6-3). The significant p-values from multiple pairwise comparisons passed false discovery rate with a threshold of alpha = 0.05. The developmental differences in MTR between *Fmr1* KO and WT mouse brains suggested a decrease of myelin components at PND 18 and 60 in the white matter of *Fmr1* KO mouse brain. Alterations in MTR suggested the macromolecule content of white matter, including myelin proteins and lipids, fluctuated during development in the *Fmr1* KO mouse brain that could severely impact myelin structure.

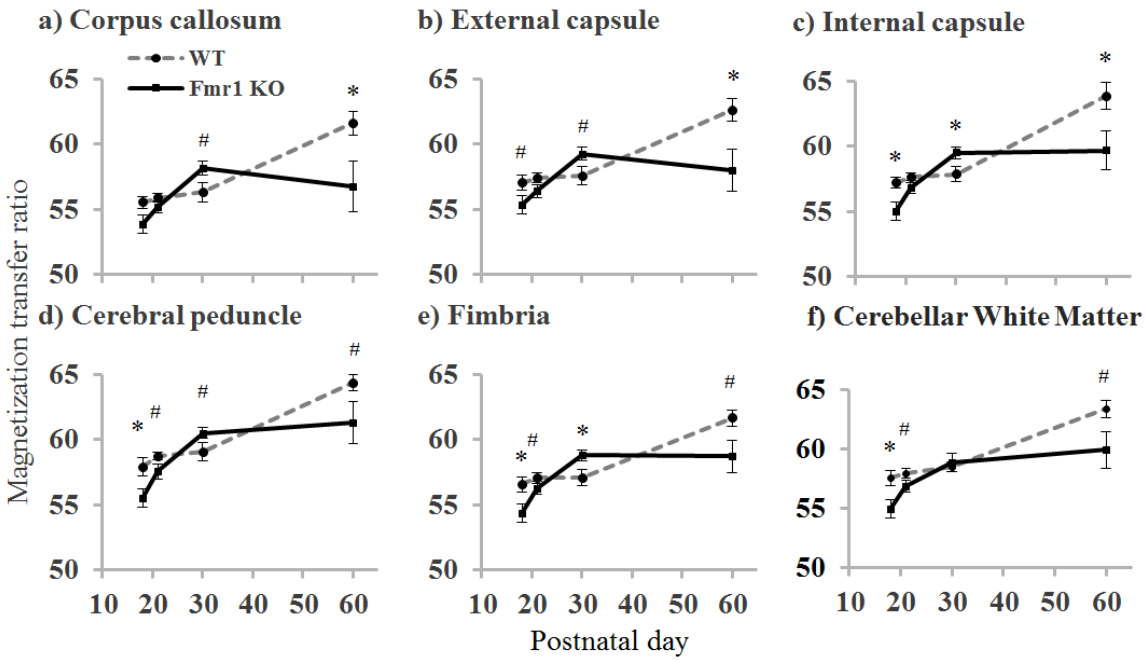

Figure 6-3: Magnetization transfer ratio (MTR; mean ± standard error) from regional white matter between WT (gray dashed line) and *Fmr1* KO mice (black solid line) in the a) the corpus callosum, b) external and c) internal capsule, d) cerebral peduncle, e) fimbria, and f) cerebellar white matter at PND 18, 21, 30, and 60. The significant (genotype X age) was found in all white matter regions. The significant genotype differences in MTR between WT and *Fmr1* KO mice are marked with * $p < 0.05$. Near significant genotype trends are marked with # $p < 0.10$. The significant p-values passed false discovery rate (alpha = 0.05).

MTR	Region	df	F-value	p-value
Genotype	Corpus callosum	1	6.722	**0.011**
	External capsule	1	8.406	**< 0.001**
	Internal capsule	1	9.365	**< 0.001**
	Cerebral peduncle	1	7.511	**0.008**
	Fimbria	1	6.722	**0.011**
	Cerebellar white matter	1	12.007	**0.001**
Age	Corpus callosum	3	12.382	**< 0.001**
	External capsule	3	11.332	**< 0.001**
	Internal capsule	3	23.117	**< 0.001**
	Cerebral peduncle	3	24.028	**< 0.001**
	Fimbria	3	19.115	**< 0.001**
	Cerebellar white matter	3	17.315	**< 0.001**
Genotype X age	Corpus callosum	3	6.568	**< 0.001**
	External capsule	3	6.492	**< 0.001**
	Internal capsule	3	7.111	**< 0.001**
	Cerebral peduncle	3	4.565	**0.005**
	Fimbria	3	6.417	**< 0.001**
	Cerebellar white matter	3	2.913	**0.040**
Error	Corpus callosum	73		
	External capsule	73		
	Internal capsule	73		
	Cerebral peduncle	73		
	Fimbria	73		
	Cerebellar white matter	73		

n	WT	*Fmr1* KO
PND 18	9	9
PND 21	14	12
PND 30	12	13
PND 60	6	6

Table 6-6: Summary of two-way ANOVA for MTR. The F-value and p-value for genotype, age, and genotype X age interaction are presented. Statistically significant effects (p-value of 0.05 or less) are indicated in bold. An independent Student's T-test was performed if there was a significant (genotype X age) interaction.

6.3.4. Myelin staining

To directly determine myelin content in our animals we stained tissue with Black Gold II, a histological indicator of myelin. Figure 6-4a shows myelin staining of a representative section from each genotype at each age. Myelin density was decreased in *Fmr1* KO mouse brain at PND 18 in the external capsule ($t(6.88)$, $p<0.001$), internal capsule ($t(3.50)$, $p<0.001$), and fimbria ($t(2.01)$, $p<0.05$) compared to the corresponding

regions of the WT mouse brain (Figure 6-4c, d, and f, respectively). Myelin density at PND 21 was increased in the cerebral peduncle of *Fmr1* KO mouse brain compared to the WT ($t(2.10)$, $p<0.05$). By PND 30, the myelin density increased in *Fmr1* KO mouse brain, including the external capsule ($t(4.82)$, $p<0.001$), internal capsule ($t(2.11)$, $p<0.05$), cerebral peduncle ($t(2.45)$, $p<0.05$), and fimbria ($t(4.61)$, $p<0.001$) compared to the corresponding regions of the WT mouse brain (Figure 6-4b, c, d, e, and f, respectively). In contrast to PND 30, at PND 60 the myelin density in *Fmr1* KO mouse brain decreased compared to the WT in the external capsule ($t(6.61)$, $p<0.001$) (Figure 6-4c). The significant p-values passed false discovery rate (alpha = 0.05) for multiple pairwise comparisons. In agreement with the MTR data, many of the white matter regions in *Fmr1* KO mouse brains had decreased myelin density at PND 18 followed by increased levels at PND 30 and decreased at PND 60 compared to the corresponding regions of WT mouse brain (Figure 6-4). An age related increase in myelin density in the *Fmr1* KO mouse brain between PND 18 to PND 30, whereas the increase with age was more pronounced in the WT mouse brain between PND 30 to PND 60 (Figure 6-4). Myelin density measured from Black Gold II staining showed significant interaction of (genotype X age) in the external capsule, internal capsule, cerebral peduncle and fimbria (Table 6-7).

In addition, the myelin staining in the white matter regions of *Fmr1* KO mice had different developmental time courses than the WT mice (Figure 6-4). In WT mice myelin density increased steeply between PND 30 and PND 60 in the corpus callosum and external capsule whereas in *Fmr1* KO mice steep increases occurred between PND 18 and PND 30 and tended to level off thereafter. In the internal capsule, cerebral

peduncle and hippocampal fimbria of WT mice myelin staining increased steadily from PND 18 to PND 60, whereas in *Fmr1* KO mice the slopes of increase tended to decrease after PND 30. The alterations in myelin density in developing *Fmr1* KO mouse brain suggest that FMRP can influence white matter maturation, potentially by regulation of the mRNA of myelin proteins (Darnell et al., 2011).

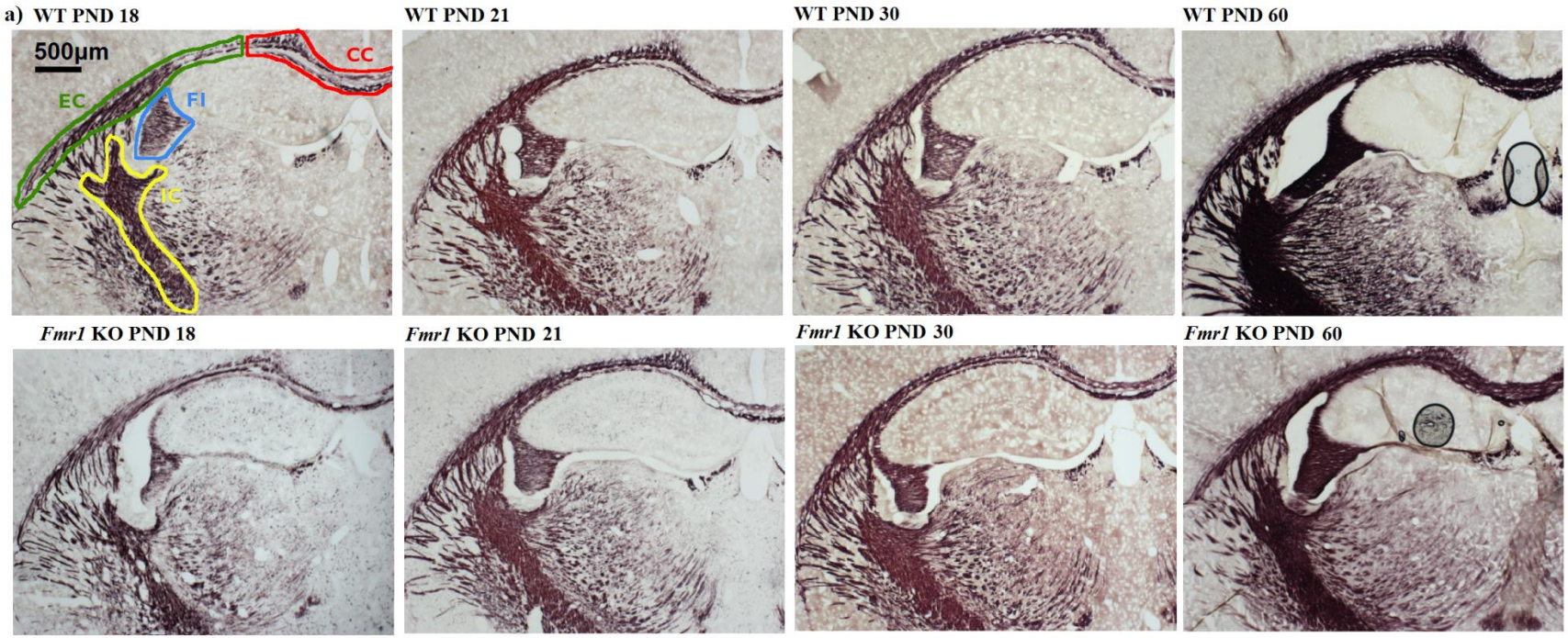
a) WT PND 18
500µm
CC
EC
FI
IC
WT PND 21
WT PND 30
WT PND 60
Fmr1 KO PND 18
Fmr1 KO PND 21
Fmr1 KO PND 30
Fmr1 KO PND 60

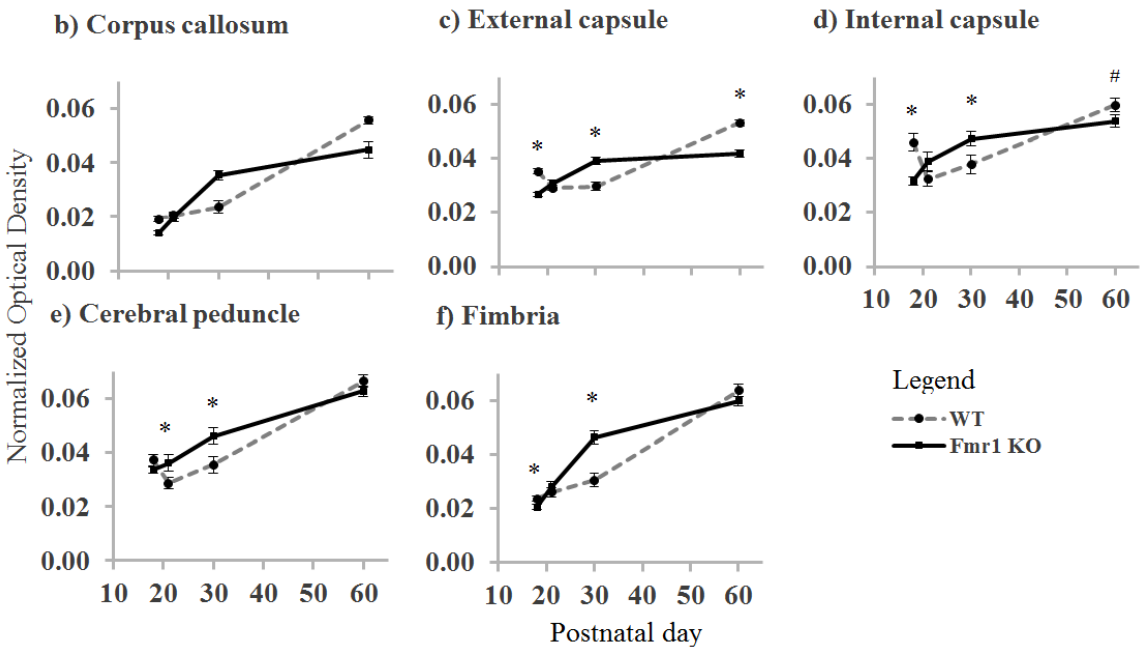

Figure 6-4: a) Representative images of myelin staining with Black Gold II in WT and *Fmr1* KO mouse brains. a) Approximate ROIs are drawn in a) with corpus callosum in red, external capsule in green, internal capsule in yellow, and fimbria in blue. The cerebral peduncle is not shown but is posterior to the internal capsule. The images were taken between Bregma -1.70 to -2.30 at PND 18, 21, 30 and 60. The scale bar represents 500 µm. Myelin density was measured by integrated optical density normalized to the area of the ROI. Myelin density determined by IOD (mean ± standard error) in white matter regions including the: b) corpus callosum, c) external capsule, d) internal capsule, e) cerebral peduncle and f) fimbria. Normalized optical densities in WT brain are shown with a gray dashed line and *Fmr1* KO optical density values are shown by a black solid line for each white matter region. Significant differences between *Fmr1* KO and WT myelin density were indicated with * $p < 0.05$, near significant differences were indicated with # $p < 0.10$. The significant p-values passed false discovery rate (alpha = 0.05).

Black Gold II	Region	df	F-value	p-value
Genotype	Corpus callosum	1	1.730	0.191
	External capsule	1	28.056	< **0.001**
	Internal capsule	1	5.313	**0.023**
	Cerebral peduncle	1	0.959	0.329
	Fimbria	1	6.748	**0.010**
Age	Corpus callosum	3	18.787	< **0.001**
	External capsule	3	129.770	< **0.001**
	Internal capsule	3	80.925	< **0.001**
	Cerebral peduncle	3	60.244	< **0.001**
	Fimbria	3	15.299	< **0.001**
Genotype X age	Corpus callosum	3	1.469	0.226
	External capsule	3	12.287	< **0.001**
	Internal capsule	3	3.960	**0.010**
	Cerebral peduncle	3	2.993	**0.033**
	Fimbria	3	3.665	**0.014**
Error	Corpus callosum	133		
	External capsule	133		
	Internal capsule	133		
	Cerebral peduncle	133		
	Fimbria	133		

n	WT	*Fmr1* KO
PND 18	6	6
PND 21	6	6
PND 30	6	6
PND 60	6	6

Table 6-7: Summary of two-way ANOVA for Black Gold II staining of myelin. The F-value and p-value for genotype, age, and (genotype X age) interaction are presented. Statistically significant effects (p-value of 0.05 or less) are indicated in bold. An independent Student's T-test was performed if there was a significant (genotype X age) interaction.

6.4. DISCUSSION

Myelination of axons starts prenatally in the human brain, continues into adulthood and only declines around middle-age; whereas myelination in rodents begins postnatally and continues throughout adulthood (Andersen, 2003; Xie et al., 2013). Moreover, the developmental process of myelination varies regionally (Quarles et al., 2012). Post-mortem studies have shown that axons and myelin sheaths undergo conspicuous growth during the first two years of human life (Kinney et al., 1988); whereas the peak of myelination in the rodent brain occurs between PND 20-21 (Semple

et al., 2013). Alterations to the normal maturation pattern due to abnormalities in the myelination process during childhood and adolescence have been correlated with psychotic symptomatology (Hyde et al., 1992) and white matter abnormalities have been observed in FXS and in autism spectrum disorder (Haas et al., 2009; Hazlett et al., 2012; Hoeft et al., 2010; Hoeft et al., 2011).

6.4.1. Myelination delay in white matter in the developing *Fmr1* KO mouse

Our results demonstrate an abnormal pattern of change in myelin density during early postnatal development in *Fmr1* KO mice compared to WT mice (Figures 6-3 and 6-4). The results of MTR and myelin density measurements show similar patterns of change in the *Fmr1* KO mouse brain, suggesting that histological changes in myelin are reflected with MTR in the fixed brain. Magnetization transfer imaging is sensitive to the macromolecules in white matter, in particular proteins and lipids in myelin (Stanisz et al., 1999). The MTR from this present study suggested altered concentrations of white matter macromolecules, including lipids and proteins, at different stages of brain development that could contribute to altered myelin composition in *Fmr1* KO mice. Previous in-depth research demonstrated that cholesterol and myelin lipids contribute significantly to the MT effect (Koenig et al., 1990; Stanisz et al., 1999). In addition, a previous study with the myelin basic protein deficient Shriverer mouse revealed no differences in Black Gold II staining compared to controls, further suggesting that myelin with Black Gold II staining has greater specificity to lipids (Savaskan, Weinmann, Heimrich, & Eyupoglu, 2009). Therefore, because myelin composition is composed of 70-85% lipids (Quarles et al., 2012) and due to the similarities in myelin density and MTR in the *Fmr1* KO mouse

brain found in this study, the altered MTR in the *Fmr1* KO mouse brain likely reflects differences in lipid content. It has been shown that male FXS patients (4-20+ years) have reduced plasma cholesterol, low and high-density lipoprotein compared to the normal control population (Berry-Kravis et al., 2015). Although it has not been determined whether brain cholesterol levels might be altered in FXS patients or *Fmr1* KO mice, normal myelination in the brain mainly depends on cholesterol synthesized in the brain (Jurevics & Morell, 1995) and cholesterol is known to be heavily incorporated into myelin particularly during the peak of myelination (Saher et al., 2005). Furthermore, cholesterol deficiency could contribute to malfunction of neurotransmission and has been associated with neurodegenerative diseases (Zhang & Liu, 2015).

The polyribosomal FMRP complex has been shown to bind to the mRNAs of many myelin proteins and likely regulates their translation (Darnell et al., 2011). FMRP binds to the mRNA of myelin basic protein and repress translation (Wang et al., 2004). Furthermore, FMRP concentration is higher in oligodendrocyte precursor cells and immature oligodendrocytes compared to mature oligodendrocytes when myelin basic protein concentration increases (Wang et al., 2004). Levels of myelin basic protein mRNA in oligodendrocytes *in vitro* are elevated in the absence of FMRP (Wang et al., 2004). The concentrations of myelin basic protein and 2' 3'-cyclic-nucleotide 3'-phosphodiesterase (CNP) at PND 7 and PND 15 are decreased in cerebellar white matter in *Fmr1* KO mice (Pacey et al., 2013). The reduced concentrations of myelin basic protein and CNP, as well as myelin thickness in cerebellar white matter gradually normalized with age in *Fmr1* KO mouse brain suggesting a developmental delay in myelination (Pacey et al., 2013). The MTR results in the present study show similar

patterns in cerebellar white matter, including an early reduction in MTR at PND 18 that becomes less pronounced with increasing age (Figure 6-3f). At PND 21 and 30, we found no differences between the *Fmr1* KO and WT mice in MTR in cerebellar white matter. Similarly, Pacey et al. (Pacey et al., 2013), reported no difference in myelin thickness, myelin basic protein and CNP concentrations in cerebellar white matter between *Fmr1* KO and WT mice at PND 30. In the present study, the differences in myelin density and MTR at PND 18, 30 and 60 in the *Fmr1* KO mice compared to the WT suggests that alterations in forebrain and midbrain white matter could span many critical periods of brain development.

Reduced MTR have been associated with pathological states of demyelination and axonal degeneration in multiple sclerosis both in patients and in preclinical models (Bonnier et al., 2014; Ou et al., 2009; Schmierer et al., 2004; Thiessen et al., 2013). In an animal model of multiple sclerosis, decreasing MTR was found in the corpus callosum and external capsule of mice treated with cuprizone, an agent that caused demyelination (Thiessen et al., 2013). In addition, similar MTR values were found between *in vivo* and *ex vivo* imaging of the mouse model of multiple sclerosis by Thiessen et al. (Thiessen et al., 2013). Thus, the decrease of MTR and myelin density found in white matter of *Fmr1* KO mice may indicate delayed myelination in the present study.

6.4.2. Contribution of altered brain metabolites to myelination in the *Fmr1* KO mice

Alteration in brain metabolite levels could also contribute to myelin changes in *Fmr1* KO mice. Reduced *N*-acetylaspartate was reported in cortex and cerebellum at PND 12 (Davidovic et al., 2011) and we found a genotype effect from repeated measures

ANOVA in *N*-acetylaspartate and reduced *N*-acetylaspartate/tCr was found in hippocampus at PND 18 in *Fmr1* KO mice (Chapter 5, Figure 5-3a) (Shi et al., 2012). *N*-acetylaspartate serves as an important precursor to the formation of myelin lipids in oligodendrocytes (Burri et al., 1991; Moffett et al., 2007; Urenjak et al., 1992). Therefore, reduction of *N*-acetylaspartate in the *Fmr1* KO mouse brain may contribute to the decreased myelin density reported in this study at PND 18 (Figure 6-4).

Myo-inositol is continuously incorporated and broken down from phosphatidylinositol in lipids (Shears, 1989). Phosphatidylinositol is phosphorylated by phosphoinositide 3 kinase (PI3K) (Peltier et al., 2007; Sanchez et al., 2004), and phosphorylation of phosphatidylinositol can promote dissociation of the myelin basic protein and actin complex from the lipid vesicle membrane (Boggs et al., 2012). Increased PI3K activity has been reported in the hippocampus of *Fmr1* KO mouse (Sharma et al., 2010), and if PI3K phosphorylates phosphatidylinositol in white matter then that may contribute to myelin layer instability by disrupting attachment of myelin basic proteins to the myelin membrane. In contrast, attachment of myelin basic protein to oligodendrocyte membranes requires phosphatidylinositol 4,5-bisphosphate; reduction of phosphatidylinositol 4,5-bisphosphate led to detachment of myelin basic proteins from oligodendrocyte membrane and loss of myelin compaction in the corpus callosum (Nawaz et al., 2009). The hippocampus of *Fmr1* KO mice revealed a reduction in *myo*-inositol/tCr at PND 30 compared to the WT mice (Chapter 5, Figure 5-3c), which may result in altered phosphatidylinositol levels and PI3K signaling (Shi et al., 2012). Taken together, the results suggest that the decrease observed in *myo*-inositol/tCR may contribute to alterations in myelin structure at PND 30 in the *Fmr1* KO mouse brain.

6.4.3. Implications for functional brain networks in the *Fmr1* KO mouse

The alteration in myelin density during brain development suggests that the process of myelination is dysregulated during development in *Fmr1* KO brain, and this could adversely influence neuronal function and potentially have a negative impact on the formation and maturation of brain networks. Axons that form long distance connections in the brain network showed altered morphology with increased axonal branching and misguided axon growth in the *Drosophila* model of FXS (Pan et al., 2004). Thus, early disruptions in myelin and axon formation could potentially change the formation and integrity of the brain network in *Fmr1* KO mice. Evidence for this concept was also found in recent work on both FXS patients and the *Fmr1* KO mice, which showed significant reductions in functional connectivity measured by resting state functional MRI (Haberl et al., 2015; S. S. Hall et al., 2013). The deficit in the myelin density during development in the *Fmr1* KO brain could also serve to further reinforce altered brain networks. Although this study did not investigate changes in neural networks with age, the findings from diffusion tensor imaging (Chapter 7), a common method to study axon organization in the brain (Argyridis, et al., 2013; Haberl et al., 2015; Mori & Zhang, 2006; Ou et al., 2009; Paydar et al., 2014; Thiessen et al., 2013), may provide further insights into the consequences of altered myelination with respect to axons in developing *Fmr1* KO brain.

The white matter regions studied are essential for communication between brain regions. The corpus callosum connects the left and right hemispheres and reaches all cortical regions (Hofer & Frahm, 2006). The external capsule is connected to the corpus

callosum and relays information between cortices as well as between the corticostriatal pathways (Hofer & Frahm, 2006; Vasung et al., 2010). Reduced myelin density at PND 18 and 60 suggest altered myelin content in the external capsule that could contribute to reduction of functional connectivity in the resting state networks of *Fmr1* KO mice (Haberl et al., 2015) and FXS patients (Hall et al., 2016). In addition, the connections in the corticostriatal pathway could be altered due to excessive striatal fiber density reported in young FXS children (Haas et al., 2009). The internal capsule and cerebral peduncle are part of the corticospinal pathway that passes along afferent and efferent signals from the motor cortex to the spinal cord (Feeney & Wier, 1979; Jang & Seo, 2015). The corticospinal pathway is essential in learning and refining motor skills and FXS patients as well as *Fmr1* KO mice exhibit a variety of motor related deficits and inability to learn motor skills (Garber et al., 2008; Padmashri et al., 2013). The hippocampal fimbria is composed of axons originating in the hippocampus and serves as an intermediary between the entorhinal cortex and the hippocampus (Amaral et al., 2016). Hippocampal dysfunction has been widely reported in FXS and the *Fmr1* KO model including increased metabotropic glutamate receptor 5 dependent long-term depression, increased immature dendritic spines, and elevated protein synthesis (Bilousova et al., 2009; Huber et al., 2002; Qin et al., 2005). The hippocampal fimbria was identified as the only white matter region to have elevated protein synthesis in the adult *Fmr1* KO mouse (Qin et al., 2005). The present study, in conjunction with previous reports, provides ample evidence to support the possibility that altered pattern of myelination in different regions may have an impact on the timely maturation of brain networks.

6.4.4. White matter volume in the FXS brain

Previous MRI studies have established alterations in brain volume as pathological in FXS, including changes in regional gray and white matter volumes of cortical and subcortical regions, compared to normally developing children (Gothelf et al., 2008; Hazlett et al., 2012; Hoeft et al., 2010; Reiss et al., 1994). An earlier study from our group reported increased volume of the hippocampus in *Fmr1* KO brains compared to WT brains (Chapter 5, Figure 5-1) (Shi et al., 2012). Although the current findings did not show consistent differences in white matter volume between *Fmr1* KO and WT mouse brains, the data agree with a recent study that reported only minor volume differences in the C57Bl6J *Fmr1* KO mouse brain compared to WT (Lai et al., 2016). The C57Bl6J strain of *Fmr1* KO mouse was chosen for this study because previous findings from our group showed alterations in brain metabolites during development (Shi et al., 2012). In addition, Pacey et al. (Pacey et al., 2013) reported decreased cerebellar volume and delayed myelination, including reduced myelin proteins and myelin thickness in the C57Bl6J *Fmr1* KO mouse. While the C57Bl6J *Fmr1* KO mouse in the present study did not reveal volume differences in white matter regions, other methods used in this study showed evidence of alterations in myelin and white matter in developing *Fmr1* KO mice.

6.4.5. Imaging the fixed brain

The imaging findings along with results from myelin staining suggest that measurement of T_2 and MTR could be used to better understand the microstructure of FXS brain *in vivo*. However, the current findings have to be taken in context of the

limitations of the study. It is likely that the T_2 and MTR values measured *in vivo* would be different from those measured in a fixed tissue sample because the fixative solution has been shown to affect the T_2 and MTR values compared to *in vivo* measurements (Schmierer et al., 2008; Shepherd et al., 2009). Therefore, precautions based on previous studies between fixed and *in vivo* brain samples were taken to minimize differences in T_2 relaxation and MTR in the fixed brain (Schmierer et al., 2008; Shepherd et al., 2009). Our goal in this study was to obtain an accurate assessment of white matter development by obtaining high-resolution volumetric, T_2, and MTR data. Thus, we elected to perform these measurements in a fixed brain to stabilize brain structure, allow longer imaging durations and eliminate confounds of animal motion. Fixed *Fmr1* KO mouse brains have been used to study volume changes in the past (Ellegood et al., 2010; Lai et al., 2016; Pacey et al., 2013). In addition, it has been shown that the trends in the data from fixed samples would be similar to *in vivo* with T_2 (Shepherd et al., 2009) and with MTR following immersion of brain tissue in PBS (Thiessen et al., 2013). The findings of the current study regarding the utility of T_2-relaxation and MTR in revealing developmental changes in the *Fmr1* KO mouse are compelling, future studies should focus on using these techniques *in vivo* to assess their utility as imaging markers for FXS and also to assess whether such changes alter brain connectivity in the *Fmr1* KO mouse.

6.5. Conclusions

In this study, we demonstrated altered levels of myelin and macromolecules in the white matter of *Fmr1* KO mouse brain at developmental ages compared to the corresponding regions of the WT mouse brain. White matter and myelin alterations were

found during times that coincided with key stages of brain development including early myelination, the peak of myelination and synaptogenesis, neural network development and maturation in the *Fmr1* KO mouse brain. The findings show dysregulation of myelination and white matter maturation in the *Fmr1* KO mouse brain during development and suggest complex changes in white matter development. We observed delayed myelination before the peak of myelination at PND 18, then at PND 30 myelin density increased suggesting compensation to the delayed myelination and then lowered myelin levels in adult *Fmr1* KO mouse brain compared to the WT. Differences in white matter and myelin between the *Fmr1* KO and WT mouse brains were prevalent during development and could contribute to changes in the brain networks of the *Fmr1* KO mouse.

CHAPTER 7: DIFFUSION PROPERTIES OF THE *FMR1* KO BRAIN AND REPRESENTATION OF AXON FIBERS

7.1. INTRODUCTION

The diffusion properties of gray and white matter were examined in this chapter to determine whether axons could contribute to altered brain morphology in the developing *Fmr1* KO mouse. In addition to myelin deficits, evidence of altered axonal growth patterns and morphology have been reported in animal models of FXS (Bureau et al., 2008; Pacey et al., 2013; Pan et al., 2004). FMRP is normally observed at axonal growth cones and along the axon shafts of cultured WT neurons (Antar et al., 2006). In the *Fmr1* KO neurons, axon growth cones display excess filopodia and reduced axon motility compared to the WT neurons, which can potentially limit axon growth and decrease the chances of the axon connecting with dendritic spines (Antar et al., 2006). Irregular axon morphology has also been reported in the adult *Drosophila* model of FXS, including increased axonal branching and protrusion of branched axons into other regions normally not observed in the WT brain (Pan et al., 2004). Diffuse axon arbors, which display shorter and more dispersed axons, have been demonstrated in neurons connecting layer 4 to layer 2/3 in somatosensory cortex of developing *Fmr1* KO mice (PND 13-15) and showed no differences by PND 20 compared to WT (Bureau et al., 2008). The diffuse axon arbor phenotype may be the result of altered axon pruning in *Fmr1* KO mouse brain (Bureau et al., 2008). The studies in the animal models of FXS suggest that FMRP may play a role in axon guidance and pruning (Antar et al., 2006; Bureau et al., 2008; Pan et al., 2004).

Microstructural changes in axons and myelin during normal development and

under pathological conditions are best studied by MRI using diffusion tensor imaging (DTI) (Argyridis et al., 2013; Haberl et al., 2015; Mori & Zhang, 2006; Ou et al., 2009; Paydar et al., 2014; Thiessen et al., 2013). DTI is able to report information on water mobility within biological tissue in multiple directions from which the microstructural environment of the tissue can be inferred (Mori & Zhang, 2006). Originally, measures of water diffusivity were based on the assumption that water diffusion is isotropic, being able to diffuse in any direction if unhindered in an uniform sample (Mori & Zhang, 2006). The diffusion distances are typically modeled by a Gaussian distribution, an assumption that water diffusion distances after a certain diffusion time follow a normal distribution (Mori & Zhang, 2006). However, diffusion is hindered in both gray and white matter due to morphological structures, with white matter exhibiting more anisotropic diffusion because of restriction in water diffusion across the axon and myelin membranes, and the gray matter exhibiting more isotropic diffusion behavior (Mori & Zhang, 2006). Given the heterogeneity of tissues and tissue type, more recently the diffusion of water has been modeled by the diffusion tensor, composed of eigenvectors that align parallel (e_1, in the axial direction) and perpendicular (e_2 and e_3, two radial directions) to axon bundles. The eigenvectors correspond to eigenvalues (λ_1, λ_2, λ_3), which represent the diffusivity along these three principal diffusion directions in the brain after obtaining information from at least 6 directions of diffusion sensitization (Mori & Zhang, 2006; Mukherjee et al., 2002).

Developmentally mean diffusivity (MD), a measure of the average distance water molecules diffuse after a period of time, decreases as the brain develops due to more restriction in water diffusion (Lebel et al., 2012; Qiu et al., 2008). Fractional anisotropy

(FA), a measure of the preferential direction of diffusion (Mori & Zhang, 2006), increases in white matter during development as the water molecule is freely able to diffuse along the axon due to relatively less restricted diffusion while it is more restricted across the axon. Barriers to diffusion are encountered perpendicular to the axon from cellular membranes and myelin, making diffusion more anisotropic along the direction of the axon (Neil et al., 2002; Paydar et al., 2014; Qiu et al., 2008). Both MD and FA remain the most reported parameters with respect to white matter health and axonal organization during development (Lebel et al., 2012; Paydar et al., 2014; Qiu et al., 2008). The developmental decrease of MD and increase of FA are observed in gray and white matter during normal human (birth to 30 years) and rodent brain (PND 0-21) development, though the rate of change varies by region (Bockhorst et al., 2008; Lebel et al., 2012; Paydar et al., 2014). In the aged brain MD increases and FA decreases in humans (50+ years) and rodents (16-18 months) (de Groot et al., 2016; Sun et al., 2005)

While MD and FA generally represent maturation and health of the normal human and rodent brain, axial diffusion (AD, represents the eigenvalue λ_1) is a measure of diffusion parallel to the fiber and is generally used as a biomarker to characterize axon morphology. An increase of axon density and axonal branching has been associated with a decrease in AD (Kumar et al., 2012; Lebel et al., 2012; Qiu et al., 2008). Radial diffusion (RD, represents the average eigenvalues λ_2 and λ_3), is a measure of diffusion perpendicular to the fiber and is generally used as a biomarker for myelination in healthy developing brain (Lebel et al., 2012; Mukherjee et al., 2002). Changes in myelination are often associated with change in RD; a decrease in RD was observed with increase in myelination during brain development (Kumar et al., 2012; Lebel et al., 2012; Mukherjee

et al., 2002). Conversely, RD was found to increase during demyelination in multiple sclerosis and demyelinated animal models, along with increased MD and reduced FA (Ou et al., 2009; Song et al., 2002; Thiessen et al., 2013).

The Gaussian model of diffusion assumes that water diffuses uniformly in brain tissue. However, this is a simplistic assumption since water mobility in brain tissue is much more complex, where membranes and compartments contribute to highly heterogeneous diffusion environment (Fieremans et al., 2011; Jensen & Helpern, 2010). The diffusion kurtosis model was proposed to account for this complexity and to better represent the microstructure of the brain biologically (Fieremans et al., 2011; Jensen & Helpern, 2010; Steven et al., 2014). Diffusion kurtosis imaging (DKI), an extension of DTI, models the water diffusion process as non-Gaussian (Fieremans et al., 2011; Jensen & Helpern, 2010; Steven et al., 2014) and DKI can provide higher sensitivity into myelin and axon microstructure in human and rodent brains (Cheung et al., 2009; Fieremans et al., 2011; Jensen & Helpern, 2010).

The goal of this study is to determine microstructural properties of axons in the developing brains of *Fmr1* KO mice compared to the WT. In this study, DKI technique was used to study the whole brain and regional white and gray matter morphological characteristics to provide additional insight into axonal and myelin development in *Fmr1* KO mouse brain. Diffusion and kurtosis parameters were measured in fixed brains of *Fmr1* KO and WT mice at ages that have been previously shown to correspond to critical periods of development in the rodent brain, at postnatal day 18 (PND 18) and PND 21 before and during peak of myelination and synaptogenesis, respectively; at PND 30 during neural network development, and at PND 60 during maturation of the neural

networks when the mouse is considered an adult (Semple et al., 2013). The same developmental ages were used as described in Chapter 6 to better understand the nature of the developing white matter, which is composed of axons and myelin, and the findings in the current study could provide further insights into the morphology of white matter in *Fmr1* KO mice.

7.2. METHODS

7.2.1. Animal procedure

Fmr1 KO mice (JAX B6.129P2-$^{Fmr1\text{tmICgr}}$ mice; Jackson Laboratory, Bar Harbor, ME, USA) from a C57Bl6J background were bred in a mouse colony at the University of Maryland, Baltimore. Wild-type mice (JAX C57Bl6J; WT) were also bred in a mouse colony at the University of Maryland, Baltimore. The Institutional Animal Care and Use Committee at the University of Maryland, Baltimore approved the protocol for this study. Food and water were given *ad libitum*. All mice were weaned at PND 21.

Male *Fmr1* KO and WT mice were obtained from a total of ten different litters to prevent litter effect. We studied mice at PND 18 (12 *Fmr1* KO, 10 WT), PND 21 (11 *Fmr1* KO, 13 WT), PND 30 (15 *Fmr1* KO, 12 WT), and PND 60 (6 *Fmr1* KO, 6 WT). At PND 18, 21, 30, and 60, male mice were anesthetized with 4% isofluorane and then perfused through the left ventricle of the heart with 1X phosphate buffered saline (PBS) and followed by 4% paraformaldehyde (PFA). The whole brain was removed from the skull and placed in PFA to continue fixation for 48 hours. The fixed brain was then immersed in PBS for at least 48 hours before imaging. This post-fixation procedure was reported to preserve brain tissue diffusion properties so that it was comparable to *in vivo*

diffusion parameters (Shepherd et al., 2009). Prior to imaging, the fixed brain was placed in a customized conical tube that was filled with Fluroinert (3M, St. Paul, MN), a compound that has no MR signal and minimizes susceptibility artifacts.

7.2.2. Magnetic resonance imaging

All experiments were performed on a Bruker Biospec 7.0 Tesla 30 cm horizontal bore scanner using Paravision 5.1 software (Bruker Biospin MRI, Ettlingen, Germany). A four-channel Bruker ^{1}H surface array coil was used as the receiver and a Bruker 72-mm linear-volume coil as the transmitter. T_2-weighted 3D anatomical images were obtained covering a 15 mm thick with TE/TR of 11/2500ms at a resolution of 113 μm × 150 μm × 170 μm, using two signal averages. Diffusion kurtosis images were acquired with the spin echo DTI sequence in the coronal plane. Thirty diffusion directions were applied at diffusion weightings of b = 0.7 ms/μm^2, 2.1 ms/μm^2, and 4.0 ms/μm^2. The three b-values were chosen to show diffusion signal attenuation for the kurtosis model (Steven et al., 2014). Higher b-values compared to *in vivo* values were chosen to obtain higher diffusion sensitivity and a better estimate of kurtosis (Sun et al., 2003). The chosen b-values have been shown to provide diffusion attenuated images with sufficient signal to noise such that they preserve the information on diffusion anisotropy, MD, AD, and RD, while at the same time providing kurtosis information. Five images with no diffusion at b = 0 ms/μm^2 were acquired. The field of view used for imaging the brain was 1.88cm × 1.50cm x 1.2cm which provided a spatial resolution of 293μm × 234μm x 1000μm at a TR/TE 6000/27.7ms, and one average.

7.2.3. DKI reconstruction

The maps of mean, axial, and radial diffusivity (MD, AD, and RD, respectively), fractional anisotropy (FA), mean, axial, and radial kurtosis (MK, AK, and RK, respectively) were calculated from a custom MatLab program (Xu et al., 2011; Zhuo et al., 2012) based on model described in Jensen et al. 2010 (Jensen & Helpern, 2010).

Diffusion-weighted signals from all four b-values (b = 0, 0.7, 2.1, 4.0ms/μm^2) and 30 directions were fitted voxel-wise using non-linear least squares fit to the equation from Zhuo et al. (Zhuo et al., 2012):

$$\ln S(\mathbf{g},b) = \ln S_0 - b\sum_{i=1}^{3}\sum_{j=1}^{3} g_i g_j D_{ij} + \frac{1}{6}b^2 MD^2 \sum_{i=1}^{3}\sum_{j=1}^{3}\sum_{k=1}^{3}\sum_{l=1}^{3} g_i g_j g_k g_l W_{ijkl} \qquad [1]$$

where,

$\mathbf{g} = (g_1, g_2, g_3)$ is the unit-vector direction of the diffusion gradient.

$S(\mathbf{g},b)$ is the diffusion-weighted signal at a particular b-value with direction **g**.

S_0 is the MR signal with no diffusion weighting (b = 0 ms/μm^2) and is the average of all the five b=0 volumes that were acquired.

MD is the mean diffusivity (μm^2/ms).

D_{ij} is element of the 3x3 diffusion tensor, **D**.

W_{ijkl} is element of the 3x3x3x3 4th order diffusion kurtosis tensor, **W**.

Since **D** and **W** are both symmetric matrices, with 6 independent elements of the diffusion tensor and 15 independent elements for diffusion kurtosis tensor, a total of 21 parameters were fitted using equation [1]. The apparent diffusion coefficient $D_{app}(\mathbf{g})$ and apparent kurtosis $K_{app}(\mathbf{g})$ for each direction **g** were then calculated from equations from Zhuo et al. (Zhuo et al., 2012):

$$D_{app}(\mathbf{g}) = \sum_{i=1}^{3}\sum_{j=1}^{3} g_i g_j D_{ij} \quad [2]$$

$$K_{app}(\mathbf{g}) = \frac{MD^2}{D_{app}(\mathbf{g})^2}\sum_{i=1}^{3}\sum_{j=1}^{3}\sum_{k=1}^{3}\sum_{l=1}^{3} g_i g_j g_k g_l W_{ijkl} \quad [3]$$

The three eigenvalues λ_1, λ_2, λ_3 ($\lambda_1 \geq \lambda_2 \geq \lambda_3$) and the corresponding eigenvectors (e_1, e_2, e_3) were derived through eigen-decomposition of the diffusion tensor. The λ_1 eigenvalue aligns parallel (axial direction) while λ_2 and $\lambda_3$align perpendicular (two radial directions) to the diffusion tensor. The diffusion parameters, MD, FA, AD, and RD were calculated as follows from Zhuo et al. (Zhuo et al., 2012):

$$MD = \frac{\lambda_1 + \lambda_2 + \lambda_3}{3} \quad [4]$$

$$FA = \frac{\sqrt{3[(\lambda_1 - MD)^2 + (\lambda_2 - MD)^2 + (\lambda_3 - MD)^2]}}{\sqrt{2(\lambda_1^2 + \lambda_2^2 + \lambda_3^2)}} \quad [5]$$

$$AD = \lambda_1, \; RD = \frac{\lambda_2 + \lambda_3}{2}, \quad [6]$$

Diffusion kurtosis related parameters were derived from the diffusion kurtosis tensor described in Jensen et al. 2010 (Jensen & Helpern, 2010). The mean kurtosis (MK) was calculated by averaging the K_{app} in all 30 directions.

$$MK = \frac{1}{N}\sum_{i=1}^{N}(K_{app})_i \quad [7]$$

Axial kurtosis (AK) and radial kurtosis (RK), which characterize the kurtosis along the axial and radial diffusion directions, respectively, were derived as in Jensen et al. (Jensen & Helpern, 2010) after first transforming **W** to the coordinates defined by the three eigenvectors of the diffusion tensor as:

$$\hat{W}_{ijkl} = \sum_{i'=1}^{3}\sum_{j'=1}^{3}\sum_{k'=1}^{3}\sum_{l'=1}^{3} e_{i'i}e_{j'j}e_{k'k}e_{l'l}W_{i'j'k'l'} \quad [8]$$

$$AK = \frac{(\lambda_1+\lambda_2+\lambda_3)^2}{9\lambda_1^2}\hat{W}_{1111} \quad [9]$$

$$RK = G_1(\lambda_1,\lambda_2,\lambda_3)\hat{W}_{2222} + G_1(\lambda_1,\lambda_3,\lambda_2)\hat{W}_{3333} + G_2(\lambda_1,\lambda_2,\lambda_3)\hat{W}_{2233} \quad [10]$$

Where $G_1(\lambda_1,\lambda_2,\lambda_3) = \frac{(\lambda_1+\lambda_2+\lambda_3)^2}{18\lambda_2(\lambda_2-\lambda_3)^2}(2\lambda_2 + \frac{\lambda_3^2-3\lambda_2\lambda_3}{\sqrt{\lambda_2\lambda_3}})$ and

$$G_2(\lambda_1,\lambda_2,\lambda_3) = \frac{(\lambda_1+\lambda_2+\lambda_3)^2}{3(\lambda_2-\lambda_3)^2}(\frac{\lambda_2+\lambda_3}{\sqrt{\lambda_2\lambda_3}} - 2)$$

7.2.4. Analysis of gray and white matter regions

To assess the characteristics of the microstructural changes during development, regions of interest (ROI) were drawn manually on the FA map at each time point using FSLview (Analysis Group, FMRIB, Oxford, UK) for the whole brain; gray matter regions, including the caudate putamen and thalamus; and white matter regions, including the corpus callosum, external capsule, internal capsule, cerebral peduncle, fimbria, and cerebellar white matter. The ROI of the whole brain covered both gray and white matter regions from the prefrontal cortex to the cerebellum, excluding the ventricles. Average regional diffusion parameter values were extracted from the ROIs using a custom MATLAB program (Xu et al., 2011).

7.2.5. White matter fiber tractography

A deterministic fiber tractography map of the brain was generated from the principle diffusion direction to show fiber tracts throughout the brain (Mukherjee et al., 2008; Tsurugizawa et al., 2013). The density map was generated using

TrackVisDiffusion Toolkit software (TrackVis Diffusion Toolkit, Charlestown, MA) from the DKI image. The fiber density represents a scalar value of the number of fibers that passed through the white and gray matter ROI (Torgerson et al., 2013). The same manually drawn ROIs of white and gray matter regions used to extract diffusion and kurtosis values were imported onto the density map. Fiber tracts were then filtered to only display the tracts emanating from specific white and gray matter regions which included the corpus callosum, external capsule, internal capsule, cerebral peduncle, fimbria, caudate putamen, and thalamus.

7.2.6. Statistics

A two-way analysis of variance (ANOVA) was performed on each of the DTI and DKI parameters by region to assess the effect of genotype, age, as well as the interactions between these variables using SPSS (IBM Corp. 2013, IBM SPSS Statistics for Windows, Version 22.0. Armonk, NY). Post-hoc analysis with genotype and age was performed with an independent Student's t-test if the interaction of (genotype X age) showed significance with $p < 0.05$. To control for multiple pairwise comparisons, a false discovery rate with threshold of alpha = 0.05 was performed on the p-values. The threshold assumes 5% of significant p-values may be false positives, and if a significant p-value does not pass false discovery rate then that p-value may be a false positive.

7.3. RESULTS

The diffusion and kurtosis parameters for the whole brain of *Fmr1* KO and WT mice at PND 18, 21, 30 and 60 are presented in Table 7-1. A significant interaction of

(genotype X age) was found in MD, AD, and RD of the whole brain (Tables 7-2, 7-3, and 7-4, respectively). The *Fmr1* KO mice showed reduced MD in the whole brain at PND 21 ($t(3.16)$, $p<0.005$) and at PND 30 ($t(2.67)$, $p<0.01$) (Table 7-1). The *Fmr1* KO mice showed reduced AD in the whole brain at PND 21 ($t(3.39)$, $p<0.005$) and at PND 30 ($t(2.32)$, $p<0.05$) (Table 7-1). The *Fmr1* KO mice showed reduced RD in the whole brain at PND 21 ($t(2.88)$, $p<0.005$) and at PND 30 ($t(2.77)$, $p<0.05$) (Table 7-1). Outlier diffusion values were observed in two PND 60 WT brains and were removed from further analysis. A significant decrease of diffusivity was observed in the whole brain of *Fmr1* KO mice at PND 21 and 30, which led us to investigate specific white and gray matter regions.

Whole Brain		WT	SE	*Fmr1* KO	SE	n	WT	*Fmr1* KO
MD	PND 18	0.405	0.007	0.416	0.011	PND 18	10	12
($\mu m^2/ms$)	PND 21	0.402	0.003	**0.372**	0.009	PND 21	13	11
	PND 30	0.400	0.006	**0.377**	0.006	PND 30	12	15
	PND 60	0.401	0.010	0.428	0.021	PND 60	4	6
AD	PND 18	0.486	0.009	0.496	0.013			
($\mu m^2/ms$)	PND 21	0.483	0.005	**0.441**	0.012			
	PND 30	0.481	0.007	**0.459**	0.007			
	PND 60	0.478	0.013	0.504	0.023			
RD	PND 18	0.365	0.007	0.376	0.011			
($\mu m^2/ms$)	PND 21	0.361	0.003	**0.337**	0.008			
	PND 30	0.359	0.006	**0.336**	0.006			
	PND 60	0.362	0.009	0.390	0.020			
FA	PND 18	0.200	0.006	0.190	0.009			
	PND 21	0.199	0.006	0.185	0.005			
	PND 30	0.198	0.003	0.213	0.006			
	PND 60	0.190	0.003	0.178	0.009			
MK	PND 18	0.780	0.073	0.765	0.072			
	PND 21	0.784	0.035	0.838	0.055			
	PND 30	0.795	0.057	0.712	0.058			
	PND 60	0.912	0.034	0.732	0.045			
AK	PND 18	0.779	0.051	0.783	0.051			
	PND 21	0.777	0.026	0.897	0.048			
	PND 30	0.820	0.046	0.744	0.052			
	PND 60	0.875	0.024	0.750	0.038			
RK	PND 18	0.800	0.088	0.768	0.087			
	PND 21	0.810	0.042	0.817	0.062			
	PND 30	0.795	0.071	0.712	0.061			
	PND 60	0.962	0.043	0.743	0.053			

Table 7-1: Whole brain DTI and DKI parameters between WT and *Fmr1* KO mice at PND 18, 21, 30, and 60. The table shows the mean and standard error (SE) of DTI parameters of mean diffusivity (MD), axial diffusivity (AD), radial diffusivity (RD), and fractional anisotropy (FA), as well as the mean and SE of DKI parameters of mean kurtosis (MK), axial kurtosis (AK), and radial kurtosis (RK). Significant differences are shown in bold between *Fmr1* KO and WT mice. The significant p-values passed false discovery rate (alpha = 0.05) for multiple pairwise comparisons in the whole brain.

7.3.1. Diffusion tensor parameter changes in *Fmr1* KO brain

7.3.1.1. Mean diffusivity

Similar to the MD in the whole brain, no differences in MD were observed at PND 18 and 60 in any white and gray matter regions between *Fmr1* KO and WT mice.

The *Fmr1* KO mice showed reduced MD at PND 21 in the corpus callosum ($t(3.87)$, $p<0.001$), external capsule ($t(2.44)$, $p<0.05$), fimbria ($t(3.23)$, $p<0.005$), and thalamus ($t(3.116)$, $p<0.005$) compared to WT (Fig 7-1). Reduced MD was also observed in the *Fmr1* KO mice at PND 30 in the corpus callosum ($t(2.95)$, $p<0.01$), external capsule ($t(2.89)$, $p<0.01$), caudate putamen ($t(2.10)$, $p<0.05$), and thalamus ($t(2.93)$, $p<0.01$) (Figure 7-1). A significant interaction of (genotype X age) was observed with MD in the corpus callosum, external capsule, fimbria, caudate putamen, and thalamus (Table 7-2). The significant p-values passed false discovery rate (alpha = 0.05) for multiple pairwise comparisons of MD in the whole brain, corpus callosum, external capsule, fimbria, caudate putamen, and thalamus. The reduced MD at PND 21 and 30 in the *Fmr1* KO mouse brain likely indicate altered maturation process in both white and gray matter.

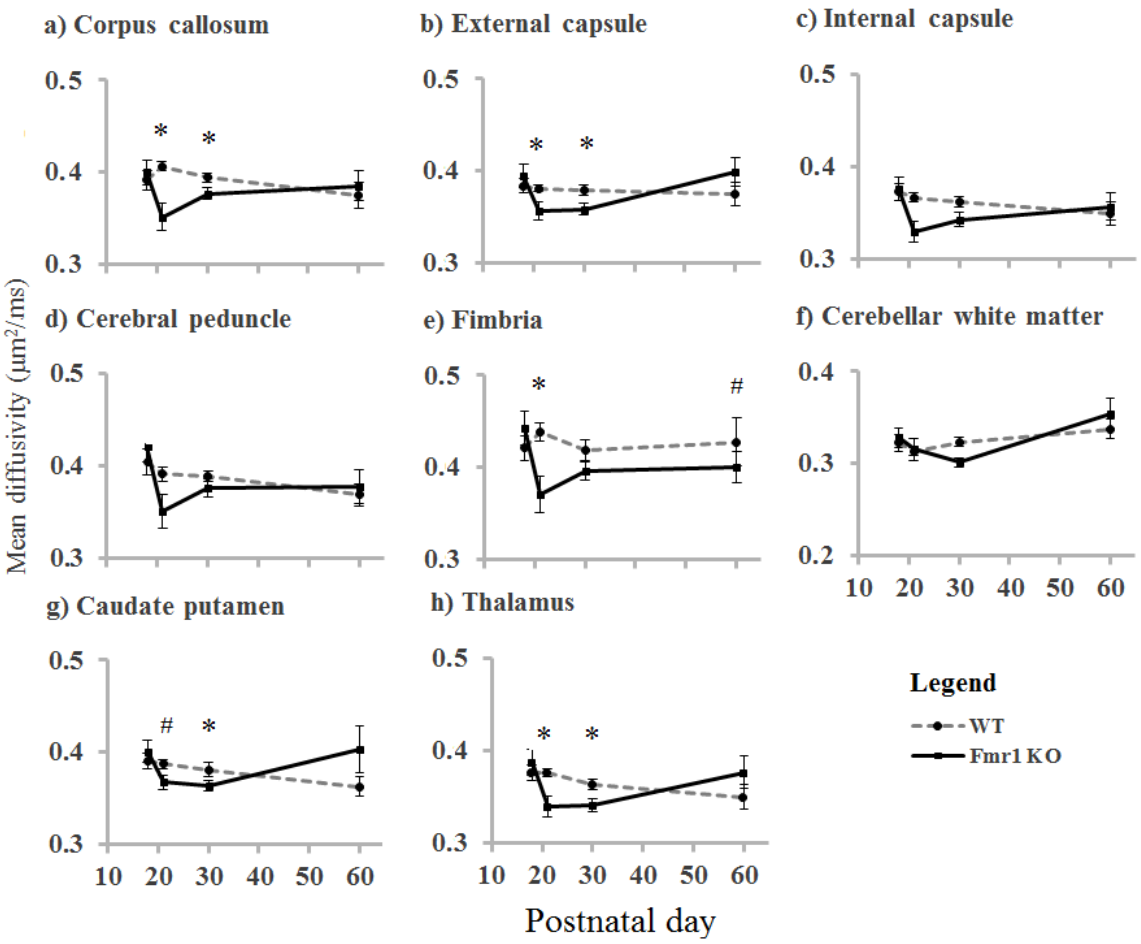

Figure 7-1: Temporal changes in mean diffusion (MD) (μm^2/ms; mean ± SE) in *Fmr1* KO (black solid line) in comparison with WT (gray dashed line) mouse brains. MD was measured in white matter regions including the a) corpus callosum, b) external capsule, c) internal capsule, d) cerebral peduncle, e) fimbria, and f) cerebellar white matter. Gray matter regions measured include the g) caudate putamen and h) thalamus. Significant differences between genotypes at each time point are denoted * $p < 0.05$ and near significant values # $p < 0.10$. The significant p-values passed false discovery rate (alpha = 0.05) for the corpus callosum, external capsule, fimbria, caudate putamen, and thalamus.

Mean Diffusion		df	F-value	p-value
Genotype	Whole brain	1	0.297	0.588
	Corpus callosum	1	4.238	**0.043**
	External capsule	1	0.334	0.565
	Internal capsule	1	2.822	0.097
	Cerebral peduncle	1	1.083	0.301
	Fimbria	1	5.262	**0.025**
	Cerebellar white matter	1	0.000	1.000
	Caudate putamen	1	0.133	0.716
	Thalamus	1	0.839	0.363
Age	Whole brain	3	4.857	**0.004**
	Corpus callosum	3	1.161	0.330
	External capsule	3	3.711	**0.015**
	Internal capsule	3	3.649	**0.016**
	Cerebral peduncle	3	3.995	**0.011**
	Fimbria	3	1.340	0.268
	Cerebellar white matter	3	3.831	**0.013**
	Caudate putamen	3	2.699	0.052
	Thalamus	3	3.990	**0.011**
Genotype X age	Whole brain	3	3.980	**0.011**
	Corpus callosum	3	4.541	**0.006**
	External capsule	3	3.409	**0.022**
	Internal capsule	3	2.515	0.065
	Cerebral peduncle	3	1.958	0.128
	Fimbria	3	3.309	**0.025**
	Cerebellar white matter	3	1.503	0.221
	Caudate putamen	3	3.191	**0.028**
	Thalamus	3	3.904	**0.012**
Error	Whole brain	75		
	Corpus callosum	75		
	External capsule	75		
	Internal capsule	75		
	Cerebral peduncle	75		
	Fimbria	75		
	Cerebellar white matter	75		
	Caudate putamen	75		
	Thalamus	75		

n	WT	*Fmr1* KO
PND 18	10	12
PND 21	13	11
PND 30	12	15
PND 60	4	6

Table 7-2: Summary of two-way ANOVA results for mean diffusion. The F-value and p-value for genotype, age, and interaction of (genotype X age) are presented. An interaction with a p-value of 0.05 or less was considered significant (in bold) and allowed further pairwise comparisons. An independent Student's T-test was performed if there was a significant interaction of (genotype X age).

7.3.1.2. Axial diffusivity

Axial diffusivity (AD) is diffusion along the direction of the axon, thus is considered a measure of axonal organization, and this measure may provide insight into axon density and axonal branching in developing *Fmr1* KO mouse brain. No differences

in AD were observed in white and gray matter regions at PND 18 and 60 between *Fmr1* KO and WT mice. The *Fmr1* KO mice showed reduced AD at PND 21 in the corpus callosum ($t(3.23)$, $p<0.005$), external capsule ($t(2.83)$, $p<0.01$), fimbria ($t(3.20)$, $p<0.005$), and thalamus ($t(3.291)$, $p<0.005$) (Figure 7-2). Reduced AD was also observed in *Fmr1* KO mice at PND 30 in the corpus callosum ($t(2.63)$, $p<0.05$) and thalamus ($t(3.14)$, $p<0.005$) compared to WT (Figure 7-2). A significant interaction of (genotype X age) was observed with AD in the whole brain, corpus callosum, external capsule, fimbria, and thalamus (Table 7-3). The significant p-values passed false discovery rate (alpha = 0.05) for multiple pairwise comparisons of AD in the whole brain, corpus callosum, external capsule, fimbria, and thalamus. In general, the AD in white and gray matter regions of the WT mouse brain did not change between ages, which was in agreement with *in vivo* findings in the C57Bl6J WT mice from PND 21 to 56 (Hammelrath et al., 2016). In *Fmr1* KO mice, AD decreased between PND 18 to 21 and increased from PND 21 to 30. The reduction of AD in the *Fmr1* KO mouse brain at PND 21 and 30 suggested alterations in axonal organization, including increased axonal branching and increased fiber density.

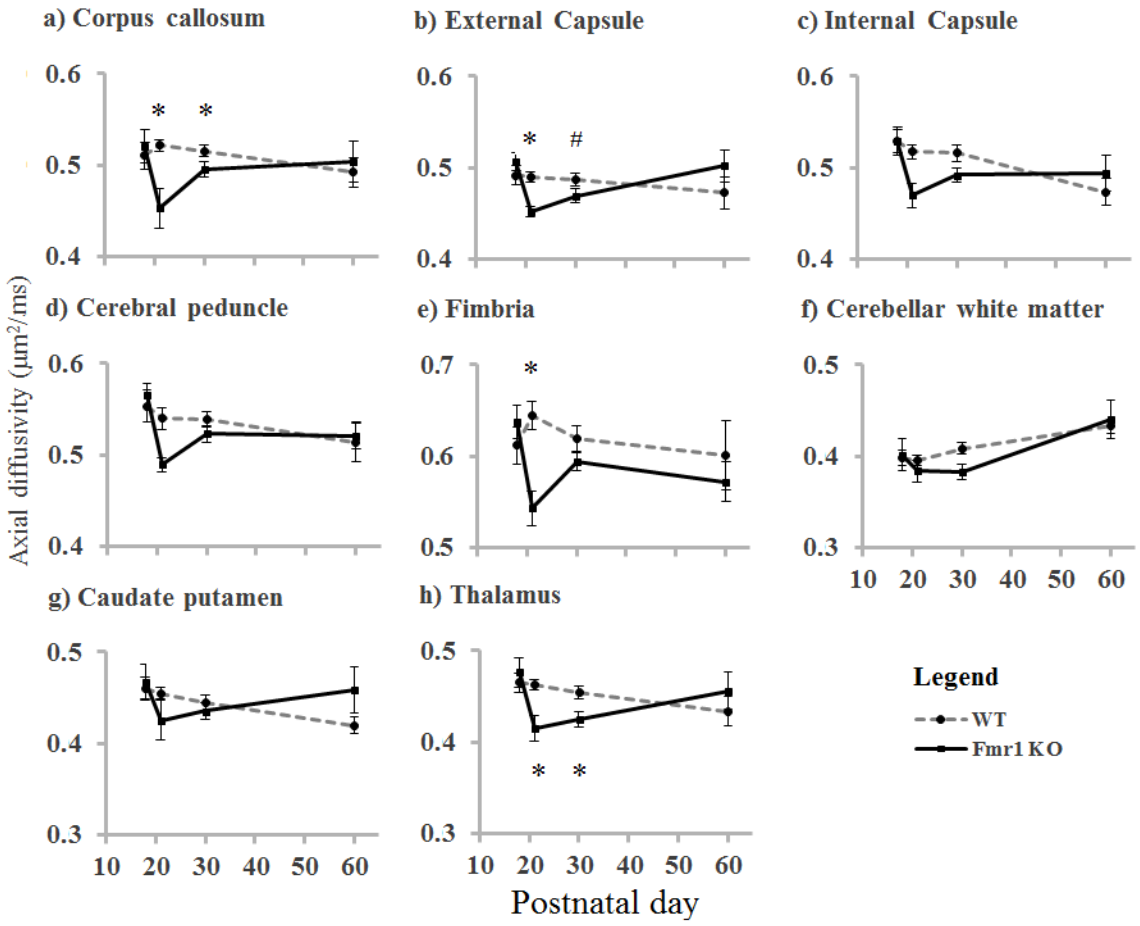

Figure 7-2: Temporal change in axial diffusion (AD) (μm^2/ms; mean ± SE) in *Fmr1* KO (black solid line) in comparison with WT (gray dashed line) mouse brains. AD was measured in white matter regions including the a) corpus callosum, b) external capsule, c) internal capsule, d) cerebral peduncle, e) fimbria, and f) cerebellar white matter. Gray matter regions measured include the g) caudate putamen and h) thalamus. Significant differences between genotypes at each time point are denoted * $p < 0.05$ and near significant values # $p < 0.10$. The significant p-values passed false discovery rate (alpha = 0.05) in the corpus callosum, external capsule, fimbria, and thalamus.

Axial Diffusion		df	F-value	p-value
Genotype	Whole brain	1	0.740	0.393
	Corpus callosum	1	3.557	0.063
	External capsule	1	0.336	0.564
	Internal capsule	1	2.047	0.157
	Cerebral peduncle	1	1.731	0.192
	Fimbria	1	4.705	**0.033**
	Cerebellar white matter	1	0.752	0.389
	Caudate putamen	1	0.000	1.000
	Thalamus	1	2.201	0.142
Age	Whole brain	3	3.966	**0.011**
	Corpus callosum	3	1.435	0.239
	External capsule	3	2.856	**0.043**
	Internal capsule	3	3.455	**0.021**
	Cerebral peduncle	3	2.658	0.054
	Fimbria	3	0.939	0.426
	Cerebellar white matter	3	5.043	**0.003**
	Caudate putamen	3	2.398	0.075
	Thalamus	3	3.432	**0.021**
Genotype X age	Whole brain	3	3.742	**0.015**
	Corpus callosum	3	3.386	**0.022**
	External capsule	3	3.425	**0.021**
	Internal capsule	3	2.015	0.119
	Cerebral peduncle	3	1.416	0.245
	Fimbria	3	3.280	**0.025**
	Cerebellar white matter	3	0.973	0.410
	Caudate putamen	3	2.512	0.065
	Thalamus	3	3.545	**0.018**
Error	Whole brain	75		
	Corpus callosum	75		
	External capsule	75		
	Internal capsule	75		
	Cerebral peduncle	75		
	Fimbria	75		
	Cerebellar white matter	75		
	Caudate putamen	75		
	Thalamus	75		

n	WT	*Fmr1* KO
PND 18	10	12
PND 21	13	11
PND 30	12	15
PND 60	4	6

Table 7-3: Summary of two-way ANOVA for axial diffusivity. The F-value and p-value for genotype, age, and interaction of (genotype X age) are presented. An interaction with a p-value of 0.05 or less was considered significant (in bold) and allowed further pairwise comparison. An independent Student's T-test was performed if there was a significant interaction of (genotype X age).

7.3.1.3. Radial diffusivity

Radial diffusivity (RD) is the diffusion perpendicular to the direction of the axon and is associated with diffusion restricted by the presence of myelin (Song et al., 2002).

No differences were observed in RD at the whole brain, as well as within white and gray matter regions at PND 18 and PND 60 were observed between *Fmr1* KO and WT mice. The *Fmr1* KO mice showed reduced RD at PND 21 in the corpus callosum ($t(4.08)$, $p<0.001$), fimbria ($t(3.14)$, $p<0.005$), and thalamus ($t(2.980)$, $p<0.01$) (see Figure 7-3). Reduced RD was also observed in the *Fmr1* KO mice at PND 30 in the corpus callosum ($t(2.65)$, $p<0.05$), external capsule ($t(3.19)$, $p<0.005$), caudate putamen ($t(2.54)$, $p<0.05$), and thalamus ($t(2.63)$, $p<0.05$) (see Figure 7-3). A significant interaction of (genotype X age) was observed with RD in the corpus callosum, external capsule, fimbria, caudate putamen, and thalamus (Table 7-4). The significant p-values passed false discovery rate (alpha = 0.05) for multiple pairwise comparisons of RD in the whole brain, corpus callosum, external capsule, fimbria, caudate putamen, and thalamus. The RD in white and gray matter regions in WT mice did not change between ages, which agreed with *in vivo* findings in the C57Bl6J WT mice from PND 21 to 56 (Hammelrath et al., 2016). In *Fmr1* KO mice, RD decreased between PND 18 to 21, which suggests increased myelin density or more packed fibers at PND 21 and 30 in *Fmr1* KO mice.

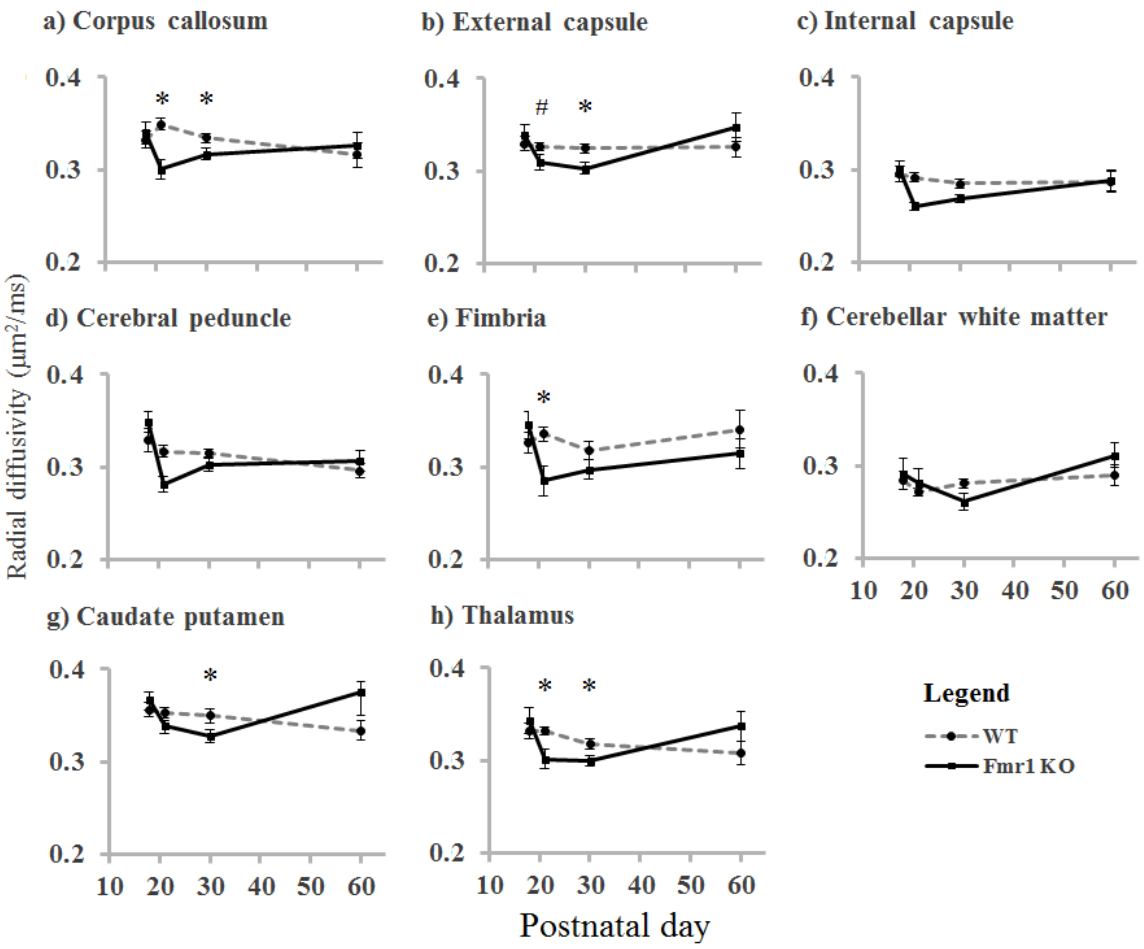

Figure 7-3: Temporal changes in radial diffusion (RD) (μm^2/ms; mean ± SE) in *Fmr1* KO (black solid line) in comparison with WT (gray dashed line) mouse brains. RD was measured in white matter regions including the a) corpus callosum, b) external capsule, c) internal capsule, d) cerebral peduncle, e) fimbria, and f) cerebellar white matter. Gray matter regions measured include the g) caudate putamen and h) thalamus. Significant differences between genotypes at each time point are denoted * $p < 0.05$ and near significant values # $p < 0.10$. The significant p-values passed false discovery rate (alpha = 0.05) in the corpus callosum, external capsule, fimbria, caudate putamen, and thalamus.

Radial Diffusion		df	F-value	p-value
Genotype	Whole brain	1	0.108	0.744
	Corpus callosum	1	4.019	**0.049**
	External capsule	1	0.288	0.593
	Internal capsule	1	2.746	0.102
	Cerebral peduncle	1	0.634	0.428
	Fimbria	1	4.841	**0.031**
	Cerebellar white mat	1	0.425	0.516
	Caudate putamen	1	0.219	0.641
	Thalamus	1	0.267	0.607
Age	Whole brain	3	5.307	**0.002**
	Corpus callosum	3	0.955	0.419
	External capsule	3	4.337	**0.007**
	Internal capsule	3	3.534	**0.019**
	Cerebral peduncle	3	4.746	**0.004**
	Fimbria	3	2.245	0.090
	Cerebellar white mat	3	3.151	**0.030**
	Caudate putamen	3	2.808	**0.045**
	Thalamus	3	4.264	**0.008**
Genotype X age	Whole brain	3	3.978	**0.011**
	Corpus callosum	3	4.692	**0.005**
	External capsule	3	3.224	**0.027**
	Internal capsule	3	2.392	0.075
	Cerebral peduncle	3	2.231	0.092
	Fimbria	3	2.847	**0.043**
	Cerebellar white mat	3	1.762	0.162
	Caudate putamen	3	3.559	**0.018**
	Thalamus	3	3.872	**0.012**
Error	Whole brain	75		
	Corpus callosum	75		
	External capsule	75		
	Internal capsule	75		
	Cerebral peduncle	75		
	Fimbria	75		
	Cerebellar white mat	75		
	Caudate putamen	75		
	Thalamus	75		

n	WT	*Fmr1* KO
PND 18	10	12
PND 21	13	11
PND 30	12	15
PND 60	4	6

Table 7-4: Summary of two-way ANOVA for radial diffusivity. The F-value and p-value for genotype, age, and interaction of (genotype X age) are presented. An interaction with a p-value of 0.05 or less was considered significant (in bold) and allowed further pairwise comparison. An independent Student's T-test was performed if there was a significant interaction of (genotype X age).

7.3.1.4. Fractional anisotropy

Fractional anisotropy (FA) is a commonly used marker for white matter health that increases with brain development and is often used as a parameter to indicate axonal

organization (Mori & Zhang, 2006). The FA value close to 0 represents isotropic diffusion and a value closer to 1 represents highly anisotropic diffusion (Mori & Zhang, 2006; Paydar et al., 2014). No differences in FA were observed in gray and white matter regions at PND 18 and PND 60 between *Fmr1* KO and WT mice. The *Fmr1* KO mice showed increased FA in the external capsule at PND 30 ($t(2.78)$, $p<0.05$) and the caudate putamen ($t(2.64)$, $p<0.05$) compared to WT (Figure 7-4). A significant interaction of (genotype X age) was observed with FA in the external capsule and caudate putamen (Table 7-5). The significant p-value passed false discovery rate (alpha = 0.05) for multiple pairwise comparisons of FA in the external capsule only. The increase of FA in the *Fmr1* KO mouse brain was likely driven by increased myelination as reduced RD in the caudate putamen and showed near significant decrease in the external capsule at PND 30 (see Figure 7-3b and 3g), whereas no change in AD was observed in the external capsule and caudate putamen in the *Fmr1* KO mouse brain at PND 30 (Figure 7-2b and g).

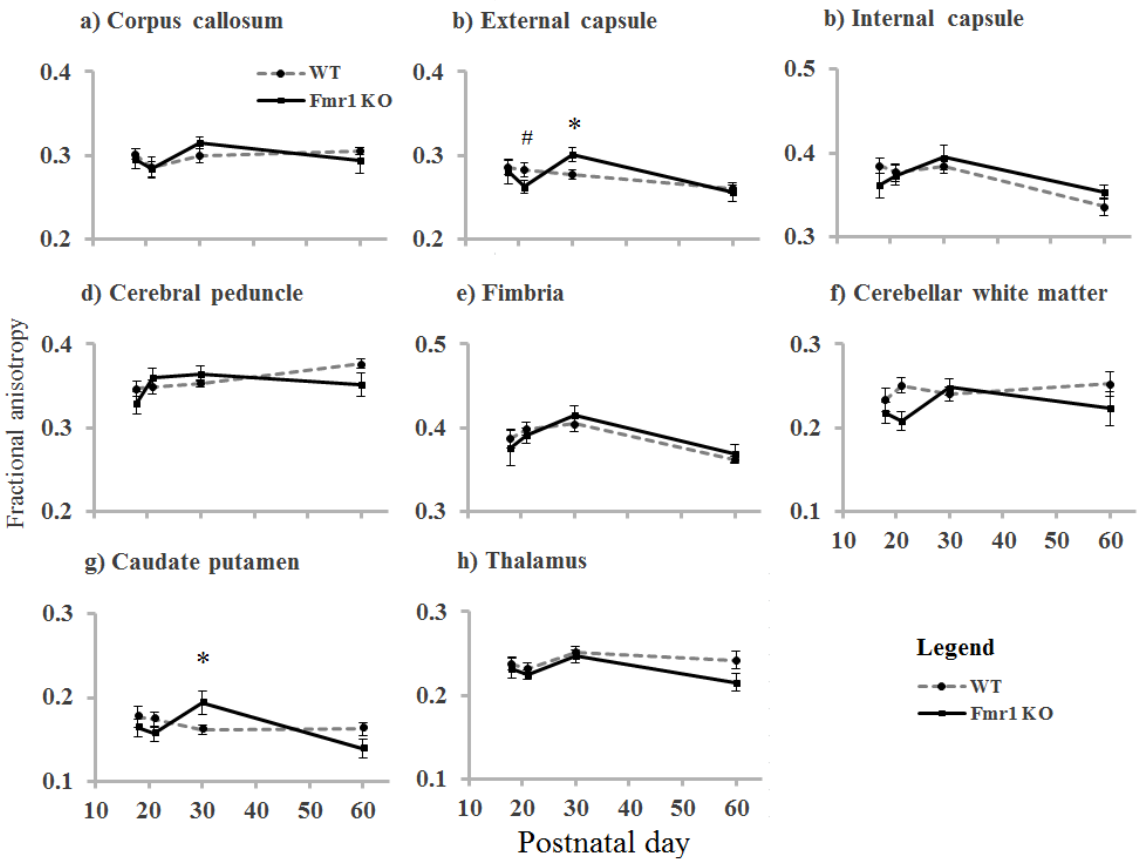

Figure 7-4: Temporal changes in fractional anisotropy (FA) (mean ± SE) in *Fmr1* KO (black solid line) in comparison with WT (gray dashed line) mouse brains. FA was measured in white matter regions including the a) corpus callosum, b) external capsule, c) internal capsule, d) cerebral peduncle, e) fimbria, and f) cerebellar white matter. Gray matter regions measured include the g) caudate putamen and h) thalamus. Significant differences between genotypes at each time point are denoted * $p < 0.05$ and near significant values # $p < 0.10$. The significant p-values passed false discovery rate (alpha = 0.05) for the external capsule and did not pass for the caudate putamen.

Fractional Anisotropy		df	F-value	p-value
Genotype	Whole brain	1	1.222	0.273
	Corpus callosum	1	0.045	0.833
	External capsule	1	0.035	0.853
	Internal capsule	1	0.048	0.827
	Cerebral peduncle	1	0.433	0.513
	Fimbria	1	0.034	0.854
	Cerebellar white matter	1	4.850	**0.031**
	Caudate putamen	1	0.440	0.509
	Thalamus	1	3.020	0.086
Age	Whole brain	3	3.000	**0.036**
	Corpus callosum	3	1.808	0.153
	External capsule	3	3.491	**0.020**
	Internal capsule	3	2.360	0.078
	Cerebral peduncle	3	2.606	0.058
	Fimbria	3	3.446	**0.021**
	Cerebellar white matter	3	1.107	0.352
	Caudate putamen	3	1.846	0.146
	Thalamus	3	3.312	0.025
Genotype X age	Whole brain	3	2.346	0.080
	Corpus callosum	3	0.418	0.740
	External capsule	3	2.895	**0.041**
	Internal capsule	3	0.830	0.481
	Cerebral peduncle	3	1.830	0.149
	Fimbria	3	0.338	0.798
	Cerebellar white matter	3	1.933	0.132
	Caudate putamen	3	3.740	**0.015**
	Thalamus	3	0.449	0.718
Error	Whole brain	75		
	Corpus callosum	75		
	External capsule	75		
	Internal capsule	75		
	Cerebral peduncle	75		
	Fimbria	75		
	Cerebellar white matter	75		
	Caudate putamen	75		
	Thalamus	75		

n	WT	*Fmr1* KO
PND 18	10	12
PND 21	13	11
PND 30	12	15
PND 60	4	6

Table 7-5: Summary of two-way ANOVA for fractional anisotropy (FA). The F-value and p-value for genotype, age, and interaction of (genotype X age) are presented. An interaction with a p-value of 0.05 or less was considered significant (in bold) and allowed further pairwise comparisons. An independent Student's T-test was performed if there was a significant interaction of (genotype X age).

7.3.1.5. Fiber density

No significant effect of genotype or interaction with genotype was observed with fiber density in two-way ANOVA, and hence no pairwise comparisons were performed

(Table 7-6). The fiber density values represent the number of axons or axon bundles in white and gray matter regions in *Fmr1* KO and WT mice are presented in Table 7-7. The results show that the number of axons or axon bundles were not different between *Fmr1* KO and WT mice in the regions studied.

The fiber density in the corpus callosum increased with age between PND 30 and 60 in both *Fmr1* KO and WT mice (Table 7-7). In contrast, fiber density in the internal capsule decreased with age in both *Fmr1* KO and WT mice (Table 7-7). The age-related changes to fiber density may be the result of maturation in white matter tracts and may suggest refinement of cortical connections bridged by the corpus callosum (Hofer & Frahm, 2006) as well as the corticospinal pathway which includes the internal capsule (Feeney & Wier, 1979; Jang & Seo, 2015).

Fiber density		df	F-value	p-value
Genotype	Corpus callosum	1	2.100	0.151
	External capsule	1	1.223	0.272
	Internal capsule	1	3.869	0.053
	Cerebral peduncle	1	0.055	0.814
	Fimbria	1	2.860	0.095
	Caudate putamen	1	2.585	0.112
	Thalamus	1	0.001	0.982
Age	Corpus callosum	3	4.196	**0.008**
	External capsule	3	2.664	0.054
	Internal capsule	3	3.396	**0.022**
	Cerebral peduncle	3	1.586	0.200
	Fimbria	3	0.138	0.937
	Caudate putamen	3	1.237	0.302
	Thalamus	3	2.456	0.070
Genotype X age	Corpus callosum	3	0.461	0.710
	External capsule	3	1.744	0.165
	Internal capsule	3	0.700	0.555
	Cerebral peduncle	3	0.782	0.507
	Fimbria	3	0.952	0.420
	Caudate putamen	3	0.679	0.568
	Thalamus	3	1.908	0.136
Error	Corpus callosum	75		
	External capsule	75		
	Internal capsule	75		
	Cerebral peduncle	75		
	Fimbria	75		
	Caudate putamen	75		
	Thalamus	75		

n	WT	*Fmr1* KO
PND 18	10	12
PND 21	13	11
PND 30	12	15
PND 60	4	6

Table 7-6: Summary of two-way ANOVA for fiber density. The F-value and p-value for genotype, age, and interaction of (genotype X age) are presented. A p-value of 0.05 or less was considered significant (in bold). No significant interaction of (genotype X age) was found in fiber density values.

Fiber density					
Regions	PND	WT	SE	*Fmr1* KO	SE
Corpus callosum	18	13.82	0.68	14.21	0.84
	21	12.33	0.79	13.89	1.08
	30	14.84	0.78	14.90	0.62
	60	15.68	0.84	17.46	0.96
External capsule	18	15.20	0.54	16.61	0.72
	21	16.55	0.65	17.41	0.78
	30	18.27	0.80	17.06	0.42
	60	15.78	1.08	17.07	0.51
Internal capsule	18	16.32	0.76	14.21	0.77
	21	15.24	0.67	15.26	0.65
	30	14.77	1.11	13.52	0.43
	60	13.27	0.68	11.84	0.94
Cerebral peduncle	18	14.11	1.03	12.96	0.72
	21	13.06	0.92	14.54	0.99
	30	14.70	1.02	14.33	0.84
	60	15.57	1.12	16.31	0.50
Fimbria	18	21.92	1.59	22.22	1.31
	21	24.11	1.66	20.66	0.90
	30	24.19	1.32	21.08	0.82
	60	23.43	1.45	22.69	1.00
Caudate putamen	18	13.58	0.68	12.93	0.77
	21	14.03	0.51	14.27	0.81
	30	14.02	0.59	12.86	0.32
	60	15.21	0.50	13.60	0.73
Thalamus	18	17.05	1.00	15.81	0.77
	21	16.63	0.56	15.96	0.78
	30	16.03	0.79	18.35	0.97
	60	19.21	0.89	18.88	1.07

Table 7-7: Fiber density between WT and *Fmr1* KO mice at PND 18, 21, 30 and 60. White matter regions include the corpus callosum, external capsule, internal capsule, cerebral peduncle, and fimbria. Gray matter regions include the caudate putamen and thalamus. Fiber density was calculated with TrackVis software. The fiber density represents a scalar value of the number of fibers, including axons or axon bundles that passed through the white and gray matter ROI.

7.3.2. Diffusion kurtosis parameter changes in the *Fmr1* KO brain

Diffusion kurtosis imaging (DKI), an extension of DTI, measures the extent of non-Gaussianity in a dimensionless parameter. A kurtosis value approaching 0 indicates Gaussian diffusion distribution. Higher kurtosis indicating greater heterogeneity in the diffusion distribution of the brain, which has been associated with presence of cellular structures and membranes (Steven et al., 2014). The whole brain measure of kurtosis parameters did not show significant differences between *Fmr1* KO and WT mice (Table 7-1).

7.3.2.1. Mean Kurtosis

Mean kurtosis (MK) is the average of diffusion kurtosis along all directions and shows degree of deviation from the Gaussian distribution of diffusion (Steven et al., 2014). Increased kurtosis is observed during brain development and often interpreted as an increase in the complexity of gray and white matter including cellular structures, axons and myelin (Paydar et al., 2014). However, no significant interaction of (genotype X age) was observed with MK in white and gray matter regions (Table 7-6 and Figure 7-5 respectively).

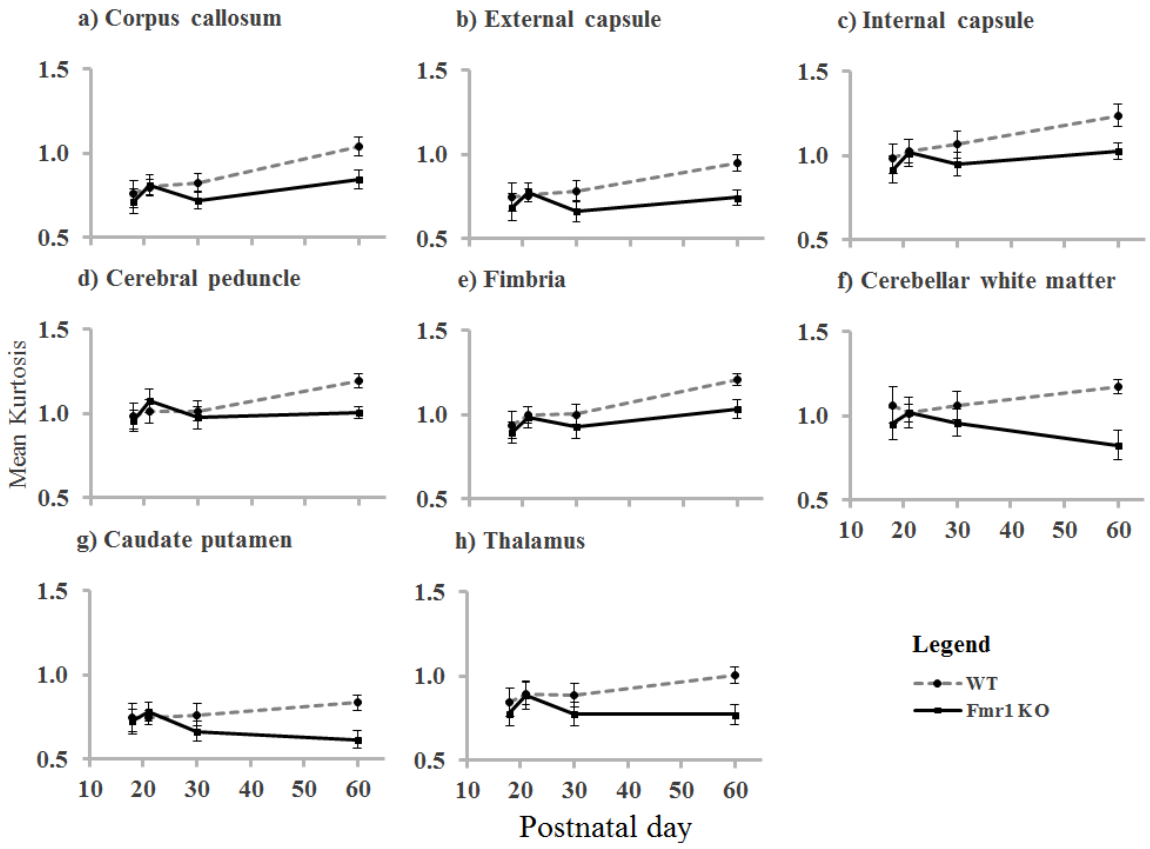

Figure 7-5: Temporal changes in mean kurtosis (MK) (mean ± SE) in *Fmr1* KO (solid black line) in comparison with WT (gray dashed line) mouse brains. MK was measured in white matter regions including the a) corpus callosum, b) external capsule, c) internal capsule, d) cerebral peduncle, e) fimbria, and f) cerebellar white matter. Gray matter regions measured include the g) caudate putamen and h) thalamus. No significant interaction of (genotype X age) was found in the regions studied.

Mean Kurtosis		df	F-value	p-value
Genotype	Whole brain	1	1.501	0.225
	Corpus callosum	1	2.620	0.110
	External capsule	1	2.817	0.097
	Internal capsule	1	2.564	0.114
	Cerebral peduncle	1	0.468	0.496
	Fimbria	1	1.914	0.171
	Cerebellar white matter	1	4.272	**0.042**
	Caudate putamen	1	1.653	0.202
	Thalamus	1	2.368	0.128
Age	Whole brain	3	0.529	0.664
	Corpus callosum	3	2.234	0.091
	External capsule	3	0.926	0.433
	Internal capsule	3	1.044	0.378
	Cerebral peduncle	3	0.718	0.544
	Fimbria	3	2.154	0.101
	Cerebellar white matter	3	0.012	0.998
	Caudate putamen	3	0.249	0.862
	Thalamus	3	0.365	0.779
Genotype X age	Whole brain	3	1.073	0.366
	Corpus callosum	3	0.825	0.484
	External capsule	3	0.807	0.494
	Internal capsule	3	0.467	0.706
	Cerebral peduncle	3	0.760	0.520
	Fimbria	3	0.440	0.725
	Cerebellar white matter	3	0.947	0.423
	Caudate putamen	3	1.093	0.358
	Thalamus	3	0.532	0.662
Error	Whole brain	75		
	Corpus callosum	75		
	External capsule	75		
	Internal capsule	75		
	Cerebral peduncle	75		
	Fimbria	75		
	Cerebellar white matter	75		
	Caudate putamen	75		
	Thalamus	75		

n	WT	*Fmr1* KO
PND 18	10	12
PND 21	13	11
PND 30	12	15
PND 60	4	6

Table 7-8: Summary of two-way ANOVA for mean kurtosis. The F-value and p-value for genotype, age, and interaction of (genotype X age) are presented. A p-value of 0.05 or less was considered significant (in bold). No significant interaction of (genotype X age) was found with MK.

7.3.2.2. Axial Kurtosis

Axial kurtosis (AK) is the kurtosis along the axial direction of the diffusion tensor (Steven et al., 2014). AK is generally low in white matter because diffusion in the axons is relatively unhindered along the axon, and this parameter shows the least deviation from

the Gaussian distribution of diffusion (Steven et al., 2014). Near significant (genotype X age) interactions were observed in the whole brain ($p = 0.076$), corpus callosum ($p = 0.064$), cerebral peduncle ($p = 0.086$), and fimbria ($p = 0.050$) (Table 7-6). We decided to proceed with pairwise comparisons in AK between *Fmr1* KO and WT mice since near significant interaction of (genotype X age) was found in white matter regions. No differences in AK were observed at PND 18, 30, and 60 between *Fmr1* KO and WT mice in the whole brain, as well as the white matter regions (Table 7-9 and Figure 7-6). At P21, *Fmr1* KO mice showed increased AK in the whole brain ($t(2.24)$, $p=0.035$), cerebral peduncle ($t(2.20)$, $p<0.05$), and fimbria ($t(2.17)$, $p<0.05$) compared to the WT mice (Figure 7-6). A near significant decrease of AK was also found in the corpus callosum of *Fmr1* KO mice at PND 30 compared to the WT mice ($p = 0.062$).

Developmental changes in AK were also observed in WT and *Fmr1* KO mice. The increase of AK was observed from PND 18 to 21in the whole brain, cerebral peduncle and fimbria of *Fmr1* KO mouse brain and then decreased from PND 21 to PND 30. The increase of AK was more prominent in WT mouse brain from PND 30 to 60, suggestive of age-related increase of kurtosis expected in the developing rodent brain (Cheung et al. 2016).

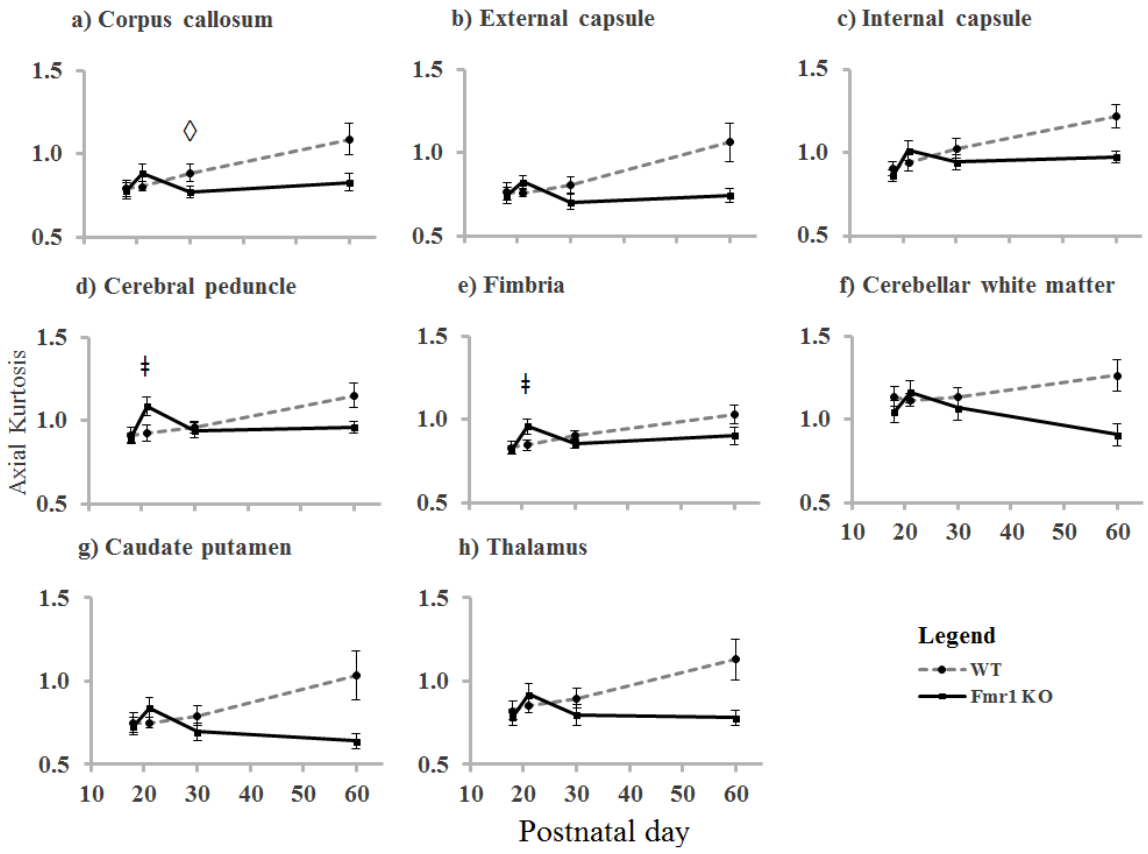

Figure 7-6: Temporal changes in axial kurtosis (AK) (mean ± SE) in *Fmr1* KO (solid black line) in comparison with WT (gray dashed line) mouse brains. AK was measured in white matter regions including the a) corpus callosum, b) external capsule, c) internal capsule, d) cerebral peduncle, e) fimbria, and f) cerebellar white matter. Gray matter regions measured include the g) caudate putamen and h) thalamus. Only near significant interaction of (genotype X age) was observed with AK. Therefore significant differences between genotypes at each time point are denoted differently compared to other figures, ǂ $p < 0.05$ and near significant values ◊ $p < 0.10$.

Axial Kurtosis		df	F-value	p-value
Genotype	Whole brain	1	0.273	0.603
	Corpus callosum	1	1.020	0.316
	External capsule	1	1.304	0.257
	Internal capsule	1	1.058	0.307
	Cerebral peduncle	1	0.418	0.520
	Fimbria	1	0.066	0.798
	Cerebellar white matter	1	3.827	0.054
	Caudate putamen	1	0.700	0.405
	Thalamus	1	0.951	0.333
Age	Whole brain	3	0.736	0.534
	Corpus callosum	3	1.117	0.348
	External capsule	3	0.485	0.694
	Internal capsule	3	2.478	0.068
	Cerebral peduncle	3	1.570	0.204
	Fimbria	3	2.193	0.096
	Cerebellar white matter	3	0.603	0.615
	Caudate putamen	3	0.730	0.537
	Thalamus	3	0.501	0.683
Genotype X age	Whole brain	3	2.388	0.076
	Corpus callosum	3	2.522	0.064
	External capsule	3	1.900	0.137
	Internal capsule	3	1.641	0.187
	Cerebral peduncle	3	2.282	0.086
	Fimbria	3	2.719	0.050
	Cerebellar white matter	3	1.493	0.224
	Caudate putamen	3	2.003	0.121
	Thalamus	3	1.141	0.338
Error	Whole brain	75		
	Corpus callosum	75		
	External capsule	75		
	Internal capsule	75		
	Cerebral peduncle	75		
	Fimbria	75		
	Cerebellar white matter	75		
	Caudate putamen	75		
	Thalamus	75		

n	WT	*Fmr1* KO
PND 18	10	12
PND 21	13	11
PND 30	12	15
PND 60	4	6

Table 7-9: Summary of two-way ANOVA for axial kurtosis. The F-value and p-value for genotype, age, and interaction of (genotype X age) are presented. An interaction with p-value of 0.05 or less was considered significant (in bold). However, the whole brain, corpus callosum, cerebral peduncle, and fimbria revealed near significant interaction of (genotype X age) ($p < 0.10$) and we proceeded with pairwise comparisons using an independent Student's T-test.

7.3.2.3. Radial Kurtosis

Radial kurtosis (RK) measures tissue heterogeneity along the radial direction of

an axon (Steven et al., 2014). In white matter, RK is generally high due to cellular membranes and myelin sheaths resulting in greater non-Gaussian distribution (Kelm et al., 2016; Steven et al., 2014). No significant interaction of (genotype X age) was observed with RK in white and gray matter regions (Table 7-10 and Figure 7-7).

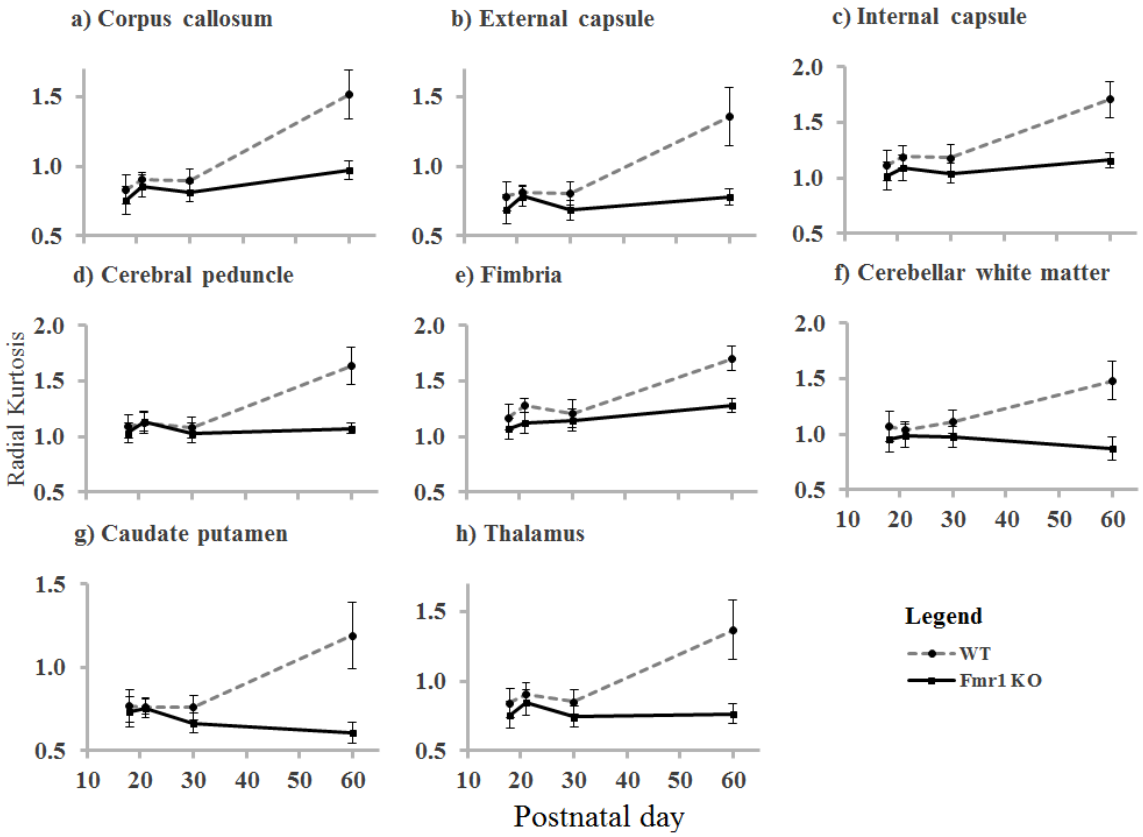

Figure 7-7: Temporal changes in radial kurtosis (RK) (mean ± SE) in *Fmr1* KO (solid black line) in comparison with WT (gray dashed line) mouse brains. RK was measured in white matter regions including the a) corpus callosum, b) external capsule, c) internal capsule, d) cerebral peduncle, e) fimbria, and f) cerebellar white matter. Gray matter regions measured include the g) caudate putamen and h) thalamus. No significant interaction of (genotype X age) was found in the regions studied.

Radial Kurtosis		df	F-value	p-value
Genotype	Whole brain	1	2.295	0.134
	Corpus callosum	1	3.427	0.068
	External capsule	1	3.318	0.072
	Internal capsule	1	3.184	0.078
	Cerebral peduncle	1	1.349	0.249
	Fimbria	1	2.985	0.088
	Cerebellar white matter	1	5.184	**0.026**
	Caudate putamen	1	2.488	0.119
	Thalamus	1	2.859	0.095
Age	Whole brain	3	0.558	0.645
	Corpus callosum	3	3.026	**0.035**
	External capsule	3	0.972	0.411
	Internal capsule	3	0.969	0.412
	Cerebral peduncle	3	0.700	0.555
	Fimbria	3	1.698	0.175
	Cerebellar white matter	3	0.149	0.930
	Caudate putamen	3	0.138	0.937
	Thalamus	3	0.429	0.733
Genotype X age	Whole brain	3	0.648	0.587
	Corpus callosum	3	0.454	0.715
	External capsule	3	0.416	0.742
	Internal capsule	3	0.251	0.861
	Cerebral peduncle	3	0.646	0.588
	Fimbria	3	0.292	0.831
	Cerebellar white matter	3	0.745	0.529
	Caudate putamen	3	0.824	0.485
	Thalamus	3	0.348	0.790
Error	Whole brain	75		
	Corpus callosum	75		
	External capsule	75		
	Internal capsule	75		
	Cerebral peduncle	75		
	Fimbria	75		
	Cerebellar white matter	75		
	Caudate putamen	75		
	Thalamus	75		

n	WT	*Fmr1* KO
PND 18	10	12
PND 21	13	11
PND 30	12	15
PND 60	4	6

Table 7-10: Summary of two-way ANOVA for radial diffusivity. The F-value and p-value for genotype, age, and interaction of (genotype X age) are presented. A p-value of 0.05 or less was considered significant (in bold). No significant interaction of (genotype X age) was found with RK.

7.4. DISCUSSION

7.4.1. Insight regarding axonal fibers of the developing *Fmr1* KO mouse brain

The decrease of AD in white and gray matter regions at PND 21 (Figure 7-2) and increased AK at PND 21 in white matter regions (Figure 7-6) were observed in *Fmr1* KO

mice. The decrease of AD and increase of AK suggests altered axonal organization including the possibility of increased axonal branching and reduced axonal pruning in the *Fmr1* KO mice. Increased axonal branching was reported in the *Drosophila* model of FXS (Pan et al., 2004) and co-culture of the *Fmr1* KO mouse astrocytes and WT mouse neurons resulted in the increase of axonal branching in WT neurons (Jacobs & Doering, 2010). In somatosensory cortex of developing *Fmr1* KO mice, diffuse axon arbors with shorter and more disperse axons compared to WT mice were found, suggesting deficits in axonal guidance and axon pruning in *Fmr1* KO mouse brain (Bureau et al., 2008). In addition, the current study did not find differences in fiber density between *Fmr1* KO and WT mice, which suggest the increase in AD at PND 21 and PND 30 in *Fmr1* KO mouse brain is more likely attributed to alterations in axonal organization than changes in the number of axons. AK is low in white matter due to the relatively unrestricted diffusion of water along the axial direction (Steven et al., 2014). However, the increased AK in the immature *Fmr1* KO mouse brain at PND 21 suggests a potential increase in tissue heterogeneity that can hinder the unrestricted diffusion along the axial direction and further supports alterations in axonal organization.

The alterations of AD and AK in *Fmr1* KO mouse brain were transient, found during the peak of synaptogenesis between PND 20-21and neural network development between PND 25-35 (Semple et al., 2013), and equilibrated to WT levels by PND 60. Alterations in axon organization during these critical periods may result in deficits with neuronal signaling. Reduced axon motility has been reported in *Fmr1* KO neuron that may contribute to the inability to form connections with dendritic spines and contribute to higher density of immature dendritic spines (Antar et al., 2006). Thus, the decrease of AD

and increase of AK in the developing *Fmr1* KO mouse brain may suggest developmental abnormalities in axon organization during the formation of the neural network.

7.4.2. Insight regarding myelination in the developing *Fmr1* KO mouse brain

Proper myelination is essential to maintaining the health of the axon and for the proper conduction of neuronal signals that travel along the axon (Quarles et al., 2012). The decreased RD in white and gray matter regions in the *Fmr1* KO mice at PND 21 and 30 show that diffusion was more restricted along the radial direction and may suggest an increase in myelin compaction or more densely packed myelinated fibers. This notion of increased myelination in *Fmr1* KO mice is supported by our findings of increased myelin density in the external and internal capsules, cerebral peduncle, and fimbria of *Fmr1* KO mice at PND 30 as described in Chapter 6 (Figure 6-4). A previous study by Pacey et al. (Pacey et al., 2013) showed that myelin thickness and the number of myelinated axons were reduced in the cerebellar white matter of immature *Fmr1* KO mice (PND 7) and normalized by PND 15. Furthermore, Pacey et al. (Pacey et al., 2013) reported increased amount of sparsely myelinated axons (myelin thickness of 60 nm or less), and a reduction in the number of heavily myelinated axons (myelin thickness of 100-120+ nm) in the cerebellar white matter in the immature *Fmr1* KO mice (PND 7). Differences were no longer observed in the distribution of myelin thickness by PND 15, suggesting myelin differences were only present in early cerebellar white matter development between *Fmr1* KO and WT mice (Pacey et al., 2013). Similarly, the current study did not find (genotype X age) differences with RD in the cerebellar white matter between *Fmr1* KO and WT mice in the ages studied (Figure 7-4f). The decreased RD found in the current

study supports the findings of increased myelination at PND 30 and may also indicate greater compaction of myelin or densely packed myelinated fibers in white matter regions in *Fmr1* KO mouse brain.

7.4.3. Alterations in diffusivity in the brains of *Fmr1* KO mice and FXS patients

In the current study, no differences were found in diffusion and kurtosis parameters at PND 60 between *Fmr1* KO and WT mice (Figures 7-1 through 7-7). However, recent *in vivo* DTI findings in adult (PND 63-84) C57Bl6J *Fmr1* KO mice showed increased MD and decreasing FA in the corpus callosum compared to the corresponding region in WT mouse brain (Haberl et al., 2015). The differences in findings by Haberl et al. (Haberl et al., 2015) to the current study may be due to the wider age range for adult mice used by Haberl et al. (Haberl et al., 2015) and/or the small sample size in the present study at PND 60 (n=4 WT and n=6 *Fmr1* KO). While the mouse brain is considered adult by PND 60, it has also been reported that specific developmental processes including ongoing myelination (Semple et al., 2013) and maturation of the prefrontal cortex (Kolb et al., 2012) may not be complete. It may be possible that further changes occur at older ages in the white matter of *Fmr1* KO mice where an increase in MD and decrease in FA have been reported (Haberl et al., 2015). Reduced FA and increased AD and RD were also reported in girls with FXS (7-14 years) in the internal capsule, thalamus, and precentral gyrus compared to normal controls (Villalon-Reina et al., 2013). The study by Barnea-Goraly et al. (Barnea-Goraly et al., 2003) also reported decreased FA in the white matter pathways from the frontal-striatal and parietal to somatosensory cortices in female adolescent and adult FXS patients (13-

23 years) compared to normal controls. While our study also shows evidence of increased MD and decreased FA in the preclinical model of FXS, a notable difference is that our study is on adult male *Fmr1* KO mice whereas the FXS patients in the above studies were all female.

Findings from the fixed brains in the current study were consistent with MD and FA trends reported in FXS patients compared to IQ-matched controls (Green et al., 2015; Hall et al., 2016). A DTI study with FXS patients ages (10-23 years) showed increased FA in many white matter pathways in the forebrain, including regions of the inferior longitudinal fasciculus, the uncinated fasciculus, the cingulate gyrus, compared to IQ-matched controls (Hall et al., 2016). In addition, decreased MD between the white matter of the temporal and occipital lobes was reported in FXS patients compared to IQ-matched controls, suggesting aberrant axonal growth and pruning due to the lack of FMRP regulation in the FXS brain (Hall et al., 2016). In young adults with FXS (23 ± 3 years), increasing FA and decreasing RD were found in white matter regions of the inferior longitudinal fasciculus connecting the superior and medial temporal gyri and in the inferior fronto-occipital fasciculus in FXS patients compared to IQ-matched controls (Green et al., 2015). These two studies with FXS patients demonstrate alterations in DTI parameters specific to FXS pathology as the FXS patients were compared to developmentally delayed patients of similar IQ (Green et al., 2015; Hall et al., 2016).

7.4.4. Diffusivity in normally developing rodents

It is necessary to compare our diffusivity data to other studies with the developing WT mice to ensure the findings in our controls reflected normal development in the

mouse brain. The AD and RD values in our study were similar to the values reported by Sun et al. (Sun et al., 2003) in the *in vivo* and fixed mouse brain. In addition, they reported AD and RD values in white and gray matter were not different between *in vivo* and fixed mouse brain. Bockhorst et al. (Bockhorst et al., 2008) studied the developmental change in FA, MD, AD and RD of the corpus callosum and internal capsule in *in vivo* WT rat brains at PND 0 (birth), 2, 4, 6, 8, 14, 21, 28, 42 and 56. Increased FA and decreased MD, AD, and RD were found between only PND 0-21 in the developing corpus callosum of WT rats and no changes were observed at older ages in the corpus callosum (Bockhorst et al., 2008). A recent *in vivo* study of the developing C57Bl6J mouse brain showed no differences with MD, AD, RD, and FA at PND 21, 56, 84 and 168 in the whole brain, white matter regions of the corpus callosum, external and internal capsule, and fimbria, as well as gray matter regions of the caudate putamen and thalamus (Hammelrath et al., 2016). The findings in the current study with WT mice also showed no developmental change in MD, AD, and RD between PND 18-60 in white and gray matter regions. The effect of age found in our data may be influenced by the decrease in *Fmr1* KO mice from PND 18 to 21, whereas no significant differences were observed in MD, AD, and RD between ages in WT mice. Another *in viv*o cross sectional DTI study using C57Bl6J mice at PND 30, 50 and 70 showed no changes between ages with MD in the corpus callosum, external and internal capsule (Kumar et al., 2012). Furthermore, FA decreased from PND 50 to PND 70 in the corpus callosum, external and internal capsule of C57Bl6J mice (Kumar et al., 2012). Similarly, we found significant effect of age in the external capsule and near significant effect of age in the internal capsule in both *Fmr1* KO and WT mice (Figure 7-4). Therefore, the WT mice used in this

study demonstrated similar developmental trajectory compared to DTI parameters reported in the developing rodent brain.

7.5. CONCLUSIONS

The current study used DTI and DKI to determine developmental differences in white and gray matter microstructure between *Fmr1* KO and WT mice. Our results showed evidence of abnormal microstructure in white and gray matter regions in the *Fmr1* KO mouse brain, including decreased MD, AD, and RD during developmental stages at PND 21 and 30. Furthermore, increased FA was observed in the *Fmr1* KO mouse brain at PND 30. The reduced diffusion parameters indicated more restricted diffusion environment in the *Fmr1* KO mouse brain at PND 21 and 30; the decrease in AD suggests a possible alteration in axonal organization, while the decrease in RD suggests an increased compaction of myelin in the brains of *Fmr1* KO mice compared to the WT mice. No differences were found in fiber density in white matter regions indicating that the number of axons or axon bundles were not different between *Fmr1* KO and WT mice. Further investigations using immunohistological staining of axons are needed to confirm findings of altered axon organization and electron microscopy to determine changes in myelin thickness in the developing *Fmr1* KO mice.

CHAPTER 8: RESTING STATE NETWORKS IN THE DEVELOPING *FMR1* KO MOUSE BRAIN

8.1. INTRODUCTION

8.1.1. Functional connectivity and resting state networks in the brain

Resting state functional magnetic resonance imaging (fMRI) is a common method to study the large-scale topological organization of the brain through temporal correlation of the spontaneous low frequency fluctuations in the blood oxygen level dependent (BOLD) signal (Thompson et al., 2015; van den Heuvel & Hulshoff Pol, 2010). The BOLD signal arises from differences between the diamagnetic properties of oxygenated hemoglobin and the paramagnetic deoxygenated hemoglobin, (Ogawa et al., 1990). Neural activity leads to increased cerebral blood flow of oxygenated hemoglobin and results in increase of BOLD signal; thus the BOLD signal is an indirect measure of brain activity (Buxton & Frank, 1997; Ogawa et al., 1990). The correlation of spontaneous BOLD signal between two brain regions is measured by functional connectivity and is organized into functional brain networks known as resting state networks (Mantini et al., 2007). Identified resting state networks in adult human brain include the default mode, attention, salience, auditory, visual and somatomotor networks (Mantini et al., 2007, Peters et al., 2016). Determining functional connectivity of resting state networks is important to the study of FXS since previous studies have reported neural network dysfunction, including altered neuronal activity and imbalance of excitatory/inhibitory neuronal signaling in the neocortex of the *Fmr1* KO mouse brain (Gibson et al., 2008; Harlow et al., 2010).

8.1.2. Imbalance of neuronal signaling in the developing *Fmr1* KO mice

The imbalance of excitatory and inhibitory signaling has been demonstrated in the somatosensory cortex of the developing C57Bl6J *Fmr1* KO mice. Decreased LTP in somatosensory cortex has been reported during the critical period of synaptic plasticity in the developing *Fmr1* KO mice brain (PND 3-10) (Harlow et al., 2010). Furthermore, increased membrane excitability in excitatory neurons and decreased membrane excitability of fast spiking inhibitory neurons has also been reported in somatosensory cortex of the developing *Fmr1* KO mouse brain (PND 14 and PND 28) (Gibson et al., 2008). Synchronous depolarization of neighboring excitatory neurons has been observed due to this increase in membrane excitability in excitatory neurons resulting in abnormally elevated neocortical circuit excitability in developing *Fmr1* KO mouse brain (Gibson et al., 2008). The alterations in the neocortical circuits of *Fmr1* KO mouse brain have led to further investigations into the brain networks of FXS patients and *Fmr1* KO mice respectively (Haberl et al., 2015; Hall et al., 2013).

8.1.3. Altered functional connectivity in FXS and the *Fmr1* KO mice

A recent study by Haberl et al. (Haberl et al., 2015), using resting state functional MRI (rs-fMRI) has revealed decreased functional connectivity between the visual cortex and somatosensory, motor and auditory cortices, as well as the caudate putamen and hippocampus in the brain of adult C57Bl6J *Fmr1* KO mice compared to WT (9-12 weeks old). In addition, fluorescent viral tracer injection in visual cortex demonstrated an increase of local neuronal connections within the visual cortex of adult *Fmr1* KO mouse

brain while long-distance neuronal connections to cortical and subcortical regions are decreased (Haberl et al., 2015).

The increase of neuronal hyperconnectivity may contribute to local neural network excitability in the visual cortex of adult *Fmr1* KO mouse (Haberl et al., 2015). It should be noted that functional connectivity is a measure of the correlation of BOLD signal between two brain regions and decreased functional connectivity is not the same as decreased brain activity. Rather a decrease in functional connectivity is reflective of how asynchronous the temporal BOLD signal is between the same two regions of WT and *Fmr1* KO mouse brains. Thus, the decrease of functional connectivity in the resting state networks reflects altered functional organization in the brain network in *Fmr1* KO mice. The findings by Haberl et al. (Haberl et al., 2015) demonstrate hyperconnectivity of neuronal connections within the visual cortex, whereas functional connectivity between cortical and subcortical brain regions decrease (Haberl et al., 2015).

Alterations in functional connectivity are reported in children and adolescents with FXS (ages 10-16) (Hall et al., 2013). Specifically, reduced functional connectivity is found in brain regions including the frontal, temporal, parietal, and occipital lobes, which are associated with the attention, default mode, somatomotor, and visual, and auditory resting state networks (Hall et al., 2013). The study by Hall et al. (Hall et al., 2013) only compared FXS patients to IQ-matched controls, and not to normal controls, to distinguish between alterations in functional connectivity specific to FXS. The reduced functional connectivity suggests that alterations in resting state networks may potentially underlie behavioral and cognitive deficits specific to FXS patients (Hall et al., 2013). The neuronal hyperconnectivity in *Fmr1* KO mouse brain may contribute to decreased

functional connectivity since more neuronal activity in visual cortex will result in higher BOLD signal in the visual cortex than the other brain regions. Similarly, elevated neocortical excitability in somatosensory cortex can also result in higher BOLD signal and reduced functional connectivity in the *Fmr1* KO mouse brain. These neurological features may also contribute to the decreased functional connectivity observed in FXS patients (Hall et al., 2013).

8.1.4. Resting state networks in the rodent brain

Established resting state networks reflect processing of auditory, visual, somatosensory and motor information (Biswal et al., 1997; Mantini et al., 2007). In addition, higher order networks like the DMN, attention and salience networks regulate emotion, cognition, and sense of self (Mantini et al., 2007; Peters et al., 2016; Seeley et al., 2007). Human resting state networks were discussed in Chapter 2. The networks relating to sensory input (somatomotor, auditory, and visual) as well as the default mode network have been demonstrated in adult rats and mice (Bajic et al., 2016; Jonckers, et al., 2011; Lu et al., 2012; Sierakowiak et al., 2015). Currently, only one study has reported the default mode and somatomotor resting state networks in the immature rat brain (PND 13-15) (Bajic et al., 2016).

Previous findings demonstrated altered neuronal activity in somatosensory cortex of the immature *Fmr1* KO mice (Gibson et al., 2008; Harlow et al., 2010), as well as reports of hypersensitivity to electrical stimuli and poor motor coordination and learning in developing *Fmr1* KO mouse (Padmashri et al., 2013; Zhang et al., 2014). The deficiencies in the somatosensory and motor cortices of *Fmr1* KO mouse brain suggest

the somatomotor network is also altered. The rodent somatomotor network includes the somatosensory and motor cortices, as well as regions of the prefrontal cortex, caudate putamen, and thalamus. The somatomotor network is present in the immature (PND 13-17) and adult (20-24 weeks) rodent brains (Bajic et al., 2016; Liska et al., 2015; Lu et al., 2012; Sierakowiak et al., 2015).

The auditory network is of interest because FXS patients show hypersensitivity to auditory stimuli (Hall et al., 2009) and the *Fmr1* KO mice are susceptible to audiogenic seizures, especially during development (Musumeci et al., 2000). Haberl et al. (Haberl et al., 2015) reported decreased functional connectivity between the visual cortex to the auditory, somatosensory, and motor cortices, as well as to the caudate putamen in the adult *Fmr1* KO mice (9-12 weeks old), which suggests reduced functional connectivity in the somatomotor, visual and auditory networks in the adult *Fmr1* KO mouse brain.

Hall et al. (Hall et al., 2013) have reported reduced functional connectivity in the default mode network, including the insular and parietal cortices as well as the superior frontal gyrus, in children and adolescents with FXS. In the normal human brain, the default mode network is a group of interconnected brain regions that show corresponding BOLD signal when the brain is at rest and not focused on a goal-oriented task and is also involved social, emotional, and introspective processes (Buckner et al., 2008; Li et al., 2014). Social and emotional deficits are well documented in FXS patients, including social avoidance and eye gaze aversion, as well as irritability and violent behavior (Bailey et al., 2009; Garber et al., 2008; Hall et al., 2006; Watson et al., 2008). The default mode network has also been identified in the immature and adult rodent brains, showing functional connectivity between the prefrontal, cingulate, granular and parietal

cortices (Bajic et al., 2016; Hutchison et al., 2010; Lu et al., 2012; Sforazzini et al., 2014). Thus the developing *Fmr1* KO mouse brain may show deficits in functional connectivity in many resting state networks, similar to previous finding in adolescent FXS patients (Hall et al., 2013) and adult *Fmr1* KO mice (Haberl et al., 2015).

8.1.5. The effect of anesthesia on resting state networks in the rodent brain

The effect of anesthesia on brain function deserves special consideration due to the reduction of BOLD signal from anesthetics (Jonckers et al., 2015; Nasrallah et al., 2016; Pan et al., 2015; Sierakowiak et al., 2015). Anesthesia can suppress brain metabolism (Gyulai, 2004) and reduce functional connectivity in the brain (Jonckers et al., 2015; Pan et al. 2015). Isoflurane inhalation reduces cerebral blood flow and doses of 2% or higher can significantly reduce BOLD signal (Jonckers et al., 2015). However, BOLD signals have been reported under light anesthesia between 1-1.5% isoflurane in adult rodents (Haberl et al., 2015; Hutchison et al., 2010; Jonckers et al., 2015; Sforazzini et al., 2014). Adult mice and rats anesthetized with 1-1.5% isoflurane show functional connectivity between the frontal orbital, cingulate, granular and parietal cortices that is indicative of a default mode network (Hutchison et al., 2010; Jonckers et al., 2011; Sforazzini et al., 2014). Similarly, indications of the somatomotor, auditory and visual networks are reported in anesthetized adult mice and rats with 1-1.5% isoflurane (Jonckers et al., 2011; Sierakowiak et al., 2015). Despite the known limitations of isoflurane on BOLD signal, isoflurane is still commonly used in resting state fMRI for longitudinal studies in rodents because of the short recovery time and low mortality rates (Jonckers et al., 2015). However, repeated isoflurane exposure must be carefully

controlled in developmental studies. Repeat exposure to 1.5% isoflurane for 2 hours for three consecutive days between PND 7-10 has been shown to cause apoptosis in the hippocampus of C57Bl6J WT mice (Yi et al., 2015). Yi et al. (Yi et al., 2015) also reported that mice with early isoflurane exposure (PND 7-10) show poor performance in the Morris water maze in adulthood, including increased escape latency and reduced number of platform crossings. Although the effect of anesthesia on the BOLD signal even at lower levels is not completely known, anesthesia must be carefully controlled when studying functional connectivity in rodents, especially during development.

8.1.5. Study aim

Functional connectivity studies in the adult rodent brain have shown evidence of the default mode, somatosensory, auditory, and visual resting state networks (Hutchison et al., 2010; Lu et al., 2012; Sforazzini et al., 2014). Functional connectivity is observed under light anesthesia (1-1.5% isofluorane) albeit with lower BOLD signal (Jonckers et al., 2015; Nasrallah et al., 2016; Pan et al. 2015; Sierakowiak et al., 2015). However, there is only one study currently demonstrating resting state networks in the immature rat brain (Bajic et al., 2016) and none studying the immature mouse brain. Thus, the purpose of this study is to characterize developmental changes in functional connectivity in WT and *Fmr1* KO mouse brains. The current study focuses on functional connectivity in the somatomotor, auditory, visual, and default mode networks, all of which were previously established in WT adult rodent brain (Jonckers et al., 2015; Lu et al., 2012; Sierakowiak et al., 2015). Functional connectivity in these networks was reduced in brains of FXS patients and *Fmr1* KO mice (Haberl et al., 2015; Hall et al., 2013). We assessed

functional connectivity changes during the developmental stage (PND 30) and early adulthood (PND 60) in *Fmr1* KO mice compared to WT. The rationale for using PND 30 as the development stage is supported by evidence that synaptic pruning continues during this period in rodents and by PND 60 the rodent brain is matured and brain networks are developed (Semple et al., 2013). We predicted that functional connectivity changes in WT mice from PND 30 to PND 60 would indicate normal brain development. From previous reports showing altered neural network formation and reduced functional connectivity in *Fmr1* KO mice (Gibson et al., 2008; Haberl et al., 2015; Harlow et al., 2010), we hypothesized that the functional connectivity in the somatomotor network would decrease in the *Fmr1* KO mice compared to the WT mice.

8.2. MATERIALS AND METHODS

8.2.1. Animal procedure

The current study used B6.129P2-*Fmr1*^{tm1Cgr} (*Fmr1* KO) mice (Jackson Laboratory, Bar Harbor, ME, USA) from a C57BL6J background and WT mice (JAX C57Bl/6J mice; Jackson Laboratory, Bar Harbor, ME, USA) bred in the animal facility at the University of Maryland, Baltimore. The animal protocol was approved by the Institutional Animal Care and Use Committee at the University of Maryland, Baltimore. All mice were weaned at PND 21. The mice were genotyped using methods previously described in Bakker et al. (Bakker et al., 1994) and described in Chapter 4. Food and water were provided *ad libitum*. Six WT mice and 6 *Fmr1* KO mice were studied; no mice died during scanning.

8.2.2. Magnetic resonance imaging

8.2.2.1. Anesthesia

A MDS Matrix Isoflurane Vaporizer, Model VIP 3000, was used to deliver 100% oxygen containing 2.5% isoflurane at 1 liter/minute to the mice to induce anesthesia in an induction chamber. Once the mouse was anesthetized it was removed from the induction chamber and placed in a small animal holder in a prone position with its head held in place with a bite bar and ear pins. A circulating warm water pad was placed over the mouse to maintain body temperature at 36–37°C. Isoflurane was then gradually reduced to a maintenance dose of 1.5% for the duration of the MRI scan. The breathing rate of the mouse was monitored during the scan (SA Instruments, Stony Brook, NY, USA). MRI studies were performed at PND 30 and PND 60 on *Fmr1* KO and WT mice, and each mouse was under isoflurane anesthesia for approximately 2 hours per MRI scan.

8.2.2.2. Image acquisition

All imaging was performed on a Bruker Biospec 7.0 Tesla 30 cm horizontal bore scanner using Paravision 5.1 software (Bruker Biospin MRI, Ettlingen, Germany). A Bruker 72-mm linear-volume coil was the transmitter and a four-channel Bruker ^{1}H surface array coil was used as the receiver. Prior to imaging, magnetic field inhomogeneity was adjusted using the FASTMAP technique (Gruetter, 1993b). An anatomical T_2 image was performed first, with parameters: TE/TR = 19 ms/3000 ms, 4 averages, 1mm slice thickness and 10 slices covering the cerebral cortex. The spatial resolution was 150 μm x 150 μm over a field of view (FOV) of 1.5 cm x 1.5 cm. Three rs-fMRI scans were performed per mice at each age with a spin-echo echo planar imaging

sequence. The rs-fMRI scan parameters were: TE/TR = 27.69 ms/1000 ms, spatial resolution 312 μm X 312 μm, FOV 1.5 cm x 1.5 cm, 10 slices with a thickness of 1 mm that covered the cerebral cortex and was spatially matched to the anatomical image. A total of 600 volumes (time series) were collected during each rs-fMRI scan. After the MRI, the mouse was allowed to recover in its home cage with littermates and then returned to the colony. Images were converted into the standard image format (digital imaging and communications in medicine format) in preparation for image pre-processing.

A WT mouse brain was fixed at PND 30 and scanned following procedures in Chapter 5. This WT mouse brain was scanned with 3D TurboRARE T2 image over a slab of 15 mm thickness, isotropic resolution 150 μm^3 , TE/TR =11/2500 ms, 2 averages. The high resolution anatomical image was used as the template during pre-processing steps.

8.2.3. Data analysis

8.2.3.1. Pre-processing procedures

Pre-processing of the rs-fMRI images was necessary before further analysis to correct for motion and physiological noise which can result in spurious functional connectivity (Pan et al. 2015). Pre-processing was performed using Statistical Parametric Mapping (SPM) (SPM, London, UK) and Analysis of Functional NeuroImages (AFNI) software (AFNI, National Institute of Health, Bethesda, MD). The pre-processing procedure of images is shown in Figure 8-1. In SPM, image pre-processing pipeline included slice timing correction, which adjusted for the different times of slice acquisition to make it appear that BOLD signal for each time series was collected at once.

Then motion correction was performed, which ensured each voxel in the time series were in the same location. Then the rs-fMRI image was registered to the high resolution anatomical image of the mouse, where the rs-fMRI image was adjusted by translational (x, y, z) and rotational parameters (roll, pitch, yaw) to fit the anatomical image. The anatomical images obtained at PND 30 and PND 60 were similarly then registered to a template mouse brain using SPM. The template mouse brain is a 3D high-resolution anatomical image of a fixed male WT mouse brain at PND 30 from our lab.

Further pre-processing and motion correction were performed in AFNI, including despiking which removed short, high amplitude signal most likely result of motion from the time series, detrending process which removed noise from low-frequency drifts in the time series that could arise from artifacts and movement, smoothing with a 0.6 mm full width half maximum Gaussian kernel to average signal intensities between voxels to improve signal to noise ratio, correction of translational (x, y, z) and rotational movements (roll, pitch, yaw), and band-pass filtering of BOLD signal with the frequency range of 0.01-0.1 Hz to remove cardiac and respiratory physiological noise (Cox, 1996). These pre-processing steps were necessary to remove motion, correct imaging artifacts and physiological noise; all of which could have led to false correlation of BOLD signal between regions (Pan et al. 2015).

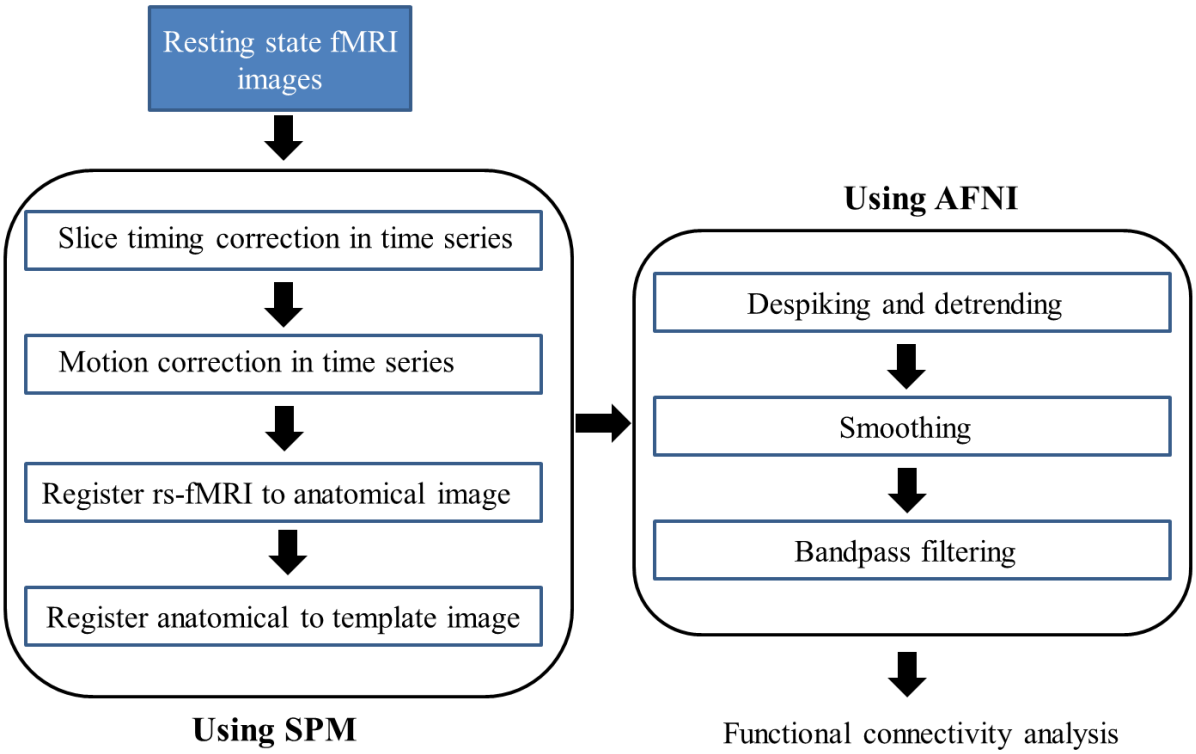

Figure 8-1: Flowchart of pre-processing procedures with the rs-fMRI images. Slice timing and motion correction, as well as image registration, were performed using Statistical Parametric Mapping (SPM). Further pre-processing of the rs-fMRI images were performed using Analysis of Functional NeuroImages (AFNI) software, including despiking, detrending, smoothing, and bandpass filtering. Calculation of functional connectivity was performed after pre-processing steps.

8.2.3.2. Calculation of functional connectivity

A custom mouse brain atlas with 26 unilateral cortical and subcortical ROIs was drawn on the WT mouse brain template (Figure 8-2) using a previously established anatomical reference of the mouse brain (Franklin & Paxinos, 2007). For each rs-fMRI image, the time series from each rs-fMRI scan was extracted from each ROI. The correlation of low frequency BOLD signal between each ROI pairs was calculated with Pearson's correlation coefficient and then converted into a z-score with Fisher's transformation. The z-scores from the 3 scans were then averaged for each seed to target region in each mouse brain, which represents functional connectivity in the mouse. Three

rs-fMRI scans were preformed and averaged to increase BOLD signal from the mice.

Two sets of connectivity matrices were developed. The first matrix was generated to highlight the longitudinal differences in functional connectivity, measured by z-scores, from PND 30 to 60 in WT and *Fmr1* KO group in each of the paired ROIs. The second matrix highlighted the differences in functional connectivity between WT and *Fmr1* KO mice at PND 30 and PND 60 for each of the paired ROIs. The connectivity matrices with respect to genotype showed the difference in z-scores between WT and *Fmr1* KO mice. Regions were analyzed unilaterally to differentiate intra- and inter- hemispheric functional connectivity. Functional connectivity from ROIs associated with the somatomotor, auditory, visual, and default mode networks was used for statistical analysis (Jonckers et al., 2011; Mantini et al., 2007). The hippocampal ROI (numbers 25 and 26 in Figure 8-2) did not belong to these networks and was not used.

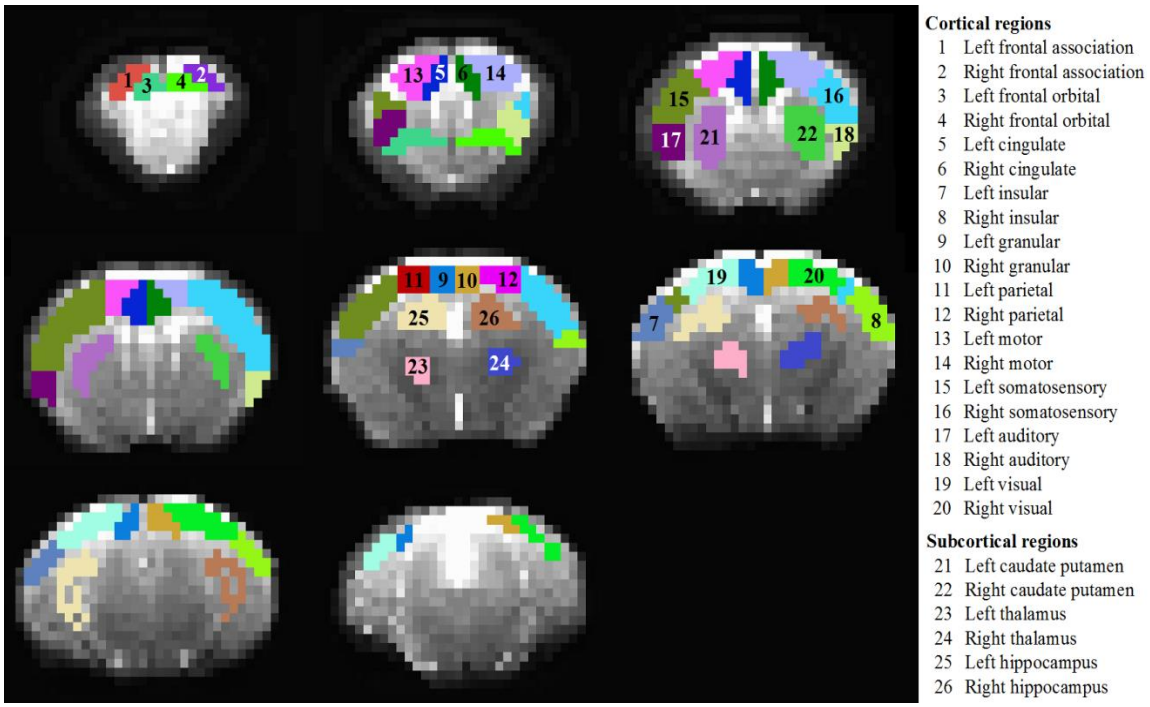

Figure 8-2: The mouse brain atlas. Unilateral region of interests were drawn manually with AFNI in cortical and subcortical regions. The number in the ROI corresponds to the ROI label.

8.2.4. Statistical analysis

The connectivity z-scores were analyzed using repeated measures analysis of variance (RMANOVA) for each of the paired regions in SPSS (IBM Corp. 2013. IBM SPSS Statistics for Windows, Version 22.0. Armonk, NY). To analyze the effect of development on functional connectivity, a 2-way RMANOVA was performed, the between subject factor was genotype (WT and *Fmr1* KO) and the within subject factor was age (PND 30 and PND 60). Genotype and age effects were analyzed by Student's t-tests if the interaction of (age X genotype) was statistically significant ($p < 0.05$). To control for multiple comparisons, the false discovery rate was calculated with a threshold of alpha = 0.05, which assumes 5% of significant p-values are false. The significant p-values reported are uncorrected but not passing the false discovery rate may indicate that

the p-value is a false positive.

8.3. RESULTS

8.3.1. Developmental differences in the somatomotor network

To date, no studies have investigated the developmental change in functional connectivity in the somatomotor network in developing WT or *Fmr1* KO mouse brain. Therefore, it was essential to first determine longitudinal differences in functional connectivity from PND 30 to PND 60 in WT and *Fmr1* KO mice. Knowing the longitudinal differences, we then compared genotype differences between *Fmr1* KO mice and WT at each time point. Significant within group interaction of (age X genotype) was found in the functional connectivity between the left somatosensory cortex and right thalamus ($F(1,20) = 5.63$, $p = 0.040$), and between the right somatosensory cortex and right caudate putamen ($F(1,20) = 5.39$, $p = 0.030$). Near significant within group interaction of (age X genotype) was found in functional connectivity between the right motor cortex and right somatosensory cortex ($p = 0.081$), between the left motor cortex and left frontal orbital cortex ($p = 0.096$), between the left somatosensory cortex and left thalamus ($p = 0.087$), as well as between the right somatosensory cortex and left caudate putamen ($p = 0.083$). Significant interactions were further analyzed using Student's t-tests for time related changes (pairwise comparison of PND 30 and PND 60) and genotype related differences (pairwise comparison of WT and *Fmr1* KO at each time point).

In the somatomotor network of WT mice, functional connectivity between the left somatosensory cortex and the right thalamus decreased from PND 30 to PND 60 ($t(2.80)$,

p = 0.019), and between the right somatosensory cortex and right caudate putamen (p = 0.083) (Figure 8-3 a and c) were significant or close to statistically significant. No significant differences were found in functional connectivity between PND 30 and 60 in the *Fmr1* KO mice (Figure 8-3b). In the somatomotor network, the WT mice showed a developmental decrease of functional connectivity from PND 30 to PND 60. In contrast, functional connectivity in *Fmr1* KO mice did not change from PND 30 to PND 60, suggesting a lack of functional connectivity that may indicate a delay in development of the somatomotor network.

Comparison between genotypes revealed lower functional connectivity between the left somatosensory cortex and right thalamus (t(2.41), p = 0.037) in the *Fmr1* KO mice compared to the WT mice at PND 30 (Figure 8-3c and 8-4a). No differences in functional connectivity were found at PND 60 (Figure 8-4b). The significant p-values passed false discovery rate (alpha = 0.05), which controlled for multiple pairwise comparisons of functional connectivity between the left somatosensory cortex and right thalamus, but did not pass for significant p-values between the right somatosensory cortex and the right caudate putamen. During brain development, functional connectivity in the somatomotor network was lower in *Fmr1* KO mice compared to WT at PND 30, but at PND 60 there were no differences between the genotypes.

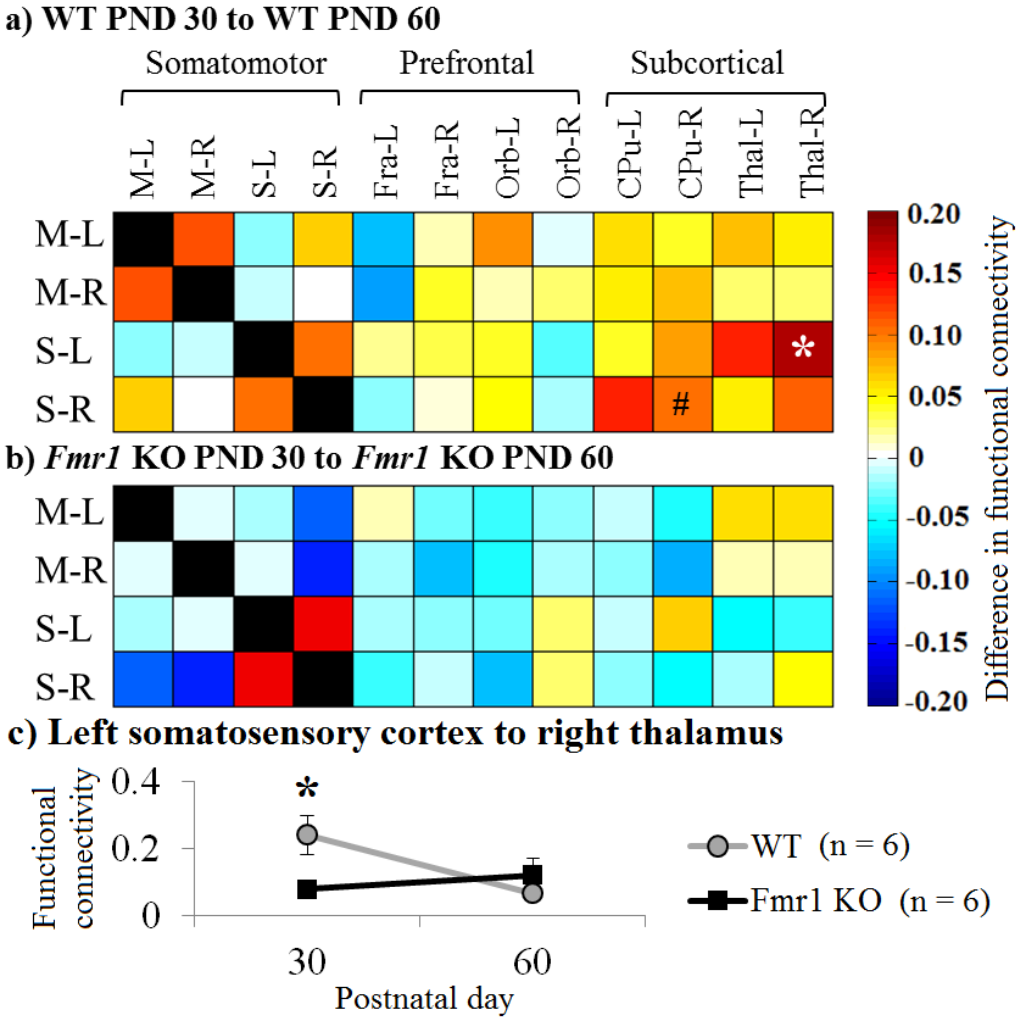

Figure 8-3: Difference in functional connectivity between PND 30 and PND 60 in the somatomotor network in *Fmr1* KO and WT mice. The difference in functional connectivity, as measured by z-scores, between PND 30 to PND 60 is presented as connectivity matrices in the a) WT mice and b) *Fmr1* KO mice. In figures a and b, greater functional connectivity at PND 30 is indicated by positive difference of z-scores (yellow-red) and greater functional connectivity at PND 60 is indicated by negative difference of z-scores (blue). A black square represents no functional connectivity because the seed and target regions are the same. The brain regions from the somatomotor network include the motor cortex (M), and somatosensory cortex (S). Prefrontal cortex regions include the frontal association cortex (Fra) and frontal orbital cortex (Orb). Functional connectivity from the motor and somatosensory cortex to the caudate putamen (CPu) and the thalamus (Thal) are also presented. Functional connectivity within left (L) or right (R) brain hemispheres represents intra-hemispheric functional connectivity (e.g. M-L to S-L). Inter-hemispheric functional connectivity is represented by L to R and vise versa (e.g. M-L to S-R). Longitudinal change in functional connectivity (mean ± standard error) between c) the left somatosensory cortex to the right thalamus in WT (gray line) and *Fmr1* KO (black line) mice at PND 30 and 60. Significant differences of functional connectivity from PND 30 to PND 60 are represented by * $p < 0.05$ and near significant differences # $p < 0.10$. The significant p-

values passed false discovery rate (alpha = 0.05) for multiple pairwise comparisons of functional connectivity between the left somatosensory cortex and right thalamus but did not pass for pairwise comparisons between the right somatosensory cortex and right caudate putamen.

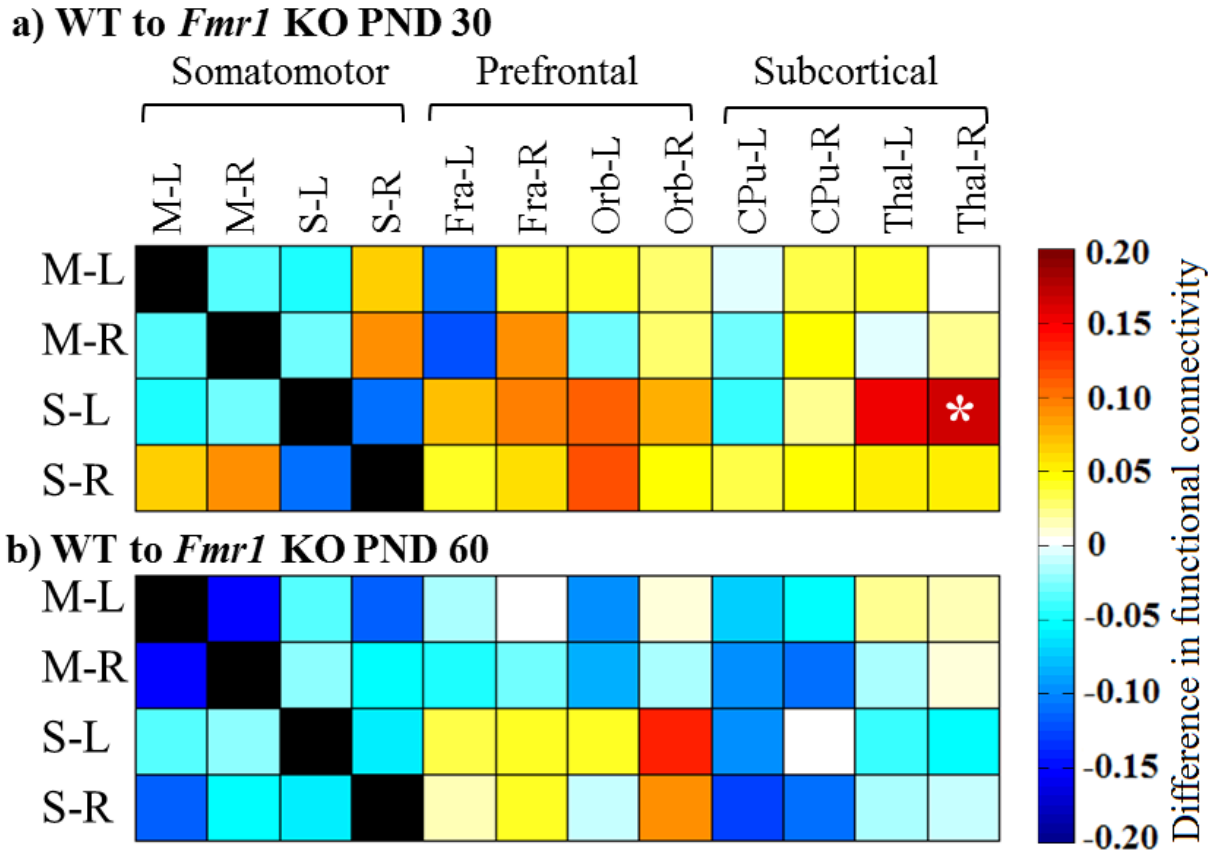

Figure 8-4: Difference in functional connectivity between *Fmr1* KO and WT mice at PND 30 and PND 60 in the somatomotor network. The difference in functional connectivity (z-scores) between WT (n = 6) and *Fmr1* KO (n = 6) mice is presented as connectivity matrices at a) PND 30 and b) PND 60. In figures a and b, greater functional connectivity in WT mice are indicated by positive difference of z-scores (yellow-red) and greater functional connectivity in *Fmr1* KO mice is indicated by negative difference of z-scores (blue). The brain regions from the somatomotor network include the motor cortex (M), and somatosensory cortex (S). Prefrontal cortex regions include the frontal association cortex (Fra) and frontal orbital cortex (Orb). Functional connectivity from the motor and somatosensory cortex to the caudate putamen (CPu) and the thalamus (Thal) are also presented. Significant differences in functional connectivity from PND 30 to PND 60 are represented by * $p < 0.05$ and near significant differences # $p < 0.10$. The significant p-values passed false discovery rate (alpha = 0.05) for multiple pairwise comparisons of functional connectivity.

8.3.2. Developmental differences in the auditory and visual networks

Significant within group interaction of (age X genotype) was found in functional connectivity between the right auditory cortex and left somatosensory cortex $F(1,20) = 9.59$, $p = 0.011$ and between the left auditory cortex and right motor cortex $F(1,20) = 5.40$, $p = 0.043$. No significant within group interaction of (age X genotype) was found in functional connectivity between the visual cortex and other regions.

In the auditory network, decreased functional connectivity between the right auditory cortex and left somatosensory cortex was observed in WT mice ($t(2.66)$, $p = 0.024$) from PND 30 to PND 60. Increased connectivity in the same paired region was also observed in *Fmr1* KO mice ($t(-2.42)$, $p = 0.036$) from PND 30 to PND 60 (Figure 8-5). Functional connectivity between the left auditory cortex and right motor cortex was increased in *Fmr1* KO mice from PND 30 to PND 60 ($t(-2.25)$, $p = 0.048$) (Figure 8-5b and c).

Comparison between genotypes revealed decreased functional connectivity between the right auditory cortex and left somatosensory cortex ($t(4.44)$, $p = 0.001$), as well as between the left auditory cortex and right motor cortex in *Fmr1* KO mice compared to WT at PND 30 ($t(3.43)$, $p = 0.006$) (Figure 8-6a). The significant p-values passed false discovery rate (alpha = 0.05) for multiple pairwise comparisons of functional connectivity between the right auditory cortex and left somatosensory cortex, and only passed for functional connectivity between the left auditory cortex and right motor cortex between genotypes at PND 30. Furthermore, the findings of the current study demonstrate deficits in interhemispheric functional connectivity in the auditory network of *Fmr1* KO mice at PND 30. However, the decrease in functional connectivity at PND

30 was not different at PND 60 between genotypes (Figure 8-5c and 8-6b). The findings have shown reduced functional connectivity in *Fmr1* KO mouse brain at PND 30 which may suggest a delay in the auditory network development because at PND 60 the differences were no longer observed. The results in the current study show differences in the trajectory of maturation in the auditory network, but not the visual network, between *Fmr1* KO and WT mice.

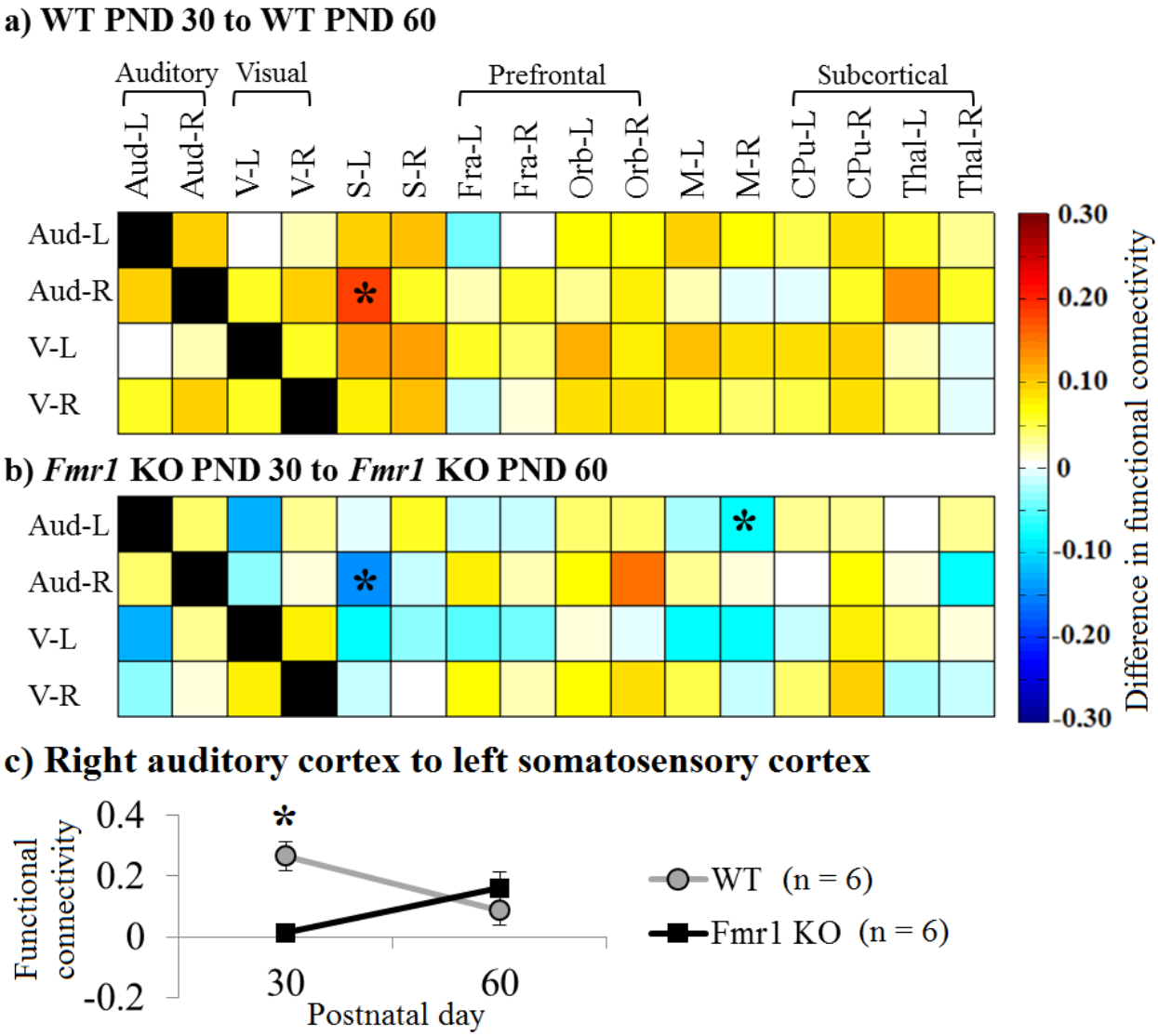

Figure 8-5: Difference in functional connectivity between PND 30 and PND 60 in the auditory and visual networks in *Fmr1* KO and WT mice. The difference in functional connectivity, as measured by z-scores, between PND 30 to PND 60 is presented as connectivity matrices in the a) WT mice and b) *Fmr1* KO mice. In figures a and b, greater functional connectivity at PND 30 is indicated by positive difference of z-scores (yellow-red) and greater functional connectivity at PND 60 is indicated by negative difference of z-scores (blue). The brain regions from the auditory network include the auditory (Aud), visual (V) and somatosensory (S) cortices. Functional connectivity of the caudate putamen (CPu) and the thalamus (Thal) are also presented. Longitudinal change in functional connectivity (mean ± standard error) between c) the right auditory cortex to left somatosensory cortex in WT (gray line) and *Fmr1* KO (black line) mice at PND 30 and 60. Significant differences in functional connectivity from PND 30 to PND 60 are represented by * $p < 0.05$ and near significant differences # $p < 0.10$. The significant p-values passed false discovery rate (alpha = 0.05) for multiple pairwise comparisons of functional connectivity between the right auditory cortex and left somatosensory cortex, but not between the left auditory cortex and right motor cortex.

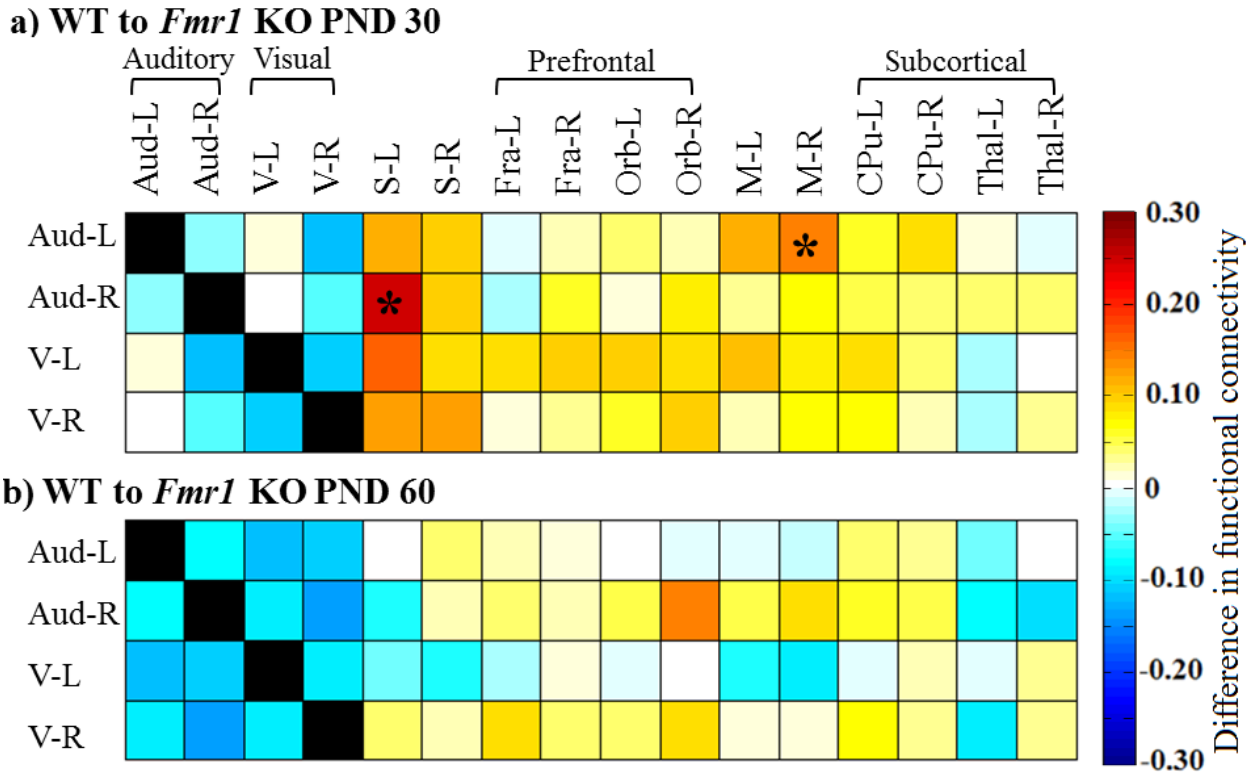

Figure 8-6: Difference in functional connectivity between *Fmr1* KO and WT mice at PND 30 and PND 60 in the auditory and visual networks. The difference in functional connectivity (z-scores) between WT (n = 6) and *Fmr1* KO (n = 6) mice is presented as connectivity matrices at a) PND 30 and b) PND 60. In figures a and b, greater functional connectivity in the WT mice are indicated by positive difference of z-scores (yellow-red) and greater functional connectivity in *Fmr1* KO mice is indicated by negative difference of z-scores (blue). The brain regions from the auditory network include the auditory (Aud), visual (V) and somatosensory (S) cortices. Functional connectivity of the caudate putamen (CPu) and the thalamus (Thal) are also presented. Significant differences in functional connectivity from PND 30 to PND 60 are represented by * $p < 0.05$ and near significant differences # $p < 0.10$. The significant p-values passed false discovery rate (alpha = 0.05) for multiple pairwise comparisons of functional connectivity.

8.3.3. Developmental differences in the default mode network

Significant within group interaction of (age X genotype) was found in functional connectivity between the left granular cortex and left caudate putamen $F(1,20) = 7.53$, $p = 0.021$, and between the left parietal cortex and left frontal orbital cortex $F(1,20) = 11.18$, $p = 0.007$. Near significant within group interaction of (age X genotype) was found between the left parietal cortex and right frontal association cortex ($p = 0.055$). No

within group interactions were observed in the cingulate cortex.

In the default mode network, a near significant decrease in functional connectivity was found between the left granular cortex and left caudate putamen ($p = 0.077$) in WT mice from PND 30 to PND 60 (Figure 8-7a and c). Functional connectivity between the left parietal cortex and left frontal orbital cortex decreased from PND 30 to PND 60 ($t(-2.55)$, $p = 0.029$) (Figure 8-7b and c) in *Fmr1* KO mice. Between PND 30 to PND 60, functional connectivity decreased in WT mice whereas functional connectivity was increased in *Fmr1* KO mice. However, it was surprising how few developmental differences were observed between *Fmr1* KO and WT mice, which may suggest that the default mode network matured by PND 30 or may reflect the effect of anesthesia on the default mode network.

Comparison between genotype revealed decreased functional connectivity between the left parietal cortex and left frontal orbital cortex ($t(2.67)$, $p = 0.022$) and between the left granular cortex and left caudate putamen ($t(2.38)$, $p = 0.039$) in *Fmr1* KO mice compared to WT at PND 30 (Figure 8-8a). At PND 60, the no functional connectivity differences were observed between *Fmr1* KO and WT mice. The significant p-values from multiple pairwise comparisons did not pass the false discovery rate (alpha = 0.05). The reduced functional connectivity in the default mode network in the *Fmr1* KO mouse brain was only found at PND 30 but not at PND 60 in comparison to WT. We have found similar patterns of reduced functional connectivity in the somatomotor and auditory networks of *Fmr1* KO mouse brain compared to the WT at PND 30 and no differences in functional connectivity at PND 60, suggesting an overall delay development in the resting state networks in *Fmr1* KO mice.

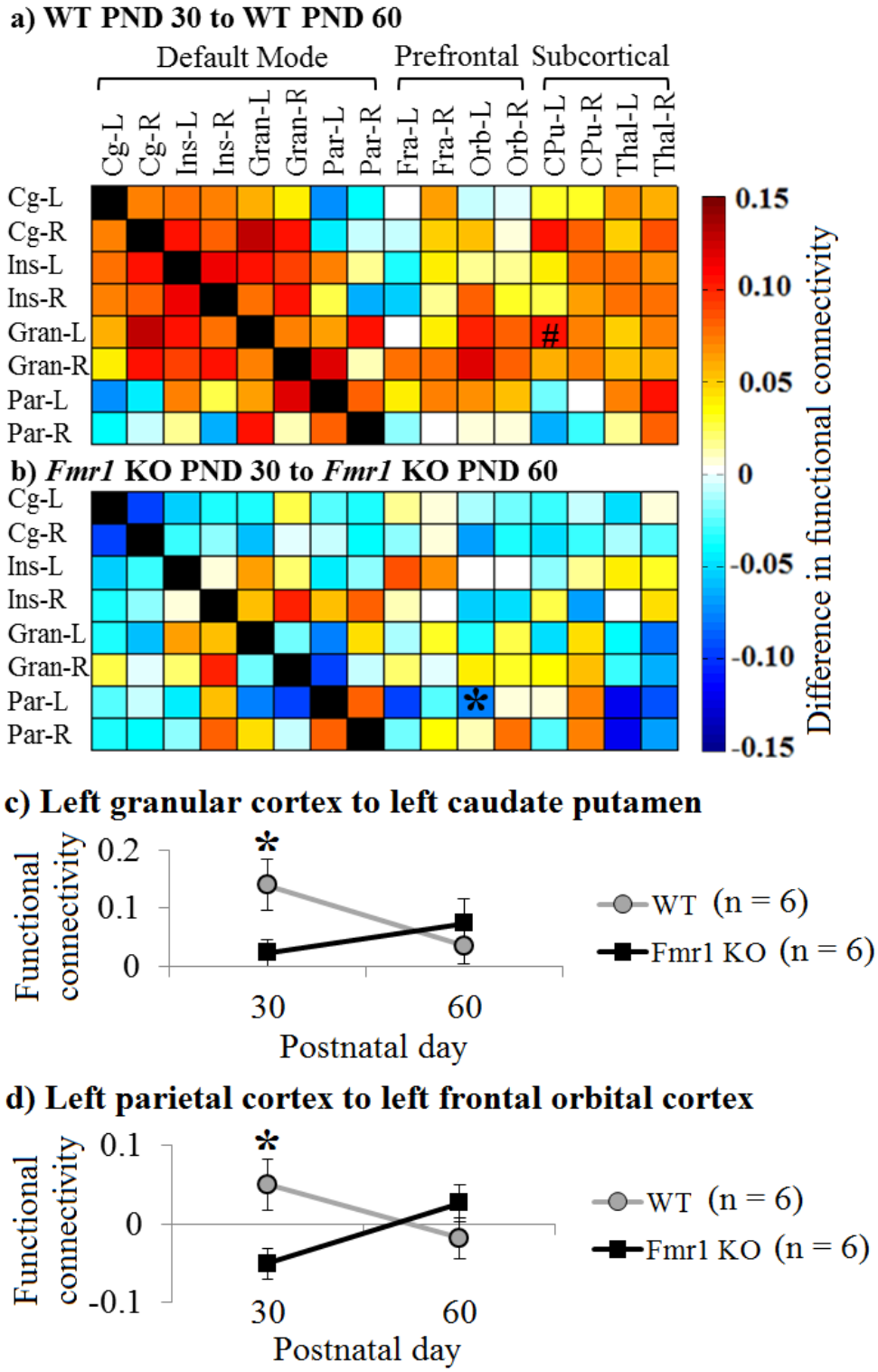

Figure 8-7: Difference in functional connectivity between PND 30 and PND 60 in the default mode network in *Fmr1* KO and WT mice. The difference in functional connectivity, as measured by z-scores, between PND 30 to PND 60 is presented as connectivity matrices in the a) WT mice and b) *Fmr1* KO mice. In figures a and b, greater functional connectivity at PND 30 is indicated by positive difference of z-scores

(yellow-red) and greater functional connectivity at PND 60 is indicated by negative difference of z-scores (blue). The brain regions from the default mode network include the cingulate cortex (Cg), granular cortex (Gran), insular cortex (Ins), and parietal cortex (Par). Prefrontal cortex regions include the frontal association cortex (Fra) and frontal-orbital cortex (Orb). Functional connectivity from the cortical regions of the default mode network to the caudate putamen (CPu) and the thalamus (Thal) are also presented. Longitudinal change in functional connectivity (mean ± standard error) between c) the left granular cortex to the left caudate putamen and d) left parietal cortex to left frontal orbital cortex in WT (gray line) and *Fmr1* KO (black line) mice at PND 30 and 60. Significant differences in uncorrected T-tests of functional connectivity from PND 30 to PND 60 are represented by * $p < 0.05$ and near significant differences # $p < 0.10$. The significant p-values from multiple pairwise comparisons did not pass the false discovery rate (alpha = 0.05).

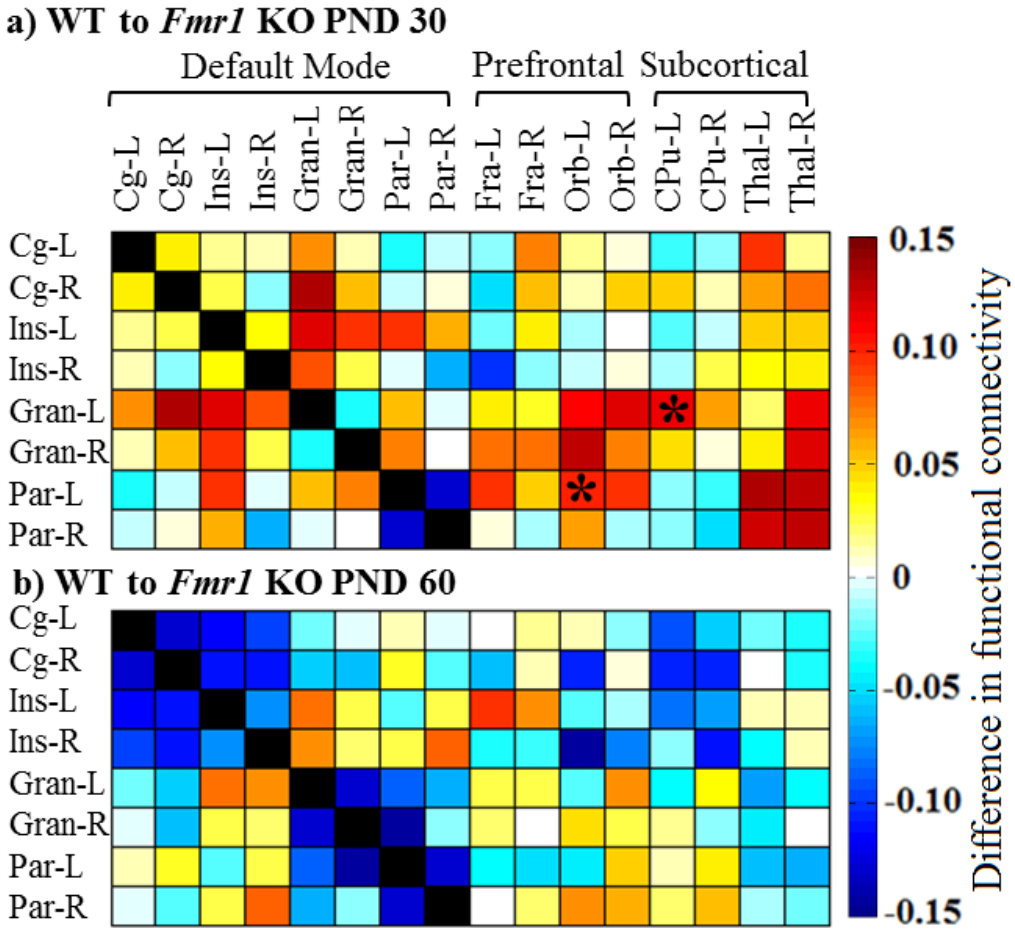

Figure 8-8: Difference in functional connectivity between *Fmr1* KO and WT mice at PND 30 and PND 60 in the default mode network. The difference in functional connectivity (z-scores) between WT (n = 6) and *Fmr1* KO (n = 6) mice is presented as connectivity matrices at a) PND 30 and b) PND 60. In figures a and b, greater functional connectivity in WT mice are indicated by positive difference of z-scores (yellow-red) and greater functional connectivity in *Fmr1* KO mice is indicated by negative difference of z-scores (blue). The brain regions from the default mode network include the cingulate cortex (Cg), granular cortex (Gran), insular cortex (Ins), and parietal cortex (Par). Prefrontal cortex regions include the frontal association cortex (Fra) and frontal-orbital cortex (Orb). Functional connectivity from the cortical regions of the default mode network to the caudate putamen (CPu) and the thalamus (Thal) are also presented. Significant differences in uncorrected T-tests of functional connectivity from PND 30 to PND 60 are represented by * $p < 0.05$ and near significant differences # $p < 0.10$. The significant p-values from multiple pairwise comparisons did not pass the false discovery rate (alpha = 0.05).

8.4. DISCUSSION

8.4.1. Developmental changes in functional connectivity

The current study found decreased functional connectivity in the somatomotor, auditory, and default mode networks in *Fmr1* KO mice at PND 30. The decrease in functional connectivity in developing *Fmr1* KO mouse brain agreed with the finding of decreased functional connectivity among somatosensory, motor and auditory cortices by Haberl et al. (Haberl et al., 2015) in adult *Fmr1* KO mouse brain (PND 63-84). However, while Haberl et al. (Haberl et al., 2015) have reported reduced connectivity in the visual network, the current study did not find any differences in this network in *Fmr1* KO mouse. Functional connectivity among regions of the parietal, insular and prefrontal cortex in the default mode network was reduced in FXS patients (10-16 years old) compared to IQ-matched controls (Hall et al., 2013) and the present study found decreased functional connectivity between the parietal cortex and frontal orbital cortex in *Fmr1* KO mice at PND 30 compared to WT. Thus, our findings in the developing *Fmr1* KO mouse brain at PND 30 agree with previous reports in adult *Fmr1* KO mice (Haberl et al., 2015) and young FXS patients (Hall et al., 2013), suggesting that functional connectivity is reduced during brain development and maturation in comparison to the WT.

The decrease in functional connectivity found in the somatomotor, auditory and default mode networks at PND 30 were transient and the decreases were no longer observed at PND 60 in *Fmr1* KO mice compared to WT, which suggests a delay in maturation of the resting state networks. In Chapter 7, we reported decreased axial diffusivity (AD) as possible indications of altered axon organization, such as increased

axonal branching, in *Fmr1* KO mouse brain at PND 21 and 30. It may be possible that altered axon organization at PND 30 may reflect to reduced functional connectivity found in the current study in *Fmr1* KO mouse brain. In addition, the decreased AD was only observed during a short time period in *Fmr1* KO mouse brain and was similar to WT levels at PND 60. Thus, the changes in functional connectivity may possibly reflect morphological development in the brains of *Fmr1* KO mice. However, the normalized functional connectivity in *Fmr1* KO mouse brain at PND 60 may be transient, as Haberl et al. (Haberl et al., 2015) showed decreased functional connectivity in adult *Fmr1* KO mice between PND 63-84. Therefore, our finding at PND 60 indicates that functional connectivity between immature and adult *Fmr1* KO mice may not be constitutively decreased.

Decreased functional connectivity in the somatomotor, auditory, and default mode networks in WT mice from PND 30 to PND 60 may reflect the refinement of the functional brain network (Figures 8-1, 8-2 and 8-3). A comparison of the functional connectivity in healthy human infants (55 ± 20 days) to adults (30 ± 2 years) showed potential developmental patterns of functional connectivity within resting state networks (Wylie et al., 2014).The default mode network in human infant brains showed greater functional connectivity between the medial prefrontal and anterior cingulate cortices compared to adults (Wylie et al., 2014). The default mode network in human adult brains showed greater functional connectivity with the insular cortex as well as between the posterior cingulate and parietal cortices compared to infants (Wylie et al., 2014). In the auditory network, adults show greater functional connectivity within regions of the superior temporal gyrus while infants show greater functional connectivity in the

posterior region of the superior temporal gyrus (Wylie et al., 2014). Adults also show greater functional connectivity with the primary visual cortex compared to infants (Wylie et al., 2014). Therefore, functional connectivity does not only increase with age, rather changes in functional connectivity during development may reflect refinement of the resting state networks (Wylie et al., 2014). Similarly, the decrease of functional connectivity in WT mice between PND 30 to PND 60 in the current study may reflect refinement of the resting state networks.

8.4.1.1. Somatomotor network

The decrease in functional connectivity at PND 30 in the *Fmr1* KO mouse brain observed in this study may contribute to tactile hypersensitivity in *Fmr1* KO mice (Zhang et al., 2014). The somatosensory cortex of developing *Fmr1* KO mice displayed developmental deficits including a delay in the window of synaptic plasticity from PND 4-10, whereas the WT window was from PND 3-7 (Harlow et al., 2010). In addition, Gibson et al. (Gibson et al., 2008) reported the imbalance of excitatory/inhibitory signaling in the somatosensory cortex that led to increased synchronous depolarization of neighboring excitatory neurons, which resulted in elevated neocortical circuit excitability in developing *Fmr1* KO mouse brain (PND 14 and PND 28). In anesthetized C57Bl6J *Fmr1* KO mice (PND 25-35), electrical hindpaw stimulation led to faster depolarization in the primary somatosensory cortex and leading to faster depolarization of the primary motor cortex compared to the WT, which demonstrated elevated neural network excitability between two cortical regions in the developing *Fmr1* KO mouse (Zhang et al. 2014). The increased membrane excitability and hyperactivity in somatosensory cortex in

developing *Fmr1* KO mouse brain (Gibson et al., 2008; Zhang et al. 2014) may be reflected by the decrease in functional connectivity in the somatomotor network in *Fmr1* KO mice at PND 30.

8.4.1.2. Auditory network

The decrease in functional connectivity in the auditory network of *Fmr1* KO mice at PND 30 may suggest susceptibility to audiogenic seizures. High incidences of auditory seizures were reported (40-90%) in FVB *Fmr1* KO mice at PND 17, PND 22, PND 35, and PND 45, following exposure to auditory stimuli greater than 100 decibels (Musumeci et al., 2000). Neurons in auditory cortex of adult FVB *Fmr1* KO mice (1-4 months) demonstrated hypersensitivity to auditory stimuli by firing significantly greater numbers of action potentials compared to WT mice (Rotschafer & Razak, 2013). In a tasked-based fMRI study of female FXS patients (11-24 years) compared to age-matched normal controls, patients were asked to discriminate between two audio tones of varying lengths and press the corresponding buttons for the longer tone (Hall et al., 2009). The female FXS patients showed increased BOLD signal in the medial frontal gyrus, superior and temporal gyrus and the cerebellum compared to the normal controls, indicating increased brain activity in brain regions associated with auditory processing (Hall et al., 2009). Thus, the reduced functional connectivity in the auditory network found in the current study and in previous studies with FXS patients and adult *Fmr1* KO mice (Haberl et al., 2015; Hall et al., 2013) may suggest hypersensitivity to auditory stimuli (Hall et al., 2009; Musumeci et al., 2000; Rotschafer & Razak, 2013; Zhang 2014).

8.4.1.3. Visual network

No developmental change was reported in the visual network between *Fmr1* KO and WT mice at PND 30 and PND 60 (Figure 8-4a). In contrast to the findings in the current study, Haberl et al. (Haberl et al., 2015) reported reduced functional connectivity in the primary visual cortex and auditory and motor cortices, as well as the hippocampus and caudate putamen in adult C57Bl6J *Fmr1* KO mouse brains (PND 63-84) compared to WT (Haberl et al., 2015). The difference in ages between these two studies suggests functional connectivity in the visual network may decrease as the *Fmr1* KO mouse brain matures. The study by Haberl et al. (Haberl et al., 2015) demonstrated that widespread reduction of functional connectivity may be characteristic of adult *Fmr1* KO mouse brain. Reduced functional connectivity in the visual network was also reported in FXS patients (10-16 years), with the exception of increased functional connectivity between the primary visual cortex and the thalamus, compared to IQ-matched controls (Hall et al., 2013). Sensitivity to light has not been reported in the FXS population. However, a recent study showed that the *Drosophila* Fmr1 protein binds and suppresses translation of the photoreceptor rhodopsin mRNA; light exposure removed Fmr1 protein suppression on rhodopsin mRNA and increased rhodopsin protein levels (Wang et al., 2017). Furthermore, over expression of the Fmr1 protein in *Drosophila* reduced light sensitivity (Wang et al., 2017). Although Wang et al. (Wang et al., 2017) did not report rhodopsin levels in the *Drosophila* model of FXS; their study suggests rhodopsin protein levels may be increased without translational repression of the rhodopsin mRNA by the Fmr1 protein. In addition, the FXS population has a higher likelihood of having vision problems compared to the normal population, including nearsightedness, farsightedness,

astigmatism, and nystagmus (repetitive and rapid eye movement) (Kidd et al., 2014). These vision problems may reflect alterations of processing visual information in the brain and may suggest reduced functional connectivity in the visual network in FXS patients.

8.4.1.4. Default mode network

The current study found decreased functional connectivity in the default mode network in *Fmr1* KO mice at PND 30 but was not different at PND 60 compared to the WT (Figure 8-8). Fair et al. (Fair et al., 2008) reported functional connectivity between neighboring brain regions in the default mode network in healthy children (7-9 years old), including between the medial prefrontal cortex and superior frontal regions, as well as between the posterior cingulate and lateral parietal cortices. In contrast, the default mode network of healthy adults (21-31 years old) showed that functional connectivity increased between non-neighboring brain regions, including between the medial prefrontal cortex and superior frontal region to the lateral parietal and posterior cingulate cortices (Fair et al., 2008). The present study found decreased functional connectivity between the parietal cortex to the frontal orbital cortex and between the granular cortex to the caudate putamen in *Fmr1* KO mice compared to WT at PND 30 (Figure 8-8a). The decrease in functional connectivity may reflect delayed development of anterior to posterior functional connectivity in the default mode network in *Fmr1* KO mice at PND 30.

8.4.2. Functional connectivity alterations in the autism spectrum disorder and relation to FXS

Patients with FXS share common behavioral and cognitive deficits with patients diagnosed with autism spectrum disorder (ASD), and 46% of children with FXS are also diagnosed with ASD (Bailey et al., 2008). Thus, findings in resting state networks of ASD patients may contextualize changes found in FXS patients and *Fmr1* KO mice to shared behavioral and cognitive deficits. However, it should be noted that 16-38% of patients with ASD, without FXS, have been categorized with intellectual disability compared to over 90% of FXS patients categorized with intellectual disability (Abbeduto et al., 2014).

In children with ASD (3.5 ± 0.8 years), decreased functional connectivity has been reported between the visual cortex to the motor and somatosensory cortices compared to normal controls, and the reduced functional connectivity was indicative of hypersensitivity to visual and auditory stimuli (Shen et al., 2016). In an older group of ASD patients (15-52 years) reduced functional connectivity was reported in the default mode network, between the medial prefrontal cortex and angular gyrus of the parietal lobe compared to normal controls; although no change in the attention network was found (Kennedy & Courchesne, 2008). Normally, the activation of default mode and attention networks are anti-correlated, meaning the activation of default mode network results in the deactivation of the attention network (Li et al., 2014; Raichle et al., 2001). In ASD patients, Kennedy et al. (Kennedy & Courchesne, 2008) did not find anti-correlation of default mode and attention networks, suggesting that the imbalance of these two networks contribute to altered cognitive abilities. FXS patients showed reduced functional connectivity in the default mode, attention, salience, somatomotor and visual networks compared to IQ-matched developmentally delayed controls (Hall et al., 2013).

Both FXS and ASD share similar alterations in functional connectivity (Hall et al., 2013; Kennedy & Courchesne, 2008; Shen et al., 2016). However, the FXS patients showed large-scale reduction of functional connectivity compared to IQ-matched controls (Hall et al., 2013), which may reflect greater incidence of intellectual disability in FXS compared to ASD patients (Abbeduto et al., 2014).

8.5. CONCLUSIONS

The reduction of functional connectivity in the somatomotor, auditory, and default mode networks was found in *Fmr1* KO mice compared to WT at PND 30. However, the reduced functional connectivity observed at PND 30 was not observed at PND 60 between *Fmr1* KO and WT mice. Our findings suggest that the development of the somatomotor, auditory, and default mode networks were delayed in brains of *Fmr1* KO mice. The decrease in functional connectivity in the somatomotor and auditory networks may underlie hypersensitivity to tactile and auditory stimuli, respectively.

CHAPTER 9: INTERVENTIONS FOR FRAGILE X SYNDROME AND PILOT STUDY WITH METFORMIN TREATMENT IN THE DEVELOPING *FMR1* KO MOUSE BRAIN

9.1. TREATMENT OUTCOME MEASURES FOR FXS

A greater number of intervention studies in FXS patients have started incorporating children and adolescents with FXS (Berry-Kravis et al., 2016; Dziembowska et al., 2013; Leigh et al., 2013; Paribello et al., 2010; Utari et al., 2010). As noted above, the study by Bilousova et al. (Bilousova et al., 2009) is the first study to demonstrate the beneficial effect of minocycline therapy at an early age by normalizing dendritic spine morphology and anxiety level in *Fmr1* KO mice. The encouraging results from the preclinical study with minocycline have led to studies of minocycline in children with FXS as young as three years old (Dziembowska et al., 2013; Leigh et al., 2013; Paribello et al., 2010; Utari et al., 2010). In addition, adolescent FXS patients have been included in mGluR5 antagonist, mavoglurant, clinical trials and future studies may include children with FXS (Bailey et al., 2016; Berry-Kravis et al., 2016).

FXS can be diagnosed *in utero* through testing of the amniotic fluid or placental cells for the *FMR1* mutation (de Die-Smulders et al., 2004). Delays in reaching developmental milestones usually lead to FXS diagnosis at 36 months for boys and 42 months for girls, on average (Bailey et al., 2009). Treatment for FXS has been reported as early as 3 years of age and inclusion of children in treatment studies are becoming more common, although no studies have been limited to younger age groups (Berry-Kravis et al., 2008; Berry-Kravis et al., 2012; Dziembowska et al., 2013; Leigh et al., 2013).

Treatment outcome is typically measured using Aberrant Behavior Checklist-Community (ABC-C) scores to rate negative behaviors associated with FXS including

inappropriate speech, hyperactivity, irritability, sociability, and stereotypy (Sansone et al., 2012). The scope of the ABC-C has recently been modified with added sensitivity and specificity for FXS patients, to better determine improved outcome measurements with treatment (Sansone et al., 2012). However, the ABC-C relies on caretaker and physician scoring which can be subjective (Sansone et al., 2012). Visual Analogue Scale and Clinical Global Impression scales are also utilized to measure treatment efficacy in FXS patients and also rely on caretaker or clinician scoring (Jacquemont et al., 2014). Clinicians are aware of the subjective nature of the ABC-C but behavioral symptoms of FXS varies considerably in the FXS population (Bailey et al., 2009; Garber et al., 2008; Jacquemont et al., 2014; Kidd et al., 2014). Therefore, use of the ABC-C is necessary for evaluation of treatment because it covers a wide range of behavioral symptoms associated with FXS (Gross et al., 2012; Jacquemont et al., 2014). While the continued use of ABC-C checklist and similar metrics to evaluate treatment is the clinical standard, other objective metrics may be incorporated in addition to behavioral scoring in future treatment trials for FXS patients, including brain imaging methods to study whether alterations in brain metabolism, morphology and function have normalized following treatment. Currently, imaging studies have not been incorporated in conjunction with intervention studies to measure improvement in FXS patients or *Fmr1* KO mice. Including translational imaging methods to study brain alterations and treatment effects may provide outcome measures to improve evaluation of treatment in FXS patients and help plan future treatment strategies. Similarly, assessment of novel therapies could also benefit from quantitative imaging in *Fmr1* KO mouse brain.

9.2. TREATMENTS FOR FXS

This section focuses on intervention strategies that have been commonly used in clinical trials and studies with FXS patients. Pharmaceuticals, including stimulants anticonvulsants and anti-psychotics, are frequently used to treat negative behaviors; these interventions only attenuate behavioral issues in 50-70% of FXS patients, many of the drugs used do not target specific molecular changes in FXS to improve the condition (Bailey et al., 2012; Berry-Kravis et al., 2012). Some patients that have enrolled in the treatment studies described in this section may also have been taking stimulants, anticonvulsants, and anti-psychotics during the treatment tests. All treatment studies described in this section included males and females with FXS, but the majority of FXS patients described are males.

9.2.1. Metabotropic glutamate receptor 5 antagonist

Metabotropic glutamate receptor 5 (mGluR5) antagonists have been developed to ameliorate the effects of increased mGluR5-dependent long-term depression in FXS patients (Figure 9-1) (Burket et al., 2011; Krueger & Bear, 2011; Levenga et al., 2011; Thomas et al., 2012; Yan et al., 2005), with mavoglurant being the most recent tested in clinical trials (Bailey et al., 2016; Berry-Kravis et al., 2016). A phase 2 clinical trial of treatment with mavoglurant for 20 days in adult FXS patients did not show improvement of behavior from ABC-C scoring compared to the placebo group (Jacquemont et al., 2011). Interestingly, a subset of the FXS patient group with the full *FMR1* promoter methylation showed improvement of ABC-C scores of stereotypy, hyperactivity and inappropriate speech compared to the placebo group (Jacquemont et al., 2011). However,

two additional phase 2 clinical trials with mavoglurant did not show improvements in behavior scoring in adolescents and adults with full *FMR1* promoter methylation using either ABC-C (Berry-Kravis et al., 2016) or from Clinical Global Impression-Improvement scores (Bailey et al., 2016). The investigators suggested that treatment of mavoglurant may prove beneficial in a younger FXS population (Berry-Kravis et al., 2016). In addition, side effects of fatigue and headache have been reported in many FXS patients taking mavoglurant (Jacquemont et al., 2011). While there is considerable evidence supporting the use of mGluR5 antagonists from studies in *Fmr1* KO mouse (Burket et al., 2011; Krueger & Bear, 2011; Levenga et al., 2011; Thomas et al., 2012; Yan et al., 2005), the results have not been positive when treating the FXS patients (Bailey et al., 2016; Berry-Kravis et al., 2016; Jacquemont et al., 2011).

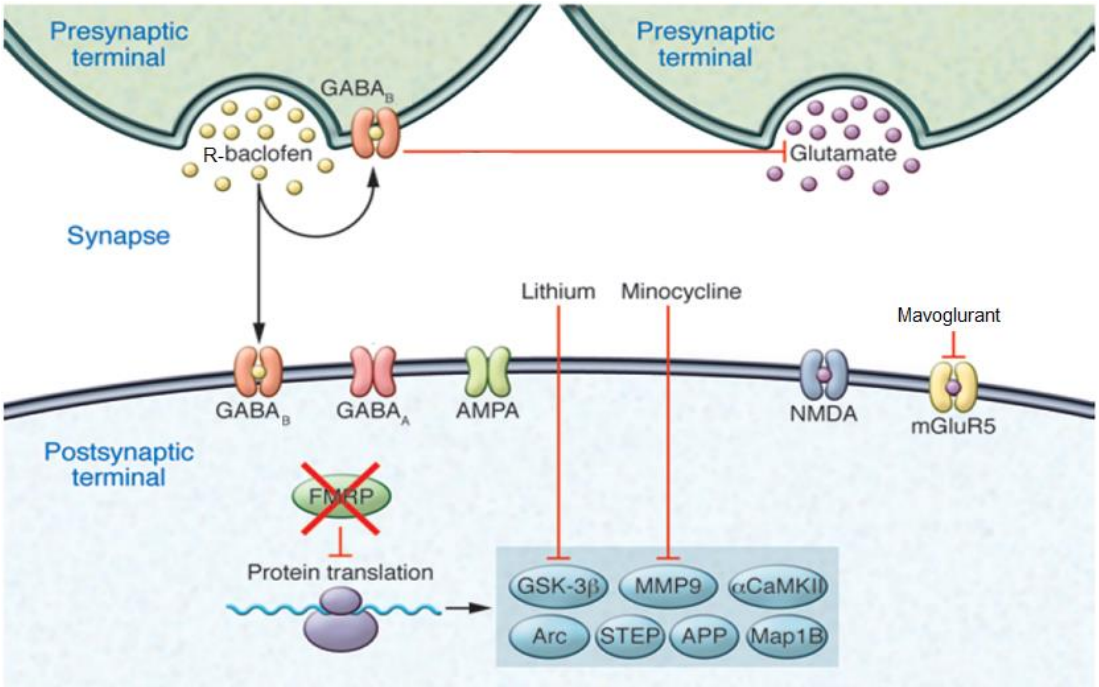

Figure 9-1: Current pharmacological interventions for FXS and their intended targets. The figure was adapted from Bagni et al. (Bagni et al., 2012).

9.2.2. $GABA_B$ receptor agonist

Studies with $GABA_B$ receptor agonist R-baclofen in *Fmr1* KO mice have shown improvement in learning and behavior, as well as normalization of elevated rate of protein synthesis and immature dendritic spine density in the *Fmr1* KO mice, reviewed in Chapter 1 (Figure 9-1) (Henderson et al., 2012; Kang et al., 2017; Qin et al., 2015). A phase 2 clinical trial with the $GABA_B$ receptor agonist R-baclofen for 1 month in FXS patients with the full mutation (6 to 39 years old) showed improvement on the Aberrant Behavior Checklist social avoidance scale, although other outcome measures did not change (Berry-Kravis et al., 2012). No distinctions were made with respect to sex due to the small number of female participants in the study with R-baclofen (Berry-Kravis et al., 2012). Common side effects included sedation and headaches with R-baclofen treatment (Berry-Kravis et al., 2012). Therefore, R-baclofen may be a promising treatment option for FXS patients, with both *Fmr1* KO mice and FXS patients showing improvement in social interaction (Berry-Kravis et al., 2012; Qin et al., 2015).

9.2.3. Lithium

Lithium is commonly used to treat mood disorders and has shown efficacy in the treatment of FXS (Berry-Kravis et al., 2008) and *Fmr1* KO mice (Liu et al., 2011; Liu et al., 2012). Long-term lithium treatment starting at 3 weeks of age until 12 weeks has shown reduction of immature dendritic spine density in the medial prefrontal cortex and normalization of elevated rate of cerebral protein synthesis in the hippocampus, cortex, caudate putamen, thalamus, amygdala and cerebellum in *Fmr1* KO mice (Yuskaitis et al., 2010; Liu et al., 2011; Liu et al., 2012). Lithium treatment normalized hyperactivity and

social interaction behaviors, as well as improved in passive avoidance learning in *Fmr1* KO mice (Liu et al., 2011). In addition, long-term lithium treatment resulted in normalization of AKT and mTOR activity in the in the hippocampus of *Fmr1* KO mouse brain (Liu et al., 2012), and reduced the elevated activity of glycogen synthase kinase-3 in the whole brain of *Fmr1* KO mouse (Figure 9-1) (Liu et al., 2011). Three weeks of lithium treatment in adult *Fmr1* KO mice also showed a reduction of glycogen synthase kinase-3 activity, and normalized hyperactive behavior and anxiety in *Fmr1* KO mice compared to WT (Yuskaitis et al., 2010). In FXS patients (6 to 23 year old), two months of lithium treatment led to improvement in ABC-C scores of hyperactivity, inappropriate speech, and in maladaptive behavior (Berry-Kravis et al., 2008). Lithium can be toxic at high levels and requires continuous monitoring (Liu & Smith, 2014) and side effects of lithium treatment include polyuria and polydipsia as well as elevated levels of thyroid stimulating hormone in some FXS patients (Berry-Kravis et al., 2008). Thus, lithium treatment was effective in normalizing the immature dendritic spine density, protein synthesis, behavior and learning in *Fmr1* KO mice and showed improvement in sociability in children and adults with FXS (Berry-Kravis et al., 2008; Liu et al., 2012; Yuskaitis et al., 2010).

9.2.4. Minocycline

The positive results in *Fmr1* KO mice following the reduction of MMP-9 activity and improvement in behavioral tasks with the broad-spectrum antibiotic minocycline (Figure 9-1) (Bilousova et al., 2009), led to many clinical studies with this drug. Review of *Fmr1* KO mouse studies with minocycline was presented in Chapter 1. Several studies

using minocycline treatment in FXS patients showed improvement in behavior (Dziembowska et al., 2013; Leigh et al., 2013; Paribello et al., 2010). Treatment of adolescents and adults with FXS (13-32 years old) with minocycline for 2 months led to improved ABC-C scores in irritability, stereotypy, hyperactivity and inappropriate speech (Paribello et al., 2010). Only two female FXS patients participated in the study by Paribello et al. (Paribello et al., 2010), and the effect of sex was not analyzed. Treatment of children and adolescents with FXS (3-16 years old) with minocycline for 3 months showed improvement in anxiety and mood from Clinical Global Impression-Improvement score, as well as improvement in behavior from patient specific secondary troubled behavior indicated by caretakers (Leigh et al., 2013). No effect of gender has been reported (Leigh et al., 2013). A recent study showed improvement in global behavior scores in boys with FXS (3-14 years old) from Clinical Global Impression-Improvement following minocycline treatment (Dziembowska et al., 2013). In addition, this study showed minocycline treatment reduced elevated MMP-9 activity in the plasma of boys with FXS. However, there was no correlation of decreasing MMP-9 activity to global behavior scores (Dziembowska et al., 2013). Common side effects included gastrointestinal distress and staining of nails (Paribello et al., 2010; Utari et al., 2010). Minocycline treatment has proven effective in improving behavior in especially in younger FXS patients and demonstrated efficacy in young FXS patients.

9.3. PILOT STUDY FOR METFORMIN

9.3.1. Current understanding of metformin in the *Fmr1* KO mouse and FXS patients

Metformin, is a drug commonly used to treat type 2 diabetes by reducing insulin levels, glucose concentration and glucose synthesis in the body (Hatoum & McGowan, 2015). In the body, metformin uptake occurs through the organic cation transporter (OCT1), and inhibits mitochondrial complex I, although the mechanism of inhibition is currently unknown (Viollet et al., 2012), and leads to reduced ATP production (Figure 9-2a) (Hatoum & McGowan, 2015). Change in energy production leads to downstream phosphorylation and activation of the energy sensor, adenosine monophosphate-activated protein kinase (AMPK) to inhibit mammalian target of rapamycin (mTOR) and reduce glucose synthesis (Figure 9-2a) (Hatoum & McGowan, 2015). In the body, metformin has been shown to affect hepatocytes, skeletal muscles, endothelial cells, and pancreatic beta cells, as well as neurons in brain (Viollet et al., 2012).

In the *Fmr1* KO mouse brain, metformin can potentially target two major pathological features of FXS, the increased mTOR activation (Sharma et al., 2010), increased glucose metabolism (Qin et al., 2002) and protein synthesis (Qin et al. 2005). However, a recent study with 10 days of intraperitoneal injections metformin treatment, showed normalization of exaggerated mGluR5 dependent LTD in the hippocampus and normalized elevated MEK and ERK activation in the prefrontal cortex and hippocampus of the adolescent and adult *Fmr1* KO mice (8-12 weeks) (Figure 9-2c) (Gantois et al., 2017). In addition, no change in the activation of AMPK or the mTOR binding protein raptor (regulatory-associated protein of mTOR) was found following metformin

treatment in *Fmr1* KO mice, suggesting metformin in *Fmr1* KO mouse brain may not follow the same signaling pathway as reported in the body (Figure 9-2c) (Gantois et al., 2017; Hatoum & McGowan, 2015). Metformin treatment also normalized phosphorylation of the eukaryotic initiation factor 4E (eIF4E) and overall mRNA translation in *Fmr1* KO mouse (Figure 9-2c) (Gantois et al., 2017). In addition, short-term treatment of metformin in the adult *Fmr1* KO mice was able to normalize immature dendritic spine density in the hippocampus as well as improve social interaction behavior compared to WT (Gantois et al., 2017). It is currently unknown how metformin can modulate downstream signaling of mGluR5 but the findings from Gantois et al. (Gantois et al., 2017) show that metformin can correct neurological deficits associated with exaggerated mGluR5-dependent LTD.

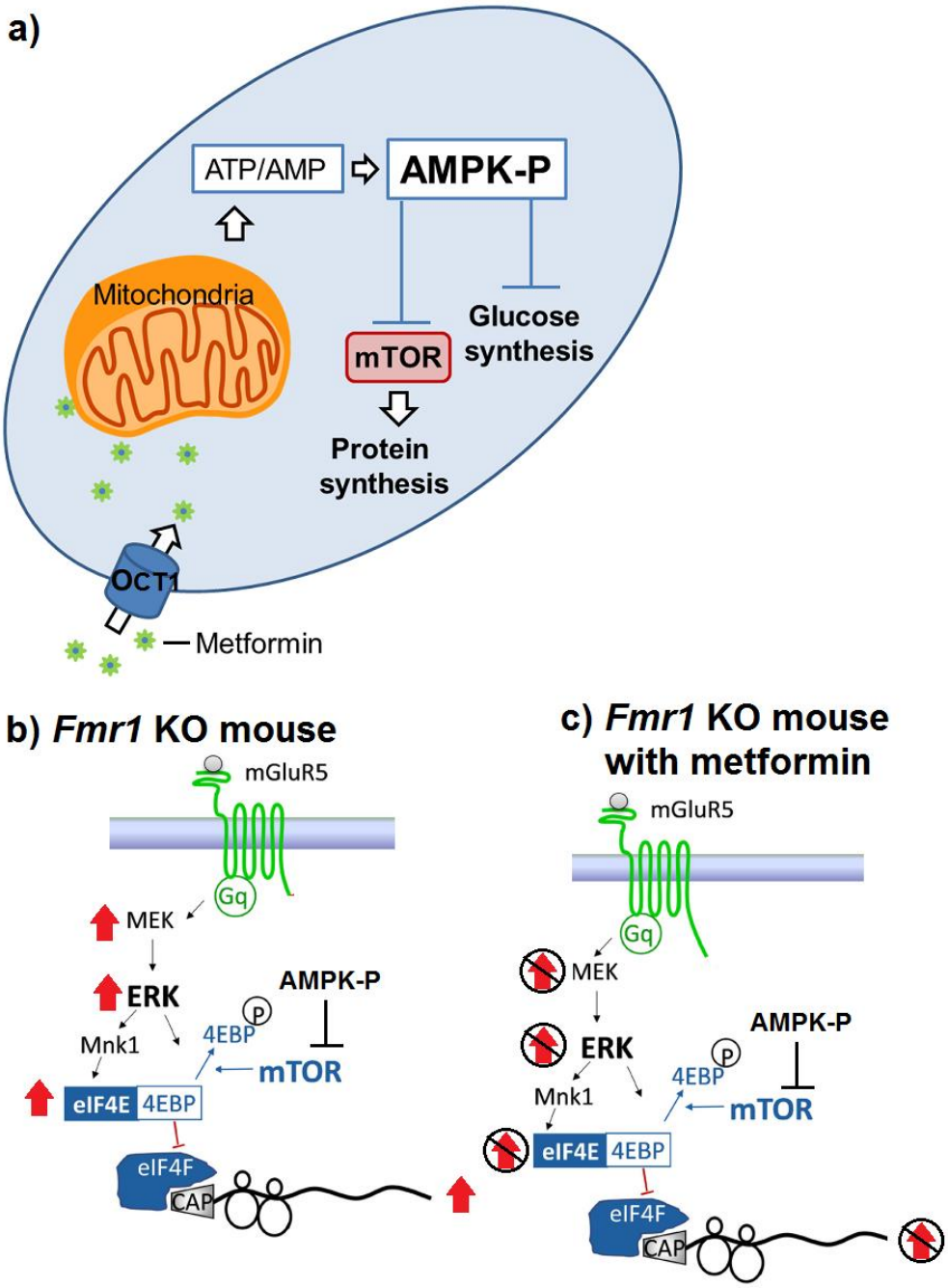

Figure 9-2: Possible metformin signaling pathways in FXS. a) The effect of metformin (green stars) in the body has been previously shown to activate Oct1and inhibit Complex I in the mitochondria, leading to phosphorylation of AMPK to inhibit mTOR activation, protein synthesis, and glucose synthesis (Hatoum & McGowan, 2015). b) In the hippocampus and prefrontal cortex of the *Fmr1* KO mouse brain, increased MEK/ERK signaling, downstream activation of eIF4E and increased mRNA levels were reported (Gantois et al., 2017). c) Short-term metformin treatment corrected MEK/ERK signaling pathway in *Fmr1* KO mouse (Gantois et al., 2017). Figures 9-2b and c were modified from Huber et al. (Huber et al., 2015).

There are also indications of metformin improving negative behaviors in FXS patients. A case study of 7 FXS patients (4.5-60 years) treated with metformin for the duration of 4 months to 1 year, showed improved Aberrant Behavior Checklist-Community Edition scores in irritability, sociability, and hyperactivity compared to their scores before metformin treatment (Dy et al., 2017). Specifically, in the 4 year old boy with FXS, 6 months of metformin treatment improved expressive language and attention, as well as decreased tantrums and hyperactivity (Dy et al., 2017). The case studies also suggest that long-term metformin treatment may be possible, although 3 out of 7 patients on metformin experienced gastrointestinal distress (Dy et al., 2017).

The current pilot study compared the effects of metformin on functional connectivity in developing *Fmr1* KO and WT mice. Treatment with metformin was started on PND 21 when the brain was still immature and continued for 39 days. Functional connectivity and magnetization transfer ratio (MTR) were measured following short-term treatment at PND 30, and functional connectivity following long-term treatment at PND 60 to assess changes in brain networks in vehicle and metformin treatent groups.

9.3.2. MATERIALS AND METHODS

9.3.2.1. Animal procedure

The current study used B6.129P2-*Fmr1*^{tm1Cgr}/J (*Fmr1* KO) mice (Jackson Laboratory, Bar Harbor, ME, USA) from a C57BL6J background and WT mice (JAX C57Bl/6J mice; Jackson Laboratory, Bar Harbor, ME, USA) bred in the animal facility at the University of Maryland, Baltimore. The animal protocol was approved by the

Institutional Animal Care and Use Committee at the University of Maryland, Baltimore. All mice were weaned at PND 21. The mice were genotyped using methods previously described in Bakker et al. (Bakker et al., 1994) and described in Chapter 4. Food and water were provided *ad libitum*. Six WT mice and 6 *Fmr1* KO mice were studied in the vehicle group. Five WT mice and 7 *Fmr1* KO mice were studied in the metformin treatment group. Three mice in the metformin group at PND 30 (2 WT and 1 *Fmr1* KO) died during imaging due to respiratory failure and their scans were excluded from the study and not included in the number of animals used.

9.3.2.2. Metformin treatment

Metformin chloride was dissolved in deionized water and administered to mice through the drinking water at a dose of 250 mg/kg (after weaning) starting at PND 21 for 39 days until PND 60. The dose was based on a previous study which showed that one 250 mg/kg dose of metformin increased AMPK activation in the kidney and liver of 5 week old male mice (Harada et al., 2010). No toxic effects were observed at a dose of 250 mg/kg (Harada et al., 2010), which was well under the lethal dose 50 (LD50) of 1450 mg/kg for metformin in mice (Moskalev et al., 2016). Deionized water was the vehicle since metformin is soluble in water. Deionized water was provided to the control group (or vehicle), whereas water with metformin chloride was provided to the metformin group *ad libitum.* The metformin solution was changed every three days and made on the day of the water change. The water levels were monitored daily and consumption was recorded every three days. Health conditions, including body mass and fur growth of the mice were checked daily. No health abnormalities were observed among animals in the

metformin treatment group. The mice were longitudinally imaged using MRI at PND 30, following a short-term metformin treatment, and at PND 60, which was considered to be long-term metformin treatment.

9.3.2.3. Magnetic resonance imaging and data analysis

This pilot study used the same methods for resting state functional MRI (rs-fMRI) and anesthesia as reported in Chapter 8, section 8.2.3. Two sets of connectivity matrices were developed for the somatomotor, auditory and visual, and the default mode networks, comparing differences in functional connectivity, as measured by the z-score, between WT and *Fmr1* KO in the vehicle group at PND 30 and PND 60 as well as the differences between the vehicle WT and metformin treated *Fmr1* KO mice at PND 30 and PND 60.

The magnetization transfer images were obtained using a FLASH T_1 technique. Acquisition parameters were slice thickness 1 mm, 4 slices, spatial resolution of 200 μm X 200 μm over a field of view of 2 cm X 2 cm, TE/TR = 2.3 ms/75.8 ms, and 8 averages. For the MT images (M_s), a Gaussian off-resonance saturation pulse was used with duration of 12.6 ms and flip angle of 140 degrees at an off-resonance frequency of 6000 Hz from the center frequency of water protons. The reference MT image (M_o) was scanned using the same parameters except without the off-resonance pulse. Calculation of magnetization transfer ratio (MTR) followed the same protocol as reported in Chapter 5. Regions of interest also included the corpus callosum, external capsule, internal capsule, cerebral peduncle, and fimbria.

9.3.2.4. Statistical analysis

The connectivity z-scores were analyzed using repeated measures analysis of variance (RMANOVA) for functional connectivity of each paired region. To analyze the effect of metformin treatment on functional connectivity, a 3-way RMANOVA was performed, the between subject factors were genotype (WT and *Fmr1* KO) and treatment (vehicle and metformin), the within subject factor was age (PND 30 and PND 60). Functional connectivity between treatment groups was analyzed if the interaction of (age X genotype X treatment) was statistically significant ($p < 0.05$). Genotype, treatment and age effects were analyzed by Student's t-tests if the interaction was statistically significant. In each white matter region, MTR was analyzed using two-way ANOVA at PND 30, with genotype and treatment as between subject factors. A significant interaction of (genotype X treatment) ($p < 0.05$) allowed further pairwise comparison using independent Student's t-test and corrected for multiple comparisons. Statistical analyses were performed in SPSS (IBM Corp. 2013. IBM SPSS Statistics for Windows, Version 22.0. Armonk, NY). Multiple pairwise comparisons were controlled by calculating the false discovery rate with a threshold of alpha = 0.05, which assumes 5% of significant p-values were false.

9.3.3. RESULTS

9.3.3.1. Effect of Metformin on Functional Connectivity Networks

In the somatomotor network, significant within group interaction of (age X genotype X treatment) was found in functional connectivity between the right motor cortex and right frontal association cortex ($F(1,20) = 5.38$, $p = 0.031$). Short-term metformin treatment from PND 21 to PND 30 increased functional connectivity between

these two regions in WT mice compared to the vehicle WT at PND 30 (t(-2.55), p = 0.031), whereas metformin treatment in *Fmr1* KO mice did not change functional connectivity when compared to vehicle *Fmr1* KO mice (Figure 9-3c). In the vehicle group, functional connectivity was higher in *Fmr1* KO mice at PND 30 (t(-2.55), p = 0.029) compared to WT, but was not different at PND 60 (Figure 9-3a). In the metformin group, long-term metformin treatment from PND 21 to PND 60 increased functional connectivity in *Fmr1* KO mice compared to the WT (t(-2.59), p = 0.027) (Figure 9-3c). Functional connectivity increased in metformin *Fmr1* KO mice compared to the vehicle WT at PND 30 (t(-3.05), p = 0.011) (Figure 9-3c). The significant p-values did not pass false discovery rate, with threshold of alpha = 0.05. Thus, the results suggest metformin treatment may not alter functional connectivity between the right motor cortex to the right frontal association cortex in *Fmr1* KO mouse.

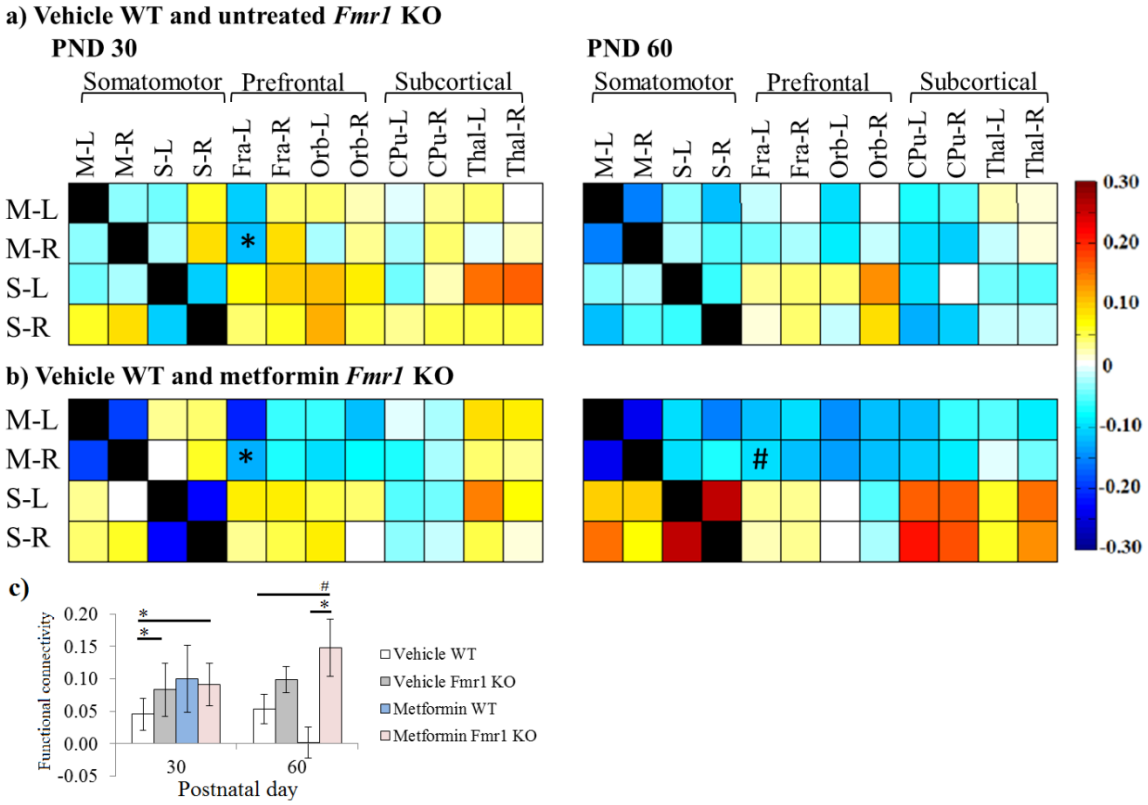

Figure 9-3: The effect of metformin treatment on functional connectivity of the somatomotor network in brains of *Fmr1* KO and WT mice. The figure shows connectivity matrices between seed to target regions at PND 30 (left) and PND 60 (right). The matrices show the difference in functional connectivity (z-scores) between a) the WT mice and *Fmr1* KO mice in the vehicle group, b) vehicle WT mice and metformin treated *Fmr1* KO mice. The difference in functional connectivity is represented by the color bar on the right, with greater *Fmr1* KO functional connectivity represented by negative z-scores (blue) and greater functional connectivity in the WT shown in the positive z-scores (red). Functional connectivity is shown in bar graphs (mean ± standard error) c) between the right motor cortex and left frontal association cortex in WT (white bar) and *Fmr1* KO mice (gray bar) in vehicle group, as well as WT (blue bar) and *Fmr1* KO mice (pink bar) in metformin treatment group at PND 30 and 60. The brain regions from the somatomotor network include the motor cortex (M), and somatosensory cortex (S). Prefrontal cortex regions include the frontal association cortex (Fra) and frontal orbital cortex (Orb). Functional connectivity from the motor and somatosensory cortex to the caudate putamen (CPu) and the thalamus (Thal) are also presented. Significant differences in functional connectivity between WT and *Fmr1* KO mice are represented by * $p < 0.05$ and near significant differences # $p < 0.10$. The significant p-values did not pass false discovery rate (alpha = 0.05).

In the auditory network, significant within group interaction of (age X genotype X treatment) was found in functional connectivity between the right auditory cortex and left

somatosensory cortex F(1,20) = 4.75, p = 0.041. Short and long-term metformin treatment did not change functional connectivity between these two regions in WT mice compared to vehicle WT (Figure 9-4c). In contrast, short-term metformin treatment increased functional connectivity in *Fmr1* KO mice compared to vehicle *Fmr1* KO mice at PND 30 (t(-2.61), p = 0.024, did not pass false discovery rate (alpha = 0.05)) (Figure 9-4c). In the vehicle group, functional connectivity was lower in *Fmr1* KO mice at PND 30 compared to WT (t(4.44), p = 0.001, passed false discovery rate (alpha = 0.05)) (Figure 9-4 a and c). Furthermore, no difference in functional connectivity was observed in metformin *Fmr1* KO mice compared to vehicle WT at PND 30 (Figure 9-4b). Thus, short-term metformin treatment may be able to increase functional connectivity in *Fmr1* KO mouse brain (Figure 9-4 b and c).

In the visual network, significant within group interactions of (age X genotype X treatment) F(1,20) = 4.74, p = 0.042 was found in functional connectivity between the left and right visual cortex. Metformin treatment decreased functional connectivity in WT mice compared to vehicle WT at PND 60 (t(2.30), p = 0.047), and a near significant increase was observed at PND 30 (Figure 9-4d). No change was observed with metformin treatment in *Fmr1* KO mice compared to vehicle *Fmr1* KO mice at both ages (Figure 9-4d). Functional connectivity was not different between genotype in the vehicle group at both ages (Figure 9-4 a and c). Following long-term metformin treatment, functional connectivity was higher in metformin *Fmr1* KO mice compared to vehicle WT (t(-2.51), p = 0.029) and metformin WT mice (t(-3.14), p = 0.010) (Figure 9-4d). The significant p-values from multiple pairwise comparisons did not pass the false discovery rate (alpha = 0.05). The results suggest that metformin may increase functional connectivity between

the left and right visual cortex in *Fmr1* KO mice following long-term treatment.

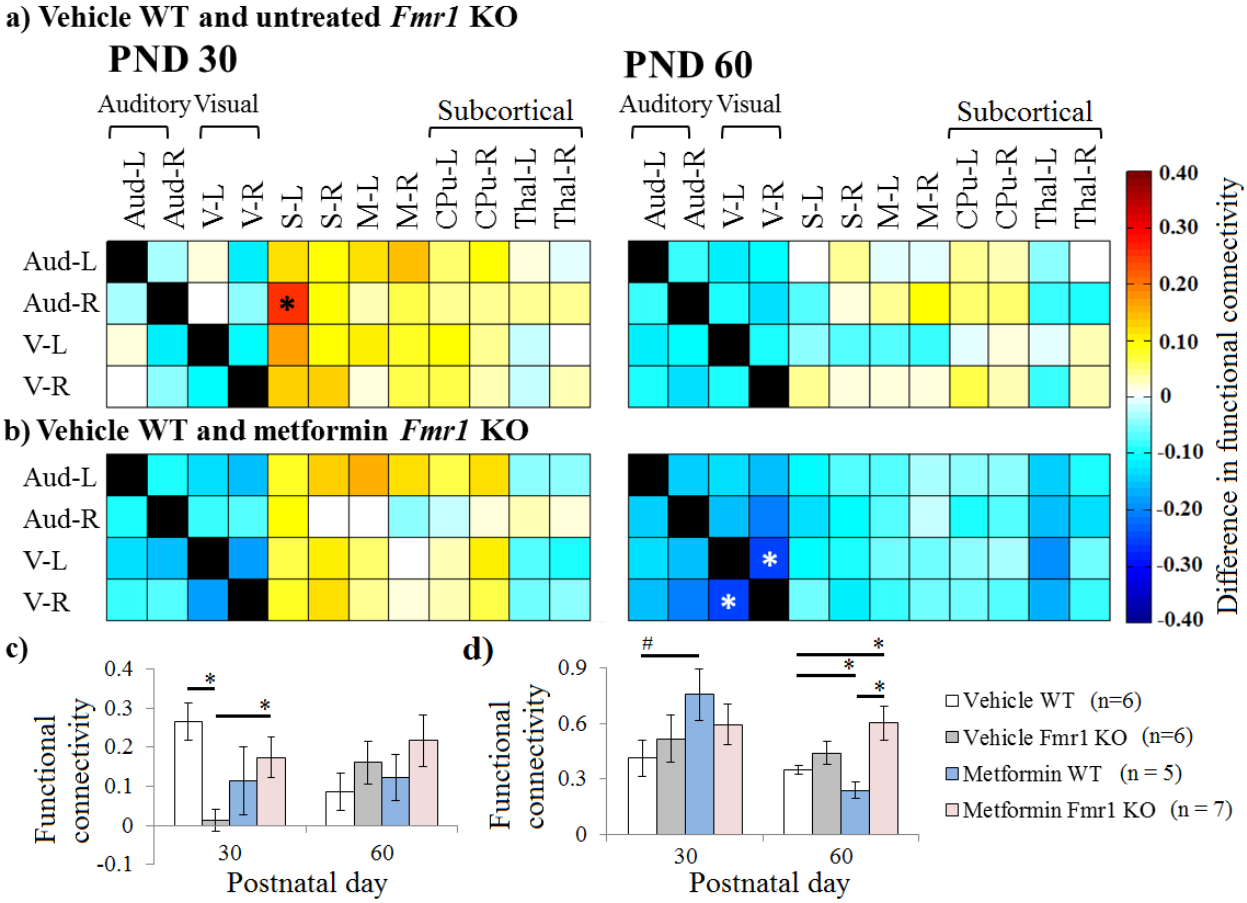

Figure 9-4: The effect of metformin treatment on functional connectivity matrix of the auditory and visual networks in the brains of *Fmr1* KO and WT mice. The figure shows difference matrices in functional connectivity between seed to target regions at PND 30 (left) and PND 60 (right). The connectivity matrices show the difference in functional connectivity (z-scores) between a) WT and *Fmr1* KO mice in the vehicle group, b) vehicle WT mice and metformin *Fmr1* KO mice. The difference in functional connectivity is represented by the color bar on the right, with greater *Fmr1* KO functional connectivity represented by negative z-scores (blue) and greater functional connectivity in the WT shown in the positive z-scores (red). Functional connectivity is shown in bar graphs (mean ± standard error) c) between the right auditory cortex and left somatosensory, and d) functional connectivity between the left and right visual cortex in WT (white bar) and *Fmr1* KO mice (gray bar) in the vehicle group, as well as WT (blue bar) and *Fmr1* KO mice (pink bar) in the metformin treatment group at PND 30 and 60. The brain regions from the auditory network include the auditory (Aud), visual (V) and somatosensory (S) cortices. Functional connectivity of the caudate putamen (CPu) and the thalamus (Thal) are also presented. Significant in functional connectivity between WT and *Fmr1* KO mice are represented by * $p < 0.05$ and near significant differences # $p < 0.10$. The significant p-values from pairwise comparisons only passed the false discovery rate (alpha = 0.05) in functional connectivity between right auditory cortex and left somatosensory cortex between vehicle WT and vehicle *Fmr1* KO mice at PND 30.

In the default mode network, no significant within group interactions of (age X genotype X treatment) was found. Near significant within group interactions of (age X genotype X treatment) was found in functional connectivity between the right granular cortex and right insular cortex, between the right parietal cortex and left caudate putamen ($p = 0.073$), and between the right parietal cortex and right caudate putamen ($p = 0.077$). The data suggest that functional connectivity is not affected by metformin treatment in the default mode network or may be due to the effect of anesthesia.

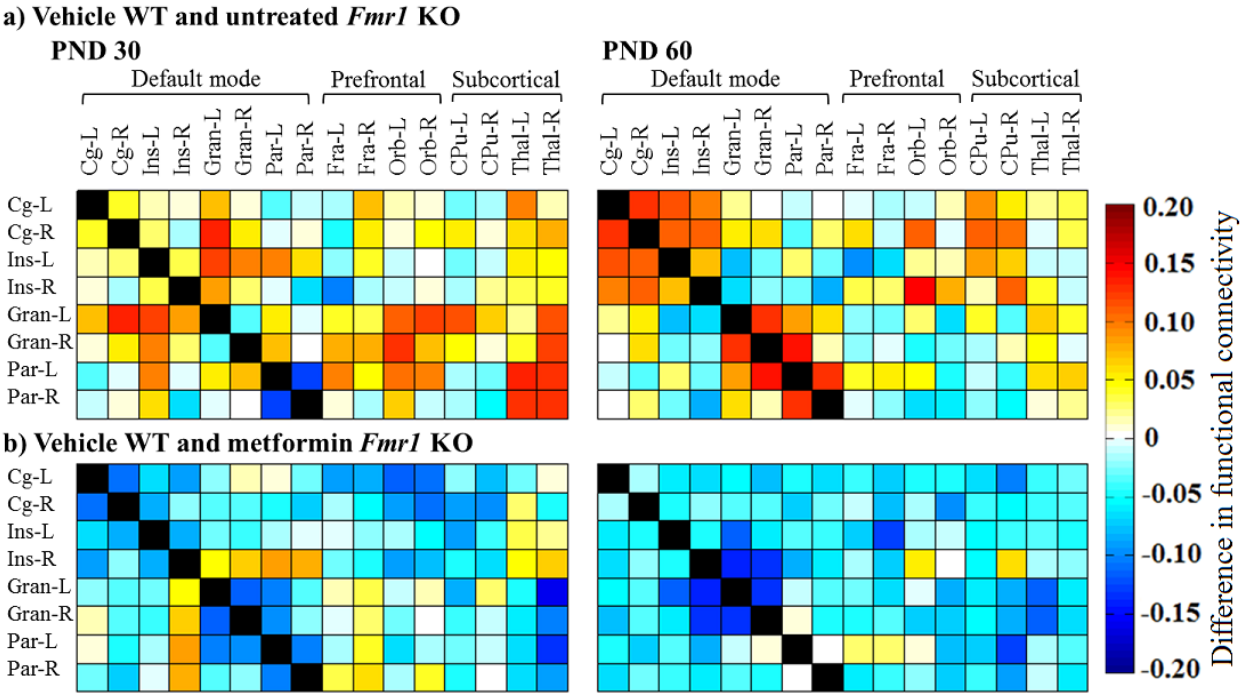

Figure 9-5: The effect of metformin treatment on functional connectivity matrix of the default mode network in the brains of *Fmr1* KO and WT mice. The figure shows connectivity matrices between seed to target regions at PND 30 (left) and PND 60 (right). The matrices show difference between a) the WT mice and *Fmr1* KO mice in the vehicle group and b) vehicle WT mice and metformin *Fmr1* KO mice. The difference in functional connectivity (z-scores) is represented by the color bar on the right, with greater *Fmr1* KO functional connectivity represented by negative z-scores (blue) and greater functional connectivity in the WT shown in the positive z-scores (red). The brain regions from the default mode network include the cingulate cortex (Cg), granular cortex (Gran), insular cortex (Ins), and parietal cortex (Par). Prefrontal cortex regions include the frontal association cortex (Fra) and frontal-orbital cortex (Orb). Functional connectivity from the cortical regions of the default mode network to the caudate putamen (CPu) and the thalamus (Thal) are also presented. No significant interaction of (age X genotype X treatment) in functional connectivity was found in the default mode network.

9.3.3.2. Changes in MTR following metformin treatment

A significant interaction of (genotype X treatment) was found in all white matter regions studied at PND 30 (Table 9-1). Short-term metformin treatment consistently increased MTR in metformin WT compared to vehicle WT in the corpus callosum (t(2.48), p = 0.034), external capsule (t(3.38), p = 0.008), internal capsule

(t(2.76), p = 0.022), cerebral peduncle (t(3.45), p = 0.008), and fimbria (t(3.51), p = 0.006) (Figure 9-6). Consequently, in the metformin treatment group MTR of WT mice was significantly higher compared to *Fmr1* KO mice in the corpus callosum (t(2.49), p = 0.032), external capsule (t(3.29), p = 0.008), cerebral peduncle (t(2.86), p = 0.017), and fimbria (t(3.74), p = 0.004) (Figure 9-6 a, b, d, and e). The significant p-values passed false discovery rate (alpha = 0.05) from multiple pairwise comparisons in the external capsule, cerebral peduncle and fimbria. The findings in the present study showed that metformin treatment significantly affected WT mice at PND 30, whereas metformin treatment did not affect MTR in *Fmr1* KO mice.

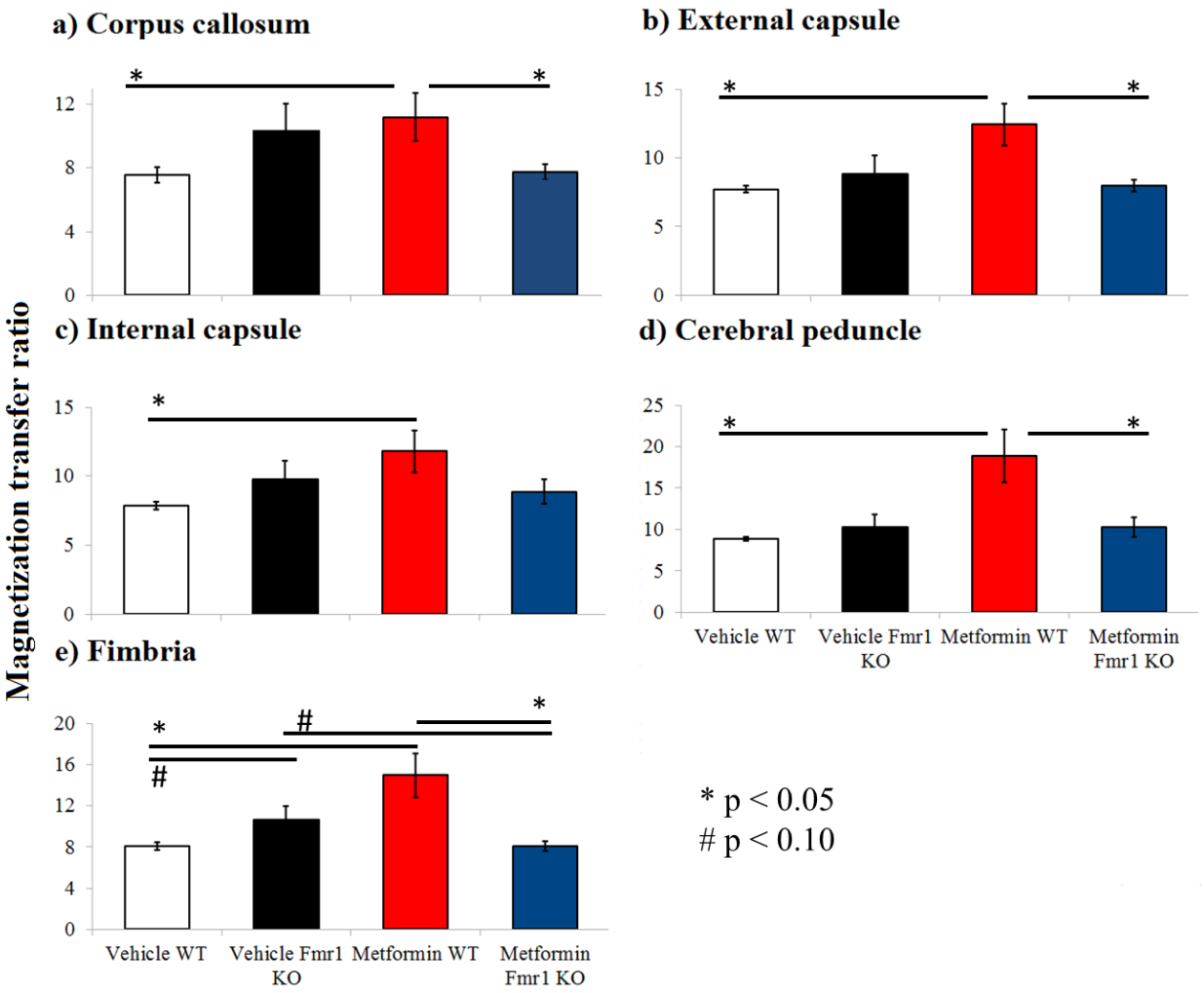

Figure 9-6: The effect of short-term metformin treatment on MTR in white matter regions of *Fmr1* KO and WT mice. The MTR (mean ± standard error) of vehicle WT (white bar; n = 6), vehicle *Fmr1* KO mice (black bar; n = 6), metformin WT (red bar; n = 5), metformin *Fmr1* KO mice (blue bar; n = 7) are shown in the a) the corpus callosum, b) external capsule, c) internal capsule, d) cerebral peduncle, and e) fimbria at PND 30. The significant differences in MTR from uncorrected T-tests between WT and *Fmr1* KO mice in vehicle and treatment groups are marked with * $p < 0.05$ and near significant differences are marked with # $p < 0.10$. The significant p-values passed false discovery rate (alpha = 0.05) in the external capsule, cerebral peduncle and fimbria.

Two way ANOVA MTR	Region	df	F-value	p-value
Genotype	Corpus callosum	1	0.08	0.785
	External capsule	1	2.99	0.099
	Internal capsule	1	0.24	0.630
	Cerebral peduncle	1	4.42	**0.048**
	Fimbria	1	3.53	0.075
Treatment	Corpus callosum	1	0.20	0.659
	External capsule	1	3.98	0.060
	Internal capsule	1	2.03	0.170
	Cerebral peduncle	1	8.82	**0.008**
	Fimbria	1	3.58	0.073
Genotype X	Corpus callosum	1	8.20	**0.010**
Treatment	External capsule	1	8.61	**0.008**
	Internal capsule	1	4.93	**0.038**
	Cerebral peduncle	1	8.66	**0.008**
	Fimbria	1	17.22	< **0.001**
Error	Corpus callosum	20		
	External capsule	20		
	Internal capsule	20		
	Cerebral peduncle	20		
	Fimbria	20		

n	
Vehicle WT	6
Vehicle *Fmr1* KO	6
Metformin WT	5
Metformin *Fmr1* KO	7

Table 9-1: Summary of two-way ANOVA for MTR in *Fmr1* KO and WT mice in metformin and vehicle groups. The F-value and p-value for genotype, treatment, and interaction of (genotype X treatment) are presented. An interaction with p-value of 0.05 or less was considered significant (in bold). An independent Student's T-test was performed if there was a significant interaction of (genotype X treatment).

9.3.3.4. Conclusions from the pilot study with metformin

A recent study demonstrated that metformin corrected many of the neurological deficits in the adult *Fmr1* KO mouse (Gantois et al., 2017), thus we predicted that metformin treatment would also be able to correct deficits in developing *Fmr1* KO mouse brain. We found that metformin appeared to modulate functional connectivity, but the

efficacy of metformin in correcting functional connectivity and MTR in our results was inconclusive. This may be due to the small number of animals used or the effect of anesthesia. Additional preclinical studies that investigate metabolic, molecular and behavioral changes following metformin treatment are needed to understand the effect of metformin on the developing brain.

CHAPTER 10: CONCLUSIONS AND FUTURE DIRECTIONS

10.1. DEVELOPMENTAL ALTERATIONS IN THE *FMR1* KO MOUSE BRAIN

In the course of this study, we have found developmental alterations in *Fmr1* KO mouse brain compared to the WT in metabolite levels (Chapter 5), white matter morphology (Chapters 6 and 7), and functional connectivity (Chapter 8). These studies have provided some indications of the neuropathology underlying brain development in *Fmr1* KO mouse brain at specific ages during critical periods of brain development during the peak of myelination and synaptogenesis (PND 20-21), neural network development (PND 25-35) and maturation (PND 60+) (Semple et al. 2013).

Previous studies in the hippocampus of the developing *Fmr1* KO mouse described exaggerated mGluR5-dependent LTD (Huber et al. 2002), altered PI3K-mTOR signaling (Sharma et al. 2010), and increased immature dendritic spine density (Bilousova et al. 2009). This led us to ask whether alterations in metabolite concentrations could be related to changes in signal transduction and neuronal function. In Chapter 5, we characterized hippocampal metabolite levels related to neurotransmission, signal transduction and osmoregulation using ^{1}H magnetic resonance spectroscopy in *Fmr1* KO mice compared to WT at PND 18, 21, and 30. We found consistently increased taurine levels in hippocampus of *Fmr1* KO mice at all ages studied. Taurine is an important brain osmolyte that is known to protect against the effects of glutamate excitotoxicity (El Idrissi et al. 1999). Taurine has also been shown to activate $GABA_A$ receptors (Wu et al. 2003). We also found decreased *myo*-inositol levels at PND 30 in the hippocampus of *Fmr1* KO mice, which could indicate altered myelin basic protein binding to the lipid membrane and possibly alter myelin compaction (Nawaz et al. 2009). The potential

alteration of myelin properties in the developing *Fmr1* KO mouse brain led to further investigations of myelin and white matter.

Morphological alterations in myelin and white matter were studied in the fixed brain of *Fmr1* KO mice compared to WT at PND 18, 21, 30 and PND 60 (Chapter 6). We hypothesized that myelination is decreased in the *Fmr1* KO mouse brain; however, we found that myelin density, measured by optical density from Black Gold II staining, varied at each age. While we did find decreased myelin density in white matter regions in the forebrain and midbrain in the *Fmr1* KO mice at PND 18 and 60, we also found that myelin density at PND 21 was comparable to the WT and myelin density was increased at PND 30 (Figure 6-4). This is the first study to investigate myelin alterations in the forebrain and midbrain of developing *Fmr1* KO mice and our findings suggest possible changes in the time course of myelin formation which may be due to the lack of FMRP regulation on mRNA translation of myelin proteins. The results of myelin density and magnetization transfer ratio (MTR) showed similar effects in *Fmr1* KO mice (Figure 6-3). Our findings suggesting that future studies of white matter can incorporate magnetization transfer imaging to further understand myelin formation in *Fmr1* KO mice or FXS patients.

Although we observed altered myelin density and MTR at different ages, regional white matter volumes were not different between *Fmr1* KO and WT mice (Figure 6-1), suggesting that molecular alterations found in white matter content were not reflected in the measurement of white matter macrostructure. Therefore, we conducted further studies of white matter microstructure in the fixed *Fmr1* KO mouse brain at PND 18, 21, 30 and 60 using diffusion tensor imaging (DTI) to provide additional insights into myelin and

axonal properties. Decreased mean diffusivity was found at PND 21 and 30 in gray and white matter in *Fmr1* KO mouse brain compared to WT brain. This finding indicates greater restriction of water diffusion and suggests an alteration in white and gray matter development. Decreased radial diffusivity (RD) was observed at PND 21 and 30 in white matter regions of *Fmr1* KO brain, indicating that water diffusion is restricted in the direction perpendicular to the axon. The decreased RD suggests that myelin may be more tightly compacted or the fibers were more densely packed in white matter regions in *Fmr1* KO brain at PND 21 and 30 compared to WT. Decreased axial diffusivity (AD) was also observed in white matter regions of *Fmr1* KO mouse at PND 21 and 30. The decreased AD in *Fmr1* KO mice suggested morphological changes to axons in white matter including increased axon fiber density and/or altered axon organization, which can limit diffusion along the axon. Since we did not find significant differences in fiber density between *Fmr1* KO and WT mice, the decrease in AD was most likely due to alterations in axonal organization, such as increased axonal branching or more diffuse axon arborization. The decrease of AD and RD were transient in the developing *Fmr1* KO mouse brain and were not different compared to AD and RD in WT brain levels at PND 60. However, alteration in myelin compaction and axon organization during brain development may have long-lasting consequences in the maturation of the *Fmr1* KO mouse brain. Currently, white matter development in *Fmr1* KO mice is not well understood, and the studies in Chapters 6 and 7 showed indications of myelin and axon alterations in white matter in *Fmr1* KO mice at PND 18, 21, 30 and 60. Furthermore, the differences in brain microstructure during development between *Fmr1* KO and WT mouse brains may also contribute to changes in the functional brain networks in the *Fmr1*

KO mouse.

To further investigate the functional brain network, we studied functional connectivity in resting state networks in *Fmr1* KO and WT mouse brains at PND 30 and 60. Functional connectivity was reduced between regions associated with the somatomotor and auditory networks in *Fmr1* KO mouse brain compared to WT at PND 30 (Figures 8-2 and 8-3). Altered functional connectivity between regions associated with the default mode network was also observed in *Fmr1* KO mice at PND 30 (Figure 8-3). To the best of our knowledge this was the first study to show reduction of functional connectivity in developing *Fmr1* KO mouse brain. However, functional connectivity in all the three networks was similar between *Fmr1* KO and WT mice by PND 60, which suggests that there is a delay in the development of resting state networks in *Fmr1* KO mouse brain. We found that functional connectivity in WT mice was decreasing from PND 30 to 60, which may indicate refinement of resting state networks during development; whereas functional connectivity in brains of *Fmr1* KO mice did not change between PND 30 to 60 (Figures 8-3, 8-5, and 8-7). While we did not expect the functional connectivity to be similar between genotypes at PND 60, this novel finding suggests that functional connectivity may change with development and/or maturation in *Fmr1* KO mouse brain. However, other studies showed large-scale reduction of functional connectivity in adult *Fmr1* KO mice (Haberl et al. 2015) and children and adolescents with FXS (Hall et al. 2013), suggesting more longitudinal studies are needed in the developing *Fmr1* KO mouse brain. Further studies using *Fmr1* KO mouse are necessary to determine whether the alterations in resting state networks at PND 30 may suggest hypersensitivity to tactile and auditory responses. A summary of the differences

between *Fmr1* KO and WT mice at each age studied is shown in Figure 10-1.

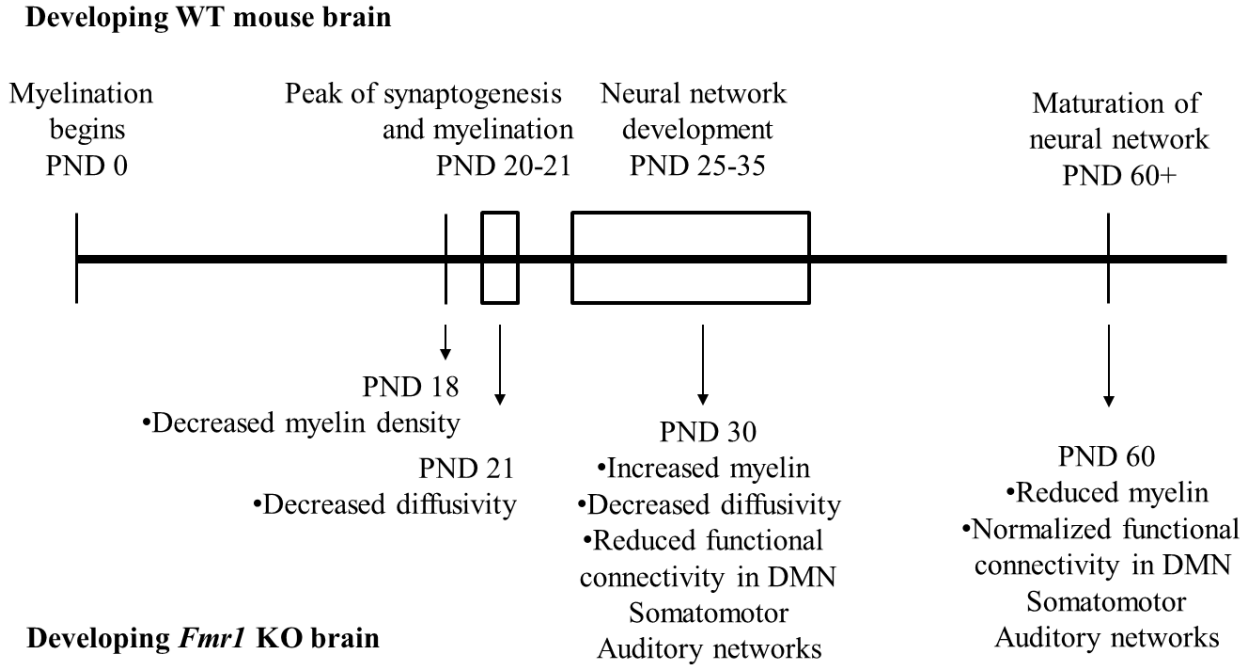

Figure 10-1: Summary of findings in the developing *Fmr1* KO mouse brain compared to the WT mouse brain at PND 18, 21, 30 and 60. The critical periods for the WT mouse brain is presented based on previously findings in the developing rodent brain (Semple et al. 2013). Specific differences at the ages studied between WT and *Fmr1* KO mice are indicated by the arrows.

10.2. FUTURE DIRECTIONS FOR STUDYING BRAIN DEVELOPMENT IN RODENT MODELS OF FXS

Our studies have shown altered myelin density and MTR in white matter during brain development in *Fmr1* KO mice. The change in myelin density may be caused by a delay in the maturation of oligodendrocyte precursor cells. FMRP has been found in oligodendrocyte precursor cells and immature oligodendrocytes, but FMRP levels declined as the oligodendrocyte matured (Wang et al. 2004). While the role of FMRP in the maturation of oligodendrocyte precursor cells is unknown, reduced levels of NG2 proteoglycan protein, a marker for oligodendrocyte precursor cells, is reported in the

cerebellar white matter of *Fmr1* KO mice at PND 7 and was normalized at PND 15 (Pacey et al., 2013). Decreased concentrations of myelin basic protein and CNP, markers of mature oligodendrocytes, were also observed at PND 7 and 15, and were normalized by PND 30, suggesting delayed maturation of oligodendrocytes (Pacey et al., 2013). Therefore, to determine if maturation of the oligodendrocyte precursor cell is hindered, the abundance of mature oligodendrocytes compared to oligodendrocyte precursor cells will need to be determined by immunohistochemistry in white matter regions in the forebrain and midbrain at PND 7, 15, and 30 in *Fmr1* KO and WT mice. Studying markers of oligodendrocyte precursor cells and oligodendrocytes would provide insight into whether the reduction of mature oligodendrocytes can contribute to a delay in myelination in *Fmr1* KO mouse brain. In addition, potential alterations of MEK/ERK and PI3K-mTOR signaling pathways in oligodendrocyte precursor cells can be studied in *Fmr1* KO mouse brain, and whether inhibitors of these pathways can affect maturation of oligodendrocytes could also be determined. Elevated activity in MEK/ERK and PI3K-mTOR signaling pathways have been reported in gray matter regions of *Fmr1* KO mice (Gantois et al., 2017), and oligodendrocytes in *Fmr1* KO mouse brain may also display alterations in signaling transduction pathways. Electron microscopy could provide morphological information regarding myelin microstructure and density and axon number to complement the signal transduction information in the immature brain of *Fmr1* KO mice.

Future studies in *Fmr1* KO mouse may consider expanding the age range to get a better understanding of the full developmental trajectories in the brain. The work in this thesis only covered PND 18, 21, 30 and 60 to specifically study structural differences in

white matter and at PND 30 and 60 to study functional network organization in developing *Fmr1* KO mouse brain. At PND 60 we found decreased myelin density and MTR, suggesting that myelin deficit can be ongoing since myelination continues well into adulthood in normally developing WT mice (18 months old) (Xie et al. 2013). Pacey et al. (Pacey et al., 2013) have reported increased myelin basic protein concentration in the cerebellum of adult *Fmr1* KO mouse brain compared to the WT (2-4 months and 7-15 months old), suggesting that myelin levels may be increased in adult *Fmr1* KO mice older than PND 60. Thus, our data and the findings from Pacey et al. (Pacey et al., 2013) suggests that myelination may be altered in the adult *Fmr1* KO mice, and further studies at older adult ages in *Fmr1* KO mice measuring myelin density, MTR, and myelin thickness may show continued defects in myelination.

Functional connectivity was reduced in brains of *Fmr1* KO mice compared to WT brain at PND 30 and was not different compared to brains of WT mice at PND 60. However, Haberl et al. (Haberl et al. 2015) reported decreased functional connectivity in adult *Fmr1* KO mice (9-12 weeks). Taken together, these studies suggest functional connectivity was reduced in immature and adult *Fmr1* KO mouse brain and the normalization at PND 60 that we observed may be transient. Therefore, future studies measuring functional connectivity may consider including more animals per age and including older ages than used in the present study.

The reduced functional connectivity in the somatomotor and auditory networks in the *Fmr1* KO mice at PND 30 may be indicative of tactile and auditory hypersensitivity (Castren et al. 2003; Gibson et al., 2008; Miller et al., 1999; Zhang et al. 2014). Future studies may consider correlating functional connectivity in the auditory networks to the

severity of induced audiogenic seizures. Functional connectivity can also be compared before and after a learning task, such as Morris water maze, to determine whether functional connectivity can change following a learning task in *Fmr1* KO mice compared to WT. In addition, a functional MRI test can be used to study tactile hypersensitivity, such as applying heat to the hindpaw in the *Fmr1* KO mouse. Incorporation of sensory response tests as well as learning tasks can improve our understanding of resting state networks as well as brain function in *Fmr1* KO mouse.

Future studies can also include studying brain development during the first two weeks of life. Harlow et al. (Harlow et al. 2010) showed a delay in the window of synaptic plasticity in the somatosensory cortex of *Fmr1* KO mice which displayed peak LTP potentiation at PND 6-7, whereas the peak LTP potentiation was at PND 3 in WT mice. Studying mouse brain at earlier ages may reveal an age related increase of FA and decrease of MD, which has been shown to change rapidly during the first two weeks in the rat brain (Bockhorst et al. 2008), and may possibly show differences in the morphology of *Fmr1* KO brain associated with early myelination, axonal growth and functional connectivity. However, given the small size of the mouse pup during the first two weeks, the quality of imaging is of concern and one may have to choose much higher field strength to obtain reliable functional information. Alternatively, one may consider performing imaging studies on the *Fmr1* KO rat model.

Future imaging studies may be better suited in the *Fmr1* KO rat compared to the mice especially during brain development because the larger brain size will improve image resolution and can reduce movement artifacts from breathing due to greater body mass. In addition, BOLD signal will be greater in the rat brain due to the larger blood

supply. Resting state networks have been reported in the immature WT rat brain (PND 13-15) (Bajic et al. 2016) so it would be feasible to study functional connectivity at earlier ages in the *Fmr1* KO rat brain. As mentioned in Chapter 1, the adult *Fmr1* KO rats can be trained to stay still during a scan without anesthesia during an fMRI task (Kenkle et al. 2016) and can be trained to study resting state networks in awake *Fmr1* KO rat. A previous study in our group demonstrated successful training of awake adult WT rats to remain still during magnetic resonance imaging and spectroscopy (Xu et al.2013). Therefore, future imaging studies can be improved by using the *Fmr1* KO rat model.

10.3. TREATMENT WITH METFORMIN

In Chapter 9, we tested the efficacy of short and long-term metformin treatment in normalizing functional connectivity in developing and adult *Fmr1* KO mice. *Fmr1* KO and WT mice were treated with metformin or given the vehicle from PND 21 to 60. We found a few instances where metformin changed functional connectivity, but the results were inconclusive regarding the efficacy of metformin. The use of anesthesia and the small number of animals used could have contributed to our inconclusive findings. Additional preclinical studies that investigate the anatomical, molecular and behavioral changes following metformin treatment are needed to determine if this drug might be useful for treatment of FXS patients.

10.4. FUTURE DIRECTIONS FOR STUDYING METFORMIN TREATMENT IN FXS

The imaging experiments described in section 10.2 can also be applied to studying the efficacy of metformin on auditory and tactile hypersensitivity as well as

changes in functional connectivity following a learning task in *Fmr1* KO mice or rats. Short-term treatment with metformin reduced the incidence of audiogenic seizures in adult *Fmr1* KO mouse (Gantois et al., 2017). Since metformin reduces glucose synthesis in the body (Hatoum & McGowan, 2015), it is important that future studies determine whether both short and long-term metformin treatment can alter brain glucose metabolism in developing *Fmr1* KO and WT mice.

Finally, more studies on the long-term effect of metformin are needed, including studies of behavior and learning, and studies of signal transduction pathways in *Fmr1* KO mice. Short-term metformin treatment was able to normalize social behavior, immature dendritic spine density, elevated mGluR5-dependent LTD and elevated MEK/ERK signaling in *Fmr1* KO mice (Gantois et al., 2017). A recent report of 7 case studies showed metformin treatment in FXS patients for 4 months-1 year improved ABC-C scores (Dy et al., 2017). The use of metformin is relatively novel for treatment of FXS and there is still much to be studied with respect to metformin treatment in the *Fmr1* KO mouse.

References

Abbeduto, L., McDuffie, A., & Thurman, A. J. (2014). The fragile X syndrome-autism comorbidity: What do we really know? *Frontiers in Genetics, 5*, 355. doi:10.3389/fgene.2014.00355 [doi]

Amaral, R. S., Park, M. T., Devenyi, G. A., Lynn, V., Pipitone, J., Winterburn, J., . . . Alzheimer's Disease Neuroimaging Initiative. (2016). Manual segmentation of the fornix, fimbria, and alveus on high-resolution 3T MRI: Application via fully-automated mapping of the human memory circuit white and grey matter in healthy and pathological aging. *Neuroimage,* doi:S1053-8119(16)30581-X [pii]

Andersen, S. L. (2003). Trajectories of brain development: Point of vulnerability or window of opportunity? *Neuroscience and Biobehavioral Reviews, 27*(1-2), 3-18. doi:S0149763403000058 [pii]

Antar, L. N., Li, C., Zhang, H., Carroll, R. C., & Bassell, G. J. (2006). Local functions for FMRP in axon growth cone motility and activity-dependent regulation of filopodia and spine synapses. *Molecular and Cellular Neurosciences, 32*(1-2), 37-48. doi:S1044-7431(06)00044-3 [pii]

Anticevic, A., Hu, S., Zhang, S., Savic, A., Billingslea, E., Wasylink, S., . . . Pittenger, C. (2014). Global resting-state functional magnetic resonance imaging analysis identifies frontal cortex, striatal, and cerebellar dysconnectivity in obsessive-compulsive disorder. *Biological Psychiatry, 75*(8), 595-605. doi:10.1016/j.biopsych.2013.10.021 [doi]

Argyridis, I., Li, W., Johnson, G. A., & Liu, C. (2013). Quantitative magnetic susceptibility of the developing mouse brain reveals microstructural changes in the

white matter. *Neuroimage, 88C*, 134-142. doi:S1053-8119(13)01118-X [pii]

Ashley, C. T.,Jr, Wilkinson, K. D., Reines, D., & Warren, S. T. (1993). FMR1 protein: Conserved RNP family domains and selective RNA binding. *Science (New York, N.Y.), 262*(5133), 563-566.

Attwell, D., & Laughlin, S. B. (2001). An energy budget for signaling in the grey matter of the brain. *Journal of Cerebral Blood Flow and Metabolism : Official Journal of the International Society of Cerebral Blood Flow and Metabolism, 21*(10), 1133-1145. doi:10.1097/00004647-200110000-00001 [doi]

Bagni, C., Tassone, F., Neri, G., & Hagerman, R. (2012). Fragile X syndrome: Causes, diagnosis, mechanisms, and therapeutics. *The Journal of Clinical Investigation, 122*(12), 4314-4322. doi:10.1172/JCI63141 [doi]

Bailey, D. B.,Jr, Berry-Kravis, E., Wheeler, A., Raspa, M., Merrien, F., Ricart, J., . . . Apostol, G. (2016). Mavoglurant in adolescents with fragile X syndrome: Analysis of clinical global impression-improvement source data from a double-blind therapeutic study followed by an open-label, long-term extension study. *Journal of Neurodevelopmental Disorders, 8*, 1-015-9134-5. Epub 2015 Dec 15. doi:10.1186/s11689-015-9134-5 [doi]

Bailey, D. B.,Jr, Raspa, M., Bishop, E., & Holiday, D. (2009). No change in the age of diagnosis for fragile x syndrome: Findings from a national parent survey. *Pediatrics, 124*(2), 527-533. doi:10.1542/peds.2008-2992 [doi]

Bailey, D. B.,Jr, Raspa, M., Bishop, E., Olmsted, M., Mallya, U. G., & Berry-Kravis, E. (2012). Medication utilization for targeted symptoms in children and adults with fragile X syndrome: US survey. *Journal of Developmental and Behavioral*

Pediatrics : JDBP, 33(1), 62-69. doi:10.1097/DBP.0b013e318236c0e1

Bailey, D. B.,Jr, Raspa, M., Olmsted, M., & Holiday, D. B. (2008). Co-occurring conditions associated with FMR1 gene variations: Findings from a national parent survey. *American Journal of Medical Genetics.Part A, 146A*(16), 2060-2069. doi:10.1002/ajmg.a.32439 [doi]

Bailey, D. B., Raspa, M., Holiday, D., Bishop, E., & Olmsted, M. (2009). Functional skills of individuals with fragile x syndrome: A lifespan cross-sectional analysis. *American Journal on Intellectual and Developmental Disabilities, 114*(4), 289-303. doi:10.1352/1944-7558-114.4.289-303

Bajic, D., Craig, M. M., Borsook, D., & Becerra, L. (2016). Probing intrinsic resting-state networks in the infant rat brain. *Frontiers in Behavioral Neuroscience, 10*, 192. doi:10.3389/fnbeh.2016.00192 [doi]

Baker, K. B., Wray, S. P., Ritter, R., Mason, S., Lanthorn, T. H., & Savelieva, K. V. (2010). Male and female Fmr1 knockout mice on C57 albino background exhibit spatial learning and memory impairments. *Genes, Brain, and Behavior, 9*(6), 562-574. doi:10.1111/j.1601-183X.2010.00585.x [doi]

Bakker, C. E., Verheij, C., & Willemsen, R. (1994). Fmr1 knockout mice: A model to study fragile X mental retardation. the dutch-belgian fragile X consortium. *Cell, 78*(1), 23-33.

Bardoni, B., Davidovic, L., Bensaid, M., & Khandjian, E. W. (2006). The fragile X syndrome: Exploring its molecular basis and seeking a treatment. *Expert Reviews in Molecular Medicine, 8*(8), 1-16. doi:S1462399406010751 [pii]

Barnea-Goraly, N., Eliez, S., Hedeus, M., Menon, V., White, C. D., Moseley, M., &

Reiss, A. L. (2003). White matter tract alterations in fragile X syndrome: Preliminary evidence from diffusion tensor imaging. *American Journal of Medical Genetics.Part B, Neuropsychiatric Genetics : The Official Publication of the International Society of Psychiatric Genetics, 118B*(1), 81-88. doi:10.1002/ajmg.b.10035

Baslow, M. H. (2010). Evidence that the tri-cellular metabolism of N-acetylaspartate functions as the brain's "operating system": How NAA metabolism supports meaningful intercellular frequency-encoded communications. *Amino Acids, 39*(5), 1139-1145. doi:10.1007/s00726-010-0656-6 [doi]

Bassell, G. J., & Warren, S. T. (2008). Fragile X syndrome: Loss of local mRNA regulation alters synaptic development and function. *Neuron, 60*(2), 201-214. doi:10.1016/j.neuron.2008.10.004

Bear, M. (1998). Development and learning. *Mechanistic Relationships between Development and Learning, ,* 205.

Bear, M. F., Huber, K. M., & Warren, S. T. (2004). The mGluR theory of fragile X mental retardation. *Trends in Neurosciences, 27*(7), 370-377. doi:10.1016/j.tins.2004.04.009 [doi]

Bernardi, S., Anagnostou, E., Shen, J., Kolevzon, A., Buxbaum, J. D., Hollander, E., . . . Fan, J. (2011). In vivo 1H-magnetic resonance spectroscopy study of the attentional networks in autism. *Brain Research, 1380,* 198-205. doi:10.1016/j.brainres.2010.12.057 [doi]

Berry-Kravis, E., Des Portes, V., Hagerman, R., Jacquemont, S., Charles, P., Visootsak, J., . . . von Raison, F. (2016). Mavoglurant in fragile X syndrome: Results of two randomized, double-blind, placebo-controlled trials. *Science Translational Medicine,*

8(321), 321ra5. doi:10.1126/scitranslmed.aab4109 [doi]

Berry-Kravis, E., Levin, R., Shah, H., Mathur, S., Darnell, J. C., & Ouyang, B. (2015). Cholesterol levels in fragile X syndrome. *American Journal of Medical Genetics.Part A, 167A*(2), 379-384. doi:10.1002/ajmg.a.36850 [doi]

Berry-Kravis, E., Sumis, A., Hervey, C., & Mathur, S. (2012). Clinic-based retrospective analysis of psychopharmacology for behavior in fragile x syndrome. *International Journal of Pediatrics, 2012*, 843016. doi:10.1155/2012/843016; 10.1155/2012/843016

Berry-Kravis, E., Sumis, A., Hervey, C., Nelson, M., Porges, S. W., Weng, N., . . . Greenough, W. T. (2008). Open-label treatment trial of lithium to target the underlying defect in fragile X syndrome. *Journal of Developmental and Behavioral Pediatrics : JDBP, 29*(4), 293-302. doi:10.1097/DBP.0b013e31817dc447

Berry-Kravis, E. M., Hessl, D., Rathmell, B., Zarevics, P., Cherubini, M., Walton-Bowen, K., . . . Hagerman, R. J. (2012). Effects of STX209 (arbaclofen) on neurobehavioral function in children and adults with fragile X syndrome: A randomized, controlled, phase 2 trial. *Science Translational Medicine, 4*(152), 152ra127. doi:4/152/152ra127 [pii]

Bifulco, M., Laezza, C., Stingo, S., & Wolff, J. (2002). 2',3'-cyclic nucleotide 3'-phosphodiesterase: A membrane-bound, microtubule-associated protein and membrane anchor for tubulin. *Proceedings of the National Academy of Sciences of the United States of America, 99*(4), 1807-1812. doi:10.1073/pnas.042678799 [doi]

Bilousova, T. V., Dansie, L., Ngo, M., Aye, J., Charles, J. R., Ethell, D. W., & Ethell, I. M. (2009). Minocycline promotes dendritic spine maturation and improves

behavioural performance in the fragile X mouse model. *Journal of Medical Genetics, 46*(2), 94-102. doi:10.1136/jmg.2008.061796

Birken, D. L., & Oldendorf, W. H. (1989). N-acetyl-L-aspartic acid: A literature review of a compound prominent in 1H-NMR spectroscopic studies of brain. *Neuroscience and Biobehavioral Reviews, 13*(1), 23-31. doi:S0149-7634(89)80048-X [pii]

Biswal, B. B., Van Kylen, J., & Hyde, J. S. (1997). Simultaneous assessment of flow and BOLD signals in resting-state functional connectivity maps. *NMR in Biomedicine, 10*(4-5), 165-170. doi:10.1002/(SICI)1099-1492(199706/08)10:4/5<165::AID-NBM454>3.0.CO;2-7 [pii]

Bockhorst, K. H., Narayana, P. A., Liu, R., Ahobila-Vijjula, P., Ramu, J., Kamel, M., . . . Perez-Polo, J. R. (2008). Early postnatal development of rat brain: In vivo diffusion tensor imaging. *Journal of Neuroscience Research, 86*(7), 1520-1528. doi:10.1002/jnr.21607 [doi]

Boggs, J. M., Rangaraj, G., & Dicko, A. (2012). Effect of phosphorylation of phosphatidylinositol on myelin basic protein-mediated binding of actin filaments to lipid bilayers in vitro. *Biochimica Et Biophysica Acta, 1818*(9), 2217-2227. doi:10.1016/j.bbamem.2012.04.006 [doi]

Bonnier, G., Roche, A., Romascano, D., Simioni, S., Meskaldji, D., Rotzinger, D., . . . Granziera, C. (2014). Advanced MRI unravels the nature of tissue alterations in early multiple sclerosis. *Annals of Clinical and Translational Neurology, 1*(6), 423-432. doi:10.1002/acn3.68 [doi]

Bostrom, C. A., Majaess, N. M., Morch, K., White, E., Eadie, B. D., & Christie, B. R. (2015). Rescue of NMDAR-dependent synaptic plasticity in Fmr1 knock-out mice.

Cerebral Cortex (New York, N.Y.: 1991), 25(1), 271-279. doi:10.1093/cercor/bht237 [doi]

Bray, S., Hirt, M., Jo, B., Hall, S. S., Lightbody, A. A., Walter, E., . . . Reiss, A. L. (2011). Aberrant frontal lobe maturation in adolescents with fragile X syndrome is related to delayed cognitive maturation. *Biological Psychiatry, 70*(9), 852-858. doi:10.1016/j.biopsych.2011.05.038

Brennan, F. X., Albeck, D. S., & Paylor, R. (2006). Fmr1 knockout mice are impaired in a leverpress escape/avoidance task. *Genes, Brain, and Behavior, 5*(6), 467-471. doi:GBB183 [pii]

Broide, R. S., & Leslie, F. M. (1999). The alpha7 nicotinic acetylcholine receptor in neuronal plasticity. *Molecular Neurobiology, 20*(1), 1-16. doi:10.1007/BF02741361

Brown, V., Jin, P., Ceman, S., Darnell, J. C., O'Donnell, W. T., Tenenbaum, S. A., . . . Warren, S. T. (2001). Microarray identification of FMRP-associated brain mRNAs and altered mRNA translational profiles in fragile X syndrome. *Cell, 107*(4), 477-487.

Bruno, J. L., Shelly, E. W., Quintin, E. M., Rostami, M., Patnaik, S., Spielman, D., . . . Reiss, A. L. (2013). Aberrant basal ganglia metabolism in fragile X syndrome: A magnetic resonance spectroscopy study. *Journal of Neurodevelopmental Disorders, 5*(1), 20-1955-5-20. doi:10.1186/1866-1955-5-20 [doi]

Buckner, R. L., Andrews-Hanna, J. R., & Schacter, D. L. (2008). The brain's default network: Anatomy, function, and relevance to disease. *Annals of the New York Academy of Sciences, 1124*, 1-38. doi:10.1196/annals.1440.011 [doi]

Bureau, I., Shepherd, G. M., & Svoboda, K. (2008). Circuit and plasticity defects in the

developing somatosensory cortex of FMR1 knock-out mice. *The Journal of Neuroscience : The Official Journal of the Society for Neuroscience, 28*(20), 5178-5188. doi:10.1523/JNEUROSCI.1076-08.2008

Burket, J. A., Herndon, A. L., Winebarger, E. E., Jacome, L. F., & Deutsch, S. I. (2011). Complex effects of mGluR5 antagonism on sociability and stereotypic behaviors in mice: Possible implications for the pharmacotherapy of autism spectrum disorders. *Brain Research Bulletin, 86*(3-4), 152-158. doi:10.1016/j.brainresbull.2011.08.001

Burri, R., Steffen, C., & Herschkowitz, N. (1991). N-acetyl-L-aspartate is a major source of acetyl groups for lipid synthesis during rat brain development. *Developmental Neuroscience, 13*(6), 403-411.

Buxton, R. B., & Frank, L. R. (1997). A model for the coupling between cerebral blood flow and oxygen metabolism during neural stimulation. *Journal of Cerebral Blood Flow and Metabolism : Official Journal of the International Society of Cerebral Blood Flow and Metabolism, 17*(1), 64-72. doi:10.1097/00004647-199701000-00009 [doi]

Castren, M., Paakkonen, A., Tarkka, I. M., Ryynanen, M., & Partanen, J. (2003). Augmentation of auditory N1 in children with fragile X syndrome. *Brain Topography, 15*(3), 165-171.

Cea-Del Rio, C. A., & Huntsman, M. M. (2014). The contribution of inhibitory interneurons to circuit dysfunction in fragile X syndrome. *Frontiers in Cellular Neuroscience, 8*, 245. doi:10.3389/fncel.2014.00245 [doi]

Cheng, C., Sourial, M., & Doering, L. C. (2012). Astrocytes and developmental plasticity in fragile x. *Neural Plasticity, 2012*, 197491. doi:10.1155/2012/197491

Cheung, M. M., Hui, E. S., Chan, K. C., Helpern, J. A., Qi, L., & Wu, E. X. (2009). Does diffusion kurtosis imaging lead to better neural tissue characterization? A rodent brain maturation study. *Neuroimage, 45*(2), 386-392. doi:10.1016/j.neuroimage.2008.12.018 [doi]

Choi, C. H., McBride, S. M., Schoenfeld, B. P., Liebelt, D. A., Ferreiro, D., Ferrick, N. J., . . . Jongens, T. A. (2010). Age-dependent cognitive impairment in a drosophila fragile X model and its pharmacological rescue. *Biogerontology, 11*(3), 347-362. doi:10.1007/s10522-009-9259-6

Chugani, D. C. (2012). Neuroimaging and neurochemistry of autism. *Pediatric Clinics of North America, 59*(1), 63-73, x. doi:10.1016/j.pcl.2011.10.002; 10.1016/j.pcl.2011.10.002

Coffee, B., Keith, K., Albizua, I., Malone, T., Mowrey, J., Sherman, S. L., & Warren, S. T. (2009). Incidence of fragile X syndrome by newborn screening for methylated FMR1 DNA. *American Journal of Human Genetics, 85*(4), 503-514. doi:10.1016/j.ajhg.2009.09.007

Cox, R. W. (1996). AFNI: Software for analysis and visualization of functional magnetic resonance neuroimages. *Computers and Biomedical Research, an International Journal, 29*(3), 162-173. doi:S0010480996900142 [pii]

CURTIS, D. R., & WATKINS, J. C. (1960). The excitation and depression of spinal neurones by structurally related amino acids. *Journal of Neurochemistry, 6*, 117-141.

Danbolt, N. C. (2001). Glutamate uptake. *Progress in Neurobiology, 65*(1), 1-105. doi:S0301-0082(00)00067-8 [pii]

Dansie, L. E., Phommahaxay, K., Okusanya, A. G., Uwadia, J., Huang, M., Rotschafer,

S. E., . . . Ethell, I. M. (2013). Long-lasting effects of minocycline on behavior in young but not adult fragile X mice. *Neuroscience, 246*, 186-198. doi:10.1016/j.neuroscience.2013.04.058 [doi]

D'Antuono, M., Merlo, D., & Avoli, M. (2003). Involvement of cholinergic and gabaergic systems in the fragile X knockout mice. *Neuroscience, 119*(1), 9-13.

Darnell, J. C., Fraser, C. E., Mostovetsky, O., & Darnell, R. B. (2009). Discrimination of common and unique RNA-binding activities among fragile X mental retardation protein paralogs. *Human Molecular Genetics, 18*(17), 3164-3177. doi:10.1093/hmg/ddp255

Darnell, J. C., Van Driesche, S. J., Zhang, C., Hung, K. Y., Mele, A., Fraser, C. E., . . . Darnell, R. B. (2011). FMRP stalls ribosomal translocation on mRNAs linked to synaptic function and autism. *Cell, 146*(2), 247-261. doi:10.1016/j.cell.2011.06.013

Davidovic, L., Navratil, V., Bonaccorso, C. M., Catania, M. V., Bardoni, B., & Dumas, M. E. (2011). A metabolomic and systems biology perspective on the brain of the fragile X syndrome mouse model. *Genome Research, 21*(12), 2190-2202. doi:10.1101/gr.116764.110

Davies, S. E., Gotoh, M., Richards, D. A., & Obrenovitch, T. P. (1998). Hypoosmolarity induces an increase of extracellular N-acetylaspartate concentration in the rat striatum. *Neurochemical Research, 23*(8), 1021-1025.

de Die-Smulders, C. E., Land, J. A., Dreesen, J. C., Coonen, E., Evers, J. L., & Geraedts, J. P. (2004). Results from 10 years of preimplantation-genetic diagnostics in the netherlands. [Resultaten van 10 jaar preimplantatiegenetische diagnostiek in Nederland] *Nederlands Tijdschrift Voor Geneeskunde, 148*(50), 2491-2496.

de Groot, M., Cremers, L. G., Ikram, M. A., Hofman, A., Krestin, G. P., van der Lugt, A., . . . Vernooij, M. W. (2016). White matter degeneration with aging: Longitudinal diffusion MR imaging analysis. *Radiology, 279*(2), 532-541. doi:10.1148/radiol.2015150103 [doi]

Degaonkar, M. N., Khubchandhani, M., Dhawan, J. K., Jayasundar, R., & Jagannathan, N. R. (2002). Sequential proton MRS study of brain metabolite changes monitored during a complete pathological cycle of demyelination and remyelination in a lysophosphatidyl choline (LPC)-induced experimental demyelinating lesion model. *NMR in Biomedicine, 15*(4), 293-300. doi:10.1002/nbm.771 [doi]

Devys, D., Lutz, Y., Rouyer, N., Bellocq, J. P., & Mandel, J. L. (1993). The FMR-1 protein is cytoplasmic, most abundant in neurons and appears normal in carriers of a fragile X premutation. *Nature Genetics, 4*(4), 335-340. doi:10.1038/ng0893-335

D'Hulst, C., De Geest, N., Reeve, S. P., Van Dam, D., De Deyn, P. P., Hassan, B. A., & Kooy, R. F. (2006). Decreased expression of the GABAA receptor in fragile X syndrome. *Brain Research, 1121*(1), 238-245. doi:S0006-8993(06)02656-4 [pii]

D'Hulst, C., Heulens, I., Brouwer, J. R., Willemsen, R., De Geest, N., Reeve, S. P., . . . Kooy, R. F. (2009). Expression of the GABAergic system in animal models for fragile X syndrome and fragile X associated tremor/ataxia syndrome (FXTAS). *Brain Research, 1253*, 176-183. doi:10.1016/j.brainres.2008.11.075

D'Hulst, C., Heulens, I., Van der Aa, N., Goffin, K., Koole, M., Porke, K., . . . Kooy, R. F. (2015). Positron emission tomography (PET) quantification of GABAA receptors in the brain of fragile X patients. *PloS One, 10*(7), e0131486. doi:10.1371/journal.pone.0131486 [doi]

Diamond, I. (1971). Choline metabolism in brain. the role of choline transport and the effects of phenobarbital. *Archives of Neurology, 24*(4), 333-339.

Dictenberg, J. B., Swanger, S. A., Antar, L. N., Singer, R. H., & Bassell, G. J. (2008). A direct role for FMRP in activity-dependent dendritic mRNA transport links filopodial-spine morphogenesis to fragile X syndrome. *Developmental Cell, 14*(6), 926-939. doi:10.1016/j.devcel.2008.04.003 [doi]

Dolen, G., & Bear, M. F. (2008). Role for metabotropic glutamate receptor 5 (mGluR5) in the pathogenesis of fragile X syndrome. *The Journal of Physiology, 586*(6), 1503-1508. doi:10.1113/jphysiol.2008.150722 [doi]

Dolen, G., & Bear, M. F. (2009). Fragile x syndrome and autism: From disease model to therapeutic targets. *Journal of Neurodevelopmental Disorders, 1*(2), 133-140. doi:10.1007/s11689-009-9015-x

Dolen, G., Osterweil, E., Rao, B. S., Smith, G. B., Auerbach, B. D., Chattarji, S., & Bear, M. F. (2007). Correction of fragile X syndrome in mice. *Neuron, 56*(6), 955-962. doi:10.1016/j.neuron.2007.12.001

D'Souza, D. V., Jonckers, E., Bruns, A., Kunnecke, B., von Kienlin, M., Van der Linden, A., . . . Verhoye, M. (2014). Preserved modular network organization in the sedated rat brain. *PloS One, 9*(9), e106156. doi:10.1371/journal.pone.0106156 [doi]

Dy, A. B. C., Tassone, F., Eldeeb, M., Salcedo-Arellano, M. J., Tartaglia, N., & Hagerman, R. (2017). Metformin as targeted treatment in fragile X syndrome. *Clinical Genetics,* doi:10.1111/cge.13039 [doi]

Dziembowska, M., Pretto, D. I., Janusz, A., Kaczmarek, L., Leigh, M. J., Gabriel, N., . . . Tassone, F. (2013). High MMP-9 activity levels in fragile X syndrome are lowered

by minocycline. *American Journal of Medical Genetics.Part A, 161A*(8), 1897-1903. doi:10.1002/ajmg.a.36023 [doi]

Eichenbaum, H. (1996). Is the rodent hippocampus just for 'place'? *Current Opinion in Neurobiology, 6*(2), 187-195. doi:S0959-4388(96)80072-9 [pii]

El Idrissi, A., Boukarrou, L., Dokin, C., & Brown, W. T. (2009). Taurine improves congestive functions in a mouse model of fragile X syndrome. *Advances in Experimental Medicine and Biology, 643*, 191-198.

El Idrissi, A., Ding, X. H., Scalia, J., Trenkner, E., Brown, W. T., & Dobkin, C. (2005). Decreased GABA(A) receptor expression in the seizure-prone fragile X mouse. *Neuroscience Letters, 377*(3), 141-146. doi:10.1016/j.neulet.2004.11.087

El Idrissi, A., Neuwirth, L. S., & L'Amoreaux, W. (2010). Taurine regulation of short term synaptic plasticity in fragile X mice. *Journal of Biomedical Science, 17 Suppl 1*, S15. doi:10.1186/1423-0127-17-S1-S15

El Idrissi, A., & Trenkner, E. (1999). Growth factors and taurine protect against excitotoxicity by stabilizing calcium homeostasis and energy metabolism. *The Journal of Neuroscience : The Official Journal of the Society for Neuroscience, 19*(21), 9459-9468.

Ellegood, J., Pacey, L. K., Hampson, D. R., Lerch, J. P., & Henkelman, R. M. (2010). Anatomical phenotyping in a mouse model of fragile X syndrome with magnetic resonance imaging. *Neuroimage, 53*(3), 1023-1029. doi:10.1016/j.neuroimage.2010.03.038

Estevez, A. Y., O'Regan, M. H., Song, D., & Phillis, J. W. (1999). Hyposmotically induced amino acid release from the rat cerebral cortex: Role of phospholipases and

protein kinases. *Brain Research, 844*(1-2), 1-9. doi:S0006-8993(99)01801-6 [pii]

Fair, D. A., Cohen, A. L., Dosenbach, N. U., Church, J. A., Miezin, F. M., Barch, D. M., . . . Schlaggar, B. L. (2008). The maturing architecture of the brain's default network. *Proceedings of the National Academy of Sciences of the United States of America, 105*(10), 4028-4032. doi:10.1073/pnas.0800376105 [doi]

Fan, T. W. M. (1996). Metabolite profiling by one- and two-dimensional NMR analysis of complex mixtures. *Progress in Nuclear Magnetic Resonance Spectroscopy, 28*, 161-219.

Feeney, D. M., & Wier, C. S. (1979). Sensory neglect after lesions of substantia nigra or lateral hypothalamus: Differential severity and recovery of function. *Brain Research, 178*(2-3), 329-346. doi:0006-8993(79)90697-8 [pii]

Fieremans, E., Jensen, J. H., & Helpern, J. A. (2011). White matter characterization with diffusional kurtosis imaging. *Neuroimage, 58*(1), 177-188. doi:10.1016/j.neuroimage.2011.06.006 [doi]

Finelli, D. A., Hurst, G. C., Amantia, P.,Jr, Gullapali, R. P., & Apicella, A. (1996). Cerebral white matter: Technical development and clinical applications of effective magnetization transfer (MT) power concepts for high-power, thin-section, quantitative MT examinations. *Radiology, 199*(1), 219-226. doi:10.1148/radiology.199.1.8633148 [doi]

Finelli, D. A., Hurst, G. C., & Gullapalli, R. P. (1998). T1-weighted three-dimensional magnetization transfer MR of the brain: Improved lesion contrast enhancement. *AJNR.American Journal of Neuroradiology, 19*(1), 59-64.

Flaim, S. F. (1994). Pharmacokinetics and side effects of perfluorocarbon-based blood

substitutes. *Artificial Cells, Blood Substitutes, and Immobilization Biotechnology, 22*(4), 1043-1054. doi:10.3109/10731199409138801 [doi]

Franklin, K. B. J., & Paxinos, G. (2007). *The mouse brain in steretaxic coordinates* (3rd ed.) Academic Press.

Freund, L. S., Reiss, A. L., & Abrams, M. T. (1993). Psychiatric disorders associated with fragile X in the young female. *Pediatrics, 91*(2), 321-329.

Gabis, L., Wei, H., Azizian, A., DeVincent, C., Tudorica, A., Kesner-Baruch, Y., . . . Pomeroy, J. (2008). 1H-magnetic resonance spectroscopy markers of cognitive and language ability in clinical subtypes of autism spectrum disorders. *Journal of Child Neurology, 23*(7), 766-774. doi:10.1177/0883073808315423 [doi]

Gantois, I., Khoutorsky, A., Popic, J., Aguilar-Valles, A., Freemantle, E., Cao, R., . . . Sonenberg, N. (2017). Metformin ameliorates core deficits in a mouse model of fragile X syndrome. *Nature Medicine,* doi:10.1038/nm.4335 [doi]

Garber, K. B., Visootsak, J., & Warren, S. T. (2008). Fragile X syndrome. *European Journal of Human Genetics : EJHG, 16*(6), 666-672. doi:10.1038/ejhg.2008.61

Gholizadeh, S., Halder, S. K., & Hampson, D. R. (2015). Expression of fragile X mental retardation protein in neurons and glia of the developing and adult mouse brain. *Brain Research, 1596,* 22-30. doi:10.1016/j.brainres.2014.11.023 [doi]

Gibson, J. R., Bartley, A. F., Hays, S. A., & Huber, K. M. (2008). Imbalance of neocortical excitation and inhibition and altered UP states reflect network hyperexcitability in the mouse model of fragile X syndrome. *Journal of Neurophysiology, 100*(5), 2615-2626. doi:10.1152/jn.90752.2008

Giraudeau, C., Geffroy, F., Meriaux, S., Boumezbeur, F., Robert, P., Port, M., . . .

Valette, J. (2013). 19F molecular MR imaging for detection of brain tumor angiogenesis: In vivo validation using targeted PFOB nanoparticles. *Angiogenesis, 16*(1), 171-179. doi:10.1007/s10456-012-9310-0 [doi]

Giuffrida, R., Musumeci, S., D'Antoni, S., Bonaccorso, C. M., Giuffrida-Stella, A. M., Oostra, B. A., & Catania, M. V. (2005). A reduced number of metabotropic glutamate subtype 5 receptors are associated with constitutive homer proteins in a mouse model of fragile X syndrome. *The Journal of Neuroscience : The Official Journal of the Society for Neuroscience, 25*(39), 8908-8916. doi:25/39/8908 [pii]

Godfraind, J. M., Reyniers, E., De Boulle, K., D'Hooge, R., De Deyn, P. P., Bakker, C. E., . . . Willems, P. J. (1996). Long-term potentiation in the hippocampus of fragile X knockout mice. *American Journal of Medical Genetics, 64*(2), 246-251. doi:10.1002/(SICI)1096-8628(19960809)64:2<246::AID-AJMG2>3.0.CO;2-S [pii]

Gothelf, D., Furfaro, J. A., Hoeft, F., Eckert, M. A., Hall, S. S., O'Hara, R., . . . Reiss, A. L. (2008). Neuroanatomy of fragile X syndrome is associated with aberrant behavior and the fragile X mental retardation protein (FMRP). *Annals of Neurology, 63*(1), 40-51. doi:10.1002/ana.21243

Green, T., Barnea-Goraly, N., Raman, M., Hall, S. S., Lightbody, A. A., Bruno, J. L., . . . Reiss, A. L. (2015). Specific effect of the fragile-X mental retardation-1 gene (FMR1) on white matter microstructure. *The British Journal of Psychiatry : The Journal of Mental Science, 207*(2), 143-148. doi:10.1192/bjp.bp.114.151654 [doi]

Greenough, W. T., Klintsova, A. Y., Irwin, S. A., Galvez, R., Bates, K. E., & Weiler, I. J. (2001). Synaptic regulation of protein synthesis and the fragile X protein. *Proceedings of the National Academy of Sciences of the United States of America,*

98(13), 7101-7106. doi:10.1073/pnas.141145998 [doi]

Gross, C., Berry-Kravis, E. M., & Bassell, G. J. (2012). Therapeutic strategies in fragile X syndrome: Dysregulated mGluR signaling and beyond. *Neuropsychopharmacology : Official Publication of the American College of Neuropsychopharmacology, 37*(1), 178-195. doi:10.1038/npp.2011.137; 10.1038/npp.2011.137

Gross, C., Nakamoto, M., Yao, X., Chan, C. B., Yim, S. Y., Ye, K., . . . Bassell, G. J. (2010). Excess phosphoinositide 3-kinase subunit synthesis and activity as a novel therapeutic target in fragile X syndrome. *The Journal of Neuroscience : The Official Journal of the Society for Neuroscience, 30*(32), 10624-10638. doi:10.1523/JNEUROSCI.0402-10.2010

Grossman, A. W., Aldridge, G. M., Lee, K. J., Zeman, M. K., Jun, C. S., Azam, H. S., . . . Rhyu, I. J. (2010). Developmental characteristics of dendritic spines in the dentate gyrus of Fmr1 knockout mice. *Brain Research, 1355*, 221-227. doi:10.1016/j.brainres.2010.07.090

Grossman, A. W., Aldridge, G. M., Weiler, I. J., & Greenough, W. T. (2006). Local protein synthesis and spine morphogenesis: Fragile X syndrome and beyond. *The Journal of Neuroscience : The Official Journal of the Society for Neuroscience, 26*(27), 7151-7155. doi:26/27/7151 [pii]

Grossman, A. W., Elisseou, N. M., McKinney, B. C., & Greenough, W. T. (2006). Hippocampal pyramidal cells in adult Fmr1 knockout mice exhibit an immature-appearing profile of dendritic spines. *Brain Research, 1084*(1), 158-164. doi:10.1016/j.brainres.2006.02.044

Gruetter, R. (1993a). Automatic, localized in vivo adjustment of all first- and second-order shim coils. *Magnetic Resonance in Medicine : Official Journal of the Society of Magnetic Resonance in Medicine / Society of Magnetic Resonance in Medicine, 29*(6), 804-811.

Gruetter, R. (1993b). Automatic, localized in vivo adjustment of all first- and second-order shim coils. *Magnetic Resonance in Medicine, 29*(6), 804-811.

Gruss, M., & Braun, K. (2001). Alterations of amino acids and monoamine metabolism in male Fmr1 knockout mice: A putative animal model of the human fragile X mental retardation syndrome. *Neural Plasticity, 8*(4), 285-298. doi:10.1155/NP.2001.285

Gyulai, F. E. (2004). Anesthetics and cerebral metabolism. *Current Opinion in Anaesthesiology, 17*(5), 397-402. doi:00001503-200410000-00008 [pii]

Haas, B. W., Barnea-Goraly, N., Lightbody, A. A., Patnaik, S. S., Hoeft, F., Hazlett, H., . . . Reiss, A. L. (2009). Early white-matter abnormalities of the ventral frontostriatal pathway in fragile X syndrome. *Developmental Medicine and Child Neurology, 51*(8), 593-599. doi:10.1111/j.1469-8749.2009.03295.x

Haberl, M. G., Zerbi, V., Veltien, A., Ginger, M., Heerschap, A., & Frick, A. (2015). Structural-functional connectivity deficits of neocortical circuits in the Fmr1 (-/y) mouse model of autism. *Science Advances, 1*(10), e1500775. doi:10.1126/sciadv.1500775 [doi]

Hagerman, R., Lauterborn, J., Au, J., & Berry-Kravis, E. (2012). Fragile X syndrome and targeted treatment trials. *Results and Problems in Cell Differentiation, 54*, 297-335. doi:10.1007/978-3-642-21649-7_17

Hall, S., DeBernardis, M., & Reiss, A. (2006). Social escape behaviors in children with fragile X syndrome. *Journal of Autism and Developmental Disorders, 36*(7), 935-947. doi:10.1007/s10803-006-0132-z [doi]

Hall, S. S., Dougherty, R. F., & Reiss, A. L. (2016). Profiles of aberrant white matter microstructure in fragile X syndrome. *NeuroImage.Clinical, 11*, 133-138. doi:10.1016/j.nicl.2016.01.013 [doi]

Hall, S. S., Jiang, H., Reiss, A. L., & Greicius, M. D. (2013). Identifying large-scale brain networks in fragile X syndrome. *JAMA Psychiatry, 70*(11), 1215-1223. doi:10.1001/jamapsychiatry.2013.247 [doi]

Hall, S. S., Walter, E., Sherman, E., Hoeft, F., & Reiss, A. L. (2009). The neural basis of auditory temporal discrimination in girls with fragile X syndrome. *Journal of Neurodevelopmental Disorders, 1*(1), 91-99. doi:10.1007/s11689-009-9007-x [doi]

Hamilton, S. M., Green, J. R., Veeraragavan, S., Yuva, L., McCoy, A., Wu, Y., . . . Paylor, R. (2014). Fmr1 and Nlgn3 knockout rats: Novel tools for investigating autism spectrum disorders. *Behavioral Neuroscience, 128*(2), 103-109. doi:10.1037/a0035988 [doi]

Hammelrath, L., Skokic, S., Khmelinskii, A., Hess, A., van der Knaap, N., Staring, M., . . . Hoehn, M. (2016). Morphological maturation of the mouse brain: An in vivo MRI and histology investigation. *Neuroimage, 125*, 144-152. doi:10.1016/j.neuroimage.2015.10.009 [doi]

Harada, S., Fujita-Hamabe, W., & Tokuyama, S. (2010). The importance of regulation of blood glucose levels through activation of peripheral 5'-AMP-activated protein kinase on ischemic neuronal damage. *Brain Research, 1351*, 254-263.

doi:10.1016/j.brainres.2010.06.052 [doi]

Harauz, G., Ladizhansky, V., & Boggs, J. M. (2009). Structural polymorphism and multifunctionality of myelin basic protein. *Biochemistry, 48*(34), 8094-8104. doi:10.1021/bi901005f; 10.1021/bi901005f

Harlow, E. G., Till, S. M., Russell, T. A., Wijetunge, L. S., Kind, P., & Contractor, A. (2010). Critical period plasticity is disrupted in the barrel cortex of FMR1 knockout mice. *Neuron, 65*(3), 385-398. doi:10.1016/j.neuron.2010.01.024

Hasselmo, M. E. (2006). The role of acetylcholine in learning and memory. *Current Opinion in Neurobiology, 16*(6), 710-715. doi:10.1016/j.conb.2006.09.002

Hatoum, D., & McGowan, E. M. (2015). Recent advances in the use of metformin: Can treating diabetes prevent breast cancer? *BioMed Research International, 2015*, 548436. doi:10.1155/2015/548436 [doi]

Hazlett, H. C., Poe, M. D., Lightbody, A. A., Styner, M., MacFall, J. R., Reiss, A. L., & Piven, J. (2012). Trajectories of early brain volume development in fragile X syndrome and autism. *Journal of the American Academy of Child and Adolescent Psychiatry, 51*(9), 921-933. doi:10.1016/j.jaac.2012.07.003; 10.1016/j.jaac.2012.07.003

Heilig, C. W., Stromski, M. E., Blumenfeld, J. D., Lee, J. P., & Gullans, S. R. (1989). Characterization of the major brain osmolytes that accumulate in salt-loaded rats. *The American Journal of Physiology, 257*(6 Pt 2), F1108-16.

Henderson, C., Wijetunge, L., Kinoshita, M. N., Shumway, M., Hammond, R. S., Postma, F. R., . . . Healy, A. M. (2012). Reversal of disease-related pathologies in the fragile X mouse model by selective activation of GABAB receptors with

arbaclofen. *Science Translational Medicine, 4*(152), 152ra128. doi:4/152/152ra128 [pii]

Henkelman, R. M., Stanisz, G. J., & Graham, S. J. (2001). Magnetization transfer in MRI: A review. *NMR in Biomedicine, 14*(2), 57-64.

Heulens, I., D'Hulst, C., Van Dam, D., De Deyn, P. P., & Kooy, R. F. (2012). Pharmacological treatment of fragile X syndrome with GABAergic drugs in a knockout mouse model. *Behavioural Brain Research, 229*(1), 244-249. doi:10.1016/j.bbr.2012.01.031

Higashimori, H., Morel, L., Huth, J., Lindemann, L., Dulla, C., Taylor, A., . . . Yang, Y. (2013). Astroglial FMRP-dependent translational down-regulation of mGluR5 underlies glutamate transporter GLT1 dysregulation in the fragile X mouse. *Human Molecular Genetics, 22*(10), 2041-2054. doi:10.1093/hmg/ddt055 [doi]

Hinman, J. D., Chen, C. D., Oh, S. Y., Hollander, W., & Abraham, C. R. (2008). Age-dependent accumulation of ubiquitinated 2',3'-cyclic nucleotide 3'-phosphodiesterase in myelin lipid rafts. *Glia, 56*(1), 118-133. doi:10.1002/glia.20595 [doi]

Hinton, V. J., Brown, W. T., Wisniewski, K., & Rudelli, R. D. (1991). Analysis of neocortex in three males with the fragile X syndrome. *American Journal of Medical Genetics, 41*(3), 289-294. doi:10.1002/ajmg.1320410306 [doi]

Hoeft, F., Carter, J. C., Lightbody, A. A., Cody Hazlett, H., Piven, J., & Reiss, A. L. (2010). Region-specific alterations in brain development in one- to three-year-old boys with fragile X syndrome. *Proceedings of the National Academy of Sciences of the United States of America, 107*(20), 9335-9339. doi:10.1073/pnas.1002762107

Hoeft, F., Walter, E., Lightbody, A. A., Hazlett, H. C., Chang, C., Piven, J., & Reiss, A.

L. (2011). Neuroanatomical differences in toddler boys with fragile x syndrome and idiopathic autism. *Archives of General Psychiatry, 68*(3), 295-305. doi:10.1001/archgenpsychiatry.2010.153

Hofer, S., & Frahm, J. (2006). Topography of the human corpus callosum revisited--comprehensive fiber tractography using diffusion tensor magnetic resonance imaging. *Neuroimage, 32*(3), 989-994. doi:S1053-8119(06)00650-1 [pii]

Hoff, G. E., Van den Heuvel, M. P., Benders, M. J., Kersbergen, K. J., & De Vries, L. S. (2013). On development of functional brain connectivity in the young brain. *Frontiers in Human Neuroscience, 7*, 650. doi:10.3389/fnhum.2013.00650 [doi]

Hou, L., Antion, M. D., Hu, D., Spencer, C. M., Paylor, R., & Klann, E. (2006). Dynamic translational and proteasomal regulation of fragile X mental retardation protein controls mGluR-dependent long-term depression. *Neuron, 51*(4), 441-454. doi:S0896-6273(06)00545-9 [pii]

Hou, L., & Klann, E. (2004). Activation of the phosphoinositide 3-kinase-akt-mammalian target of rapamycin signaling pathway is required for metabotropic glutamate receptor-dependent long-term depression. *The Journal of Neuroscience : The Official Journal of the Society for Neuroscience, 24*(28), 6352-6361. doi:10.1523/JNEUROSCI.0995-04.2004 [doi]

Huber, K. M., Gallagher, S. M., Warren, S. T., & Bear, M. F. (2002). Altered synaptic plasticity in a mouse model of fragile X mental retardation. *Proceedings of the National Academy of Sciences of the United States of America, 99*(11), 7746-7750. doi:10.1073/pnas.122205699

Huber, K. M., Klann, E., Costa-Mattioli, M., & Zukin, R. S. (2015). Dysregulation of

mammalian target of rapamycin signaling in mouse models of autism. *The Journal of Neuroscience : The Official Journal of the Society for Neuroscience, 35*(41), 13836-13842. doi:10.1523/JNEUROSCI.2656-15.2015 [doi]

Hutchison, R. M., Mirsattari, S. M., Jones, C. K., Gati, J. S., & Leung, L. S. (2010). Functional networks in the anesthetized rat brain revealed by independent component analysis of resting-state FMRI. *Journal of Neurophysiology, 103*(6), 3398-3406. doi:10.1152/jn.00141.2010 [doi]

Hyde, T. M., Ziegler, J. C., & Weinberger, D. R. (1992). Psychiatric disturbances in metachromatic leukodystrophy. insights into the neurobiology of psychosis. *Archives of Neurology, 49*(4), 401-406.

Irwin, S. A., Patel, B., Idupulapati, M., Harris, J. B., Crisostomo, R. A., Larsen, B. P., . . . Greenough, W. T. (2001). Abnormal dendritic spine characteristics in the temporal and visual cortices of patients with fragile-X syndrome: A quantitative examination. *American Journal of Medical Genetics, 98*(2), 161-167.

Jacobs, S., Cheng, C., & Doering, L. C. (2012). Probing astrocyte function in fragile X syndrome. *Results and Problems in Cell Differentiation, 54*, 15-31. doi:10.1007/978-3-642-21649-7_2

Jacobs, S., & Doering, L. C. (2010). Astrocytes prevent abnormal neuronal development in the fragile x mouse. *The Journal of Neuroscience : The Official Journal of the Society for Neuroscience, 30*(12), 4508-4514. doi:10.1523/JNEUROSCI.5027-09.2010

Jacquemont, S., Berry-Kravis, E., Hagerman, R., von Raison, F., Gasparini, F., Apostol, G., . . . Gomez-Mancilla, B. (2014). The challenges of clinical trials in fragile X

syndrome. *Psychopharmacology, 231*(6), 1237-1250. doi:10.1007/s00213-013-3289-0 [doi]

Jacquemont, S., Curie, A., des Portes, V., Torrioli, M. G., Berry-Kravis, E., Hagerman, R. J., . . . Gomez-Mancilla, B. (2011). Epigenetic modification of the FMR1 gene in fragile X syndrome is associated with differential response to the mGluR5 antagonist AFQ056. *Science Translational Medicine, 3*(64), 64ra1. doi:10.1126/scitranslmed.3001708 [doi]

Jang, S. H., & Seo, J. P. (2015). The anatomical location of the corticoreticular pathway at the subcortical white matter in the human brain: A diffusion tensor imaging study. *Somatosensory & Motor Research, 32*(2), 106-109. doi:10.3109/08990220.2014.986326 [doi]

Jensen, J. H., & Helpern, J. A. (2010). MRI quantification of non-gaussian water diffusion by kurtosis analysis. *NMR in Biomedicine, 23*(7), 698-710. doi:10.1002/nbm.1518 [doi]

Jonckers, E., Delgado y Palacios, R., Shah, D., Guglielmetti, C., Verhoye, M., & Van der Linden, A. (2014). Different anesthesia regimes modulate the functional connectivity outcome in mice. *Magnetic Resonance in Medicine, 72*(4), 1103-1112. doi:10.1002/mrm.24990 [doi]

Jonckers, E., Shah, D., Hamaide, J., Verhoye, M., & Van der Linden, A. (2015). The power of using functional fMRI on small rodents to study brain pharmacology and disease. *Frontiers in Pharmacology, 6*, 231. doi:10.3389/fphar.2015.00231 [doi]

Jonckers, E., Van Audekerke, J., De Visscher, G., Van der Linden, A., & Verhoye, M. (2011). Functional connectivity fMRI of the rodent brain: Comparison of functional

connectivity networks in rat and mouse. *PloS One, 6*(4), e18876. doi:10.1371/journal.pone.0018876 [doi]

Jurevics, H., & Morell, P. (1995). Cholesterol for synthesis of myelin is made locally, not imported into brain. *Journal of Neurochemistry, 64*(2), 895-901.

Kaneda, M. M., Caruthers, S., Lanza, G. M., & Wickline, S. A. (2009). Perfluorocarbon nanoemulsions for quantitative molecular imaging and targeted therapeutics. *Annals of Biomedical Engineering, 37*(10), 1922-1933. doi:10.1007/s10439-009-9643-z [doi]

Kang, J. Y., Chadchankar, J., Vien, T. N., Mighdoll, M. I., Hyde, T. M., Mather, R. J., . . . Moss, S. J. (2017). Deficits in the activity of presynaptic gamma-aminobutyric acid type B receptors contribute to altered neuronal excitability in fragile X syndrome. *The Journal of Biological Chemistry*, doi:jbc.M116.772541 [pii]

Kao, D. I., Aldridge, G. M., Weiler, I. J., & Greenough, W. T. (2010). Altered mRNA transport, docking, and protein translation in neurons lacking fragile X mental retardation protein. *Proceedings of the National Academy of Sciences of the United States of America, 107*(35), 15601-15606. doi:10.1073/pnas.1010564107

Kates, W. R., Abrams, M. T., Kaufmann, W. E., Breiter, S. N., & Reiss, A. L. (1997). Reliability and validity of MRI measurement of the amygdala and hippocampus in children with fragile X syndrome. *Psychiatry Research, 75*(1), 31-48.

Kayser, K., Liewald, F., Kremer, K., & Tacke, M. (1994). Integrated optical density (IOD), syntactic structure analysis, and survival in operated lung carcinoma patients. *Pathology, Research and Practice, 190*(11), 1031-1038. doi:S0344-0338(11)80898-8 [pii]

Kazdoba, T. M., Leach, P. T., Silverman, J. L., & Crawley, J. N. (2014). Modeling fragile X syndrome in the Fmr1 knockout mouse. *Intractable & Rare Diseases Research, 3*(4), 118-133. doi:10.5582/irdr.2014.01024 [doi]

Kelm, N. D., West, K. L., Carson, R. P., Gochberg, D. F., Ess, K. C., & Does, M. D. (2016). Evaluation of diffusion kurtosis imaging in ex vivo hypomyelinated mouse brains. *Neuroimage, 124*(Pt A), 612-626. doi:10.1016/j.neuroimage.2015.09.028 [doi]

Kenkel, W. M., Yee, J. R., Moore, K., Madularu, D., Kulkarni, P., Gamber, K., . . . Ferris, C. F. (2016). Functional magnetic resonance imaging in awake transgenic fragile X rats: Evidence of dysregulation in reward processing in the mesolimbic/habenular neural circuit. *Translational Psychiatry, 6*, e763. doi:10.1038/tp.2016.15 [doi]

Kennedy, D. P., & Courchesne, E. (2008). The intrinsic functional organization of the brain is altered in autism. *Neuroimage, 39*(4), 1877-1885. doi:S1053-8119(07)00995-0 [pii]

Kesler, S. R., Lightbody, A. A., & Reiss, A. L. (2009). Cholinergic dysfunction in fragile X syndrome and potential intervention: A preliminary 1H MRS study. *American Journal of Medical Genetics.Part A, 149A*(3), 403-407. doi:10.1002/ajmg.a.32697

Kidd, S. A., Lachiewicz, A., Barbouth, D., Blitz, R. K., Delahunty, C., McBrien, D., . . . Berry-Kravis, E. (2014). Fragile X syndrome: A review of associated medical problems. *Pediatrics, 134*(5), 995-1005. doi:10.1542/peds.2013-4301 [doi]

Kinney, H. C., Brody, B. A., Kloman, A. S., & Gilles, F. H. (1988). Sequence of central nervous system myelination in human infancy. II. patterns of myelination in

autopsied infants. *Journal of Neuropathology and Experimental Neurology, 47*(3), 217-234.

Kleinhans, N. M., Schweinsburg, B. C., Cohen, D. N., Muller, R. A., & Courchesne, E. (2007). N-acetyl aspartate in autism spectrum disorders: Regional effects and relationship to fMRI activation. *Brain Research, 1162*, 85-97. doi:S0006-8993(07)01021-9 [pii]

Koekkoek, S. K., Yamaguchi, K., Milojkovic, B. A., Dortland, B. R., Ruigrok, T. J., Maex, R., . . . De Zeeuw, C. I. (2005). Deletion of FMR1 in purkinje cells enhances parallel fiber LTD, enlarges spines, and attenuates cerebellar eyelid conditioning in fragile X syndrome. *Neuron, 47*(3), 339-352. doi:10.1016/j.neuron.2005.07.005

Koenig, S. H., Brown, R. D.,3rd, Spiller, M., & Lundbom, N. (1990). Relaxometry of brain: Why white matter appears bright in MRI. *Magnetic Resonance in Medicine, 14*(3), 482-495.

Kolb, B., Mychasiuk, R., Muhammad, A., Li, Y., Frost, D. O., & Gibb, R. (2012). Experience and the developing prefrontal cortex. *Proceedings of the National Academy of Sciences of the United States of America, 109 Suppl 2*, 17186-17193. doi:10.1073/pnas.1121251109 [doi]

Kronk, R., Bishop, E. E., Raspa, M., Bickel, J. O., Mandel, D. A., & Bailey, D. B.,Jr. (2010). Prevalence, nature, and correlates of sleep problems among children with fragile X syndrome based on a large scale parent survey. *Sleep, 33*(5), 679-687.

Kronk, R., Dahl, R., & Noll, R. (2009). Caregiver reports of sleep problems on a convenience sample of children with fragile X syndrome. *American Journal on Intellectual and Developmental Disabilities, 114*(6), 383-392. doi:10.1352/1944-

7588-114.6.383 [doi]

Krueger, D. D., & Bear, M. F. (2011). Toward fulfilling the promise of molecular medicine in fragile X syndrome. *Annual Review of Medicine, 62*, 411-429. doi:10.1146/annurev-med-061109-134644

Kulak, A., Duarte, J. M., Do, K. Q., & Gruetter, R. (2010). Neurochemical profile of the developing mouse cortex determined by in vivo 1H NMR spectroscopy at 14.1 T and the effect of recurrent anaesthesia. *Journal of Neurochemistry, 115*(6), 1466-1477. doi:10.1111/j.1471-4159.2010.07051.x; 10.1111/j.1471-4159.2010.07051.x

Kumar, A., Kaushik, S., Tripathi, R. P., Kaur, P., & Khushu, S. (2003). Role of in vivo proton MR spectroscopy in the evaluation of adult brain lesions: Our preliminary experience. *Neurology India, 51*(4), 474-478.

Kumar, M., Kim, S., Pickup, S., Chen, R., Fairless, A. H., Ittyerah, R., . . . Poptani, H. (2012). Longitudinal in-vivo diffusion tensor imaging for assessing brain developmental changes in BALB/cJ mice, a model of reduced sociability relevant to autism. *Brain Research, 1455*, 56-67. doi:10.1016/j.brainres.2012.03.041 [doi]

Kumar, R., Nguyen, H. D., Macey, P. M., Woo, M. A., & Harper, R. M. (2012). Regional brain axial and radial diffusivity changes during development. *Journal of Neuroscience Research, 90*(2), 346-355. doi:10.1002/jnr.22757 [doi]

La Fata, G., Gartner, A., Dominguez-Iturza, N., Dresselaers, T., Dawitz, J., Poorthuis, R. B., . . . Bagni, C. (2014). FMRP regulates multipolar to bipolar transition affecting neuronal migration and cortical circuitry. *Nature Neuroscience, 17*(12), 1693-1700. doi:10.1038/nn.3870 [doi]

Lai, J. K., Lerch, J. P., Doering, L. C., Foster, J. A., & Ellegood, J. (2016). Regional brain

volumes changes in adult male FMR1-KO mouse on the FVB strain. *Neuroscience, 318,* 12-21. doi:S0306-4522(16)00040-3 [pii]

Lebel, C., Gee, M., Camicioli, R., Wieler, M., Martin, W., & Beaulieu, C. (2012). Diffusion tensor imaging of white matter tract evolution over the lifespan. *Neuroimage, 60*(1), 340-352. doi:10.1016/j.neuroimage.2011.11.094 [doi]

Lee, J. Y., Taghian, K., & Petratos, S. (2014). Axonal degeneration in multiple sclerosis: Can we predict and prevent permanent disability? *Acta Neuropathologica Communications, 2,* 97-014-0097-7. doi:10.1186/s40478-014-0097-7 [doi]

Leigh, M. J., Nguyen, D. V., Mu, Y., Winarni, T. I., Schneider, A., Chechi, T., . . . Hagerman, R. J. (2013). A randomized double-blind, placebo-controlled trial of minocycline in children and adolescents with fragile x syndrome. *Journal of Developmental and Behavioral Pediatrics : JDBP, 34*(3), 147-155. doi:10.1097/DBP.0b013e318287cd17 [doi]

Levenga, J., de Vrij, F. M., Buijsen, R. A., Li, T., Nieuwenhuizen, I. M., Pop, A., . . . Willemsen, R. (2011). Subregion-specific dendritic spine abnormalities in the hippocampus of Fmr1 KO mice. *Neurobiology of Learning and Memory, 95*(4), 467-472. doi:10.1016/j.nlm.2011.02.009

Levenga, J., Hayashi, S., de Vrij, F. M., Koekkoek, S. K., van der Linde, H. C., Nieuwenhuizen, I., . . . Oostra, B. A. (2011). AFQ056, a new mGluR5 antagonist for treatment of fragile X syndrome. *Neurobiology of Disease, 42*(3), 311-317. doi:10.1016/j.nbd.2011.01.022

Li, J., Pelletier, M. R., Perez Velazquez, J. L., & Carlen, P. L. (2002). Reduced cortical synaptic plasticity and GluR1 expression associated with fragile X mental retardation

protein deficiency. *Molecular and Cellular Neurosciences, 19*(2), 138-151. doi:10.1006/mcne.2001.1085

Li, W., Mai, X., & Liu, C. (2014). The default mode network and social understanding of others: What do brain connectivity studies tell us. *Frontiers in Human Neuroscience, 8*, 74. doi:10.3389/fnhum.2014.00074 [doi]

Liao, A. H., Wu, S. Y., Wang, H. E., Weng, C. H., Wu, M. F., & Li, P. C. (2013). Evaluation of 18F-labeled targeted perfluorocarbon-filled albumin microbubbles as a probe for microUS and microPET in tumor-bearing mice. *Ultrasonics, 53*(2), 320-327. doi:10.1016/j.ultras.2012.06.014 [doi]

Lima, L., Obregon, F., Rousso, T., Quintal, M., Benzo, Z., & Auladell, C. (2004). Content and concentration of taurine, hypotaurine, and zinc in the retina, the hippocampus, and the dentate gyrus of the rat at various postnatal days. *Neurochemical Research, 29*(1), 247-255.

Liska, A., Galbusera, A., Schwarz, A. J., & Gozzi, A. (2015). Functional connectivity hubs of the mouse brain. *Neuroimage, 115*, 281-291. doi:10.1016/j.neuroimage.2015.04.033 [doi]

Liu, Z., & Smith, C. B. (2014). Lithium: A promising treatment for fragile X syndrome. *ACS Chemical Neuroscience,* doi:10.1021/cn500077p [doi]

Liu, Z. H., Chuang, D. M., & Smith, C. B. (2011). Lithium ameliorates phenotypic deficits in a mouse model of fragile X syndrome. *The International Journal of Neuropsychopharmacology / Official Scientific Journal of the Collegium Internationale Neuropsychopharmacologicum (CINP), 14*(5), 618-630. doi:10.1017/S1461145710000520

Liu, Z. H., Huang, T., & Smith, C. B. (2012). Lithium reverses increased rates of cerebral protein synthesis in a mouse model of fragile X syndrome. *Neurobiology of Disease, 45*(3), 1145-1152. doi:10.1016/j.nbd.2011.12.037

Liu-Yesucevitz, L., Bassell, G. J., Gitler, A. D., Hart, A. C., Klann, E., Richter, J. D., . . . Wolozin, B. (2011). Local RNA translation at the synapse and in disease. *The Journal of Neuroscience : The Official Journal of the Society for Neuroscience, 31*(45), 16086-16093. doi:10.1523/JNEUROSCI.4105-11.2011

Loffelholz, K. (1998). Brain choline has a typical precursor profile. *Journal of Physiology, Paris, 92*(3-4), 235-239.

Lohith, T. G., Osterweil, E. K., Fujita, M., Jenko, K. J., Bear, M. F., & Innis, R. B. (2013). Is metabotropic glutamate receptor 5 upregulated in prefrontal cortex in fragile X syndrome? *Molecular Autism, 4*(1), 15-2392-4-15. doi:10.1186/2040-2392-4-15 [doi]

Lu, H., Zou, Q., Gu, H., Raichle, M. E., Stein, E. A., & Yang, Y. (2012). Rat brains also have a default mode network. *Proceedings of the National Academy of Sciences of the United States of America, 109*(10), 3979-3984. doi:10.1073/pnas.1200506109 [doi]

Lu, R., Wang, H., Liang, Z., Ku, L., O'donnell, W. T., Li, W., . . . Feng, Y. (2004). The fragile X protein controls microtubule-associated protein 1B translation and microtubule stability in brain neuron development. *Proceedings of the National Academy of Sciences of the United States of America, 101*(42), 15201-15206. doi:10.1073/pnas.0404995101

Ma, Z., Perez, P., Ma, Z., Liu, Y., Hamilton, C., Liang, Z., & Zhang, N. (2016).

Functional atlas of the awake rat brain: A neuroimaging study of rat brain specialization and integration. *Neuroimage,* doi:S1053-8119(16)30315-9 [pii]

Mantini, D., Perrucci, M. G., Del Gratta, C., Romani, G. L., & Corbetta, M. (2007). Electrophysiological signatures of resting state networks in the human brain. *Proceedings of the National Academy of Sciences of the United States of America, 104*(32), 13170-13175. doi:0700668104 [pii]

Martin, B. S., & Huntsman, M. M. (2012). Pathological plasticity in fragile x syndrome. *Neural Plasticity, 2012,* 275630. doi:10.1155/2012/275630

Martinez, M., & Mougan, I. (1998). Fatty acid composition of human brain phospholipids during normal development. *Journal of Neurochemistry, 71*(6), 2528-2533.

Massa, P. T., Wu, C., & Fecenko-Tacka, K. (2004). Dysmyelination and reduced myelin basic protein gene expression by oligodendrocytes of SHP-1-deficient mice. *Journal of Neuroscience Research, 77*(1), 15-25. doi:10.1002/jnr.20155

McBride, S. M., Bell, A. J., & Jongens, T. A. (2012). Behavior in a drosophila model of fragile X. *Results and Problems in Cell Differentiation, 54*, 83-117. doi:10.1007/978-3-642-21649-7_6

McBride, S. M., Choi, C. H., Wang, Y., Liebelt, D., Braunstein, E., Ferreiro, D., . . . Jongens, T. A. (2005). Pharmacological rescue of synaptic plasticity, courtship behavior, and mushroom body defects in a drosophila model of fragile X syndrome. *Neuron, 45*(5), 753-764. doi:S0896-6273(05)00076-0 [pii]

McKenna, M. C., Dienel, G., Sonnewald, U., Waagepetersen, H. S., & Schousboe, A. (2011). Energy metabolism of the brain. In S. Brady, G. Siegel, R. W. Albers & D. Price (Eds.), ***Basic neurochemistry: Principles of molecular, cellular, and medical***

neurobiology (8th ed., pp. 200). Waltham, MA: Academic Press.

McKenna, M. C. (2007). The glutamate-glutamine cycle is not stoichiometric: Fates of glutamate in brain. *Journal of Neuroscience Research, 85*(15), 3347-3358. doi:10.1002/jnr.21444 [doi]

McKenna, M. C., Tildon, J. T., Stevenson, J. H., & Hopkins, I. B. (1994). Energy metabolism in cortical synaptic terminals from weanling and mature rat brain: Evidence for multiple compartments of tricarboxylic acid cycle activity. *Developmental Neuroscience, 16*(5-6), 291-300.

McKinney, M., Coyle, J. T., & Hedreen, J. C. (1983). Topographic analysis of the innervation of the rat neocortex and hippocampus by the basal forebrain cholinergic system. *The Journal of Comparative Neurology, 217*(1), 103-121. doi:10.1002/cne.902170109 [doi]

Miller, L. J., McIntosh, D. N., McGrath, J., Shyu, V., Lampe, M., Taylor, A. K., . . . Hagerman, R. J. (1999). Electrodermal responses to sensory stimuli in individuals with fragile X syndrome: A preliminary report. *American Journal of Medical Genetics, 83*(4), 268-279. doi:10.1002/(SICI)1096-8628(19990402)83:4<268::AID-AJMG7>3.0.CO;2-K [pii]

Moffett, J. R., Ross, B., Arun, P., Madhavarao, C. N., & Namboodiri, A. M. (2007). N-acetylaspartate in the CNS: From neurodiagnostics to neurobiology. *Progress in Neurobiology, 81*(2), 89-131. doi:10.1016/j.pneurobio.2006.12.003

Monyak, R. E., Emerson, D., Schoenfeld, B. P., Zheng, X., Chambers, D. B., Rosenfelt, C., . . . Jongens, T. A. (2016). Insulin signaling misregulation underlies circadian and cognitive deficits in a drosophila fragile X model. *Molecular Psychiatry,*

doi:10.1038/mp.2016.51 [doi]

Mori, S., & Zhang, J. (2006). Principles of diffusion tensor imaging and its applications to basic neuroscience research. *Neuron, 51*(5), 527-539. doi:S0896-6273(06)00634-9 [pii]

Moskalev, A., Chernyagina, E., Tsvetkov, V., Fedintsev, A., Shaposhnikov, M., Krut'ko, V., . . . Kennedy, B. K. (2016). Developing criteria for evaluation of geroprotectors as a key stage toward translation to the clinic. *Aging Cell, 15*(3), 407-415. doi:10.1111/acel.12463 [doi]

Mukherjee, P., Berman, J. I., Chung, S. W., Hess, C. P., & Henry, R. G. (2008). Diffusion tensor MR imaging and fiber tractography: Theoretic underpinnings. *AJNR.American Journal of Neuroradiology, 29*(4), 632-641. doi:10.3174/ajnr.A1051 [doi]

Mukherjee, P., Miller, J. H., Shimony, J. S., Philip, J. V., Nehra, D., Snyder, A. Z., . . . McKinstry, R. C. (2002). Diffusion-tensor MR imaging of gray and white matter development during normal human brain maturation. *AJNR.American Journal of Neuroradiology*, *23*(9), 1445-1456.

Mukonoweshuro, W., Wilkinson, I. D., & Griffiths, P. D. (2001). Proton MR spectroscopy of cortical tubers in adults with tuberous sclerosis complex. *AJNR.American Journal of Neuroradiology, 22*(10), 1920-1925.

Mullins, R. J., Xu, S., Pereira, E. F., Mamczarz, J., Albuquerque, E. X., & Gullapalli, R. P. (2013). Delayed hippocampal effects from a single exposure of prepubertal guinea pigs to sub-lethal dose of chlorpyrifos: A magnetic resonance imaging and spectroscopy study. *Neurotoxicology, 36*, 42-48. doi:10.1016/j.neuro.2013.02.002

[doi]

Musumeci, S. A., Bosco, P., Calabrese, G., Bakker, C., De Sarro, G. B., Elia, M., . . . Oostra, B. A. (2000). Audiogenic seizures susceptibility in transgenic mice with fragile X syndrome. *Epilepsia*, *41*(1), 19-23.

Narayanan, U., Nalavadi, V., Nakamoto, M., Thomas, G., Ceman, S., Bassell, G. J., & Warren, S. T. (2008). S6K1 phosphorylates and regulates fragile X mental retardation protein (FMRP) with the neuronal protein synthesis-dependent mammalian target of rapamycin (mTOR) signaling cascade. *The Journal of Biological Chemistry*, *283*(27), 18478-18482. doi:10.1074/jbc.C800055200

Nasrallah, F. A., To, X. V., Chen, D. Y., Routtenberg, A., & Chuang, K. H. (2016). Functional connectivity MRI tracks memory networks after maze learning in rodents. *Neuroimage, 127*, 196-202. doi:10.1016/j.neuroimage.2015.08.013 [doi]

Nawaz, S., Kippert, A., Saab, A. S., Werner, H. B., Lang, T., Nave, K. A., & Simons, M. (2009). Phosphatidylinositol 4,5-bisphosphate-dependent interaction of myelin basic protein with the plasma membrane in oligodendroglial cells and its rapid perturbation by elevated calcium. *The Journal of Neuroscience : The Official Journal of the Society for Neuroscience, 29*(15), 4794-4807. doi:10.1523/JNEUROSCI.3955-08.2009

Nedergaard, M., Ransom, B., & Goldman, S. A. (2003). New roles for astrocytes: Redefining the functional architecture of the brain. *Trends in Neurosciences*, *26*(10), 523-530. doi:S0166-2236(03)00266-2 [pii]

Neil, J., Miller, J., Mukherjee, P., & Huppi, P. S. (2002). Diffusion tensor imaging of normal and injured developing human brain - a technical review. *NMR in*

Biomedicine, 15(7-8), 543-552. doi:10.1002/nbm.784 [doi]

Nicholls, D. G. (2009). Mitochondrial calcium function and dysfunction in the central nervous system. *Biochimica Et Biophysica Acta, 1787*(11), 1416-1424. doi:10.1016/j.bbabio.2009.03.010 [doi]

Nimchinsky, E. A., Oberlander, A. M., & Svoboda, K. (2001). Abnormal development of dendritic spines in FMR1 knock-out mice. *The Journal of Neuroscience : The Official Journal of the Society for Neuroscience, 21*(14), 5139-5146.

Nosyreva, E. D., & Huber, K. M. (2006). Metabotropic receptor-dependent long-term depression persists in the absence of protein synthesis in the mouse model of fragile X syndrome. *Journal of Neurophysiology, 95*(5), 3291-3295. doi:01316.2005 [pii]

Ogawa, S., Lee, T. M., Kay, A. R., & Tank, D. W. (1990). Brain magnetic resonance imaging with contrast dependent on blood oxygenation. *Proceedings of the National Academy of Sciences of the United States of America, 87*(24), 9868-9872.

Oliet, S. H., Malenka, R. C., & Nicoll, R. A. (1997). Two distinct forms of long-term depression coexist in CA1 hippocampal pyramidal cells. *Neuron, 18*(6), 969-982. doi:S0896-6273(00)80336-0 [pii]

Oostra, B. A., Jacky, P. B., Brown, W. T., & Rousseau, F. (1993). Guidelines for the diagnosis of fragile X syndrome. national fragile X foundation. *Journal of Medical Genetics, 30*(5), 410-413.

Ou, X., Sun, S. W., Liang, H. F., Song, S. K., & Gochberg, D. F. (2009). The MT pool size ratio and the DTI radial diffusivity may reflect the myelination in shiverer and control mice. *NMR in Biomedicine, 22*(5), 480-487. doi:10.1002/nbm.1358 [doi]

Pacey, L. K., Xuan, I. C., Guan, S., Sussman, D., Henkelman, R. M., Chen, Y., . . .

Hampson, D. R. (2013). Delayed myelination in a mouse model of fragile X syndrome. *Human Molecular Genetics, 22*(19), 3920-3930. doi:10.1093/hmg/ddt246; 10.1093/hmg/ddt246

Padmashri, R., Reiner, B. C., Suresh, A., Spartz, E., & Dunaevsky, A. (2013). Altered structural and functional synaptic plasticity with motor skill learning in a mouse model of fragile X syndrome. *The Journal of Neuroscience : The Official Journal of the Society for Neuroscience, 33*(50), 19715-19723. doi:10.1523/JNEUROSCI.2514-13.2013 [doi]

Paluszkiewicz, S. M., Martin, B. S., & Huntsman, M. M. (2011). Fragile X syndrome: The GABAergic system and circuit dysfunction. *Developmental Neuroscience, 33*(5), 349-364. doi:10.1159/000329420

Pan, F., Aldridge, G. M., Greenough, W. T., & Gan, W. B. (2010). Dendritic spine instability and insensitivity to modulation by sensory experience in a mouse model of fragile X syndrome. *Proceedings of the National Academy of Sciences of the United States of America, 107*(41), 17768-17773. doi:10.1073/pnas.1012496107

Pan, L., Woodruff, E.,3rd, Liang, P., & Broadie, K. (2008). Mechanistic relationships between drosophila fragile X mental retardation protein and metabotropic glutamate receptor A signaling. *Molecular and Cellular Neurosciences, 37*(4), 747-760. doi:10.1016/j.mcn.2008.01.003

Pan, L., Zhang, Y. Q., Woodruff, E., & Broadie, K. (2004). The drosophila fragile X gene negatively regulates neuronal elaboration and synaptic differentiation. *Current Biology : CB, 14*(20), 1863-1870. doi:10.1016/j.cub.2004.09.085

Pan, W. J., Billings, J. C., Grooms, J. K., Shakil, S., & Keilholz, S. D. (2015).

Considerations for resting state functional MRI and functional connectivity studies in rodents. *Frontiers in Neuroscience, 9*, 269. doi:10.3389/fnins.2015.00269 [doi]

Paradee, W., Melikian, H. E., Rasmussen, D. L., Kenneson, A., Conn, P. J., & Warren, S. T. (1999). Fragile X mouse: Strain effects of knockout phenotype and evidence suggesting deficient amygdala function. *Neuroscience, 94*(1), 185-192. doi:S0306-4522(99)00285-7 [pii]

Parent, M. B., & Baxter, M. G. (2004). Septohippocampal acetylcholine: Involved in but not necessary for learning and memory? *Learning & Memory (Cold Spring Harbor, N.Y.), 11*(1), 9-20. doi:10.1101/lm.69104 [doi]

Paribello, C., Tao, L., Folino, A., Berry-Kravis, E., Tranfaglia, M., Ethell, I. M., & Ethell, D. W. (2010). Open-label add-on treatment trial of minocycline in fragile X syndrome. *BMC Neurology, 10*, 91. doi:10.1186/1471-2377-10-91

Paus, T., Collins, D. L., Evans, A. C., Leonard, G., Pike, B., & Zijdenbos, A. (2001). Maturation of white matter in the human brain: A review of magnetic resonance studies. *Brain Research Bulletin, 54*(3), 255-266. doi:S0361-9230(00)00434-2 [pii]

Paydar, A., Fieremans, E., Nwankwo, J. I., Lazar, M., Sheth, H. D., Adisetiyo, V., . . . Milla, S. S. (2014). Diffusional kurtosis imaging of the developing brain. *AJNR.American Journal of Neuroradiology, 35*(4), 808-814. doi:10.3174/ajnr.A3764 [doi]

Peltier, J., O'Neill, A., & Schaffer, D. V. (2007). PI3K/Akt and CREB regulate adult neural hippocampal progenitor proliferation and differentiation. *Developmental Neurobiology, 67*(10), 1348-1361. doi:10.1002/dneu.20506 [doi]

Peters, S. K., Dunlop, K., & Downar, J. (2016). Cortico-striatal-thalamic loop circuits of

the salience network: A central pathway in psychiatric disease and treatment. *Frontiers in Systems Neuroscience, 10*, 104. doi:10.3389/fnsys.2016.00104 [doi]

Pfeiffer, B. E., & Huber, K. M. (2009). The state of synapses in fragile X syndrome. *The Neuroscientist : A Review Journal Bringing Neurobiology, Neurology and Psychiatry, 15*(5), 549-567. doi:10.1177/1073858409333075 [doi]

Pop, A. S., Levenga, J., de Esch, C. E., Buijsen, R. A., Nieuwenhuizen, I. M., Li, T., . . . Willemsen, R. (2014). Rescue of dendritic spine phenotype in Fmr1 KO mice with the mGluR5 antagonist AFQ056/Mavoglurant. *Psychopharmacology, 231*(6), 1227-1235. doi:10.1007/s00213-012-2947-y [doi]

Provencher, S. W. (2001). Automatic quantitation of localized in vivo 1H spectra with LCModel. *NMR in Biomedicine, 14*(4), 260-264.

Qin, M., Huang, T., Kader, M., Krych, L., Xia, Z., Burlin, T., . . . Smith, C. B. (2015). R-baclofen reverses a social behavior deficit and elevated protein synthesis in a mouse model of fragile X syndrome. *The International Journal of Neuropsychopharmacology, 18*(9), 10.1093/ijnp/pyv034. doi:10.1093/ijnp/pyv034 [doi]

Qin, M., Kang, J., Burlin, T. V., Jiang, C., & Smith, C. B. (2005). Postadolescent changes in regional cerebral protein synthesis: An in vivo study in the FMR1 null mouse. *The Journal of Neuroscience : The Official Journal of the Society for Neuroscience, 25*(20), 5087-5095. doi:10.1523/JNEUROSCI.0093-05.2005

Qin, M., Kang, J., & Smith, C. B. (2002). Increased rates of cerebral glucose metabolism in a mouse model of fragile X mental retardation. *Proceedings of the National Academy of Sciences of the United States of America, 99*(24), 15758-15763.

doi:10.1073/pnas.242377399

Qin, M., Schmidt, K. C., Zametkin, A. J., Bishu, S., Horowitz, L. M., Burlin, T. V., . . . Smith, C. B. (2013). Altered cerebral protein synthesis in fragile X syndrome: Studies in human subjects and knockout mice. *Journal of Cerebral Blood Flow and Metabolism : Official Journal of the International Society of Cerebral Blood Flow and Metabolism, 33*(4), 499-507. doi:10.1038/jcbfm.2012.205 [doi]

Qin, M., Xia, Z., Huang, T., & Smith, C. B. (2011). Effects of chronic immobilization stress on anxiety-like behavior and basolateral amygdala morphology in Fmr1 knockout mice. *Neuroscience, 194*, 282-290. doi:10.1016/j.neuroscience.2011.06.047

Qiu, D., Tan, L. H., Zhou, K., & Khong, P. L. (2008). Diffusion tensor imaging of normal white matter maturation from late childhood to young adulthood: Voxel-wise evaluation of mean diffusivity, fractional anisotropy, radial and axial diffusivities, and correlation with reading development. *Neuroimage, 41*(2), 223-232. doi:10.1016/j.neuroimage.2008.02.023; 10.1016/j.neuroimage.2008.02.023

Qiu, G., Chen, S., Guo, J., Wu, J., & Yi, Y. H. (2016). Alpha-asarone improves striatal cholinergic function and locomotor hyperactivity in Fmr1 knockout mice. *Behavioural Brain Research, 312*, 212-218. doi:10.1016/j.bbr.2016.06.024 [doi]

Quarles, R. H., Macklin, W. B., & Morell, P. (2012). Myelin formation, structure and biochemistry. *Basic neurochemistry: Molecular, cellular and medical aspects* (8th ed., pp. 51) Academic Press, Inc.

Raichle, M. E., MacLeod, A. M., Snyder, A. Z., Powers, W. J., Gusnard, D. A., & Shulman, G. L. (2001). A default mode of brain function. *Proceedings of the*

National Academy of Sciences of the United States of America, 98(2), 676-682. doi:10.1073/pnas.98.2.676 [doi]

Reiss, A. L., Lee, J., & Freund, L. (1994). Neuroanatomy of fragile X syndrome: The temporal lobe. *Neurology, 44*(7), 1317-1324.

Ronesi, J. A., Collins, K. A., Hays, S. A., Tsai, N. P., Guo, W., Birnbaum, S. G., . . . Huber, K. M. (2012). Disrupted homer scaffolds mediate abnormal mGluR5 function in a mouse model of fragile X syndrome. *Nature Neuroscience, 15*(3), 431-40, S1. doi:10.1038/nn.3033; 10.1038/nn.3033

Ronesi, J. A., & Huber, K. M. (2008). Homer interactions are necessary for metabotropic glutamate receptor-induced long-term depression and translational activation. *The Journal of Neuroscience : The Official Journal of the Society for Neuroscience, 28*(2), 543-547. doi:10.1523/JNEUROSCI.5019-07.2008

Rotschafer, S., & Razak, K. (2013). Altered auditory processing in a mouse model of fragile X syndrome. *Brain Research, 1506*, 12-24. doi:10.1016/j.brainres.2013.02.038 [doi]

Rubin, Y., LaPlaca, M. C., Smith, D. H., Thibault, L. E., & Lenkinski, R. E. (1995). The effect of N-acetylaspartate on the intracellular free calcium concentration in NTera2-neurons. *Neuroscience Letters, 198*(3), 209-212. doi:030439409512014U [pii]

Rudelli, R. D., Brown, W. T., Wisniewski, K., Jenkins, E. C., Laure-Kamionowska, M., Connell, F., & Wisniewski, H. M. (1985). Adult fragile X syndrome. clinico-neuropathologic findings. *Acta Neuropathologica, 67*(3-4), 289-295.

Saher, G., Brugger, B., Lappe-Siefke, C., Mobius, W., Tozawa, R., Wehr, M. C., . . . Nave, K. A. (2005). High cholesterol level is essential for myelin membrane growth.

Nature Neuroscience, 8(4), 468-475. doi:nn1426 [pii]

Sanchez, S., Jimenez, C., Carrera, A. C., Diaz-Nido, J., Avila, J., & Wandosell, F. (2004). A cAMP-activated pathway, including PKA and PI3K, regulates neuronal differentiation. *Neurochemistry International, 44*(4), 231-242. doi:S0197018603001505 [pii]

Sansone, S. M., Widaman, K. F., Hall, S. S., Reiss, A. L., Lightbody, A., Kaufmann, W. E., . . . Hessl, D. (2012). Psychometric study of the aberrant behavior checklist in fragile X syndrome and implications for targeted treatment. *Journal of Autism and Developmental Disorders, 42*(7), 1377-1392. doi:10.1007/s10803-011-1370-2 [doi]

Savaskan, N. E., Weinmann, O., Heimrich, B., & Eyupoglu, I. Y. (2009). High resolution neurochemical gold staining method for myelin in peripheral and central nervous system at the light- and electron-microscopic level. *Cell and Tissue Research, 337*(2), 213-221. doi:10.1007/s00441-009-0815-9 [doi]

Sawicka, K., Pyronneau, A., Chao, M., Bennett, M. V., & Zukin, R. S. (2016). Elevated ERK/p90 ribosomal S6 kinase activity underlies audiogenic seizure susceptibility in fragile X mice. *Proceedings of the National Academy of Sciences of the United States of America, 113*(41), E6290-E6297. doi:1610812113 [pii]

Schmierer, K., Scaravilli, F., Altmann, D. R., Barker, G. J., & Miller, D. H. (2004). Magnetization transfer ratio and myelin in postmortem multiple sclerosis brain. *Annals of Neurology, 56*(3), 407-415. doi:10.1002/ana.20202 [doi]

Schmierer, K., Wheeler-Kingshott, C. A., Tozer, D. J., Boulby, P. A., Parkes, H. G., Yousry, T. A., . . . Miller, D. H. (2008). Quantitative magnetic resonance of postmortem multiple sclerosis brain before and after fixation. *Magnetic Resonance in*

Medicine, 59(2), 268-277. doi:10.1002/mrm.21487 [doi]

Schmued, L., Bowyer, J., Cozart, M., Heard, D., Binienda, Z., & Paule, M. (2008). Introducing black-gold II, a highly soluble gold phosphate complex with several unique advantages for the histochemical localization of myelin. *Brain Research, 1229*, 210-217. doi:10.1016/j.brainres.2008.06.129 [doi]

Schousboe, A., Westergaard, N., Waagepetersen, H. S., Larsson, O. M., Bakken, I. J., & Sonnewald, U. (1997). Trafficking between glia and neurons of TCA cycle intermediates and related metabolites. *Glia, 21*(1), 99-105. doi:10.1002/(SICI)1098-1136(199709)21:1<99::AID-GLIA11>3.0.CO;2-W [pii]

Scoville, W. B., & Milner, B. (2000). Loss of recent memory after bilateral hippocampal lesions. 1957. *The Journal of Neuropsychiatry and Clinical Neurosciences, 12*(1), 103-113. doi:10.1176/jnp.12.1.103 [doi]

Seeley, W. W., Menon, V., Schatzberg, A. F., Keller, J., Glover, G. H., Kenna, H., . . . Greicius, M. D. (2007). Dissociable intrinsic connectivity networks for salience processing and executive control. *The Journal of Neuroscience : The Official Journal of the Society for Neuroscience, 27*(9), 2349-2356. doi:27/9/2349 [pii]

Semple, B. D., Blomgren, K., Gimlin, K., Ferriero, D. M., & Noble-Haeusslein, L. J. (2013). Brain development in rodents and humans: Identifying benchmarks of maturation and vulnerability to injury across species. *Progress in Neurobiology, 106-107*, 1-16. doi:10.1016/j.pneurobio.2013.04.001 [doi]

Sforazzini, F., Schwarz, A. J., Galbusera, A., Bifone, A., & Gozzi, A. (2014). Distributed BOLD and CBV-weighted resting-state networks in the mouse brain. *Neuroimage, 87*, 403-415. doi:10.1016/j.neuroimage.2013.09.050 [doi]

Shah, D., Deleye, S., Verhoye, M., Staelens, S., & Van der Linden, A. (2016). Resting-state functional MRI and [18F]-FDG PET demonstrate differences in neuronal activity between commonly used mouse strains. *Neuroimage, 125*, 571-577. doi:10.1016/j.neuroimage.2015.10.073 [doi]

Sharma, A., Hoeffer, C. A., Takayasu, Y., Miyawaki, T., McBride, S. M., Klann, E., & Zukin, R. S. (2010). Dysregulation of mTOR signaling in fragile X syndrome. *The Journal of Neuroscience : The Official Journal of the Society for Neuroscience, 30*(2), 694-702. doi:10.1523/JNEUROSCI.3696-09.2010

Shears, S. B. (1989). Metabolism of the inositol phosphates produced upon receptor activation. *The Biochemical Journal, 260*(2), 313-324.

Shen, M. D., Li, D. D., Keown, C. L., Lee, A., Johnson, R. T., Angkustsiri, K., . . . Nordahl, C. W. (2016). Functional connectivity of the amygdala is disrupted in preschool-aged children with autism spectrum disorder. *Journal of the American Academy of Child and Adolescent Psychiatry, 55*(9), 817-824. doi:10.1016/j.jaac.2016.05.020 [doi]

Shepherd, T. M., Thelwall, P. E., Stanisz, G. J., & Blackband, S. J. (2009). Aldehyde fixative solutions alter the water relaxation and diffusion properties of nervous tissue. *Magnetic Resonance in Medicine, 62*(1), 26-34. doi:10.1002/mrm.21977 [doi]

Shi, D., Xu, S., Waddell, J., Scafidi, S., Roys, S., Gullapalli, R. P., & McKenna, M. C. (2012). Longitudinal in vivo developmental changes of metabolites in the hippocampus of Fmr1 knockout mice. *Journal of Neurochemistry, 123*, 971-981. doi:10.1111/jnc.12048; 10.1111/jnc.12048

Shinoe, T., Matsui, M., Taketo, M. M., & Manabe, T. (2005). Modulation of synaptic

plasticity by physiological activation of M1 muscarinic acetylcholine receptors in the mouse hippocampus. *The Journal of Neuroscience : The Official Journal of the Society for Neuroscience, 25*(48), 11194-11200. doi:10.1523/JNEUROSCI.2338-05.2005

Sidhu, H., Dansie, L. E., Hickmott, P. W., Ethell, D. W., & Ethell, I. M. (2014). Genetic removal of matrix metalloproteinase 9 rescues the symptoms of fragile x syndrome in a mouse model. *The Journal of Neuroscience : The Official Journal of the Society for Neuroscience, 34*(30), 9867-9879. doi:10.1523/JNEUROSCI.1162-14.2014 [doi]

Sidorov, M. S., Auerbach, B. D., & Bear, M. F. (2013). Fragile X mental retardation protein and synaptic plasticity. *Molecular Brain, 6*, 15-6606-6-15. doi:10.1186/1756-6606-6-15 [doi]

Sierakowiak, A., Monnot, C., Aski, S. N., Uppman, M., Li, T. Q., Damberg, P., & Brene, S. (2015). Default mode network, motor network, dorsal and ventral basal ganglia networks in the rat brain: Comparison to human networks using resting state-fMRI. *PloS One, 10*(3), e0120345. doi:10.1371/journal.pone.0120345 [doi]

Smith, L. E., Barker, E. T., Seltzer, M. M., Abbeduto, L., & Greenberg, J. S. (2012). Behavioral phenotype of fragile X syndrome in adolescence and adulthood. *American Journal on Intellectual and Developmental Disabilities, 117*(1), 1-17. doi:10.1352/1944-7558-117.1.1

Song, S. K., Sun, S. W., Ramsbottom, M. J., Chang, C., Russell, J., & Cross, A. H. (2002). Dysmyelination revealed through MRI as increased radial (but unchanged axial) diffusion of water. *Neuroimage, 17*(3), 1429-1436.

Sonnewald, U., & Kondziella, D. (2003). Neuronal glial interaction in different

neurological diseases studied by ex vivo 13C NMR spectroscopy. *NMR in Biomedicine, 16*(6-7), 424-429. doi:10.1002/nbm.837 [doi]

Sours, C., George, E. O., Zhuo, J., Roys, S., & Gullapalli, R. P. (2015). Hyper-connectivity of the thalamus during early stages following mild traumatic brain injury. *Brain Imaging and Behavior, 9*(3), 550-563. doi:10.1007/s11682-015-9424-2 [doi]

Spencer, C. M., Alekseyenko, O., Serysheva, E., Yuva-Paylor, L. A., & Paylor, R. (2005). Altered anxiety-related and social behaviors in the Fmr1 knockout mouse model of fragile X syndrome. *Genes, Brain, and Behavior, 4*(7), 420-430. doi:GBB123 [pii]

Sridharan, D., Levitin, D. J., & Menon, V. (2008). A critical role for the right fronto-insular cortex in switching between central-executive and default-mode networks. *Proceedings of the National Academy of Sciences of the United States of America, 105*(34), 12569-12574. doi:10.1073/pnas.0800005105 [doi]

Stafford, J. M., Jarrett, B. R., Miranda-Dominguez, O., Mills, B. D., Cain, N., Mihalas, S., . . . Fair, D. A. (2014). Large-scale topology and the default mode network in the mouse connectome. *Proceedings of the National Academy of Sciences of the United States of America, 111*(52), 18745-18750. doi:10.1073/pnas.1404346111 [doi]

Stanisz, G. J., Kecojevic, A., Bronskill, M. J., & Henkelman, R. M. (1999). Characterizing white matter with magnetization transfer and T(2). *Magnetic Resonance in Medicine : Official Journal of the Society of Magnetic Resonance in Medicine / Society of Magnetic Resonance in Medicine, 42*(6), 1128-1136. doi:10.1002/(SICI)1522-2594(199912)42:6<1128::AID-MRM18>3.0.CO;2-9 [pii]

Steven, A. J., Zhuo, J., & Melhem, E. R. (2014). Diffusion kurtosis imaging: An emerging technique for evaluating the microstructural environment of the brain. *AJR.American Journal of Roentgenology, 202*(1), W26-33. doi:10.2214/AJR.13.11365 [doi]

Sun, S. W., Neil, J. J., & Song, S. K. (2003). Relative indices of water diffusion anisotropy are equivalent in live and formalin-fixed mouse brains. *Magnetic Resonance in Medicine, 50*(4), 743-748. doi:10.1002/mrm.10605 [doi]

Sun, S. W., Song, S. K., Harms, M. P., Lin, S. J., Holtzman, D. M., Merchant, K. M., & Kotyk, J. J. (2005). Detection of age-dependent brain injury in a mouse model of brain amyloidosis associated with alzheimer's disease using magnetic resonance diffusion tensor imaging. *Experimental Neurology, 191*(1), 77-85. doi:S0014-4886(04)00374-7 [pii]

Tessier, C. R., & Broadie, K. (2012). Molecular and genetic analysis of the drosophila model of fragile X syndrome. *Results and Problems in Cell Differentiation, 54*, 119-156. doi:10.1007/978-3-642-21649-7_7

Thiessen, J. D., Zhang, Y., Zhang, H., Wang, L., Buist, R., Del Bigio, M. R., . . . Martin, M. (2013). Quantitative MRI and ultrastructural examination of the cuprizone mouse model of demyelination. *NMR in Biomedicine, 26*(11), 1562-1581. doi:10.1002/nbm.2992 [doi]

Thomas, A. M., Bui, N., Perkins, J. R., Yuva-Paylor, L. A., & Paylor, R. (2012). Group I metabotropic glutamate receptor antagonists alter select behaviors in a mouse model for fragile X syndrome. *Psychopharmacology, 219*(1), 47-58. doi:10.1007/s00213-011-2375-4

Thompson, G. J., Pan, W. J., & Keilholz, S. D. (2015). Different dynamic resting state fMRI patterns are linked to different frequencies of neural activity. *Journal of Neurophysiology, 114*(1), 114-124. doi:10.1152/jn.00235.2015 [doi]

Till, S. M., Asiminas, A., Jackson, A. D., Katsanevaki, D., Barnes, S. A., Osterweil, E. K., . . . Kind, P. C. (2015). Conserved hippocampal cellular pathophysiology but distinct behavioural deficits in a new rat model of FXS. *Human Molecular Genetics, 24*(21), 5977-5984. doi:10.1093/hmg/ddv299 [doi]

Tkac, I., Rao, R., Georgieff, M. K., & Gruetter, R. (2003). Developmental and regional changes in the neurochemical profile of the rat brain determined by in vivo 1H NMR spectroscopy. *Magnetic Resonance in Medicine, 50*(1), 24-32. doi:10.1002/mrm.10497 [doi]

Torgerson, C. M., Irimia, A., Leow, A. D., Bartzokis, G., Moody, T. D., Jennings, R. G., . . . Altshuler, L. L. (2013). DTI tractography and white matter fiber tract characteristics in euthymic bipolar I patients and healthy control subjects. *Brain Imaging and Behavior, 7*(2), 129-139. doi:10.1007/s11682-012-9202-3 [doi]

Tsurugizawa, T., Ciobanu, L., & Le Bihan, D. (2013). Water diffusion in brain cortex closely tracks underlying neuronal activity. *Proceedings of the National Academy of Sciences of the United States of America, 110*(28), 11636-11641. doi:10.1073/pnas.1303178110 [doi]

Urenjak, J., Williams, S. R., Gadian, D. G., & Noble, M. (1992). Specific expression of N-acetylaspartate in neurons, oligodendrocyte-type-2 astrocyte progenitors, and immature oligodendrocytes in vitro. *Journal of Neurochemistry, 59*(1), 55-61.

Usenius, J. P., Vainio, P., Hernesniemi, J., & Kauppinen, R. A. (1994). Choline-

containing compounds in human astrocytomas studied by 1H NMR spectroscopy in vivo and in vitro. *Journal of Neurochemistry, 63*(4), 1538-1543.

Utari, A., Chonchaiya, W., Rivera, S. M., Schneider, A., Hagerman, R. J., Faradz, S. M., . . . Nguyen, D. V. (2010). Side effects of minocycline treatment in patients with fragile X syndrome and exploration of outcome measures. *American Journal on Intellectual and Developmental Disabilities, 115*(5), 433-443. doi:10.1352/1944-7558-115.5.433

van den Heuvel, M. P., & Hulshoff Pol, H. E. (2010). Exploring the brain network: A review on resting-state fMRI functional connectivity. *European Neuropsychopharmacology : The Journal of the European College of Neuropsychopharmacology, 20*(8), 519-534. doi:10.1016/j.euroneuro.2010.03.008 [doi]

Vanderklish, P. W., & Edelman, G. M. (2002). Dendritic spines elongate after stimulation of group 1 metabotropic glutamate receptors in cultured hippocampal neurons. *Proceedings of the National Academy of Sciences of the United States of America, 99*(3), 1639-1644. doi:10.1073/pnas.032681099 [doi]

Vasung, L., Huang, H., Jovanov-Milosevic, N., Pletikos, M., Mori, S., & Kostovic, I. (2010). Development of axonal pathways in the human fetal fronto-limbic brain: Histochemical characterization and diffusion tensor imaging. *Journal of Anatomy, 217*(4), 400-417. doi:10.1111/j.1469-7580.2010.01260.x [doi]

Vekeman, F., Gauthier-Loiselle, M., Faust, E., Lefebvre, P., Lahoz, R., Duh, M. S., & Sacco, P. (2015). Patient and caregiver burden associated with fragile X syndrome in the united states. *American Journal on Intellectual and Developmental Disabilities,*

120(5), 444-459. doi:10.1352/1944-7558-120.5.444 [doi]

Verheij, C., Bakker, C. E., de Graaff, E., Keulemans, J., Willemsen, R., Verkerk, A. J., . . . Oostra, B. A. (1993). Characterization and localization of the FMR-1 gene product associated with fragile X syndrome. *Nature, 363*(6431), 722-724. doi:10.1038/363722a0 [doi]

Verkerk, A. J., Pieretti, M., Sutcliffe, J. S., Fu, Y. H., Kuhl, D. P., Pizzuti, A., . . . Zhang, F. P. (1991). Identification of a gene (FMR-1) containing a CGG repeat coincident with a breakpoint cluster region exhibiting length variation in fragile X syndrome. *Cell, 65*(5), 905-914.

Villalon-Reina, J., Jahanshad, N., Beaton, E., Toga, A. W., Thompson, P. M., & Simon, T. J. (2013). White matter microstructural abnormalities in girls with chromosome 22q11.2 deletion syndrome, fragile X or turner syndrome as evidenced by diffusion tensor imaging. *Neuroimage, 81*, 441-454. doi:10.1016/j.neuroimage.2013.04.028 [doi]

Viollet, B., Guigas, B., Sanz Garcia, N., Leclerc, J., Foretz, M., & Andreelli, F. (2012). Cellular and molecular mechanisms of metformin: An overview. *Clinical Science (London, England : 1979), 122*(6), 253-270. doi:10.1042/CS20110386 [doi]

Volk, L. J., Pfeiffer, B. E., Gibson, J. R., & Huber, K. M. (2007). Multiple gq-coupled receptors converge on a common protein synthesis-dependent long-term depression that is affected in fragile X syndrome mental retardation. *The Journal of Neuroscience : The Official Journal of the Society for Neuroscience, 27*(43), 11624-11634. doi:10.1523/JNEUROSCI.2266-07.2007

Waagepetersen, H. S., Sonnewald, U., & Schousboe, A. (2003). Compartmentation of

glutamine, glutamate, and GABA metabolism in neurons and astrocytes: Functional implications. *The Neuroscientist : A Review Journal Bringing Neurobiology, Neurology and Psychiatry, 9*(5), 398-403. doi:10.1177/1073858403254006 [doi]

Wan, L., Dockendorff, T. C., Jongens, T. A., & Dreyfuss, G. (2000). Characterization of dFMR1, a drosophila melanogaster homolog of the fragile X mental retardation protein. *Molecular and Cellular Biology, 20*(22), 8536-8547.

Wang, C., Ji, F., Hong, Z., Poh, J. S., Krishnan, R., Lee, J., . . . Zhou, J. (2016). Disrupted salience network functional connectivity and white-matter microstructure in persons at risk for psychosis: Findings from the LYRIKS study. *Psychological Medicine, 46*(13), 2771-2783. doi:10.1017/S0033291716001410 [doi]

Wang, H., Ku, L., Osterhout, D. J., Li, W., Ahmadian, A., Liang, Z., & Feng, Y. (2004). Developmentally-programmed FMRP expression in oligodendrocytes: A potential role of FMRP in regulating translation in oligodendroglia progenitors. *Human Molecular Genetics, 13*(1), 79-89. doi:10.1093/hmg/ddh009

Wang, T., Bray, S. M., & Warren, S. T. (2012). New perspectives on the biology of fragile X syndrome. *Current Opinion in Genetics & Development, 22*(3), 256-263. doi:10.1016/j.gde.2012.02.002

Wang, X., Mu, Y., Sun, M., & Han, J. (2017). Bidirectional regulation of fragile X mental retardation protein phosphorylation controls rhodopsin homoeostasis. *Journal of Molecular Cell Biology, 9*(2), 104-116. doi:10.1093/jmcb/mjw041 [doi]

Warren, K. E., Frank, J. A., Black, J. L., Hill, R. S., Duyn, J. H., Aikin, A. A., . . . Balis, F. M. (2000). Proton magnetic resonance spectroscopic imaging in children with recurrent primary brain tumors. *Journal of Clinical Oncology : Official Journal of*

the American Society of Clinical Oncology, 18(5), 1020-1026. doi:10.1200/JCO.2000.18.5.1020 [doi]

Watson, C., Hoeft, F., Garrett, A. S., Hall, S. S., & Reiss, A. L. (2008). Aberrant brain activation during gaze processing in boys with fragile X syndrome. *Archives of General Psychiatry, 65*(11), 1315-1323. doi:10.1001/archpsyc.65.11.1315

Weiler, I. J., & Greenough, W. T. (1993). Metabotropic glutamate receptors trigger postsynaptic protein synthesis. *Proceedings of the National Academy of Sciences of the United States of America, 90*(15), 7168-7171.

Weiler, I. J., & Greenough, W. T. (1999). Synaptic synthesis of the fragile X protein: Possible involvement in synapse maturation and elimination. *American Journal of Medical Genetics, 83*(4), 248-252.

Weiler, I. J., Irwin, S. A., Klintsova, A. Y., Spencer, C. M., Brazelton, A. D., Miyashiro, K., . . . Greenough, W. T. (1997). Fragile X mental retardation protein is translated near synapses in response to neurotransmitter activation. *Proceedings of the National Academy of Sciences of the United States of America, 94*(10), 5395-5400.

Wilson, B. M., & Cox, C. L. (2007). Absence of metabotropic glutamate receptor-mediated plasticity in the neocortex of fragile X mice. *Proceedings of the National Academy of Sciences of the United States of America, 104*(7), 2454-2459. doi:10.1073/pnas.0610875104

Wolff, S. D., & Balaban, R. S. (1989). Magnetization transfer contrast (MTC) and tissue water proton relaxation in vivo. *Magnetic Resonance in Medicine : Official Journal of the Society of Magnetic Resonance in Medicine / Society of Magnetic Resonance in Medicine, 10*(1), 135-144.

Wozniak, J. R., & Lim, K. O. (2006). Advances in white matter imaging: A review of in vivo magnetic resonance methodologies and their applicability to the study of development and aging. *Neuroscience and Biobehavioral Reviews, 30*(6), 762-774. doi:S0149-7634(06)00047-9 [pii]

Wu, Z. Y., & Xu, T. L. (2003). Taurine-evoked chloride current and its potentiation by intracellular Ca2+ in immature rat hippocampal CA1 neurons. *Amino Acids, 24*(1-2), 155-161. doi:10.1007/s00726-002-0314-8 [doi]

Wylie, K. P., Rojas, D. C., Ross, R. G., Hunter, S. K., Maharajh, K., Cornier, M. A., & Tregellas, J. R. (2014). Reduced brain resting-state network specificity in infants compared with adults. *Neuropsychiatric Disease and Treatment, 10,* 1349-1359. doi:10.2147/NDT.S63773 [doi]

Xie, F., Zhang, J. C., Fu, H., & Chen, J. (2013). Age-related decline of myelin proteins is highly correlated with activation of astrocytes and microglia in the rat CNS. *International Journal of Molecular Medicine, 32*(5), 1021-1028. doi:10.3892/ijmm.2013.1486 [doi]

Xu, P., Tan, H., Duong, D., Yang, Y., Kupsco, J., Moberg, K., . . . Peng, J. (2012). Stable isotope labeling with amino acids in drosophila for quantifying proteins and modifications. *Journal of Proteome Research,* doi:10.1021/pr300613c

Xu, S., Ji, Y., Chen, X., Yang, Y., Gullapalli, R. P., & Masri, R. (2013). In vivo high-resolution localized (1) H MR spectroscopy in the awake rat brain at 7 T. *Magnetic Resonance in Medicine, 69*(4), 937-943. doi:10.1002/mrm.24321 [doi]

Xu, S., Zhuo, J., Racz, J., Shi, D., Roys, S., Fiskum, G., & Gullapalli, R. (2011). Early microstructural and metabolic changes following controlled cortical impact injury in

rat: A magnetic resonance imaging and spectroscopy study. *Journal of Neurotrauma, 28*(10), 2091-2102. doi:10.1089/neu.2010.1739 [doi]

Yan, Q. J., Rammal, M., Tranfaglia, M., & Bauchwitz, R. P. (2005). Suppression of two major fragile X syndrome mouse model phenotypes by the mGluR5 antagonist MPEP. *Neuropharmacology, 49*(7), 1053-1066. doi:10.1016/j.neuropharm.2005.06.004

Yang, Q., Feng, B., Zhang, K., Guo, Y. Y., Liu, S. B., Wu, Y. M., . . . Zhao, M. G. (2012). Excessive astrocyte-derived neurotrophin-3 contributes to the abnormal neuronal dendritic development in a mouse model of fragile X syndrome. *PLoS Genetics, 8*(12), e1003172. doi:10.1371/journal.pgen.1003172 [doi]

Yao, F. S., Caserta, M. T., & Wyrwicz, A. M. (1999). In vitro proton and phosphorus NMR spectroscopic analysis of murine (C57Bl/6J) brain development. *NMR in Biomedicine, 12*(7), 463-470.

Yi, X., Cai, Y., & Li, W. (2015). Isoflurane damages the developing brain of mice and induces subsequent learning and memory deficits through FASL-FAS signaling. *BioMed Research International, 2015*, 315872. doi:10.1155/2015/315872 [doi]

Yrigollen, C. M., Martorell, L., Durbin-Johnson, B., Naudo, M., Genoves, J., Murgia, A., . . . Tassone, F. (2014). AGG interruptions and maternal age affect FMR1 CGG repeat allele stability during transmission. *Journal of Neurodevelopmental Disorders, 6*(1), 24-1955-6-24. Epub 2014 Jul 30. doi:10.1186/1866-1955-6-24 [doi]

Yudkoff, M. (1999). Diseases of amino acid metabolism. In G. J. Siegel, B. W. Agranoff, R. W. Albers, S. K. Fisher & M. D. Uhler (Eds.), *Basic neurochemistry* (6th ed.,). Philadelphia: Lippincott-Raven.

Yun, S. H., & Trommer, B. L. (2011). Fragile X mice: Reduced long-term potentiation and N-methyl-D-aspartate receptor-mediated neurotransmission in dentate gyrus. *Journal of Neuroscience Research, 89*(2), 176-182. doi:10.1002/jnr.22546; 10.1002/jnr.22546

Yuskaitis, C. J., Mines, M. A., King, M. K., Sweatt, J. D., Miller, C. A., & Jope, R. S. (2010). Lithium ameliorates altered glycogen synthase kinase-3 and behavior in a mouse model of fragile X syndrome. *Biochemical Pharmacology, 79*(4), 632-646. doi:10.1016/j.bcp.2009.09.023 [doi]

Zerbi, V., Grandjean, J., Rudin, M., & Wenderoth, N. (2015). Mapping the mouse brain with rs-fMRI: An optimized pipeline for functional network identification. *Neuroimage, 123*, 11-21. doi:10.1016/j.neuroimage.2015.07.090 [doi]

Zhang, J., & Liu, Q. (2015). Cholesterol metabolism and homeostasis in the brain. *Protein & Cell, 6*(4), 254-264. doi:10.1007/s13238-014-0131-3 [doi]

Zhang, W., Xu, C., Tu, H., Wang, Y., Sun, Q., Hu, P., . . . Liu, J. (2015). GABAB receptor upregulates fragile X mental retardation protein expression in neurons. *Scientific Reports, 5*, 10468. doi:10.1038/srep10468 [doi]

Zhang, Y., Bonnan, A., Bony, G., Ferezou, I., Pietropaolo, S., Ginger, M., . . . Frick, A. (2014). Dendritic channelopathies contribute to neocortical and sensory hyperexcitability in Fmr1(-/y) mice. *Nature Neuroscience, 17*(12), 1701-1709. doi:10.1038/nn.3864 [doi]

Zhuo, J., Xu, S., Proctor, J. L., Mullins, R. J., Simon, J. Z., Fiskum, G., & Gullapalli, R. P. (2012). Diffusion kurtosis as an in vivo imaging marker for reactive astrogliosis in traumatic brain injury. *Neuroimage, 59*(1), 467-477.

doi:10.1016/j.neuroimage.2011.07.050 [doi]